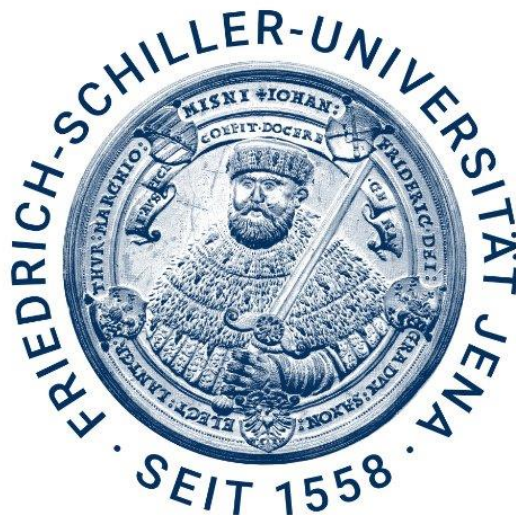# The transcription factor Miz-1 suppresses the antiviral response of hematopoietic stem cells

Dissertation

in Partial Fulfilment for the Requirements
for the Degree of

"Doctor of Philosophy" (PhD)

Submitted to the Council of the Faculty of Biological Sciences of

Friedrich Schiller University Jena

by Adam Charles Summerfield

born on 06.12.1990 in Chesterfield, United Kingdom

Listing reviewers:

Prof. Dr. Lenhard K. Rudolph,

Leibniz Institute on Aging - Fritz Lipmann Institute (FLI), Beutenbergstraße 11, 07745 Jena, Germany

Priv. Dr. Christian Kosan,

Center for Molecular Biomedicine (CMB), Department of Biochemistry, Faculty of Biological Sciences, Friedrich-Schiller-University Jena, Hans-Knöll-Str. 2, D-07745 Jena, Germany

Prof. Dr. Hartmut Geiger,

Institute of Molecular Medicine, University of Ulm, Life Sciences Building, N27 and N24, James-Franck-Ring 11c, 89081 Ulm, Germany

Date of the doctoral exam (defence):

28.06.2023

Abstract

Hematopoietic stem cells (HSC) are tasked with generating the entire blood cell repertoire whilst maintaining their long-term functionality and are well-characterised in terms of their differentiation processes. A critical factor in HSC differentiation is the transcription factor (TF) Myc, which is required for the production of mature hematopoietic cell types and to prevent the accumulation of HSCs. Myc, in other cell types, performs specific functions by recruiting binding partners, such as Myc-interacting zinc finger protein-1 (Miz-1). Miz-1 was first characterised as a growth suppressor that can be recruited and inhibited by Myc to allow cell cycle progression. Later, it was discovered that the Pox virus and zinc finger (POZ) domain of Miz-1, which is critical for Miz-1 to effectively bind DNA, is required to inhibit apoptosis during the maturation of developing B lymphocytes in response to a survival signal. However, the role of Miz-1 in the homeostasis of HSCs is unknown.

In this work, we characterise HSC and hematopoietic progenitor subsets in mice expressing a POZ domain-lacking *Miz-1* gene and find that these cells accumulate significantly when Miz-1 is deficient. We find that this is accompanied by cell cycle entry in HSCs, loss of HSC quiescence and myeloid colony-forming ability and the de-repression of interferon (IFN) and anti-viral response gene expression. The expression of CD41, which is increased in response to inflammatory stress in HSCs, was also found to be higher expressed in Miz-1-deficient HSCs. Myeloid and lymphoid progenitor cells also undergo an expansion in cell number in Miz-1 knockout bone marrow. We also determined that Miz-1 deficiency results in proteomic alterations, such as in clusters of proteins regulating RNA translation and rRNA processing, muscle contraction, vesicular and membrane trafficking and histone methylation. Our results suggested a transcriptional regulation of IFN response genes, so we investigated this in a HSC cell line using chromatin immunoprecipitation. However, we have not found that the regulation of IFN response gene expression by Miz-1 is direct. An effect on STAT1 and STAT5 phosphorylation appeared in Miz-1-deficient hematopoietic progenitors. Namely, the phosphorylation of STAT5 in response to thrombopoietin was defective, an effect known to take place when the interferon response is elevated, while the phosphorylation of STAT1 in response to IFN-γ was increased relative to controls. We also determined that the phenotypes resulting from loss of Miz-1 function in hematopoietic progenitor cells do not result from altered DNA damage or repair from damage. Thus, our work provides new insights into the function of Miz-1 as a homeostatic regulator of HSC pool size and quiescence and as a suppressor of the interferon pathway response in HSCs.

Zusammenfassung

Hämatopoetische Stammzellen (HSZ) haben die Aufgabe, das gesamte Repertoire an Blutzellen zu erzeugen und dabei ihre langfristige Funktionalität zu erhalten. Sie sind in Bezug auf ihre Differenzierungsprozesse gut charakterisiert. Ein entscheidender Faktor bei der Differenzierung von HSZ ist der Transkriptionsfaktor (TF) Myc, der für die Produktion reifer hämatopoetischer Zelltypen und zur Verhinderung der Akkumulation von HSZ erforderlich ist. In anderen Zelltypen erfüllt Myc spezifische Funktionen, indem es Bindungspartner rekrutiert, wie das Myc-interagierende Zinkfingerprotein-1 (Miz-1). Miz-1 wurde zunächst als ein Wachstumssuppressor charakterisiert, der von Myc rekrutiert und gehemmt werden kann, um die Zellzyklusprogression zu ermöglichen. Später wurde entdeckt, dass die Pox-Virus- und Zinkfinger-Domäne (POZ) von Miz-1, die für eine wirksame DNA-Bindung von Miz-1 entscheidend ist, erforderlich ist, um die Apoptose während der Reifung von sich entwickelnden B-Lymphozyten als Reaktion auf ein Überlebenssignal zu hemmen. Die Rolle von Miz-1 in der Homöostase von HSCs ist jedoch unbekannt.

In dieser Arbeit charakterisieren wir HSZ und hämatopoetische Vorläuferzellen in Mäusen, die ein Miz-1-Gen mit fehlender POZ-Domäne exprimieren, und stellen fest, dass sich diese Zellen bei einem Mangel an Miz-1 deutlich vermehren. Wir stellen fest, dass dies mit dem Eintritt in den Zellzyklus der HSZ, dem Verlust der Ruhephase der HSZ und der Fähigkeit zur Bildung von myeloischen Kolonien sowie der Unterdrückung der Expression von Interferon (IFN) und antiviraler Gene einhergeht. Es wurde auch festgestellt, dass die Expression von CD41, die als Reaktion auf entzündlichen Stress in HSZ erhöht ist, in Miz-1-defizienten HSZ stärker ausgeprägt ist. Auch die Anzahl der myeloischen und lymphoiden Vorläuferzellen nimmt im Knochenmark mit Miz-1-Knockout zu. Wir stellten außerdem fest, dass ein Miz-1-Mangel zu proteomischen Veränderungen führt, wie z. B. bei Clustern von Proteinen, die die RNA-Translation und rRNA-Verarbeitung, die Muskelkontraktion, den vesikulären und membranständigen Transport und die Histon-Methylierung regulieren. Unsere Ergebnisse deuten auf eine Transkriptionsregulierung von IFN-Antwortgenen hin, weshalb wir dies in einer HSC-Zelllinie mittels Chromatin-Immunpräzipitation untersucht haben. Wir konnten jedoch nicht feststellen, dass die Expression der IFN-Antwortgene direkt durch Miz-1 reguliert wird. Eine Auswirkung auf die STAT1- und STAT5-Phosphorylierung zeigte sich in Miz-1-defizienten hämatopoetischen Vorläuferzellen. So war die Phosphorylierung von STAT5 als Reaktion auf Thrombopoietin gestört, ein Effekt, der bekanntermaßen eintritt, wenn die Interferonantwort erhöht ist, während die Phosphorylierung von STAT1 als Reaktion auf IFN-γ im Vergleich zu den Kontrollen erhöht war. Wir haben außerdem festgestellt, dass die Phänotypen, die sich aus dem Verlust der Miz-1-Funktion in hämatopoetischen Vorläuferzellen ergeben, nicht auf veränderte DNA-Schäden oder die Reparatur von Schäden zurückzuführen sind. Unsere Arbeit bietet somit neue Einblicke in die Funktion von Miz-1 als homöostatischer Regulator der Größe des HSC-Pools und der Ruhephase sowie als Suppressor der Interferonreaktion in HSCs.

Contents

Nomenclature

BFU-E	Erythropoietin-dependent burst-forming unit
BIZ	BioInstrumenteZentrum
BM	Bone marrow
BrdU	Bromodeoxyuridine
CD	Cluster of differentiation
CDKN1B/2A	Cyclin dependent kinase inhibitor 1B/2A
CFU-GEMM	Colony forming unit-granulocyte, erythrocyte, monocyte, megakaryocyte
CFU-GM	Colony forming unit-granulocyte, macrophage
CFU-S	Colony forming unit-spleen
CFU	Colony forming unit
ChIP	Chromatin immunoprecipitation
CLP	Common lymphoid progenitor
CMB	Center for Molecular Biomedicine
CMP	Common myeloid progenitor
CMRP	Common myeloid repopulating progenitor
Ctrl	Control
DAP	Differentially abundant protein
DAPI	4′,6-diamidino-2-phenylindole
DAVID	Database for Annotation, Visualization and Integrated Discovery
DDX58 (**RIG-I**)	DExD/H-Box Helicase 58
DEG	Differentially exprressed gene
DMEM	Dulbecco's Modified Eagle Medium
dsRNA	Double-stranded ribonucleic acid
FACS	Fluorescence-activated cell sorting
FCS	Fetal calf serum
FLI	Fritz Lipmann Institute
FSC	Forward light scatter
GMP	Granulocyte-monocyte lineage-restricted progenitor
GO	Gene ontology
GSEA	Gene Set Enrichment Analysis
HPC-5	Hematopoietic progenitor cell-5 line
HSC	Hematopoietic stem cell
HSPC	Hematopoietic stem and progenitor cell
IFIT	Interferon-induced protein with tetratricopeptide repeats
IFN	Interferon
IFNAR	Interferon alpha/beta receptor
IGTP	Interferon gamma-induced GTPase
IIGP1	Interferon-Inducible GTPase 1

IL-7	Interleukin-7
IL-7R (**CD127**)	Interleukin-7 receptor alpha chain
IP	Immunoprecipitation
IRF	Interferon regulatory factor
ISG	Interferon-stimulated gene
ITGA2B	Integrin subunit alpha 2b
ITGB3	Integrin subunit beta 3
IgG	Immunoglobulin G
KDM8	Lysine demethylase 8
KO	Knockout (of the *Miz-1* POZ domain)
LMPP	Lymphomyeloid-primed progenitor
LPS	Lipopolysaccharide
LSK	Lineage-negative Sca-1-positive c-Kit-positive cells
LT	Long-term
Lin$^-$	Lineage-negative
MDS	Multidimensional scaling
MEP	Megakaryocyte-erythrocyte lineage-restricted progenitor
MERP	Megakaryocyte-erythroid repopulating progenitor
MFI	Mean fluorescence intensity
MPP	Multipotent progenitor
MS	Mass-spectometry
MX	Myxovirus resistance
Miz-1	Myc-interacting zinc finger protein-1
Mk	Megakaryocyte
MkRP	Megakaryocyte repopulating progenitor
MyRP	Myeloid repopulating progenitors
NES	Normalized enrichment score
OAS	Oligoadenylate synthetases
OASL	Oligoadenylate synthetases-like
PANTHER	Protein Analysis THrough Evolutionary Relationships
PB	Peripheral blood
PBS	Phosphate-buffered saline
PCA	Principle component analysis
PF4	Platelet factor 4
pHSC	Phenotypic hematopoietic stem cell
POZ	Pox virus and zinc finger
PPI	Protein-protein interaction
PRR	Pattern recognition receptor
qPCR	Quantitative real-time polymerase chain reaction
RBC	Red blood cell
RORC	RAR related orphan receptor C

RPKM	Reads per kilobase of transcript, per million mapped reads
RPL	Large ribosomal protein
RPM	Reads per million mapped reads
RPS	Small ribosomal protein
RTP	Room temperature
SCF	Stem cell factor
SFEM	Serum-Free Expansion Medium
SLAM	Signaling lymphocytic activation molecule
SMTNL1	Smoothelin-like protein 1
SOCS	Suppressor of cytokine signaling
SSC	Sideward light scatter
ST-HSC	Short-term hematopoietic stem cell
STAT	Signal transducer and activator of transcription
SVA	Seminal vesicle autoantigen
ScRNA-seq	Single-cell ribonucleic acid sequencing
Sca-1	Stem cell antigen 1
ssDNA	Single-stranded deoxyribonucleic acid
TF	Transcription factor
TLR	Toll-like receptor
TPO	Thrombopoietin
TSS	Transcription start site
VAMP4	Vesicle associated membrane protein 4
VWF	Von Willebrand's Factor
ZBTB17	Zinc finger and BTB domain containing 17
ZNHIT3	Zinc finger HIT-Type containing 3
γH2A.X	Gamma-histone 2A.X

1. Introduction

1.1 The hematopoietic system, stem cells and differentiation

1.1.1 The history of hematopoietic stem cell research

In 1868, the German pathologist Franz Ernst Christian Neumann noted that the bone marrow (BM) is "an important organ for blood formation" upon his observations that erythropoiesis and the formation of leukocytes take place there. Furthermore, he proposed that a common cell is responsible for the generation of all hematopoietic cells. Then, in 1909, the Russian hematologist and histologist Alexander A. Maximow developed and introduced a theory of hierarchical hematopoiesis with "stem" cells at its apex, which are mobilized by stimulants to move through a micro-environmental niche that supports these cells within the bone marrow (Konstantinov, 2000).

These ideas came dramatically into focus following the bombings of Hiroshima and Nagasaki in 1945, where many victims in the aftermath died of hematopoietic failure. A few years afterwards, hematopoietic failure in mice resulting from this radiation syndrome was found to be prevented by shielding the spleen with lead (Jacobson et al., 1950) and treatable by intravenous administration of spleen or bone marrow cells (Lorenz et al., 1951). In 1961, it was shown that a precise dilution of cells taken from the BM of mouse femurs can directly generate macroscopic colonies on the spleen of irradiated recipient mice after transplantation and that the number of the colonies formed was inversely proportional to the extent of the dilution (Till & McCulloch, 1961). These spleen colonies, referred to as colony forming units (CFU), were also shown to contain cells that are capable of repeated self-renewal (the property a cell has to generate daughter cells of the same phenotype) by forming new colonies on the spleens of other recipient mice (Siminovitch et al., 1963). This gave evidence for the hypothesis that hematopoietic organs regenerate and survive by cellular repopulation.

Observations of spleen CFUs (CFU-S) of transfused mice had revealed that they contained erythrocytic, granulocytic and megakaryocytic precursor cells. But it was still unclear which cell type was responsible for the regeneration of all others, as the ability to classify cells by their self-renewal and proliferation capacity was still lacking. In 1977, Abramson and colleagues addressed the unproven assumption of a single stem cell capable of producing CFU-S as well as lymphocytes by irradiating mouse BM and injecting these cells into stem cell-deficient recipients, observing afterwards that the chromosomal markers induced by the radiation were present in the BM, spleen and thymi of recipient mice. This included B and T lymphocytes generated in the recipient mice by stimulation with the bacterial wall component, lipopolysaccharide (LPS). Furthermore, the BM of primary recipients was injected into secondary recipients, resulting in donor lymphoid and myeloid cells being identified in recipient CFU-S which contained the same chromosomal aberrations as in the donor mouse,

showing that a particular clone of stem cells must be capable of self-renewal and multi-lineage reconstitution. Some unique karyotypes were also identified exclusively in CFU-S cells of myeloid lineage, which demonstrated the concept of lineage restriction, as this meant that some donor clones could only repopulate myeloid cells but not cells of lymphoid origin (Abramson et al., 1977).

The era of defining and identifying HSC by phenotype began in 1972 when an antibody was discovered to reduce the CFU-S forming ability of BM cells when incubated before transplantation into a recipient mouse (Golub, 1972).

1.1.2 HSC markers and functional assays

Using their splenic colony-forming assay, the process of defining HSCs according to their ability to self-renew continued and in 1979, resistance to the cytotoxic agent 5-fluorouracil, which kills dividing cells but leaves non-dividing (quiescent) cells alive, was found to spare BM cells that have regenerative capabilities greater than those of CFU-S-forming progenitor cells and could repopulate irradiated BM (Hodgson & Bradley, 1979). Quiescence was therefore identified as a characteristic indicating both the regenerative and the BM-homing capacity of HSCs.

Means of separating cells by their characteristics were also advancing: antibody-positive cells could now be separated from negative cells by fluorescence-activated cell sorting (FACS) before being injected into hosts for functional assaying. Typically after cells have been incubated with a fluorophore-conjugated antibody, FACS is used to separate those cells according to their intensity of fluorescent signal, often into marker-positive and marker-negative volumes. While the predominant method of separating cells had up until this point been density gradient centrifugation, FACS now provided a convenient means of separating cells on the basis of their size, by measuring their forward light scatter (FSC), or their granularity, measured by their sideward light scatter (SSC) and "gating" for the desired population. In 1981, Robert Coffman and Irving Weissman used FACS to segregate BM cells labelled with a leukaemia-targeting fluorescent antibody on the basis of their expression of an antigen (later named B220) and injected these cells intravenously into irradiated mice for CFU-S assaying (Coffman & Weissman, 1981). Their experiment showed that B220$^+$ cells are depleted of CFU-S activity, as opposed to unfractionated BM or B220$^-$ cells and further showed, using other methods, that B cells and certain precursors express B220. However, CFU-S assays only inform us about a progenitor cells ability to home to the spleen and provide radioprotection to a mouse over the course of two weeks, greatly limiting the scope of which cells can be studied for their self-renewal and differentiation capacities.

To address this, *in vitro* assays were developed in 1966 in which tissue sample is grown into cells, referred to as clones, as colonies on agar (Bradley & Metcalf, 1966), followed by a technique for culturing granulocyte and erythroid colonies *in vitro* developed in 1971

(Stephenson et al., 1971). Culturing of erythroid colonies on methylcellulose in 1976 then allowed them to be further resolved into short-term surviving erythroid CFUs and erythropoietin-dependent burst-forming units (BFU-E), able to survive for the duration of the assay and identified as being committed erythropoietic progenitors (Gregory, 1976). Culture on agar a year later then allowed colonies consisting of erythroid, granulocyte, neutrophil, megakaryocyte and eosinophil cells to be produced (Johnson & Metcalf, 1977). The Till-McCulloch assay later developed into the colony-forming unit (CFU) assay, which was eventually adapted to be performed on methylcellulose medium under myeloid cell-stimulating conditions. Colonies growing on the surface of the media were identified as originating from committed progenitors producing identifiable lineage-restricted colonies. These are principally the granulocyte, erythrocyte, monocyte and megakaryocytic (CFU-GEMM), granulocyte-macrophage (CFU-GM, formerly referred to as granulocyte-only CFU-C) and BFU-E colonies (Ichikawa et al., 1966), (Fauser & Messner, 1979). The CFU assay has become widely used as a means of testing the effects of different conditions on myeloid progenitor formation.

All of the aforementioned techniques, however, were only short-term assays lasting two weeks. So for the purpose of determining the long-term self-renewal and pluripotency of hematopoietic cell types, a more advanced *in vitro* cell culture technique was developed (Dexter et al., 1977), (Whitlock & Witte, 1982). This would allow investigators to examine the biochemistry of the differentiation process and, if a more defined population of input cells were used, to examine which progenitor populations are responsible for producing which kinds of committed cells. In 1986, Irving Weissman did exactly this by isolating BM cells that lacked expression of B220, the granulocyte marker Gr-1 and the macrophage marker CD11b (CD; cluster of differentiation) using FACS and subjected them to long-term culture. It was found that this subset of cells were able to differentiate into B lineage cells and using repeated dilution, were able to enrich these B cell progenitors by 100-fold compared to unfractionated BM (Muller-Sieburg et al., 1986). Weissman et al. then further determined the functional capacity of B220$^-$ Gr-1$^-$ CD11b$^-$ cells by subjecting them to CFU-S assay, finding that they were 200-fold more potent than total BM in seeding myeloid spleen colonies. Furthermore, these B220$^-$ Gr-1$^-$ CD11b$^-$ cells were far more capable of rescuing and sustaining lethally irradiated mice for more than 4 months than unseparated BM cells on a per cell basis. The result was that a 0.1% proportion of BM cells, isolated according to their cell surface marker expression pattern, had been proven to be highly enriched for lymphoid lineage cell progenitors and myeloid progenitors in addition to possessing high self-renewal capacity. However, whether the cells responsible were a single type of stem cell or a heterogeneous group of hematopoietic stem and progenitor cells (HSPCs, a term including pluripotent stem cells and multipotent progenitors), was still unknown.

FACS now allowed a more convenient means of measuring the success of the transplantation. Weissman's team further phenotypically defined HSCs in 1988 by assaying

their ability to reconstitute the committed cell types of all hematopoietic (minus erythrocyte) lineages in lethally irradiated mice, which they determined by measuring CFU-S at day 12 and B lymphocytes and neutrophils in the peripheral blood (PB) by FACS after 6 weeks (Spangrude et al., 1988). The fraction of BM cells that was chosen was FACS-selected for lacking expression of the lineage markers, Gr-1, CD11b, B220 and also the T lymphocyte markers CD4 and CD8, a battery of markers termed the lineage-negative (Lin⁻) panel. Simultaneously, the input cells were sorted for expressing the positive and negative fractions of the recently discovered stem cell antigen-1 (Sca-1). These Sca-1$^+$ Lin$^-$ cells were highly predisposed to produce the late (day 12) CFU-S, rather than the early CFU-S typical of short-term repopulating progenitors and could also form colonies on the thymus of an irradiated mouse with around a thousand-fold fewer cells than unfractionated BM could. Furthermore, fewer than 100 Sca-1$^+$ Lin$^-$ cells were necessary to completely repopulate the recipient mouse with cells of the B, T, granulocyte and macrophage lineages after 6 weeks. Committed lineage cells derived from donor mice were discerned in the recipient mouse by their expression of the CD45.2 allele. In this manner, a precise number of cells from compartments of HSPCs, identified by their cell surface molecule expression, are functionally assayed in recipient mice for their self-renewal and multilineage repopulation capacity by measuring their capability to sustain the recipient mouse's hematopoietic system over time.

The stem cell-associated receptor tyrosine kinase c-Kit, which is bound by the colony-stimulating ligand named stem cell factor (SCF). In 1991, *in vitro* and *in vivo* CFU assays were used in showing that HSPCs either lacking c-Kit expression or treated with a c-Kit antibody antagonist were unable to form colonies, evidencing that all self-renewing HSPCs express c-Kit (Okada et al., 1991), (Ogawa et al., 1991). This *in vivo* repopulation assay measured the lineage reconstitution capability of Lin$^-$ c-Kit$^+$ cells at 8 and 25 weeks after irradiation, allowing more precise identification of long-term (LT) self-renewing cell compartments. The lineage panel antibody cocktails used to negatively mark stem cells now included TER-119, a marker for erythrocytes. The results showed that while Lin$^-$ c-Kit$^-$ cell-receiving mice all died, those in receipt of regular BM cells survived, but had lower proportions of donor-derived committed cells in their peripheral blood than those that received Lin$^-$ c-Kit$^+$ cells after 8 weeks. After 25 weeks, the difference in percentages of donor-derived cells had gotten even larger, indicating that Lin$^-$ c-Kit$^+$ cells contain a greater proportion of long-term multilineage repopulating HSCs (LT-HSCs) (Okada et al., 1991).

Irving Weissman and Sean Morrison conducted a study in 1994 aiming to isolate LT-HSC further by using a 14-week competitive repopulation assay, wherein a precise number of donor cells are transplanted to a recipient together with a precise number of cells from another donor with a known repopulation potential (Morrison & Weissman, 1994). Using this technique, Weissmann and Morrison showed that Lin$^-$ Sca-1$^+$ cells expressing low levels of CD11b or CD4 possessed only transient repopulation potential, while those entirely negative for their expression possessed greater LT multilineage reconstitution potential and that this capability

resided entirely within the c-Kit$^+$ fraction, of which only 15 cells were needed to sustain a mouse for 14 weeks. The Lin$^-$ Sca-1$^+$ c-Kit$^+$ (LSK) staining scheme then became the standard of HSC isolation.

A true LT-HSC would have the property of being able to produce hematopoietic cells of all lineages for the entire duration of an organisms life. Therefore to prove that such a cell exists, an experiment would have to demonstrate that the whole of the hematopoietic system can be repopulated in a mouse by a single donor cell. This was attempted by isolating LSK according to their expression of a human stem cell marker in 1996. Expression of CD34, the human homolog of which was identified in 1983 as a HSC marker by *in vitro* CFU assay (Civin et al., 1984), was shown by Osawa et al. to have the ability to discern single LSKs capable of either transient or sustained production of differentiated myeloid and lymphoid cells (Osawa et al., 1996). LSKs that were CD34$^+$ were capable only of very brief multilineage repopulation, whereas those that were CD34$^-$ were able to produce myeloid and lymphoid cells across the time range of the repopulation experiment, which was 300 days and therefore more stringently tested for LT-HSCs than previous studies. LSKs capable of self-renewal had been shown to be CD34$^-$, but not all CD34$^-$ LSKs possessed long-term self-renewal, as only 21% of mice receiving a single CD34$^-$ LSK donor cell were able to survive the time course of the repopulation experiment. True LT-HSCs therefore, reside somewhere within the CD34$^-$ LSK compartment.

These functional assays have continued to be used to identify HSC markers, including Flt3 (CD135), a tyrosine receptor kinase, the expression of which was shown to dispose LSKs towards only being able to support reconstitution of B and T cells in the PB of recipient mice, while Flt3$^-$ LSKs remained able to support the production of myeloid, B and T cells over the long-term (Adolfsson et al., 2001). In 1997, Sean Morrison and Irving Weissman made progress organising HSPCs into a hierarchy defined by lineage-reconstituting capacity. They showed that c-Kit$^+$ cells that are CD11b$^-$ CD4$^-$ could reconstitute themselves as well as CD11b$^{lo/+}$ and CD4$^{lo/+}$ cell types in recipient mice (Morrison et al., 1997). In this way, cells were designated as being higher in the hematopoietic hierarchy if they had the ability to self-renew themselves in recipients in addition to other cell types and were referred to as multipotent progenitors (MPP). As the cell surface receptor inventory for marking HSCs had now grown to be cumbersomely long, as well as these marking strategies being unable to isolate HSCs capable of LT multilineage reconstitution in any more than 20% of mice, it became highly necessary to make the staining strategy of HSCs both more concise and definitive of HSC function. In 2005, Morrison et al. identified a group of immunoglobulin receptors, called signaling lymphocytic activation molecule (SLAM) antigens, the expression patterns of which conveniently correspond to an MPP hierarchy in mice. The aforementioned MPP cell compartments were subject to gene expression profiling which identified high CD150 expression, low CD48 and low CD41 expression as indicative of HSC status, which was then functionally verified by FACS followed by competitive reconstitution assay (Kiel et al., 2005). A single CD150$^+$ CD48$^-$ LSK was shown to yield LT multilineage reconstitution in 50% of mice, as well as engrafted at a high

rate across multiple organs. These rare cells constitute less than 0.001% of living BM cells, a quantity referred to as the cell frequency. The absolute (total) number of cells of a cell type in the BM can be found by multiplying the cell frequency by the number of cells in the bone marrow that was taken. Other studies subsequently confirmed that CD150 expression indicates LSK of greater engraftment and long-term PB reconstitution capacity, relative to non-expressing LSKs (Papathanasiou et al., 2009), especially myeloid reconstitution (Morita et al., 2010). Close to 10,000 CD150$^+$ CD48$^-$ LSKs reside in the combined femurs of a mouse, and although this depends on the mouse's age and strain, isolating cells by cell surface phenotype is still believed to be an efficient way of purifying the most pluripotent HSCs.

1.1.3 The hierarchy of the hematopoietic system

With the ability to divide cells functionally by cell surface marker, a hematopoietic lineage map had begun to emerge, which when combined with the reconstitution readout from recipient mice, also provided a time course of differentiation of the cell compartment that was transplanted. In this way, hematopoietic cell compartments, identified by their cell surface molecule phenotype, are assigned their position within the hematopoietic lineages by observing the type of cellular reconstitution they enable and the duration of time over which they are capable of said reconstitution, with delayed and prolonged reconstitution, as well as reconstitution of a broader range of cell types, each indicating a higher position in the hierarchy. For example, interleukin-7 had been shown to be an essential cytokine for B and T lymphocyte survival and development, so in 1997 researchers decided to isolate Lin$^-$ progenitor cells that express the interleukin-7 receptor alpha chain (IL-7R, CD127) and assay them for their ability to produce myeloid and lymphoid cells compared to BM cells or LSKs (Kondo et al., 1997). IL-7R$^+$ Lin$^-$ progenitors were able to reconstitute B, T and natural killer lymphocytes a week before LSKs could in competitive reconstitution assays, while unlike LSKs, could not reconstitute granulocytes or macrophages. They were therefore deemed common lymphoid progenitors (CLP); "lymphoid" due to their restricted yet comprehensive ability to repopulate the lymphoid lineage and "progenitors" due to their lesser self-renewal capacity compared to LSKs, indicated by their earlier reconstitution peak in recipient mice.

So to find the equivalent common progenitor of the myeloid lineage, Weissman and Akashi performed a similar series of experiments on the IL-7R$^-$ fraction of Lin$^-$ c-Kit$^+$ cells in the year 2000. They found that Lin$^-$ c-Kit$^+$ Sca-1$^-$ cells that were IL-7R$^-$ could be divided by CD34 and CD16/32 (a marker of myelomonocytic cells) expression into three compartments that produce distinct colony types in a CFU assay (Akashi et al., 2000). Progenitor cells that were CD16/32$^-$ CD34$^-$ gave rise to CFU-megakaryocyte-erythroid colonies when plated and only reconstituted TER-119-expressing cells when transplanted into recipient mice and were therefore designated to be megakaryocyte-erythrocyte lineage-restricted progenitors (MEP). While, progenitor cells that were CD16/32$^+$ CD34$^+$ gave rise to CFU-GM colonies and only reconstituted Gr-1$^+$ and CD11b$^+$ cells when transplanted into recipient mice and were therefore designated to be granulocyte-monocyte lineage-restricted progenitors (GMP). Furthermore, upon culturing

CD16/32⁻ CD34⁺ progenitors, it was found that MEP, GMP and mature myeloid cell types were produced, while MEP and GMP could not produce each other when cultured. Therefore, CD16/32⁻ CD34⁺ progenitors were deemed to be common myeloid progenitors (CMP), which differentiate into either the megakaryocyte-erythrocyte or the granulocyte-macrophage lineages in a mutually exclusive fashion. Moreover, none of these myeloid progenitors generated lymphoid-type cells, indicating that the expression of IL-7R, or lack thereof, is an essential junction at which a multipotent progenitor becomes either a CMP or CLP and from where a CMP may differentiate down either the megakaryocyte-erythrocyte or granulocyte-macrophage lineages: seeming to conform to a hierarchical, stepwise model of hematopoiesis.

The work done in 1994 by Morrison and Weissman had shown that HSPCs could be divided into 3 subpopulations of varying long-term reconstitution capacity, based on their CD11b and CD4 expression levels (Morrison & Weissman, 1994). Therefore, cell types with only transient self-renewal but comprehensive lineage-regeneration potential, became referred to as short-term repopulating HSCs (ST-HSC). A later study would show that LSKs lacking expression of Flt3 and CD34 possess long-term reconstituting potential of all lineages, and are therefore LT-HSCs, but upon expression of CD34, lose this capacity and become ST-HSCs that retain broad lineage reconstitution (Yang et al., 2005). These differentiation steps fit into a "classical" model of hematopoiesis as taking place before the myeloid-lymphoid bifurcation stage. In the classical model, LT-HSCs would express a set of pluripotency markers, which would change in expression level as these LT-HSCs become actively dividing and differentiating ST-HSCs, before bifurcating into CMPs or CLPs and then further on toward a committed cell type, with each stage being identifiable by a clear cell marker expression change that was conditional upon a previous cell marker expression change. However, the classical model of hematopoiesis was soon shown to be mistaken.

It was then shown, using *in vivo* and *in vitro* methods with single cells, that LSKs that coexpress CD34 and Flt3 almost entirely lose their ability to generate megakaryocytes and erythrocytes, compared to CD34⁺ Flt3⁻ LSKs (Adolfsson et al., 2005), while still retaining most of their granulocyte-monocyte generation capacity. Today, these CD34⁺ Flt3⁺ LSKs are referred to as lymphomyeloid-primed progenitors (LMPP) and the departure of megakaryocytes and erythrocytes from their differentiation repertoire compared to their Flt3-negative counterparts suggested that a type of megakaryocyte-erythroid progenitor exists that may have the option to bypass the lymphoid-myeloid differentiation partition.

In 2013, this was directly confirmed when investigators partitioned CD34⁻ LSKs into CD150⁺ CD41⁺, CD150⁺ CD41⁻ and CD150⁻ CD41⁻ subsets for single-cell transplantation into recipient mice and surprisingly found that these fractions contained cells that were myeloid-lineage restricted but also demonstrated long-term repopulation potential (Yamamoto et al., 2013). CD41 (also known as integrin alpha 2b protein), was chosen as a marker as it is known to greatly increase in expression level in HSCs during aging (Gekas & Graf, 2013). As a result of these transplantations, a new set of progenitor cell had to be defined, with reference to their

repopulation ability and are referred to as myeloid-restricted progenitors (MyRP). Based on the lineages to which these cells are restricted in repopulating, they were further defined as being common myeloid repopulating progenitors (CMRP), megakaryocyte-erythroid repopulating progenitors (MERP) and megakaryocyte repopulating progenitors (MkRP). CMRPs are capable of reconstituting platelets, erythrocytes, neutrophils and monocytes, MERPs can reconstitute platelets and erythrocytes and MkRPs only platelets. To investigate the process by which these progenitors are produced from HSCs further, the team allowed HSCs to divide once in culture and transplanted each single cell into a recipient mouse. By measuring the hematopoietic reconstitution of these recipient mice, it was shown that the transplanted cells constituted by a variety of daughter cell pairs, including HSC-HSC, HSC-MyRP and MyRP-MyRP pair types. As well as having important implications about the nature of HSC homeostasis and differentiation, this showed that HSCs could divide directly into myeloid repopulating progenitors with no intermediary differentiation steps.

In fate mapping, transposon tags of specific sequences (barcodes) are introduced to HSCs and their dissemination among daughter cells (including the original cells) are harvested. When this is coupled with FACS, this allows the nascent process of hematopoietic differentiation during homeostasis to be tracked from individual HSCs by cell marker readout. These studies converge on a differentiation model in which HSCs can be grouped on the basis of their eventual lineage commitment fates into 5 clusters. One of these clusters appears unipotent in its ability to repopulate megakaryocytes and platelets and is demarcated by the high von Willebrand's Factor (VWF) and CD41 expression levels of its cells, meaning that they are the MkRPs identified by Yamamoto et al. In this cluster, self-renewal and multilineage capacity appear at first sight to have been uncoupled, as they appear unipotent but possess LT self-renewal. Another reproducibly identifiable cluster is the LT multilineage-repopulating HSC cluster, responsible for a large proportion of megakaryocytes produced and produce cells of all other lineages at a very slow rate (Carrelha et al., 2018), (Rodriguez-Fraticelli et al., 2018), (Nestorowa et al., 2016). The lineage outputs of the remaining 3 clusters identified by studies differ in their potency to produce the erythroid, myeloid (granulocyte) and lymphoid lineages (Carrelha et al., 2018). For example, MPP1 cells, seen as the first step in the HSCs process of differentiation in the classical model, are tri-potent for erythroid, myeloid and lymphoid lineages, which paradoxically for the classical model, means they closely resemble MPP4 or LMPP cells (Rodriguez-Fraticelli et al., 2018). MPP2 cells are found to reconstitute primarily megakaryocyte and erythroid cells and small amounts of myeloid lineages, while MPP3 cells are largely bi-potent for erythroid and myeloid cell types. Contrariwise, there is heterogeneity in which HSPC clusters are accountable for the generation of each committed cell fate. Megakaryocyte production is accounted for by LT-HSC and MPP cell types equally, while B lymphocytes almost exclusively pass through MPP3 and MPP4 cells, with erythroid and myeloid cells being contributed to by a varied mix of progenitors and with little LT-HSC contribution (Rodriguez-Fraticelli et al., 2018). Erythroid cells move predominantly through an MPP2 state unlike myeloid or lymphoid progenitors (Nestorowa et al., 2016). A highly

intriguing finding by multiple independent teams is that some platelet fate-restricted HSCs retain the potential to populate all lineages upon secondary transplantation, suggesting that the MkRP cluster possesses the ability to reprogram into LT-HSCs (Yamamoto et al., 2013), (Nishikii et al., 2015), a finding also been confirmed *in vitro* (Carrelha et al., 2018), suggesting that MkRPs reside within the stem cell compartment.

The fact that different committed cell types have predominantly moved through one MPP cell type and not others tells us that HSCs and progenitors are bypassing stepwise MPP differentiation, traversing only one phenotypic MPP state, suggesting a minimum-step model of hematopoiesis. It also been shown that in human beings, MPP, CMP and MEP populations contain progenitors that are already committed to a single lineage (Notta et al., 2016) and that in mice, based on gene expression, CMP, MEP, GMP, CLP as well as T cell and dendritic cell progenitors can each be broken down into further clusters (G. Guo et al., 2013), revealing the true heterogeneity of HSPCs hidden by marking cells according to their surface molecule phenotype.

Gene expression profiling has revealed the true heterogeneity between HSPC types. Single-cell techniques offer not only cellular resolution of fate decisions, but also in transcript expression differences between populations. When RNA-sequencing, a more sensitive method of measuring gene expression than the method used to identify the SLAM markers, is performed on single cells, it is called single-cell RNA-seq (ScRNA-seq). ScRNA-seq profiling can be used to find absolute differences between individual cells in mRNA content and therefore informs us about the gene expression mechanism of differentiation at the single-cell level, allowing researchers to more distinctly resolve the HSPC clusters, whereas bulk RNA-seq reveals only relative expression differences between cell populations. The transcriptome of each cell is projected on the reconstructed differentiation path giving complete insight into the cell state transitions occurring during blood differentiation. An interesting finding is that the LT-HSC cluster, the only of the HSPC clusters to overlap with all the others, is identified by its high expression of the receptor c-Mpl, the ligand of which is the thrombopoietic cytokine thrombopoietin (TPO), while MkRPs are discriminated for by their high VWF and CD41 expression. When scRNA-seq, fate mapping and cell surface marker-based isolation of HSPCs are combined, we find that the true discriminant of HSPC fate decision making is its RNA expression profile, of which a cells surface marker expression pattern is only an imprecise indicator.

However, a model that predicts which cells are deterministically committed to particular hematopoietic fates based on either the HSPC cluster to which they belong or their transcriptomic profile is still lacking, as there is still expression variance within each cluster. These experimental findings have led to the emergence of a model which may be referred to as a "bypass", "two-tier" or "radial" model of hematopoiesis (Figure 1.1), which currently competes for favour among researchers with the stepwise model. This model envisions the terminally differentiated hematopoietic cells originating from one of five clusters of stem and

progenitor cells in a single or few steps, along a differentiation trajectory determined from the outset by gene expression of lineage-determining transcription factors (TF). These clusters, whose heterogeneity and order of differentiation is poorly approximated by cell surface phenotype, are divided into two tiers, with multipotent, slowly dividing HSCs and unipotent MkRPs possessing long-term self-renewal, and a proliferative lower tier more geared toward PB generation in which MPPs, MkRPs, CMRPs and LMPPs are represented.
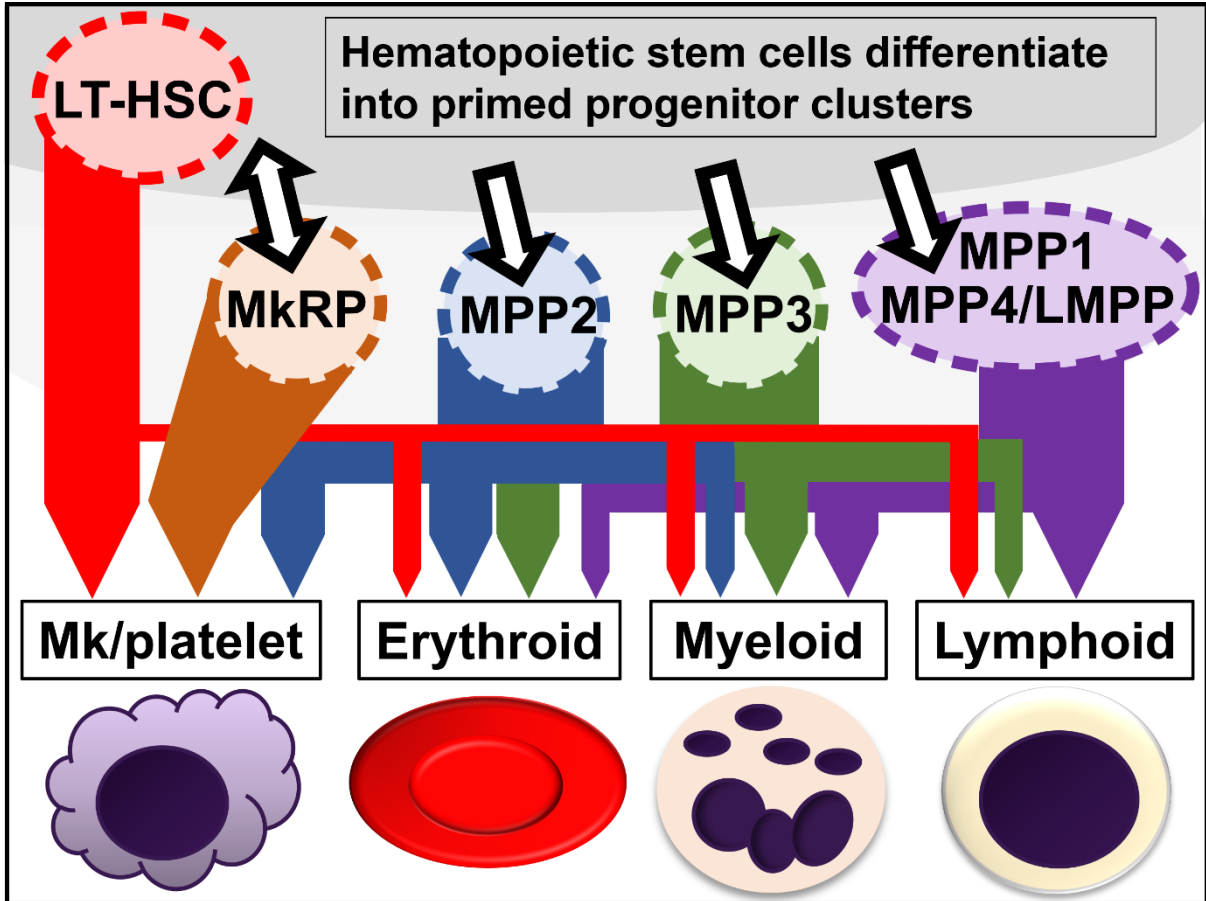
Figure 1.1.: A radial model of hematopoietic differentiation 5 clusters of HSPC type (dotted ovals), defined by their RNA transcriptome, are shown along with their potency (colored arrows) for each lineage of mature hematopoietic cell type. The approximate percentage of cells of each HSPC cluster primed for each cell fate is indicated by the width of each colored arrow. Diagram does not indicate the proportion of each mature hematopoietic cell type that is repopulated by each HSPC cluster type, nor are the relative sizes of HSPC clusters represented. To emphasise radial differentiation, black-edged white arrows represent a single differentiation step from quiescent, multilineage LT-HSCs to more rapidly repopulating progenitor types; the capacity of unipotent MkRPs to reprogram into LT-HSCs is also depicted. Diagram represents the fact that lineage fates and potencies of progenitors are not tracked by their cell surface phenotype nor the sequence of classically defined MPP progression according to the classical stepwise model of hematopoiesis. Mk; megakaryocyte.

1.1.4 Processes regulating hematopoietic differentiation

Homeostasis must be strictly coordinated so that the body has a steady supply of blood cells and platelets while reducing energy waste, loss of stem cell potency and the risk of leukaemia (Orford & Scadden, 2008). Lineage-committed blood cells have a high turnover and therefore only HSCs can sustain the system due to their multilineage capacities. The primary mechanism for regulating HSCs between a state of activity when they are needed, and a state of dormancy when they are not, is their quiescence. The first demonstration of a fraction of HSCs that exhibit long-term quiescence was in 2008 (Wilson et al., 2008), when Anne Wilson and colleagues used FACS to measure the DNA content (which doubles during the S phase of mitosis) and the intracellular Ki-67 expression (expressed in cycling cells, but not in quiescent G0 cells) of LSK populations according to their CD135 (Flt3), CD150, CD48 and CD34 expression. The fraction of these LSKs known to have the most self-renewal and LT multilineage reconstitution capacity are $CD135^-$ $CD150^+$ $CD48^-$ $CD34^-$ LSKs, referred to as HSCs and as a percentage of the population, were mostly (about 70%) in the quiescent G0 stage of the cell cycle. The expression of CD34 in $CD135^-$ $CD150^+$ $CD48^-$ LSKs (this fraction is referred to as MPP1) was correlated with a significant decrease in G0 cells, falling to 40%. Using the classical model to interpret Wilson's findings, as MPP1 express CD48 in becoming MPP2 cells (which differ from MPP1 in that they express CD48), quiescence falls lower still, before dropping to its lowest levels in MPP3 (which have low CD150 expression) and MPP4 cells (which express Flt3, also named LMPP cells). These measurements however, tell us only the levels of quiescence among HSPCs at a given point in time and therefore cannot inform us about the likelihood a type of cell will divide over a given period of time. A label-retaining assay, whereby the nucleoside dye 5-bromo-2-deoxyuridine (BrdU) is incorporated into DNA during mitosis and lost over the course of following divisions, was therefore done to measure the rate of loss of BrdU in fractions of HSPCs. When BrdU loss was measured by FACS at different time points, it was found that HSCs lose BrdU slower than any MPP cell type. A mathematical model showed that HSCs could be divided into 2 populations, into an "active" population that underwent mitosis on average every 36 days, which account for 5 out of 6 HSCs, and a "dormant" population that divided on average every 145 days. Fitting with the theory that quiescence is necessary to retain the pluripotency and self-renewal of a stem cell, multilineage reconstitution ability in recipient mice was highly enriched among dormant, label-retaining HSCs compared to active HSCs. Activated HSCs can also return to dormancy after a period of activity.

The regulation of quiescence in HSPCs involves both extrinsic and intrinsic factors, with return to or exit from quiescence being tied to differentiation. Quiescence is regulated in specific micro-environments, or niches. There are two acknowledged niches for hematopoietic cells within the BM: the endosteal niche on the marrow-side inner surface of the bone, which is lined with osteoblastic cells that quiescent HSCs colocalise with and a vascular niche where HSPCs active in the cell cycle are known to primarily reside (Wilson et al., 2008), (Kunisaki et

al., 2013). Many ligands are now known to regulate HSC quiescence, multilineage capacity and self-renewal from the cells composing these niches: two known to be essential for maintenance of the HSC pool are SCF, the ligand for c-Kit and TPO, the cytokine found to be necessary for platelet production from megakaryocytes, as well as stimulating megakaryocyte progenitor proliferation and differentiation into megakaryocytes (Kaushansky, 1997), (Gurney et al., 1994). SCF stimulation alone can induce a large percentage of HSCs to enter the cell cycle (Oedekoven et al., 2021), with the pool size of HSCs being maintained by SCF released by endothelial cells in the vascular niche (Ding et al., 2012), (Oguro et al., 2013). Similarly, the production of myeloid progenitor colonies *in vitro* depends on the presence of TPO (Buza-Vidas et al., 2006). Interestingly, TPO is required *in vivo* to restrain cell cycling and protect the pool size of LSK cells (Qian et al., 2007). It is understandable how TPO can affect HSPC pleiotropically when we consider its combination with other cytokines: TPO is necessary but insufficient for human hematopoietic colony formation *in vitro*, additionally requiring IL-6 and Flt3 ligand (Matsunaga et al., 1998). While TPO can synergise with other cytokines to form a few *in vitro* colonies, this capacity is greatly enhanced by addition of SCF. Indeed, TPO and SCF together are sufficient for progenitor colony formation (Ku et al., 1996) and they are necessary for a majority of CD34⁻ LSK to be able to divide (Ema et al., 2000), (Seita et al., 2007), especially for cumulative divisions. Cytokines achieve these effects through different molecular pathways, with SCF activating intracellular Akt and TPO inducing the phosphorylation of the signal transducer and activator of transcription 5 (STAT5) molecule (Du et al., 2012), (Nishikawa et al., 2014). Therefore, TPO and SCF act together to promote the survival and expansion of HSCs.

A common view is that HSCs must leave quiescence and enter the cell cycle in order to differentiate (Ikonomi et al., 2020). Data from single-cell RNA-sequencing experiments have shown that HSCs typically express lineage-specifying genes before entering the S phase of the cell cycle (Grinenko et al., 2018). Similarly, HSCs enter S and G2/M phases after their gene expression profiles diverge from erythrocyte and granulocyte-macrophage trajectories to a lymphocyte trajectory (Nestorowa et al., 2016). This expression program is referred to as lineage priming, and the percentage of a HSPC compartment that is primed broadly reflects how active that compartment is in the cell cycle, with very few HSCs and MPP1 cells being primed whereas most MPP2 cells are lineage-primed (Rodriguez-Fraticelli et al., 2018). Exposure to TPO induces gene expression changes in HSCs, including induction of the oncogene *c-Myc* (Comoglio et al., 2018) as well as the megakaryocyte lineage gene *VWF* (Nishikii et al., 2015). In summary, cytokines induce HSCs and progenitors to commit to programs of differentiation according to HSPC priming and they are required for mature cell production.

1.1.5 The regulation of HSC activity by Myc

The balance between self-renewal and differentiation is determined in the nuclei of HSCs by TFs such as Myc, which was discovered due to being contained in the genomes of two cancer-causing avian acute leukemia viruses (Duesberg & Vogt, 1979), (Mellon et al., 1978),

the human homolog of which was also found translocated to a highly expressed genomic region in Burkitt lymphoma patients (Finver et al., 1988). In fact, gain of function *Myc* gene aberrations are found in a majority of B lymphomas (Korać et al., 2017) and its overexpression is necessary for erythroleukemia cells to maintain a blockade on their differentiation into mature erythrocytes, showing that Myc has a differentiation-blocking role (Coppola & Cole, 1986), (Obinata et al., 1994).

Myc in fact is a gene family consisting of 3 homologous genes whose protein products are named c-Myc (referred hitherto as Myc), N-Myc and L-Myc, the first two of which play a role in regulating the differentiation of HSCs after they have left quiescence. Myc expression in hematopoietic cell types is coordinated from a genomic blood enhancer region consisting of different modules and is the only enhancer region active in the most primitive HSCs. Different TFs bind these modules, each of which is necessary for the sustained production of cells of specific lineages (Bahr et al., 2018). Myc expression in LSKs increases in response to signaling through c-Kit (Dahlin et al., 2018) in response to SCF (Yoshihara et al., 2007) and this activation can be suppressed by TPO. However, there are situations where TPO stimulation rapidly induces *c-Myc* mRNA expression, such as in CD41$^+$ LSKs (Comoglio et al., 2018) and in megakaryocytes (Chanprasert et al., 2006). Myc therefore, is required for the production of mature hematopoietic cell types to be generated and its expression is controlled by cytokine-activated signaling. Combined levels of *N-Myc* and *c-Myc* are highest in LT-HSCs and are lower in MPPs and other progenitor cell types, but this is due to loss of *N-Myc* expression (Laurenti et al., 2008), while *c-Myc* expression changes only modestly. However, certain groups of HSPCs have clearly differing *c-Myc* expression levels, as Flt3$^+$ LSK cells express higher levels of *c-Myc* transcripts than Flt3$^-$ LSK cells (Wilson et al., 2004). Changes in *c-Myc* expression levels also correlate with the onset and completion of differentiation, as it is down-regulated during megakaryocyte maturation, but up-regulated during differentiation of erythrocyte progenitors to erythrocytic blasts, and then down-regulated during further maturation (Y. Guo et al., 2009). A reduction in Myc activity correlates with a cell ending its differentiation phase (Dahlin et al., 2018). The reason for c-Myc being able to influence LT-HSC to ST-HSC differentiation despite its mRNA level remaining roughly constant is the expression of a ubiquitin ligase that marks c-Myc protein for degradation in LT-HSCs. This is reduced in expression in CD34$^+$ compared to CD34$^-$ LSK cells, allowing c-Myc protein to accumulate and stimulate cell cycle entry by reducing expression of the cell cycle inhibitor p21, which c-Myc protein suppresses (Iriuchishima et al., 2011). The sensitivity of cells that have high c-Myc activity to c-Myc inactivation is demonstrated by the widespread effects transgenic *c-Myc* inactivation in HSCs has on the hematopoietic system. This results in severe anemia and leukopenia because of impaired erythropoiesis and myelolymphopoiesis (Wilson et al., 2004), (Laurenti et al., 2008), (Baena et al., 2007) due to apoptosis of these cells (Laurenti et al., 2008) save for platelets, which are increased (Y. Guo et al., 2009). LSKs on the other hand, accumulate significantly and are unable to produce the aforementioned cell types, while progenitor cell types are nearly absent from BM (Baena et al., 2007). LSK cells are not more actively synthesizing DNA in c-

Myc$^{-/-}$ mice, however the CD150$^+$ CD48$^-$ LSK cells are (Laurenti et al., 2008), (Baena et al., 2007), as are mature Lin$^+$ cell types (Wilson et al., 2004). Interestingly, G0 HSPCs are protected from the effects of c-Myc loss, as this population remains at normal levels in mutant mice. However, Myc-deficient HSCs in control recipient mice, which suffer no hypoplasia, actually had a lower proportion of S+G2M phase cells, as well as no downregulation of c-Kit in contrast to when residing in Myc-deficient hosts. This illustrates that the proliferation-boosting effect of Myc loss is not Myc-dependent, but hypoplasia-dependent. Furthermore, Myc-KO HSPCs do not lose their HSC-progenitor gene-set identity, indicating that Myc does not preferentially determine the course of differentiation (Laurenti et al., 2008). Myc-deficient HPSCs also have impaired granulocyte, erythrocyte and megakaryocyte colony-forming capacity (Y. Guo et al., 2009), (Baena et al., 2007), completely fail to reconstitute recipients with hematopoietic cells, despite being able to home to the osteoblasts of recipient mice as well as overexpressing the relevant adhesion molecules. When c-Myc is overexpressed on the other hand, this suppresses expression of those adhesion molecules, causing HSCs to be lost from the BM and a cease of PB replenishment within weeks, likely due to premature differentiation (Wilson et al., 2004).

The emerging view on Myc activity in HSCs therefore, is that it is expressed in response to cytokine stimulation, allowing the cell to detach from the niche and differentiate as it leaves quiescence, while not specifying a specific differentiation path. HSCs depend on Myc to initiate differentiation as they enter the cell cycle and without it they will fail to form progenitors or mature cell types, due to accumulating in the cell cycle.

1.1.6 The function of Miz-1 in hematopoiesis

The activity of Myc transcription factors is modulated by binding partners which are also TFs, such as the Pox virus and zinc finger (POZ) domain containing TF Myc-interacting zinc finger protein-1 (Miz-1). Miz-1, which is encoded by the gene *ZBTB17*, was identified in 1997 in a two-hybrid cloning approach in yeast by using the basic helix-loop-helix domain of Myc as bait. It was further characterised as being able to arrest proliferation in HeLa and NIH3T3 cells when it is overexpressed via a vector but that the ability of Myc to suppress this growth arrest depended on the integrity of the POZ domain of Miz-1 (Peukert et al., 1997). The POZ domain is known to be required for most DNA binding ability of Miz-1, and it achieves this by enabling Miz-1 to tetramerize (Wanzel et al., 2008). Because lack of a POZ domain was found to correlate with Miz-1 being localised to the cytosol, and because colony formation was strongly decreased by loss of the Miz-1 POZ domain, it appeared that Miz-1 suppresses growth transcriptionally in a way inhibited by Myc, which was important because the mechanism by which Myc represses transcription was unknown.

Miz-1 was subsequently found to be highly important in development, differentiation and tumorigenesis. A full reading frame knockout of the *ZBTB17* gene causes mouse embryos to fail due to high apoptosis of ectodermal cells and therefore its effect in adult mice could not be studied (Adhikary et al., 2003). The earliest characterization of Miz-1 transcriptional activity

was its ability to inhibit cell cycle progression by directly binding the promoter region of the cell cycle inhibitor *CDKN2B* and drive its expression, which can then be reversed if c-Myc is recruited to the same region by upstream signaling and this reversal depends on the interaction between c-Myc and Miz-1 (Seoane et al., 2001), (Staller et al., 2001) (Figure 1.2A). Cell lines expressing a variant of c-Myc unable to bind Miz-1 were found to be deficient in their ability to immortalize, due to the inability of c-Myc overexpression to suppress the cell cycle inhibiting function of Miz-1. In keratinocytes, Miz-1 was discovered to induce expression of CDKN2B in response to UV irradiation, arresting the cell cycle, which c-Myc could then overcome only by binding Miz-1 (Herold et al., 2002). The same mechanism of Myc recruitment to a Miz-1 transcriptional target gene in response to pro-differentiation upstream signaling was also discovered in myeloid leukaemia cells, but in this case to suppress *CDKN1A* expression (S. Wu et al., 2003). TFs other than Myc can recruit Miz-1 to suppress cell cycle inhibitors during lymphomagenesis such as the suppression of *CDKN2B* and *CDKN1A* by Miz-1 interaction partners Gli1 (Basu et al., 2009) and BCL6 (Phan et al., 2005), respectively. Although cell cycle inhibitor suppression-dependent lymphoma formation is also known to take place via the Myc-Miz-1 interaction (van Riggelen et al., 2010).

It therefore became clear that Miz-1 has a conserved role as a transcriptional cell cycle regulator, with subsequent observations that a POZ domain deletion (*Miz-1$^{\Delta POZ}$*) in numerous tissue types or cell lines delays tumor onset and incidence supporting this notion. The *Miz-1$^{\Delta POZ}$* genotype is associated with reduced skin papilloma formation in mice (Hönnemann et al., 2012), and in the case of medullablastoma, improved survival (Vo et al., 2016) or reduced incidence (Lu et al., 2013), involving altered expression of cell cycle regulating genes. Similarly, when Miz-1 accumulates in keratinocytes due to inhibition of Mule, which marks Miz-1 for degradation, this results in an increase in Myc/Miz-1 complex formation and increased Ki-67 expression and tumorigenesis, while a knockdown of Miz-1 reduces cell proliferation (Inoue et al., 2013). There have also been observed cases where truncation of Miz-1 improves the survival rate of lymphoma, although this was found to take place through the ability of Miz-1 to inhibit apoptosis through p53, which shall be discussed later (Ross et al., 2019). Some studies also overexpressed Miz-1 in cell lines, observing that this caused cell cycle arrest or reduction in proliferation in HeLa and NIH3T3 cells (Peukert et al., 1997) and fibroblasts (Staller et al., 2001), (Herkert et al., 2010). The important role Miz-1 has been found to play in differentiation has also shed light on the manner in which it regulates the cell cycle. In neural crest stem cells, knockout of c-Myc is associated with an upregulation of cell cycle inhibitors by Miz-1, resulting in improper development in the form of a diminished cell pool size. Furthermore a c-Myc mutant unable to interact with Miz-1 had more neural crest cells in the G1 phase of the cell cycle (Kerosuo & Bronner, 2016). Mice with the *Miz-1$^{\Delta POZ}$* mutation expressed in epidermal keratinocytes experience incomplete hair follicle maturation, however unlike in the tumorigenesis models discussed until now, was associated with increased rather than reduced proliferation in these cells (Gebhardt et al., 2007). Similarly, the *Miz-1$^{\Delta POZ}$* expressed in Schwann cells (cells involved in nerve repair), resulted in mice which suffer from

late onset neuropathy as well as enlarged nerve size and fewer Schwann cells that were quiescent. This failure of mature cells that lack a Miz-1 POZ domain to arrest was found to be due to increased levels of lysine demethylase 8 (KDM8), potentially highlighting Myc-independent cell cycle regulation by Miz-1 (Fuhrmann et al., 2018). Therefore, in cases where Miz-1 inhibits cell cycle entry, Miz-1 and the Myc/Miz-1 complex, appear to mutually inhibit the function of one another with regards to regulating the cell cycle. However, this model doesn't account for the varied roles Miz-1 has been found to play in the development of different tissues.

A role for Miz-1 in the regulation of apoptosis originally appeared when NIH3T3 and colonic cancer cells in which Miz-1 expression had been knocked down had elevated percentages of cells in the sub-G1 fraction of the cell cycle in response to stress (Wanzel et al., 2005). Subsequently, targeting the *Miz-1^ΔPOZ* transgene to hematopoietic or neural progenitor cell types has revealed an anti-apoptotic function for Miz-1 in numerous cell types of these tissues. For example, mice in which neural progenitor cells lack the POZ domain in the Miz-1 gene show heightened apoptosis compared to controls in the granular layer of the brain, as do neurospheres cultured from such progenitors (Wolf et al., 2013). The lack of a Miz-1 POZ domain expressed from neural progenitors also induces apoptosis in Myc-driven medullablastomas (Vo et al., 2016). Yet the importance of Miz-1 in its regulation of apoptosis has been most extensively studied in the hematopoietic system, due to its role in the survival of lymphopoietic cell types. In 2010, using mice in which a *Miz-1^ΔPOZ* mutation is expressed in cell types of all hematopoietic lineages but not others, generated by crossing mice in which the Cre recombinase is expressed from the *Vav* gene (expressed in HSCs) with mice possessing LoxP sites flanking the POZ domain encoding exons of Miz-1, Christian Kosan et al. found that B and T lymphocytes were tremendously lacking compared to control mice (Kosan et al., 2010). This was due to high apoptosis rates in mature B cells in Miz-1-deficient mice, which can be measured by flow cytometry of labelled Annexin V, which is expressed on the surface of apoptotic cells. It was found that CLPs from *Miz-1^ΔPOZ* mice were defective in IL-7-stimulated intracellular signaling, such that the pro-survival protein BCL2 could no longer be upregulated by IL-7 and the inhibitor of this pathway, SOCS1, was very highly overexpressed in *Miz-1^ΔPOZ* CLPs compared to controls (Figure 1.2B). *Miz-1^ΔPOZ* CLPs and B cells were found to be deficient in the phosphorylation of STAT5, which can be measured by intracellular flow cytometry of fixed cells, likely due to high SOCS1 mRNA levels, which inhibits STAT5 phosphorylation by IL-7 signaling. Furthermore, the promoter regions of *SOCS1* and *BCL2* were shown to be bound by Miz-1 protein using chromatin immunoprecipitation (ChIP), which isolates protein-bound chromatin fragments, followed by quantitative real-time PCR (qPCR). With this knowledge, the investigators found that artificially inducing BCL2 and early B cell factor 1, another factor affected by Miz-1 knockout, rescued B cell production from *Miz-1^ΔPOZ* CLPs in culture. In another study, the same line of *Miz-1^ΔPOZ* mice were shown to have hypocellularity in the thymus due to apoptosis in developing T cells (Saba, Kosan, Vassen, & Möröy, 2011), compared to controls, which ordinarily must pass through a V(D)J recombination stage by

avoiding p53-mediated apoptosis. Similarly to the case in B cell development, developing T cells in *Miz-1^{ΔPOZ}* mice had higher levels of BCL2 and SOCS1 mRNA as well as defective STAT5 phosphorylation in response to IL-7 stimulation compared to controls, and developing T cell count was restored by BCL2 overexpression. However, the full generation of mature T cells hadn't been restored (Saba, Kosan, Vassen, Klein-Hitpass, et al., 2011) and DNA microarray analysis of developing T cells revealed a pronounced response of p53 target genes such as *BAX* in *Miz-1^{ΔPOZ}* mice, so *Trp53* was additionally knocked out to find out if Miz-1 coordinates a blockade of apoptosis via p53. Ablation of p53 restored the cellularity and non-apoptotic cell proportions of the developing T cells of *Miz-1^{ΔPOZ}* mice (Rashkovan et al., 2014), as well as restoring CD19 expression among pro-B cells in the BM. This was then found to be due to the ability of a Miz-1-upregulated gene, *RPL22*, to prevent p53 mRNA entry into ribosomes. Miz-1 therefore, inhibits apoptosis in lymphocytes by ensuring BCL2 is expressed in response to adequate STAT5 signaling and by inhibiting p53 mRNA translation.

However, the regulation of STAT5 signaling by Miz-1 may differ in other hematopoietic cell types. Miz-1 was found to have an important function in inhibiting apoptosis in the fetal liver, since knockout resulted hugely increased apoptosis of fetal liver cells as well as large reduction in TER-119^{+} and CD71^{+} cells, indicating incomplete erythrocyte maturation. Miz-1-deficient fetal liver cells also had no BFU-E and CFU-E colony-forming capability, unlike control cells. The embryos of these mice died due to anemia (Kosan et al., 2014). When *Miz-1^{ΔPOZ}* mutation was expressed from the Vav-Cre locus (in HSCs), adult cellularity of erythroid cell types was largely unchanged, however it was apparent that developing erythroid cells were accumulating in the spleens of Miz-1 knockout mice. When erythropoietin-induced STAT5 phosphorylation was investigated in control and knockout splenocytes, Miz-1-deficient TER-119^{+} splenocytes responded with increased phosphorylation of STAT5 compared to controls, contrary to the effect of *Miz-1^{ΔPOZ}* mutation seen in lymphocytes. The reasons for this are speculative, as, unlike in lymphocytes, *Miz-1^{ΔPOZ}* splenocytes did not have higher levels of SOCS1 at rest, nor was Miz-1 protein found to bind the *SOCS1* gene promoter. Still yet other mechanisms by which Miz-1 regulates proper STAT5 signaling may exist, as, in the mammary gland of *Miz-1^{ΔPOZ}* animals, there are both proliferation and differentiation defects and this was found to be associated with decreased STAT5 phosphorylation in mammary gland epithelial cells during lactation (Sanz-Moreno et al., 2014). In this case, it was *SOCS2*, not *SOCS1* or *SOCS3*, that was disrupted in expression level, as was the prolactin receptor, through which prolactin may induce the phosphorylation of STAT5 in mammary gland epithelial cells. These effects were concluded to be due to altered intracellular vesicular transport in *Miz-1^{ΔPOZ}* cells on the basis of ChIP-sequencing results, suggesting that the coordination of vesicular transport by Miz-1 is another mechanism by which it executes its function.
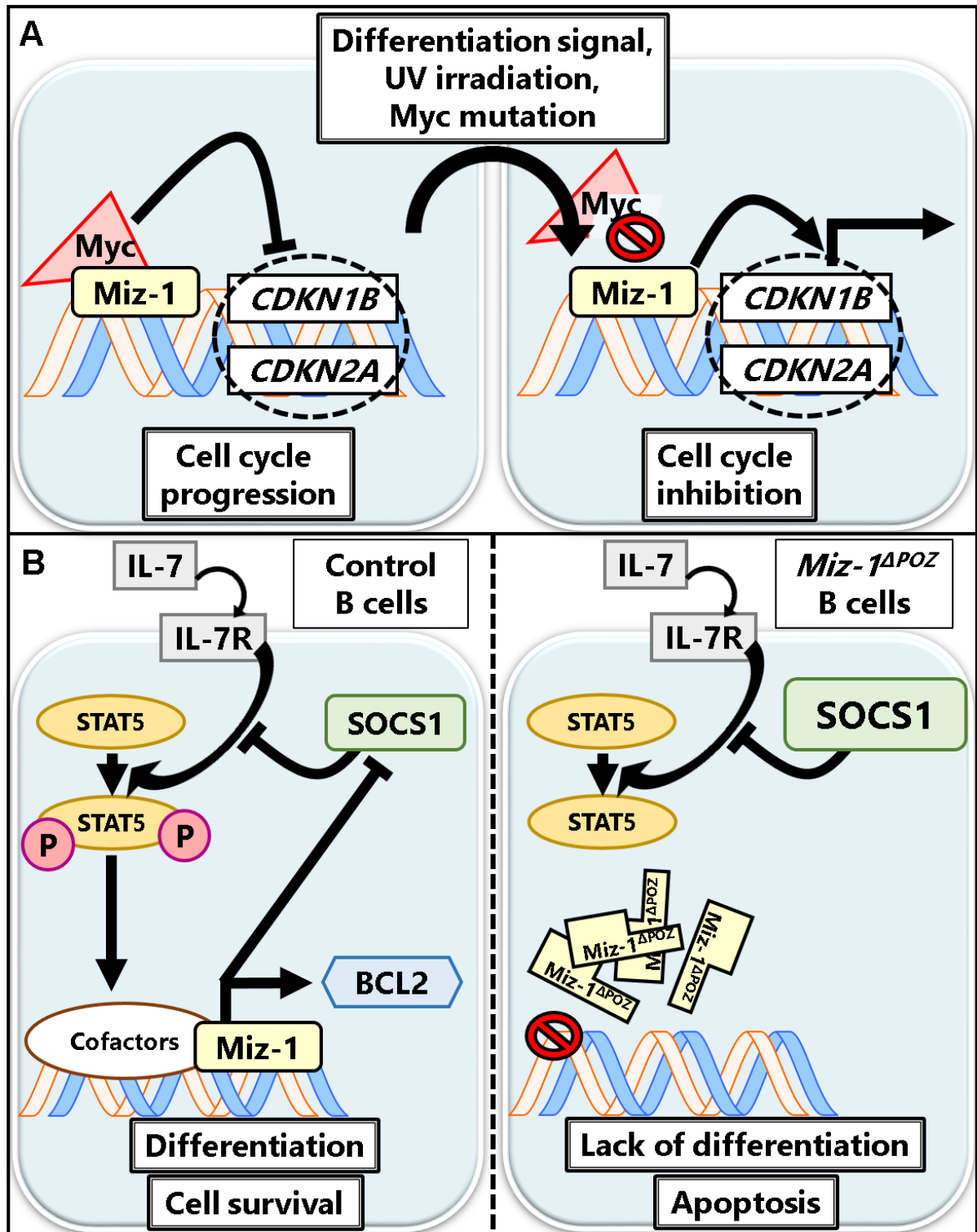
Figure 1.2.: Miz-1 is a regulator of the cell cycle and differentiation (**A**) Miz-1 binds DNA as part of a complex with Myc to suppress the expression of cell cycle inhibitors such as *CDKN1A* (myeloid leukaemia cells) and *CDKN2B* (fibroblasts), allowing the cell cycle to proceed when Myc levels are sufficient. A differentiation signal or UV irradiation can tip the balance of Myc/Miz-1 in favor of Miz-1, as can the inactivation of the Miz-1-binding of Myc, allowing Miz-1 to engage in its nascent role in the repression of cell cycle inhibitor expression. (**B**) Miz-1 promotes cell survival and inhibits apoptosis in B cell precursors to enable their differentiation. IL-7 is able to induce the expression of the survival factor

BCL2 in control B lymphocyte precursor cells, a stimulus normally relieved by SOCS1 (left). In *Miz-1*$^{\Delta POZ}$ B cell precursors, SOCS1 is no longer repressed by Miz-1 upon IL-7 stimulus, resulting in lack of STAT5 phosphorylation to activate downstream pro-survival gene expression (right). Miz-1 also cannot bind DNA to drive BCL2 expression, resulting in apoptosis and lack of differentiating cells.

Recently, a role for Miz-1 in regulating the type I interferon (IFN) pathway has been found in pancreatic cells (Muthalagu et al., 2020). Overexpression of Myc in Kras-driven pancreatic tumour cells results in suppression of the type I IFN response. In fibroblasts, this transcriptional suppression was found to depend on both Kras and Myc overexpression; contrariwise, in pancreatic adenocarcinoma cells, depletion of either Kras or Myc resulted in upregulation of IRFs, the interferon receptors, and interferon response genes. Furthermore, depletion of Miz-1 resulted in some of these type I IFN response genes being recovered in their expression and Miz-1 was shown by ChIP methods to directly bind the promoter of STAT1 and IRF7. Crucially, deletion of the Miz-1 POZ domain in Kras- and Myc-driven pancreatic tumor-bearing mice resulted in lifespan extension, due to a return in the ability of natural killer and B cells to infiltrate the tumors, facilitated by a return in protective type I IFN signaling. This illustrates yet another mechanism of the transcriptional-suppressive function of Miz-1 being recruited by Myc to facilitate tumor progression.

In summary, Miz-1 is a conserved regulator of the cell cycle, apoptosis and differentiation and this can take place through its varied effects on STAT5 phosphorylation-mediated signaling or through its participation in a complex with c-Myc. The effects of Miz-1 take place primarily through its transcriptional functions, which are highly cell type-dependent, illustrated by the findings from investigators of expression profiling of Miz-1 deficiency in cells of many different types. Loss of the Miz-1 POZ domain has been shown to induce a set of molecular phenotypes, namely defective vesicular trafficking in Purkinje (Wolf et al., 2013) and mammary gland cell types (Sanz-Moreno et al., 2014), pro-apoptotic gene expression in lymphocytes, induction of the cell cycle or mitotic processes in neural progenitor cells (Fuhrmann et al., 2018) and embryonic stem cells (Varlakhanova et al., 2011) and repression of differentiation in neural progenitor-derived tumours (Vo et al., 2016). The effect of Miz-1 POZ domain deletion in the hematopoietic stem cell compartment however, remains unknown.

1.2 The response of HSCs to infection

When the immune system is challenged with infection, HSCs are activated to support the mature immune cells which have mobilised to the infected tissue or have died as a result of infection. LSK cells transiently increase in total number in the PB in response to bacterial *E. coli* infection (Shahbazian et al., 2004). The bacterial cell wall component LPS induces LSK cells to increase in number *in vitro* (Singh et al., 2008), an effect dependent on their expression of Toll-like receptor (TLR) 4, for which LPS is an agonist. TLRs are a family of pattern recognition receptors (PRR), which are molecules that recognise pathogens for the innate immune system. LPS exposure increases the proliferation rate of LSK cells (Takizawa et al., 2011), an effect it

also has in true HSCs by increasing the proportion of them that express Ki-67 (Esplin et al., 2011).

Other TLRs recognise other kinds of pathogens. For example, TLR3 recognises intracellular double-stranded RNA (dsRNA) (Alexopoulou et al., 2001). PRRs affect their function by stimulating expression of a class of cytokines called IFN. PRRs achieve this by activating signaling cascades that result in the localisation of interferon response factors (IRF) to the nucleus, where they drive the expression of type I and II IFNs to be released by the cell and subsequently activate the innate immune response of other cells (Jefferies, 2019), (Carlin et al., 2017). Type I IFNs include IFN-α and IFN-β while type II IFN is referred to as IFN-γ. Both IFN types are expressed in response to viral and bacterial infection to induce true HSCs to proliferate, expanding their pool size, and undergo myeloid-biased differentiation, exhausting their LT-repopulation and CFU-forming capacity; but in contrast, under chronic exposure, depleting HSC pool size (Pietras et al., 2014), (Matatall et al., 2014), (Essers et al., 2009), (Baldridge et al., 2010), (Selleri et al., 1995), (Wilson et al., 2008). TLR4 signaling activated by LPS also has these effects (Esplin et al., 2011). The effect of agitating HSCs out of quiescence that IFN-α has may be due to its ability to increase c-Myc at the protein level in HSCs (Ehninger et al., 2014). But to add confusion to the picture, direct injection of type I IFNs can induce HSC apoptosis, selectively deplete them from the BM and inhibit their proliferation, illustrating that IFNs act pleiotropically based on dose, timespan and context (Smith et al., 2018). In summary, HSCs do not solely rely on signals from mature cell types to respond to infection, but respond directly through PRR-signaling.

In other hematopoietic cell types, it is known that type I IFNs are expressed at very low levels and their expression is induced by innate immune signaling pathways such as those that sense nucleic acids. 2′-5′-oligoadenylate synthases (OAS) are PRRs that detect and bind dsRNA, then activate latent ribonuclease (RNase L) to degrade viral RNAs into cleaved dsRNA, resulting in increased viral resistance (Banerjee et al., 2019). Cleaved dsRNA is then the substrate for retinoic acid-inducible gene I (RIG-I, encoded by the *DDX58* gene), (Malathi et al., 2007), another cytosolic PRR that binds cleaved cytosolic dsRNA and through a signaling cascade, activates IRF3 and IRF7 which then induce expression of type I IFNs (Wilden et al., 2009). There are also 2 OAS-like proteins (OASL1/2) in mice which have both pro- and anti-viral effects in this pathway (Choi et al., 2015). As well as serving to drive IFN expression, OAS and OAS-like proteins are induced by type I IFN (Pulit-Penaloza et al., 2012), (Eskildsen et al., 2003), thus forming a feed-forward pathway activation loop, allowing cells that have detected viral RNA to alert nearby cells to upregulate their nucleic acid degradation machinery. IFNs also stimulate the expression of other genes involved in the antiviral response, such as those expressing the 2 myxovirus resistance (MX1, MX2) proteins, which serve to trap viruses to intracellular membranes (Sadler & Williams, 2008). Another group of IFN-stimulated genes (ISG) are interferon-induced proteins with tetratricopeptide repeats (IFIT), which inhibit viral RNA translation (Diamond & Farzan, 2013). Type I IFN mediates its effects on gene expression

via intracellular signaling through IFN-α receptor (IFNAR), which induces the phosphorylation of STAT1, whereupon it forms a heterodimer with STAT2, localises to the nucleus and forms a complex with IRF9 and this complex drives the expression of interferon response genes (Au-Yeung et al., 2013). IFN-γ also stimulates phosphorylation of STAT1 in LSK cells (de Bruin et al., 2013). When dsRNA is injected into mice to stimulate IFN-α signaling, the IFN-response cluster proteins such as OAS2, OAS3, IFIT3, IFITM3 and even STAT1 and STAT2 themselves, become enriched in HSCs (Haas et al., 2015). This was measured by the investigators using proteomics. In summary, type I and II IFNs act on HSCs via STAT signaling to activate IFN-response genes, causing proliferation and harming long-term function. However, the functions of antiviral genes that respond to and can induce the IFN response, such as OAS, IFIT and MX are unexplored in HSCs.

DNA damage and anti-microbial response may indicate one another in hematopoietic cell types. In macrophages, IFN-γ and LPS signaling together are sufficient to cause the appearance of phosphorylation on the histone variant H2A.X (γH2A.X) a marker that forms foci on DNA indicating the presence of DNA double strand breaks (Morales et al., 2017). In almost opposite fashion, the type I interferon signaling pathway is known to be induced by DNA damage, also in macrophages (Härtlova et al., 2015). This is due to the cytosolic DNA sensor cyclic GMP-AMP synthase, a PRR that binds single-stranded DNA (ssDNA) fragments, and is structurally and functionally homologous to OAS1 (Hancks et al., 2015).

The cellular composition and pattern of cell surface marker expression of HSCs also changes in response to infection. Injection of dsRNA into mice induces a subset of HSCs to overexpress CD41 protein, the megakaryocyte marker, as well as VWF and platelet factor 4 (PF4). IFNAR is required for this effect to take place and therefore is assumed to rely on IFN-α signaling (Haas et al., 2015). Functional STAT1 also supports, although is not required for, this upregulation of CD41 in dsRNA-treated mice. The HSCs that strongly induce CD41 upon dsRNA-mediated (or LPS-mediated) inflammation were revealed to be a specific group of HSCs that are primed to be inflammation-responding during homeostasis and are referred to as stem-like megakaryocyte-committed progenitors; similar (or possibly identical) to MkRPs. Therefore, mice experiencing inflammation against viral infection have expanded CD41$^+$ HSC populations which overexpress megakaryocyte markers such as VWF.

1.3 The aging hematopoietic system

As they age, people suffer reduced capacity to generate high-affinity antibodies in response to vaccination, and become more likely to develop select cancers and autoimmune disorders (Larbi et al., 2008), (Grubeck-Loebenstein et al., 2009). In mice, aging influences cell types of the myeloid and lymphoid lineages differently. Aging in mice is accompanied by a reduction in the number of CLPs and their differentiating progeny: pre-pro-B, and pro-B lymphocytes. These cells also exhibit diminished responsiveness to IL-7 and proliferative potential (Miller & Allman, 2003). In contrast, CMP and GMP cells increase in absolute number (Min et al., 2006).

Myeloid cell types also increase in their representation in the PB with age, in contrast to lymphoid cell types (Dykstra et al., 2011). With regards to functionality, cells from aged donor mice tend to contribute more myeloid-type cells and fewer B lymphocytes to repopulated recipients, but have diminished ability to repopulate the BM of a recipient as a whole, than young donors (Rossi et al., 2005). That is, HSCs become myeloid-biased in repopulation capacity in old age (Rossi et al., 2005), (Sudo et al., 2000), (Porto et al., 2015), (Pang et al., 2011).

The changes that take place in HSCs during aging contribute to these effects. Phenotypic HSCs increase 10-fold in absolute numbers between the ages of 4 months to 2 years in mice (Dykstra et al., 2011), while less stringently labelled HSCs, such as CD34$^-$ Flt3$^-$ LSK cells accumulate between 3- (Porto et al., 2015) to 6-fold (Morrison et al., 1996), (Rossi et al., 2005) by 2 years of age. Furthermore, as mice age from 4 months to 1 year to 2 years of age, myeloid-biased CD150$^+$ subsets accumulate as a percentage of LSK cells (Beerman et al., 2010). Functionally, HSCs capable of multilineage reconstitution among transplanted CD34$^-$ LSK cells rise 2-fold in mice between 2 and 18 months of age, but the number of defective HSCs incapable of lymphoid reconstitution also rises by nearly 6-fold (Sudo et al., 2000). T lymphocyte-repopulating HSCs are also lost over the course of aging (Yamamoto et al., 2018). Interestingly, CD41-expressing HSPC types appear to account for much of those that accumulate with aging, as by 16 months of age, over 50% of CD34$^-$ Flt3$^-$ LSKs and CD150$^+$ CD48$^-$ LSKs are CD41-expressing, in stark contrast with young mice (Gekas & Graf, 2013). Aging and LPS exposure share the common effect of increasing CD41 expression on CD150$^+$ LSKs (Esplin et al., 2011). As CD41 expression on HSCs is an indicator of megakaryocyte lineage-priming (Rodriguez-Fraticelli et al., 2018) and because CD41$^+$ CD150$^+$ LSK cells accumulate 20-fold with aging (Yamamoto et al., 2018), it appears that most LT-HSCs enter a myeloid-biased state with age and much of this process may depend on acute inflammatory stress during the life course (Mann et al., 2018).

It is controversial whether HSCs gain or lose quiescence during aging. Old HSCs were more often in S+G2M cell stage (Morrison et al., 1996). However, other studies show quiescent LSKs (Chambers et al., 2007) in 2-year old mice were not synthesizing DNA to a greater extent than those from young mice. Others still indicate HSPCs such as CD34$^-$ LSK from old mice are less actively synthesizing DNA compared with those from young mice (Noda et al., 2009).

Transcriptomic changes in HSCs with aging reflect their defects in self-renewal and differentiation. Early studies using DNA microarray showed that myeloid-specification genes were increased in expression while lymphoid specification genes were downregulated in LSK cells with aging. More recently however, RNA-seq on quiescent CD150$^+$ LSK cells from 4-month old and 2-year old mice revealed that groups of genes involved in cell adhesion were overexpressed while those involved in DNA repair and the cell cycle were underexpressed in the older group of mice compared to young (Sun et al., 2014). Similarly in quiescent LSK cells, gene expression profiles for inflammatory responses were overexpressed, while those of DNA repair and the cell cycle were underexpressed with aging (Chambers et al., 2007). Single-cell

studies have provided even greater resolution into the gene expression differences between phenotypic groupings of HSCs by removing population-level heterogeneity: an scRNA-seq approach by Kowalczyk et al. showed that for HSCs/MPP1, MPP2 and MPP3, the main source of gene expression differences from 2 months to 2 years of age is differences in the expression of cell cycle genes (Kowalczyk et al., 2015), with differences in expression in ribosomal genes and TFs such as *STAT1* accounting for some of the rest. A bioinformatics analysis of scRNA-seq data found that a proliferation-associated cluster of genes differentially expressed over the course of aging decreased in expression level significantly, while an interferon-associated cluster were increased (Zeng et al., 2021). A recent high-resolution proteomics study also verified the enrichment of the c-Kit, CD41, VWF proteins as well as of proteins participating in the cell cycle and DNA repair processes in the HSCs of mice post-2 years of age in comparison with young mice (Zaro et al., 2020). Another scRNA-seq-based study found that certain HSPC clusters experience a delay to commitment to differentiation with age, due to alteration in the expression of TFs involved in priming, serving to explain both the expansion of HSCs as a whole and the reduction of cell number and functionality of specific progenitors as aging advances (Hérault et al., 2021).

One of the root causes of these myriad age-related changes in HSC function is believed to be their accumulation of DNA damage, influencing cellular signaling and gene expression. 1 year old and 2 year old mice HSCs show several-fold increases in the amount of DNA fragmentation (Porto et al., 2015). The foci of phosphorylated γH2A.X histone protein, which becomes phosphorylated as a consequence of signaling from the detection of DNA double-strand breaks, accumulates in number per cell between 10 and 122 weeks of age in CD34$^-$ and CD34$^+$ Flt3$^-$ LSK cells (Rossi et al., 2007).

In summary, the immune system becomes myeloid-biased and lymphoid-defective in terms of both cellularity and function with aging, due to altered transcriptional processes in HSCs, the root cause of which include intrinsic factors such as DNA damage and extrinsic factors such as inflammation, resulting in immune-related morbidity.

2. Aims of this thesis

The role of Miz-1 in hematopoietic stem cells remains to be understood and there is evidence that it regulates the cell cycle, apoptosis, differentiation and the DNA damage response in other hematopoietic cell types. It has already been shown that *Miz-1$^{\Delta POZ}$* LSKs have greater self-renewal in transplanted recipients than control LSKs and potentially a higher rate of cell cycling (Kosan et al., 2010). These facts indicate an important role of Miz-1 in the homeostasis in HSCs.

We therefore aimed to characterise the impact of loss of Miz-1 transcription factor function on hematopoietic stem and progenitor cell types and investigate the mechanisms underlying any effects. Our objectives to achieve this were to collect data from *Vav-Cre$^-$; Miz-1$^{fl/fl}$* (control) and *Vav-Cre$^+$; Miz-1$^{fl/fl}$* (*Miz-1$^{\Delta POZ}$*) mouse bone marrow cells, beginning with measuring the size of hematopoietic stem and progenitor cell compartments by flow cytometry according to established cell staining schemes. We first sought to assess the apoptosis levels and the cell cycle profiles of *Miz-1$^{\Delta POZ}$* HSCs and MPPs, by Annexin V and Ki-67 staining, to find indications of known mechanisms of Miz-1 action are taking place. A reliable functional assay, the colony-forming unit assay for the potential HSPCs have to differentiate into myeloid progenitors, was also employed to reveal any perturbation in HSPC function. A key goal was to analyse the transcriptomic profile of *Miz-1$^{\Delta POZ}$* HSCs and MPPs using RNA-sequencing for signs of any p53-dependent mechanism, as observed in *Miz-1$^{\Delta POZ}$* lymphocytes, or indicative of mechanisms active in *Miz-1$^{\Delta POZ}$* other cell types. Because Miz-1 functions primarily as a transcription factor, we sought to perform ChIP-qPCR to determine the directly-bound gene loci by Miz-1 among important differentially expressed genes identified by our RNA-sequencing experiment. We aim to specifically investigate the role DNA damage may play in *Miz-1$^{\Delta POZ}$* HSCs, as this is known to be both regulated by Miz-1 in other cell types and to be of critical importance to the function of HSCs.

By pursuing this strategy we hoped to find the effects of Miz-1 POZ domain loss in HSCs and detail the mechanism of these effects, and provide an account for the homeostatic function of Miz-1 in HSCs.
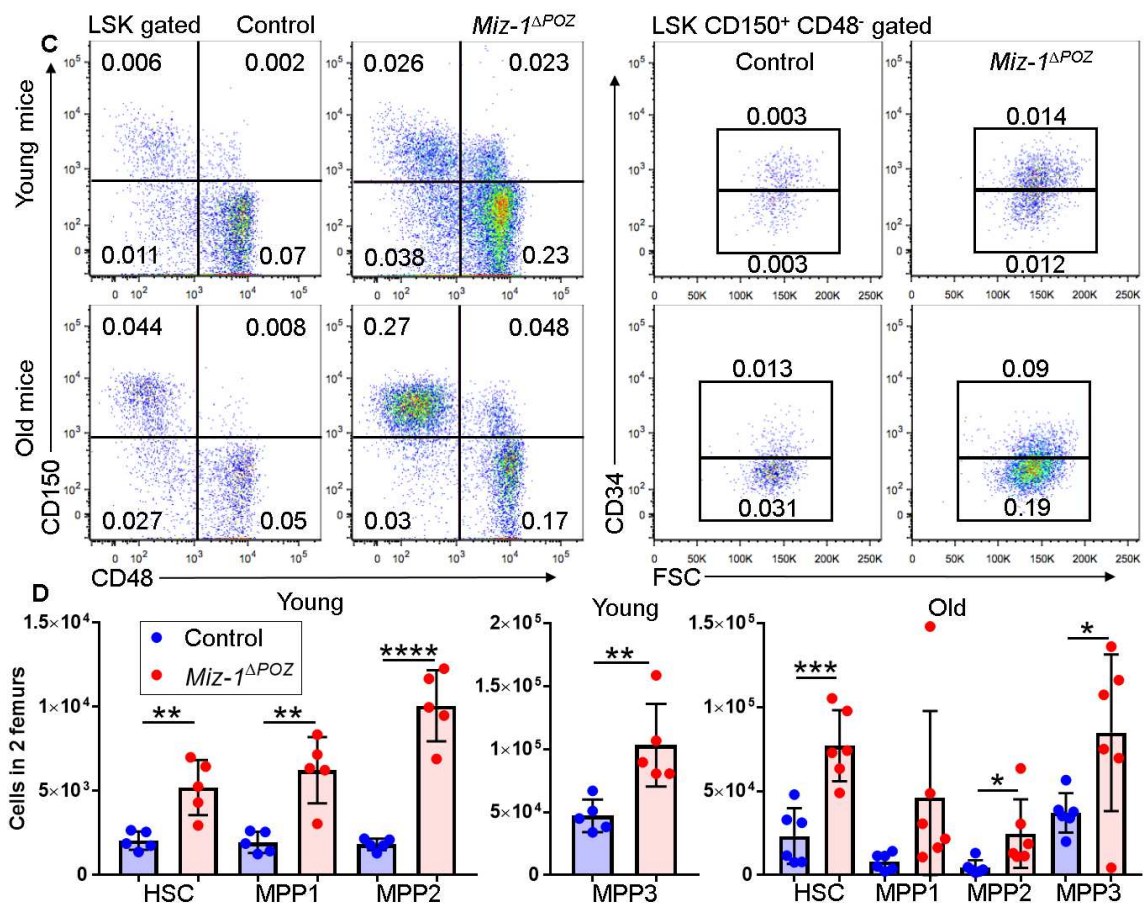
3. Results

3.1 *Miz-1* POZ domain deletion results in age-associated phenotypes in HSCs

We began by examining the effect of homozygous *Miz-1* POZ domain deletion on the composition of hematopoietic stem and progenitor cells, by analysing and comparing the bone marrow (BM) of young (10–12 week old) *Vav-Cre⁻; Miz-1^{fl/fl}* (control) and *Vav-Cre⁺; Miz-1^{ΔPOZ}* mice using flow cytometry. *Miz-1^{ΔPOZ}* mice exhibited a statistically significant, 2.3-fold increase in the number of Lineage⁻ Sca-1⁺ c-Kit⁺ (LSK) cells compared to control (Figure 3.1B) in young mice. Lineage⁻ Sca-1⁺ c-Kit⁻ (LS⁺K⁻) cells, which are lymphoid-committed cells lacking long-term repopulation capacity (Kumar et al., 2008), were also significantly increased by 5.3-fold in *Miz-1^{ΔPOZ}* mice. Using SLAM markers (CD150, CD48 and CD34) we subdivided LSKs into HSCs (CD34⁻ CD48⁻ CD150⁺ LSK), which showed a 2.5-fold increase, MPP1 (CD34⁺ CD48⁻ CD150⁺ LSK) which show a 3.2-fold increase, MPP2 (CD48⁺ CD150⁺ LSK) a 5.5-fold increase and MPP3 (CD48⁺ CD150⁻ LSK) cells, which exhibited a 2.2-fold increase (Figure 3.1D). Therefore, *Miz-1* deficiency resulted in a cellularity increase in all of the subpopulations of LSKs (including CD48⁻ CD150⁻ LSKs, data not shown) as well as their frequency in the bone marrow.
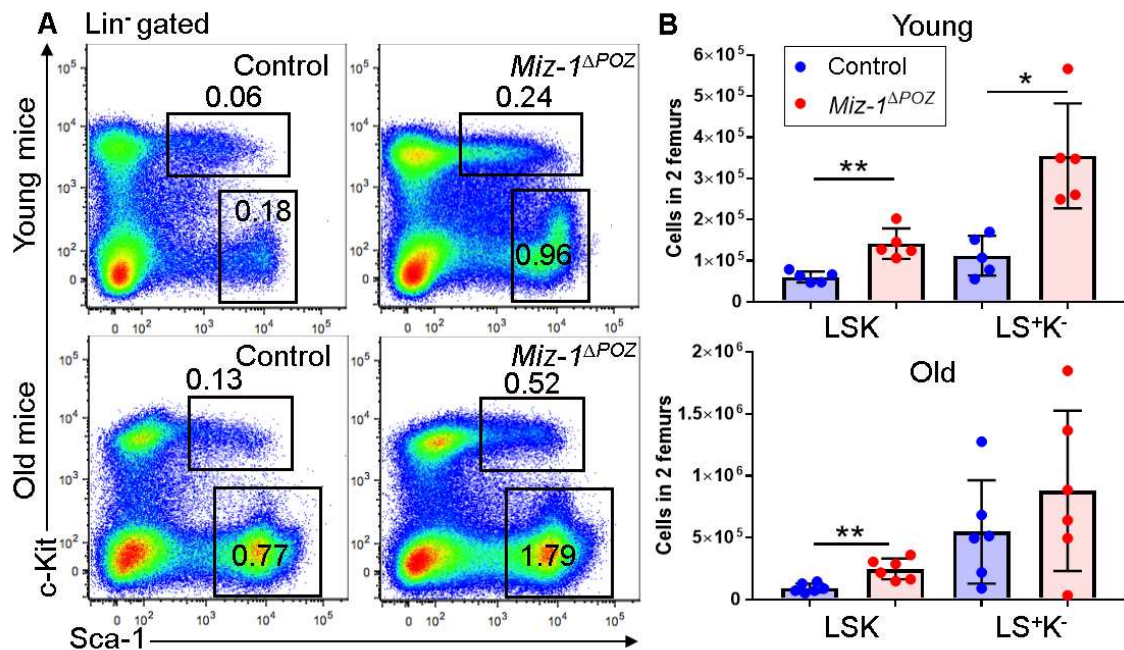
Figure 3.1.: *Miz-1* POZ domain deletion results in age-associated phenotypes in HSCs (**A**) Representative FACS plots of young (upper) and old (lower) control and *Miz-1* knockout (KO) bone marrow with LSK and LS⁺K⁻ cells resolved. The proportion of gated cells as a percentage of living FSC⁺ SSC⁺ cells are shown beside gates. (**B**) Bar graphs with overlaid dot plot of the total number of gated cells found in 2 femurs per young (upper graph) and aged (lower graph) mice, *n* = 5 (young), *n* = 6 (old); mean ± SD; *: $p < 0.05$, **: $p < 0.01$; *t* test.

As this accumulation of HSPCs resembles that seen in aging, we decided to analyse these cell compartments in 1 year to 18 month old mice. Among aged mice, the number of HSCs were higher in *Miz-1^ΔPOZ* mice than control by 3.3-fold, MPP1 by 4.9-fold, MPP2 by 5.3-fold, MPP3 by 2.3-fold (Figure 3.1D) and LSKs by 2.3-fold (Figure 3.1B). Hence, loss of *Miz-1* transcription factor function in HSPCs has an expansionary effect in both young and aged mice. We also analysed the changes that take place with age in both genotypes of mice. Aged control mice had 11-fold more HSCs than young control mice (Figure S1A) and aged *Miz-1^ΔPOZ* mice nearly 15-fold more than young *Miz-1^ΔPOZ* mice (Figure S1C). In addition, the number of MPP1 cells was nearly 5-fold higher in aged control than in young control mice (Figure S1B). Furthermore, in agreement with previous studies (Rossi et al., 2005), (Porto et al., 2015), absolute cell numbers of MPP2 and MPP3 cells were not significantly altered over the course of aging in either control or *Miz-1^ΔPOZ* mice. We observed that the number of LS$^+$K$^-$ cells were 4.9-fold higher in aged control compared to young control mice (Figure S1G). A statistically significant difference in the number of LS$^+$K$^-$ cells was not seen in young versus aged *Miz-1^ΔPOZ* mice.

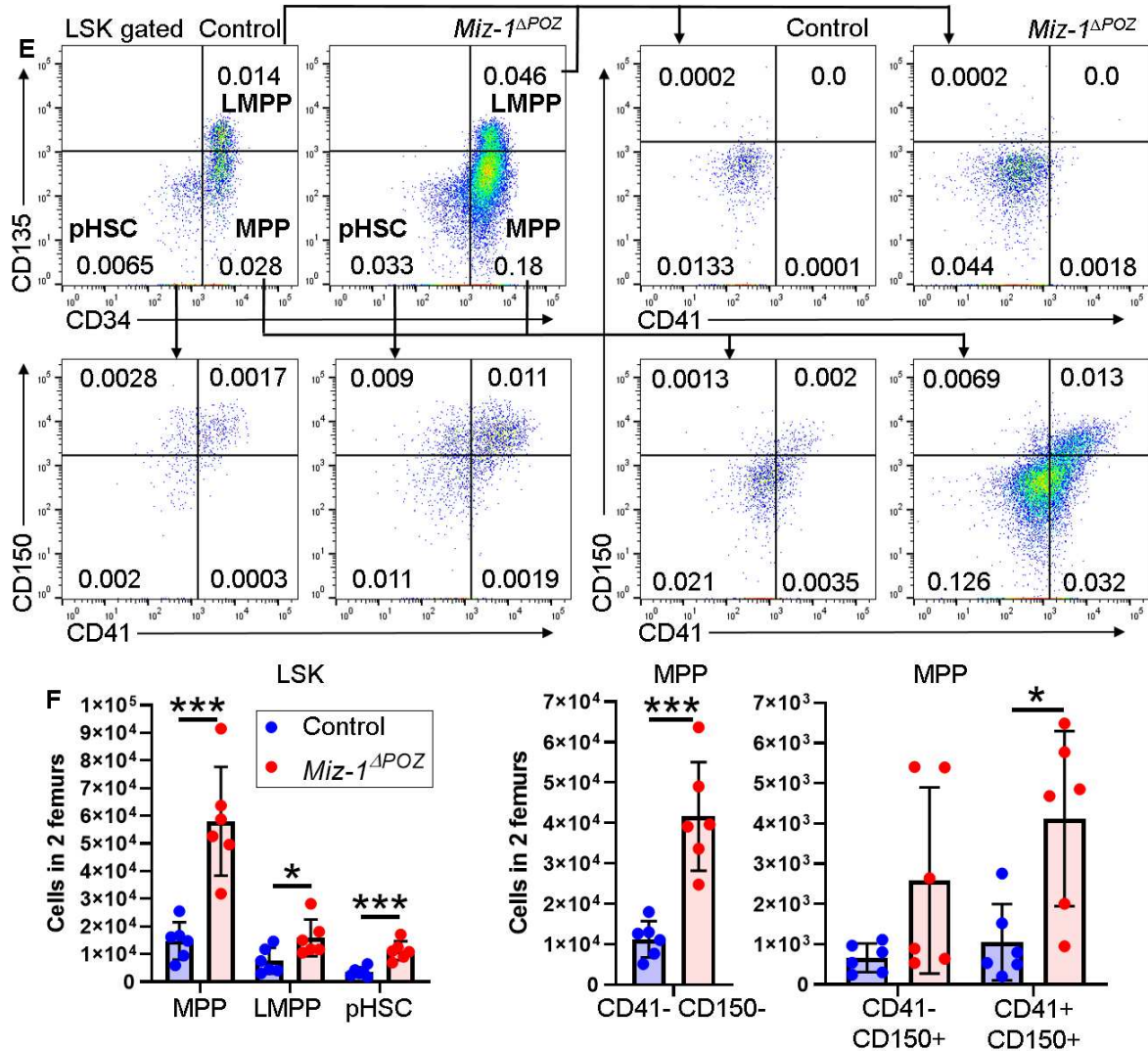**Figure 3.1.: *Miz-1* POZ domain deletion results in age-associated phenotypes in HSCs** (**C**) Representative FACS plots of LSK gated (left) and LSK CD150$^+$ CD48$^-$ gated (right) young (upper) and old (lower) control and *Miz-1* KO bone marrow with MPP2 (LSK gated, upper right quadrant), MPP3 (LSK gated, bottom right quadrant), MPP1 (LSK CD150$^+$ CD48$^-$ gated, top gate) and HSCs (LSK CD150$^+$ CD48$^-$

gated, bottom gate) resolved. (**D**) Bar graphs with overlaid dot plot of the total number of gated HSCs, MPP1 and MPP2 (bottom left), MPP3 cells (bottom middle) found in 2 femurs of young mice, n = 5 mice per genotype; mean ± SD; *: $p < 0.05$, **: $p < 0.01$, ****: $p < 0.0001$; t test. Data for HSCs, MPP1, MPP2 and MPP3 cells from aged mice are shown in the bottom right, n = 6 mice per genotype; mean ± SD; ***: $p < 0.001$; t test.

We were intrigued to find out if the HSCs of young (8–18 week old) *Miz-1$^{\Delta POZ}$* mice exhibit the age-associated phenotype of higher CD41 high-expressing compartment size and expression level. To do this, we used an alternative HSC-staining and gating strategy (Yamamoto et al., 2013) including the lymphoid marker Flt3, whereby LSKs are gated into 3 populations by CD34 and Flt3 (CD135). These are CD135$^-$ CD34$^-$ LSKs, or phenotypic HSCs (pHSC), CD135$^-$ CD34$^+$ LSKs (MPP) and CD135$^+$ CD34$^+$ LSKs, or lymphoid-primed multipotent progenitors (LMPP) (Figure 3.1E). All 3 populations of LSKs were significantly increased in absolute number by *Miz-1$^{\Delta POZ}$* mutation: pHSCs by 3.2-fold, MPPs by 3.9-fold and LMPPs by 2.1-fold (Figure 3.1F). Among CD150$^+$ pHSCs, those that were CD41$^-$ were increased by 2.4-fold in number in *Miz-1$^{\Delta POZ}$* mice compared to a 4-fold increase in those that are CD41$^+$ (Figure 3.1G). pHSCs that were negative for both markers were expanded by 3.2-fold. Therefore, those HSCs that express CD41 were disproportionately responsible for the expansion of HSCs in *Miz-1$^{\Delta POZ}$* mice. However, MPP subsets divided by CD41 and CD150 expression were all equally expanded in knockout mice, while LMPPs do not express CD150 or CD41 (Figure 3.1H). Furthermore, upon measuring the mean fluorescence intensity (MFI) of CD41 expression on the cell surfaces of LMPPs, MPPs and pHSCs by FACS, we found that in *Miz-1$^{\Delta POZ}$* MPPs and pHSCs, CD41 expression levels per cell were significantly increased (Figure 3.1I). Therefore, *Miz-1$^{\Delta POZ}$* mice also demonstrate greater CD41 cell surface expression in MPPs and HSCs as well as a greater number of those cell types expressing CD41, as is found during aging.

Young knockout mice had 28% fewer bone marrow cells in 2 femurs than control (Figure 3.1J) which was almost identical to the 27% decrease seen in comparing old (17-22 months) control mice to young control mice. However, there was no longer any statistically significant difference in bone marrow cellularity between *Miz-1$^{\Delta POZ}$* mice and controls once they reached old age. The deletion of the *Miz-1* POZ domain did not affect the level of apoptosis of LSKs in young mice as measured by Annexin V staining (Figures 3.1K, 3.1L). In summary, young *Miz-1$^{\Delta POZ}$* mice exhibited bone marrow cytopenia relative to control.

Figure 3.1.: *Miz-1* POZ domain deletion results in age-associated phenotypes in HSCs (**E**) Representative FACS plots of young control and *Miz-1* KO bone marrow with LMPP, MPP and phenotypic HSC cells resolved. Arrows from a gate to a plot indicate gating. The proportion of gated cells as a percentage of living FSC$^+$ SSC$^+$ cells are shown within gates. (**F**) Bar graphs with overlaid dot plot of the total number of gated MPPs, LMPPs and pHSCs (left), CD41$^-$ CD150$^-$ MPPs (middle) and CD150$^+$ MPPs (right) found in 2 femurs of young mice, *n* = 6 mice per genotype; mean ± SD; *: $p < 0.05$, ***: $p < 0.001$; *t* test.

These results show that deletion of the POZ domain of Miz-1 perturbs ordinary hematopoiesis throughout differentiation, resulting in an accumulation of LSKs and their subpopulations independently of LSK apoptosis. In particular, HSCs expressing CD41 are disproportionately accountable for this accumulation of stem and progenitor cells and this accumulation is present despite a reduction in total bone marrow cellularity, both phenomena of which are seen during the aging of control mice.
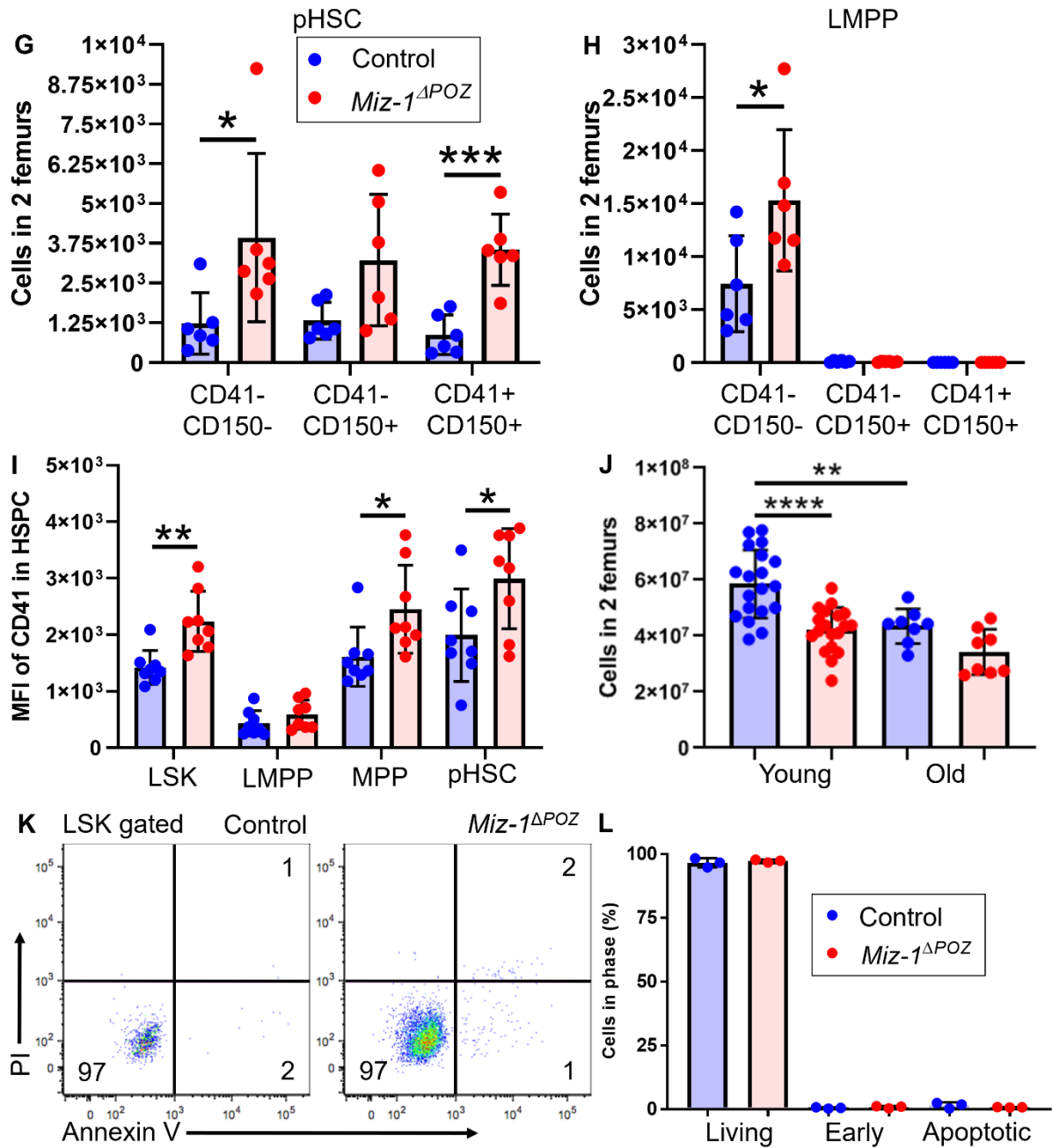
Figure 3.1.: *Miz-1* **POZ domain deletion results in age-associated phenotypes in HSCs** (**G**) Bar graph with overlaid dot plot of the total number of gated pHSCs by CD150 and CD41 subsets found in 2 femurs of young mice, n = 6 mice per genotype; mean ± SD; *: $p < 0.05$, ***: $p < 0.001$; t test. (**H**) Bar graph with overlaid dot plot of the total number of gated LMPPs by CD150 and CD41 subsets found in 2 femurs of young mice, n = 6 mice per genotype; mean ± SD; *: $p < 0.05$, ***: $p < 0.001$; t test. (**I**) Bar graphs with overlaid dot plot of the mean fluorescence intensity of CD41 of the gates of LSK, LMPP, MPP and pHSC populations in young mice, n = 8 mice per genotype; mean ± SD; *: $p < 0.05$, **: $p < 0.01$; t test. (**J**) Bar graph with overlaid dot plot of the total number of bone marrow cells counted in 2 femurs of young and old, control and *Miz-1* POZ domain deficient mice. n = 19 (young), n = 8 (old); mean ± SD; ***: $p < 0.001$, ****: $p < 0.0001$. (**K**) Levels of apoptosis in LSKs were assessed using propidium iodide (PI) and Annexin-V staining. Representative FACS plots of LSK gated control and *Miz-1* KO LSKs. The proportion of gated cells as a percentage of LSK cells are shown within gates. (**L**) Bar

graphs with dot plot overlay of the percentage of non-apoptotic (Annexin-V$^-$ PI$^-$), early apoptotic (Annexin-V$^+$ PI$^-$) and apoptotic (Annexin-V$^+$ PI$^+$) LSKs. n = 3 mice per genotype; mean ± SD.

3.2 Miz-1 maintains quiescence in HSCs

Quiescence is a functionally important property of HSCs. Since we detected an increase in stem and progenitor cells, we analysed cell cycle progression. To understand the mechanism underlying the phenotypic accumulation of LSKs and their cellular sub-compartments in *Miz-1^{ΔPOZ}* mice, we analysed their cell cycle status with anti-Ki-67 and DAPI staining by flow cytometry. We found that a significantly greater proportion of HSCs (Figures 3.2A, 3.2B), but not MPP1 or MPP2 cells (Figures 3.2C, S2A-C), have lost quiescence and entered the cell cycle in *Miz-1^{ΔPOZ}* mice. In particular, the percentages of control HSCs in the G0, G1 and S stages were 75%, 25% and 0%, respectively, whereas in *Miz-1* KO HSCs they were 55%, 43% and 2%, respectively. In addition, the proportion of MPP3 cells in the S phase rose from 15% in control to 19% in *Miz-1* KO mice. Further, we analysed the cell cycle status of 18-month old mice, but found that these differences between control and *Miz-1* KO HSCs and MPP3 cells were no longer present (Figure 3.2D). In addition, we found that the only statistically significant difference in cell cycle status between young and aged mice in either genotype was that in the S phase of MPP3, which rose from 15% in young control to 21% in aged control mice (Figure S2D) and from 19% in young *Miz-1* KO to 23% in aged *Miz-1* KO mice (Figure S2E).

These results suggest that the relative accumulation of HSCs in *Miz-1^{ΔPOZ}* mice is at least partly attributable to a loss of HSC quiescence and entry into the cell cycle.
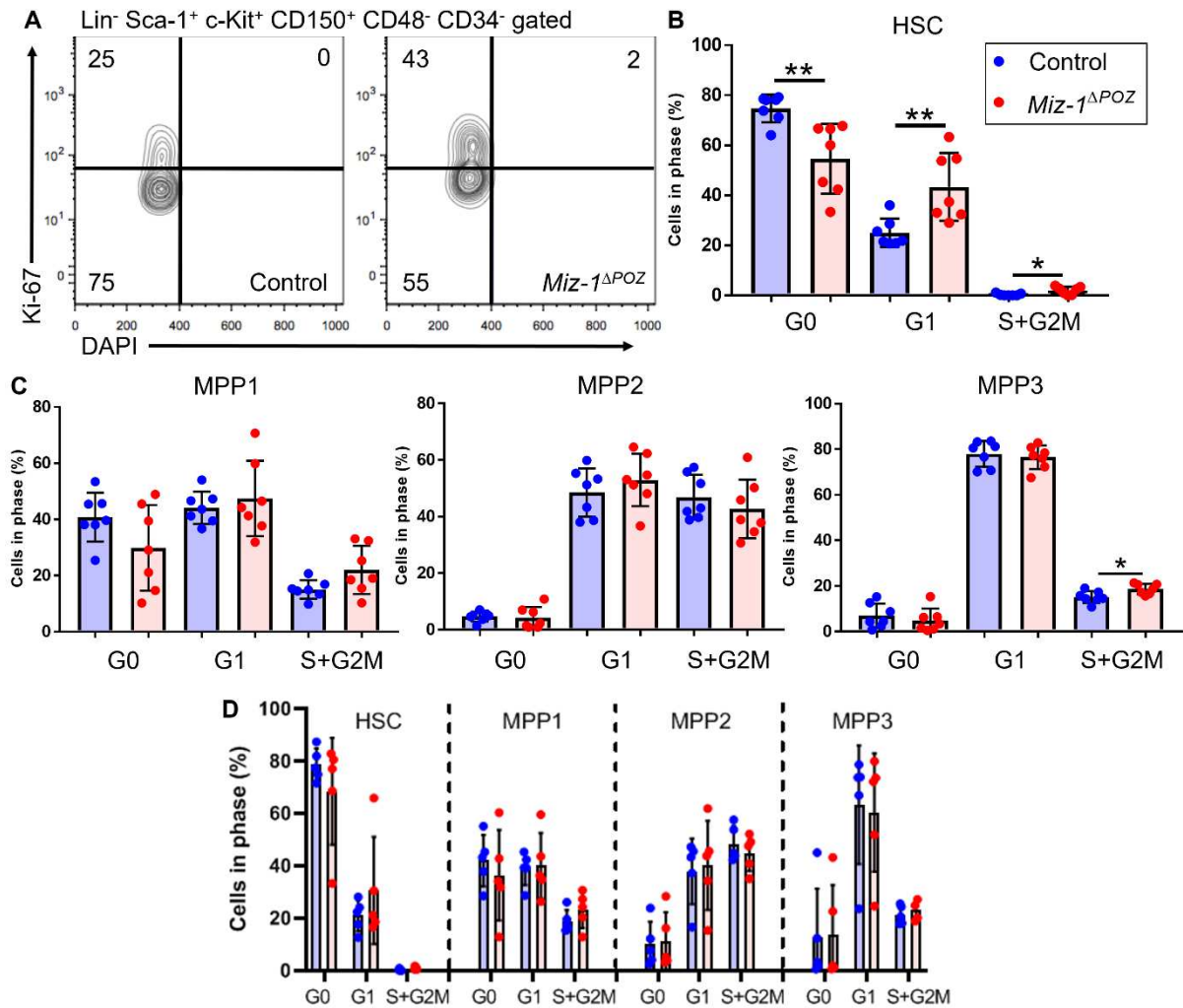
Figure 3.2.: Miz-1 maintains quiescence in HSCs (**A**) Lineage-depleted cells from the bone marrow of young mice were analysed by intracellular anti-Ki-67 and DAPI staining and flow cytometry for cell cycle status. Representative FACS plots (left) show the percentages of HSCs in the G0 (Ki-67$^-$, DAPI$^-$, lower left quadrant), G1 (Ki-67$^+$, DAPI$^-$, upper left quadrant) and S+G2M (Ki-67$^+$, DAPI$^+$, upper right quadrant) cell cycle phases. (**B**) Bar graph overlaid with dot plot showing the percentages of control and Miz-1$^{\Delta POZ}$ HSCs in each cell cycle phase. n = 7, mean ± SD. (**C**) Bar graphs with dot plot overlays displaying the mean percentage of MPP1 (left), MPP2 (middle) and MPP3 cells (right) from young mice by cell cycle phase. n = 7, mean ± SD. (**D**) Bar graphs displaying the mean percentage of HSCs, MPP1, MPP2 and MPP3 cells from aged mice by cell cycle phase. n = 5, mean ± SD.

3.3 *Miz-1* POZ domain deletion results in expansion of myeloid and lymphoid progenitor cells

Aging is not only associated with an increase in the absolute numbers of HSCs and MPP cells, but also with an increase in the number of progenitor cells of the myeloid lineage, which differentiate into macrophages, erythrocytes and megakaryocytes. CLPs, on the other hand, are known to diminish in number over the course of mouse aging (Rossi et al., 2005). To find

whether deletion of the *Miz-1* POZ domain results in a similar alteration in the number of hematopoietic progenitor cell types, we analysed the number of CMPs (resolved by lineage⁻, IL-7R⁻, Sca-1⁻, c-Kit⁺, CD16/32⁻, CD34⁺ gating), MEPs (lineage⁻, IL-7R⁻, Sca-1⁻, c-Kit⁺, CD16/32⁻, CD34⁻), GMPs (lineage⁻, IL-7R⁻, Sca-1⁻, c-Kit⁺, CD16/32⁺, CD34⁺) and CLPs (lineage⁻, IL-7R⁺, Sca-1^{mid}, c-Kit^{mid}) in control and *Miz-1$^{\Delta POZ}$* mice by flow cytometry. In young (2-3 month-old) mice, loss of the *Miz-1* POZ domain was associated with a statistically significant 1.8-fold increase in the number of MEPs and CMPs, as well as a 2.1-fold increase in GMPs (Figure 3.3A, 3.3B) and a 3-fold increase in CLPs (Figure 3.3D, 3.3E). Cell cycle analysis by way of anti-Ki-67 and DAPI staining revealed no cell cycle status changes between young control and *Miz-1$^{\Delta POZ}$* mice in myeloid progenitor cell types (Figure 3.3C).

While Miz-1 deficient mice compared to controls showed an increase in myeloid progenitors in young mice, the difference between knockout and controls in aged mice was not significant due to sample variations (Figure 3.3B). As expected in aged control mice the number of GMPs and MEPs increased with age (Figure S3A), whereas the number of CLPs decreased (Figure 3.3E). However, the increase in CMPs was not statistically significant. *Miz-1$^{\Delta POZ}$* mice showed no accumulation of myeloid progenitors with age (Figure S3B).
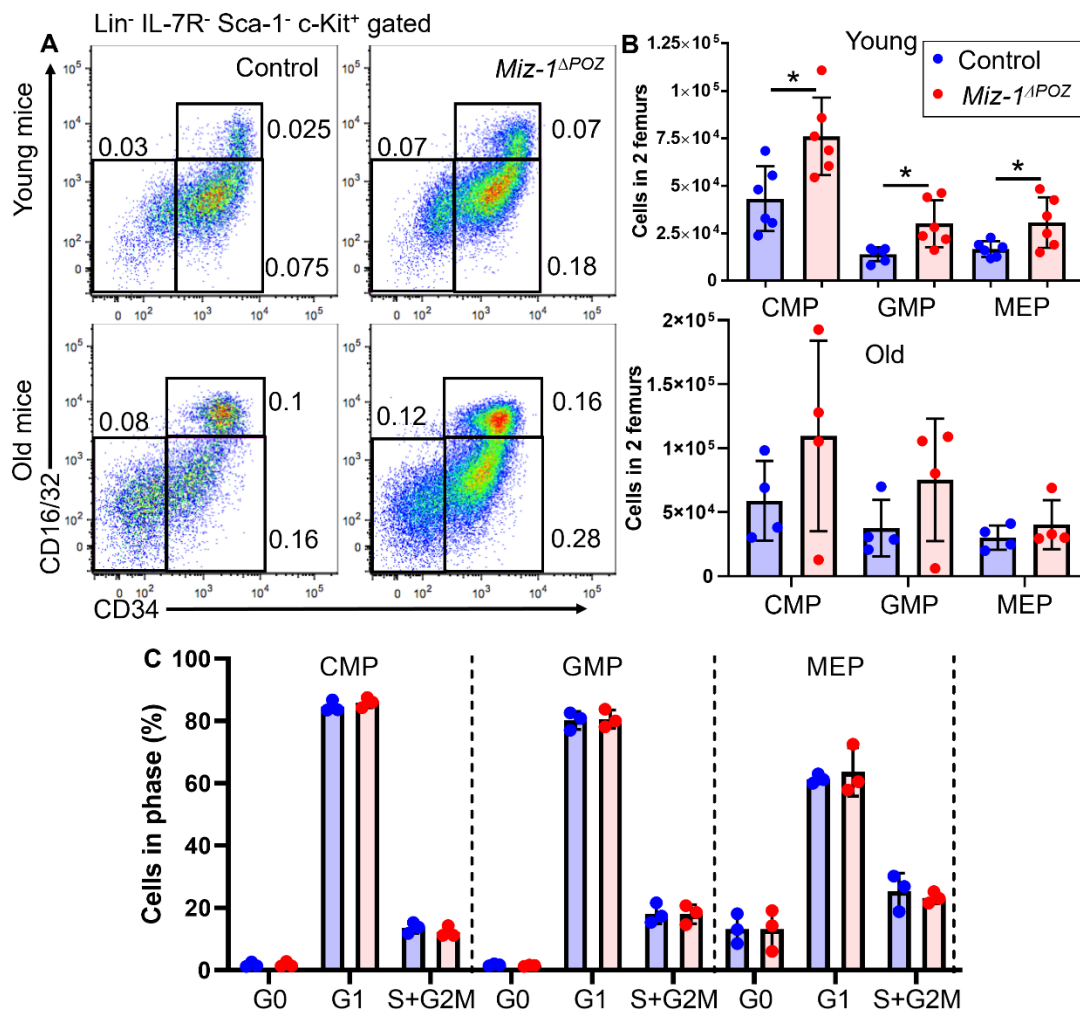
Figure 3.3.: ***Miz-1*** **POZ domain deletion results in expansion of myeloid and lymphoid progenitor cells** (**A**) Representative FACS plots of young (upper) and old (lower) control and *Miz-1* KO bone marrow with CMPs, GMPs and MEPs cells resolved. The proportion of gated cells as a percentage of living FSC⁺ SSC⁺ cells are shown beside gates. (**B**) Bar graphs overlaid with dot plot of the total number of gated cells found in 2 femurs per young (upper graph) and old (lower graph) mouse, $n = 4$, mean ± SD; *: $p < 0.05$; t test. (**C**) Bar graphs with dot plot overlay displaying the mean percentage of sorted CMPs, GMPs and MEPs, isolated from young mice, by cell cycle phase, $n = 3$, mean ± SD.

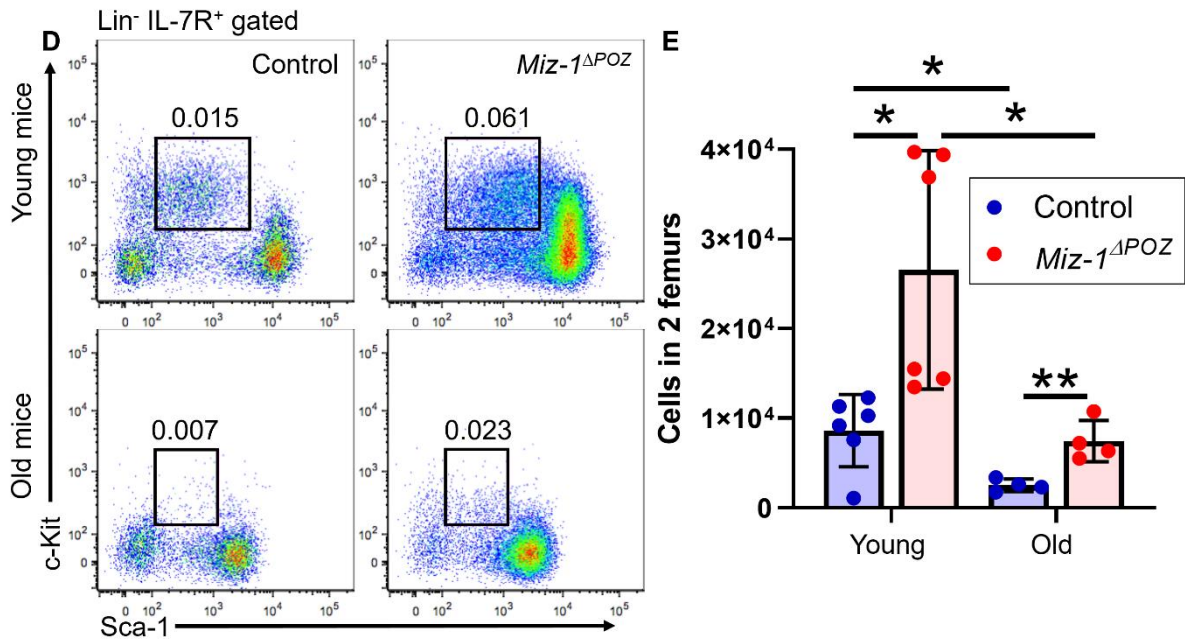**Figure 3.3.:** ***Miz-1*** **POZ domain deletion results in expansion of myeloid and lymphoid progenitor cells** (**D**) Representative FACS plots of young (upper) and old (lower) control and *Miz-1* KO bone marrow with CLP cells resolved. The proportion of gated cells as a percentage of living FSC⁺ SSC⁺ cells are shown beside gates. (**E**) Bar graphs overlaid with dot plot displaying the mean number of CLPs found in 2 femurs from young and aged control and *Miz-1^{ΔPOZ}* mice, $n = 6$ (young), $n = 4$ (old), mean ± SD; *: $p < 0.05$, **: $p < 0.01$; t test.

In agreement with published results, we reproduced the finding that CLP cell number decreases several-fold over the course of aging in control mice, as well as an increase in GMP number. However, we also found an increase in MEP with age. These results show that *Miz-1* POZ domain deficiency results in the age-associated phenotype of an accumulation of myeloid progenitor cell types, however in a trend opposite to that seen in aging, also causes accumulation of CLPs.

3.4 Loss of *Miz-1* POZ domain affects the composition of leukocytes

Because the bone marrow of *Vav-Cre; Miz-1^{ΔPOZ}* mice is cytopenic relative to that of control mice, we sought to find out if the previously described loss of lymphocytes (Kosan et al., 2010) in mice lacking a *Miz-1* POZ domain fully accounts for this effect. We tested this hypothesis

by analysing the numbers of committed hematopoietic cell types from mouse bone marrow using FACS. Similarly to previous work, there was a highly statistically significant loss of lymphocytes in *Miz-1* KO bone marrow, with lymphocytes accounting for 35% of bone marrow cells in control mice but only 10% in *Miz-1* KO mice. The percentages of other mature cell types in the bone marrow were not significantly changed in *Miz-1* KO mice. Accordingly, the number of lymphocytes in young *Miz-1$^{\Delta POZ}$* mice was 5-fold lower than in control mice. Interestingly, the number of neutrophils in young *Miz-1$^{\Delta POZ}$* mice was 1.4-fold lower than in control mice (Figure 3.4A). Whereas, erythrocytes or red blood cells (RBCs) and monocytes showed no change. To see if these differences persist in old age, we also measured committed blood cell types in aged mice. We did not find any statistically significant changes in the number of bone marrow lymphocytes, RBCs, monocytes or neutrophils between young and aged mice, in either control or *Miz-1$^{\Delta POZ}$* genotypes (Figures S4A, S4B). Of interest, there remained a statistically significant difference in the number of lymphocytes between control and *Miz-1$^{\Delta POZ}$* mice in old age, whereas the lower number of neutrophils in *Miz-1$^{\Delta POZ}$* mice relative to control disappeared. Additionally, a statistically significant 3.2-fold reduction of monocytes in *Miz-1$^{\Delta POZ}$* mice compared to controls appeared (Figure 3.4B).

These results suggest that not only is the *Miz-1* POZ domain important in HSPCs for consequent lymphopoiesis, but also for the production of neutrophils and that without it granulopoiesis becomes perturbed. Miz-1 may additionally be important in maintaining monocyte count in old age.
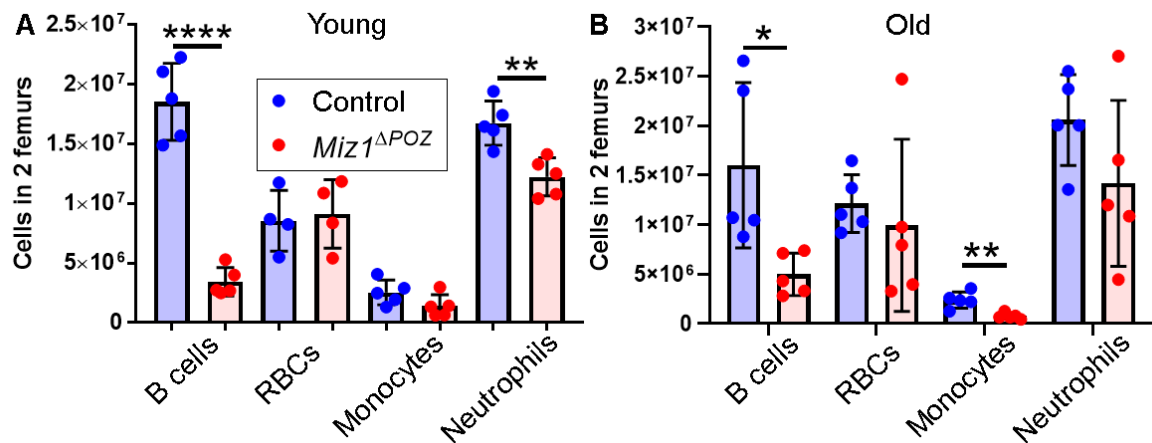
Figure 3.4.: Loss of *Miz-1* POZ domain affects the composition of leukocytes (**A**) Bar graphs overlaid with dot plot of the total number of B cells, RBCs, monocytes and neutrophils found in 2 femurs of young control and *Miz-1$^{\Delta POZ}$* mice, n = 4-5, mean ± SD; ****: $p < 0.0001$, **: $p < 0.01$; t test. (**B**) Bar graphs overlaid with dot plot of the total number of B cells, RBCs, monocytes and neutrophils found in 2 femurs of aged control and *Miz-1$^{\Delta POZ}$* mice, n = 5, mean ± SD; *: $p < 0.05$, **: $p < 0.01$; t test.

3.5 Deletion of *Miz-1* POZ domain greatly diminishes the function of HSCs

To analyse the role of the *Miz-1* POZ domain in the function of stem cells and their capacity to proliferate and differentiate into myeloid-committed precursors, colony-forming unit assays were performed (Figure S5A). Deletion of the *Miz-1* POZ domain resulted in a massive decline in the ability of bone marrow cells to form viable BFU-E (erythroblast progenitor), CFU-GM, (granulocyte-macrophage progenitor) and CFU-GEMM (myeloid progenitor) colonies on methylcellulose compared to bone marrow cells from control mice. Young control bone marrow cells were able to form an average of 65 CFU-GM colonies per 30,000 cells, whereas an equivalent number of young Miz-1-deficient BM cells could only form 4.8. Aging in control mice appeared to reduce the ability of bone marrow cells to form CFU-GM colonies, although this alteration wasn't statistically significant (Figure 3.5A). Similarly, the effect of *Miz-1* POZ domain deletion was a reduction of BFU-E colony formation from over 11.3 colonies in control to 3.8 in knockout (Figure 3.5B) and a complete amelioration of CFU-GEMM colony formation ability, which was 2.3 colonies in control and none in *Miz-1^{ΔPOZ}* cells (Figure 3.5C). Miz-1-deficient CFU-GM and BFU-E colonies appeared smaller and darker, while CFU-GEMM colonies were not observed. The effect of *Miz-1* POZ domain knockout in bone marrow taken from 18 month-old mice was also a severe loss of colony formation in all three colony types compared to control (Figures 3.5A, 3.5B, 3.5C). However, we also noticed that the number of BFU-E colonies that bone marrow cells from aged mice can form was higher than that of those taken from young mice. In particular, control bone marrow cells gained an ability to form BFU-E colonies with age, going from 11.3 in young mice to 26.6 in aged mice. In contrast, *Miz-1^{ΔPOZ}* cells from young mice formed 3.8 BFU-E colonies while those from aged *Miz-1^{ΔPOZ}* mice formed 1.4 colonies (Figure 3.5B). This finding may be consistent with data from others showing that old LT-HSC produce 1.4-fold as many colonies on methylcellulose as LT-HSC from young mice (Kowalczyk et al., 2015).

We further characterised the deficit of Miz-1-deficient stem cells in the capacity to proliferate and differentiate by re-plating the colonies produced at day 8 of the colony-forming unit assay into new methylcellulose media (Figure S5B). This showed that colonies produced from young *Miz-1^{ΔPOZ}* mice were not able to reform colonies when re-challenged with a new CFU assay (Figure 3.5D), in contrast with colonies produced from young control mice which were able to produce new colonies.
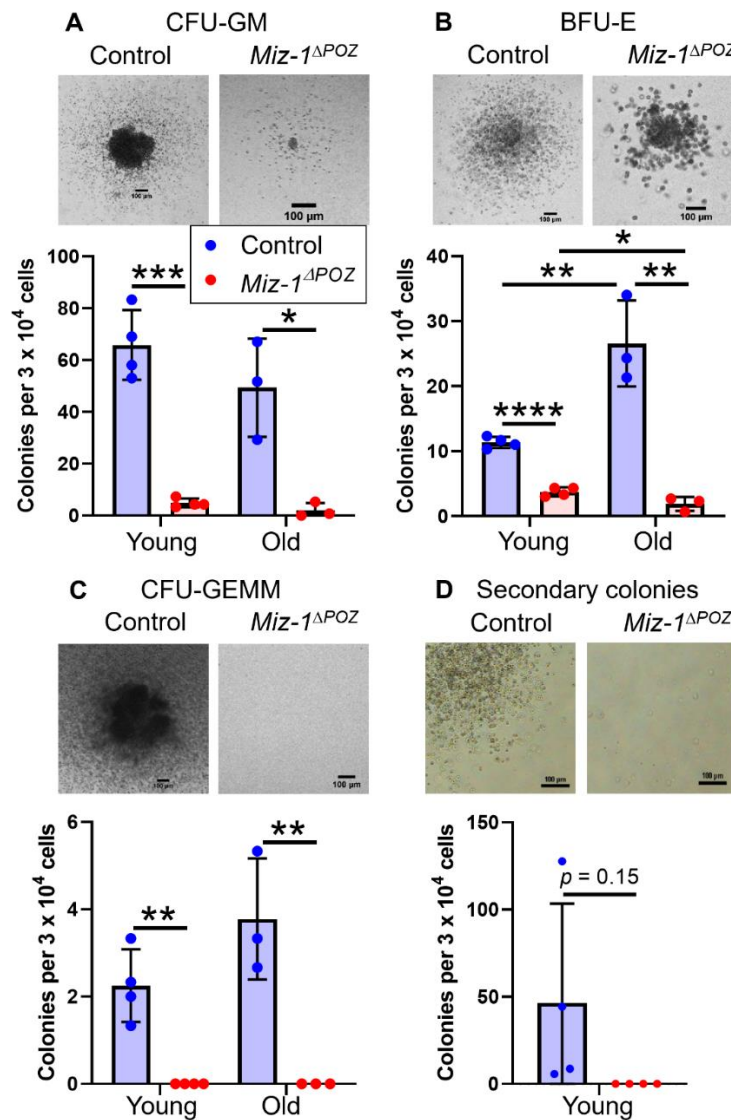
Figure 3.5.: Deletion of *Miz-1* POZ domain greatly diminishes the function of HSCs (**A**) *In vitro* colony formation of myeloid colony types from bone marrow of the indicated genotypes, counted at 8 days post culture. Representative CFU-GM colonies produced from young control and young *Miz-1^{ΔPOZ}* mice (top panel), scale bars represent 100 μm. Bar graphs with dot plot overlay representing the number of colonies of those pictured above (bottom panel). Data are means ± SD, young mice: *n* = 4, aged mice: *n* = 3, *t* test. (**B**) as in (**A**) but for BFU-E. (**C**) as in (**A**) but for CFU-GEMM. (**D**) Bar graphs with dot plot overlay representing the number of colonies formed by 30,000 re-plated colony cells, counted at 10 days after re-plating. Data are means ± SD, young mice: *n* = 4, *t* test.

These results indicate that Miz-1 protects the ability of hematopoietic stem cells to differentiate appropriately into myeloid progenitor cells and their ability to continue producing myeloid cells after an initial proliferative challenge. Miz-1 loss of function also detrimentally affects the morphology of myeloid colonies. Interestingly, we have found that BFU-E colony formation becomes enhanced as mice age, while loss of *Miz-1* POZ domain counteracts this effect.

3.6 Inactivation of Miz-1 transcriptional activity leads to the transcriptional activation of the type I interferon response pathway

In order to identify the potential underlying transcriptional processes responsible for these phenotypes, we performed RNA-sequencing transcriptome profiling on RNA from 4 biological replicates of freshly isolated CD34$^-$ and CD34$^+$ LSK cells from 4-month old mice (Figures S6A, 3.6A). RNA was sequenced following ribosomal RNA depletion. The sequencing depth was satisfactory with an average number of reads per sample of $4 \pm 0.3 \times 10^7$, which mapped onto and identified 48,526 unique transcripts. The quality of data was high, with an average of >94% of base calls ranked with a Phred quality score between Q30 and Q40. Analysis with BEDtools showed that RNA samples from *Miz-1$^{\Delta POZ}$* mice lacked reads at the *Miz-1* POZ domain locus, evidencing successful deletion. Multi-dimensional scaling (MDS) was able to discern only slight differences between LSKs from control and *Miz-1$^{\Delta POZ}$* mice, but revealed distinct CD34-high and CD34-low populations of LSKs in either genotype of mouse (Figure 3.6B). Pairwise comparison of the counts of each gene for each sample revealed that *Miz-1$^{\Delta POZ}$* samples are separated from control in CD34$^-$ LSKs (Figure 3.6C). Furthermore, *Miz-1$^{\Delta POZ}$* CD34$^-$ samples transcriptionally resembled CD34$^+$ LSKs to a greater extent than CD34$^-$ control samples did.
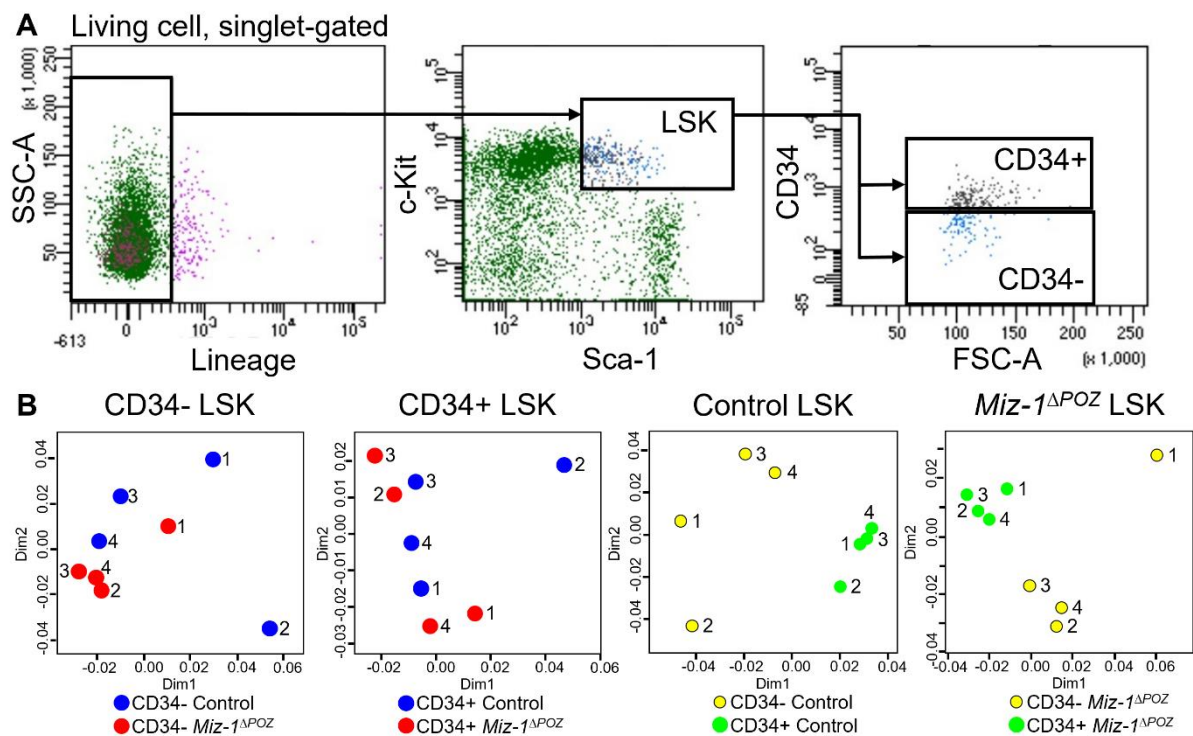
Figure 3.6.: Inactivation of Miz-1 transcriptional activity leads to the transcriptional activation of the type I interferon response pathway (**A**) FACS sorting scheme for CD34$^-$ and CD34$^+$ LSK from which RNA was isolated for RNA-sequencing. A sample from a control mouse is shown. (**B**) MDS plot revealing the characteristics in 2-dimensions of RNA-sequenced samples according to gene expression, measured in read counts. Samples are from young mice and compared by *Miz-1$^{\Delta POZ}$* genotype (left) CD34 expression (right), *n* = 4.

Our data revealed 119 differentially regulated genes (DEGs) in *Miz-1^{ΔPOZ}* CD34^{-} LSKs (DESeq p-value < 0.05), relative to control and 90 DEGs in CD34^{+} LSKs. Out of these, CD34^{-} and CD34^{+} LSKs had 34 DEGs in common (Figure 3.7M in the next section). In one or both cell types, were the mRNAs of 21 genes shown in a previous study to be directly bound by Miz-1 (Wolf et al., 2013), providing confidence in our RNA-seq approach (Figure 3.6D). In both cells types, the RIKEN transcript *2810025M15Rik* was among the 2 DEGs that were most significantly altered in expression level. The gene that was most significantly altered in expression in *Miz-1^{ΔPOZ}* CD34^{-} LSKs was *Igλc1*, followed by *2810025M15Rik* and in third was a gene not normally expressed in hematopoeitic cells, but rather in the testes, named *seminal vesicle autoantigen* (*SVA*). In *Miz-1^{ΔPOZ}* CD34^{+} LSKs, the direct genomic binding targets of Miz-1 *ZNHIT3* and *RPL22* were second and third-most significantly altered, followed by *SVA*. Of particular interest, was the overexpression of mRNAs which are expressed in the cellular response to interferon stimulation, such as interferon inducible transcripts, oligoadenylate synthetases and interferon regulatory factors (Figure 3.6E). The differential expression of a set of selected DEGs revealed by our RNA-sequencing results were verified by performing qPCR on RNA extracted from sorted CD34^{-} and CD34^{+} LSKs (Figures 3.6F, 3.6G). Furthermore, in support of our findings in flow cytometry that CD41 is expressed at a higher level in in *Miz-1^{ΔPOZ}* LSKs, CD41 mRNA *ITGA2B* was more than doubled in expression level in *Miz-1^{ΔPOZ}* CD34^{-} LSKs. Preliminary experiments measuring *RPL22* and *RORC* mRNA expression in *Miz-1^{ΔPOZ}* LSKs also showed the same trend as our RNA-seq experiment (Figure S6B).

Figure 3.6.: Inactivation of Miz-1 transcriptional activity leads to the transcriptional activation of the type I interferon response pathway (**C**) Hea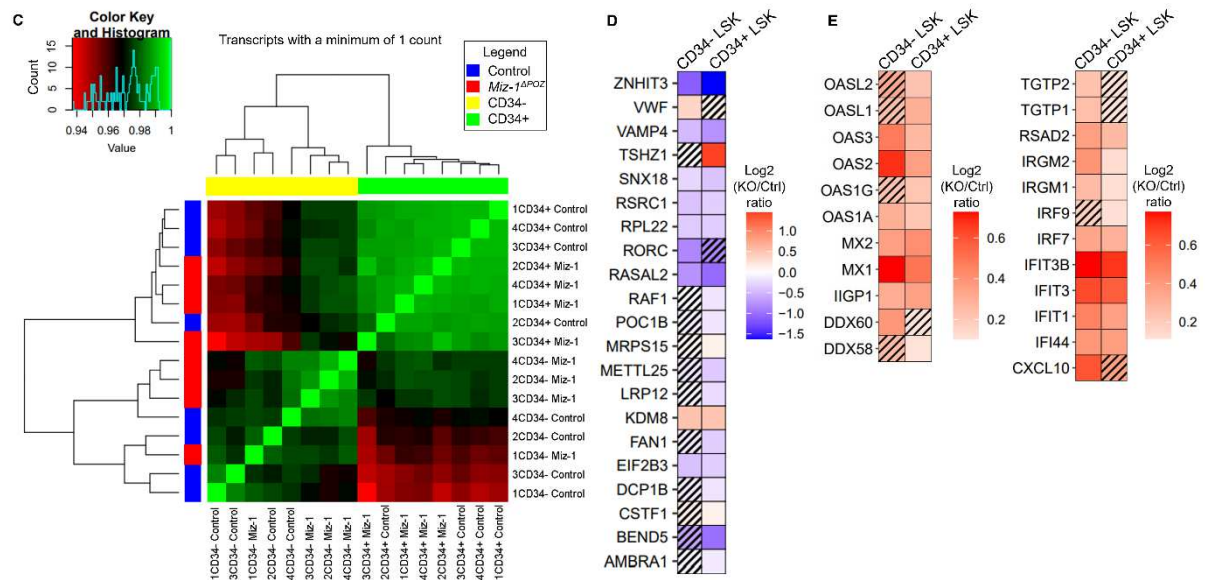t map of sample similarity in terms of gene counts. A heat map displaying comparisons of the spearman correlation of gene counts (for genes with more than one count) per gene for each sample. (**D**) Heat map of transcripts of DEGs directly bound by Miz-1, demonstrating fold expression changes in CD34^{-} and CD34^{+} LSKs. Color represents the log knockout over control ratio of the reads per kilobase million (RPKM) of each transcript, shaded-out cells do not have a statistically significant fold expression change for the indicated cell type. (**E**) Heat map of

transcripts of DEGs involved in defense response to virus and cellular response to interferon pathways, demonstrating fold expression changes in CD34⁻ (left) and CD34⁺ (right) LSKs. Color represents the log knockout over control ratio of the RPKM of each transcript, shaded-out cells have a statistically insignificant fold expression change for the indicated cell type. The functional annotation table in DAVID was used to identify the pathway each DEG is a member of.
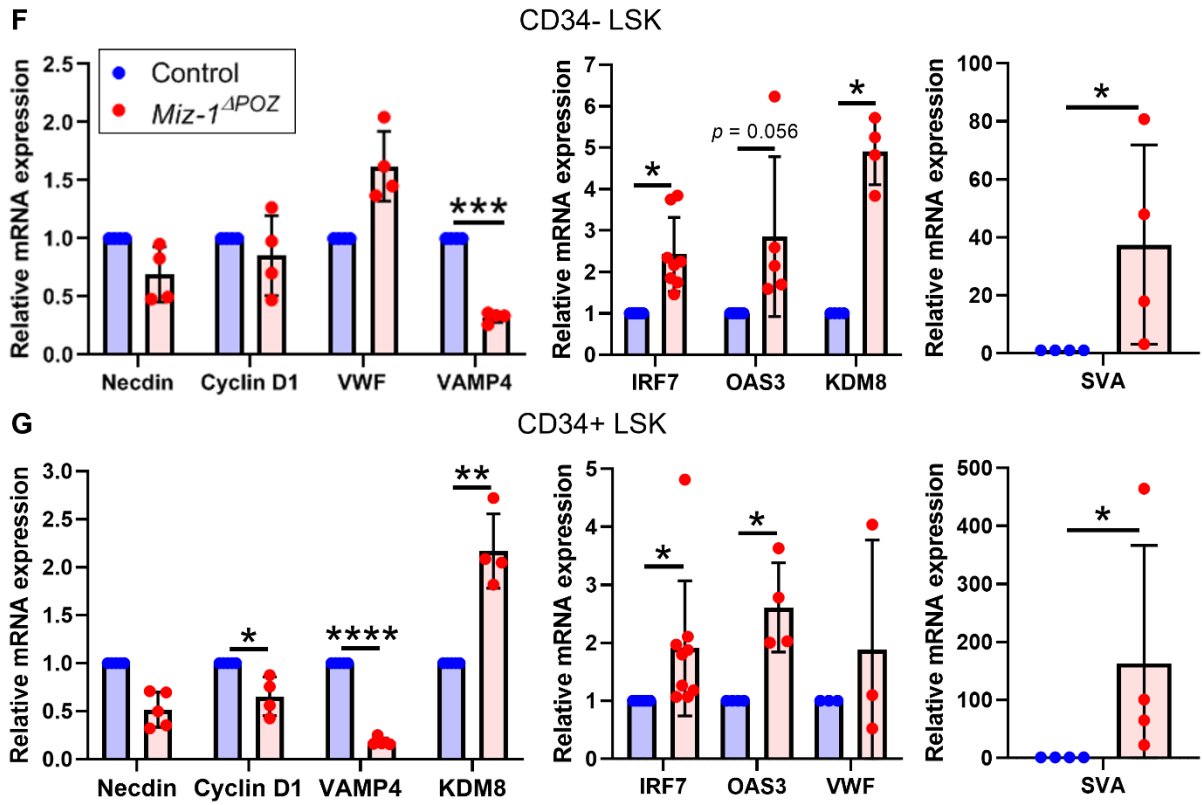
Figure 3.6.: Inactivation of Miz-1 transcriptional activity leads to the transcriptional activation of the type I interferon response pathway (**F**) Bar graph overlaid with dot-plot of qPCR results documenting the expression of selected mRNAs altered in expression level by *Miz-1ᐤᴾᴼᶻ* mutation in CD34⁻ LSKs. Graphs of *IRF7* and *OAS3* expression show data pooled from two different experiments. *n* = 8 (*IRF7*), *n* = 5 (*OAS3*), *n* = 4 (all others); error bars represent mean ± SD; *: $p < 0.05$, ***: $p < 0.001$; *t* test. (**G**) Bar graph overlaid with dot-plot of qPCR results documenting the expression of selected mRNAs altered in expression level by *Miz-1ᐤᴾᴼᶻ* mutation in CD34⁺ LSK. Graphs of *IRF7* and *OAS3* expression show data pooled from two different experiments. *n* = 9 (*IRF7*), *n* = 5 (*Necdin*), *n* = 3 (*VWF*), *n*= 4 (all others); error bars represent mean ± SD; *: $p < 0.05$, **: $p < 0.01$, ****: $p < 0.0001$; *t* test.

We used the Gene Set Enrichment Analysis (GSEA) tool to provide information about which gene clusters are significantly altered by Miz-1 transcription factor deficiency. We performed GSEA on the full readout of our RNA-seq data from both CD34⁻ and CD34⁺ LSKs, identifying 17,535 genes, using the Hallmark and Reactome pathway gene sets, which demonstrated that *Miz-1ᐤᴾᴼᶻ* LSKs have a positive enrichment of interferon response gene signatures in both LSK cell types. Among hallmark gene sets, the top two significantly enriched gene sets which correlated with the *Miz-1* KO gene signature were interferon gamma response and interferon alpha response (NOM p-value < 0.01, FDR < 0.01) and this was true for both CD34⁺ and CD34⁻

LSKs (Figure 3.6H). The most enriched Reactome gene set in *Miz-1* KO was that of interferon alpha-beta signaling in both CD34$^+$ and CD34$^-$ LSKs, while CD34$^+$ LSKs also had significant enrichment for the antiviral mechanism by IFN stimulated genes gene set (Figure 3.6I). Furthermore, in accordance with previously published results (Cabezas-Wallscheid et al., 2014), our analysis found that control LSKs transitioning from CD34$^-$ to CD34$^+$ underwent an enrichment of gene signatures associated with progression through the cell cycle (Figures S6C, S6D). The megakaryocytic and erythroid bias in the transcriptome of CD34$^-$ LSKs compared to CD34$^+$ LSKs was also reflected (Figures S6D, S6E). Interestingly, as Miz-1 deficient CD34$^-$ LSKs expressed CD34, they showed enrichment in these gene signatures, but also enrichment in the spermatogenesis gene set hallmark (data not shown).
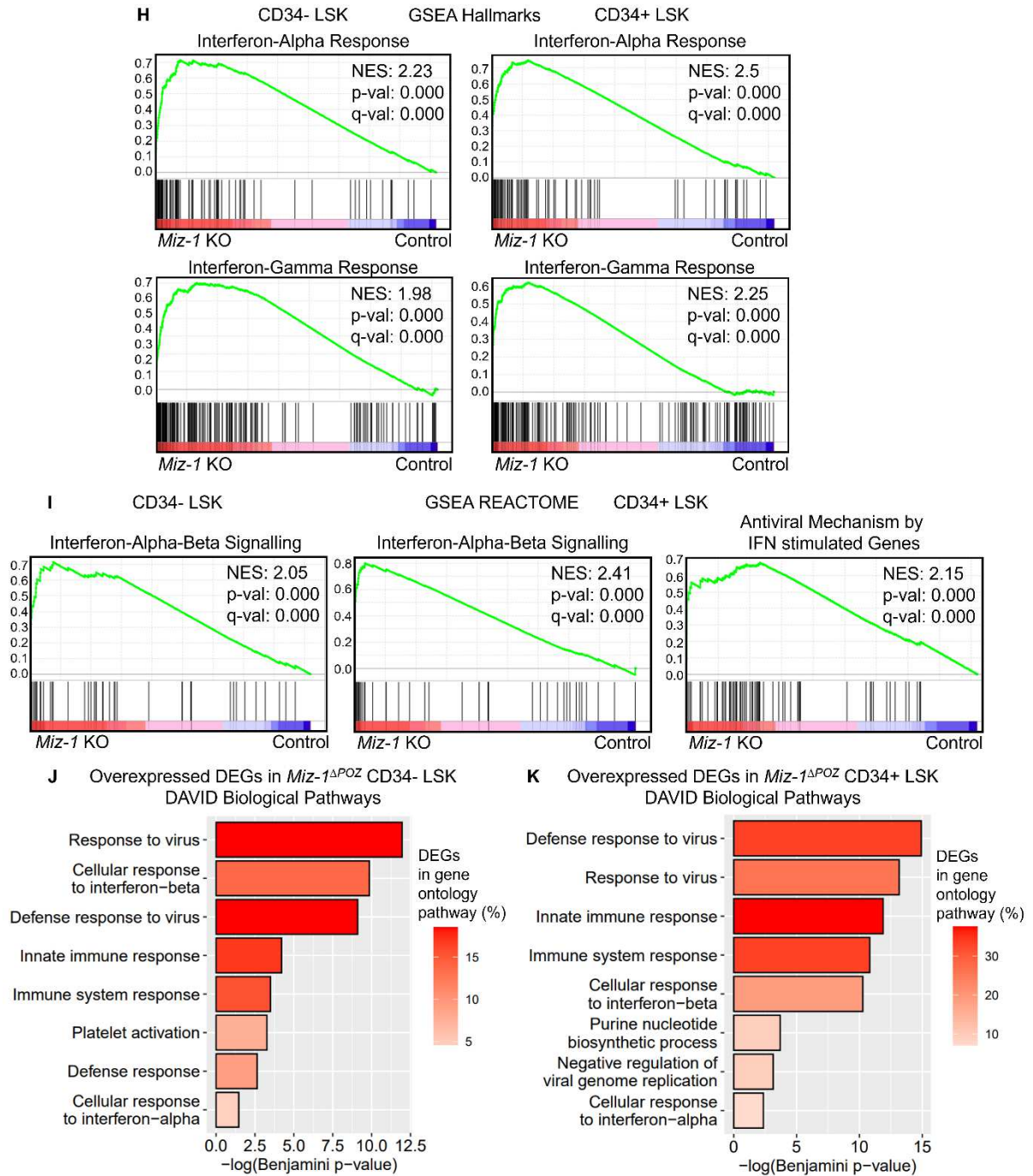
Figure 3.6.: Inactivation of Miz-1 transcriptional activity leads to the transcriptional activation of the type I interferon response pathway (**H**) Gene-set enrichment analysis profiles depicting the top „Hallmark" gene signatures enriched upon *Miz-1* POZ domain deletion in CD34^{-} (left) and CD34^{+} (right) LSKs, generated with bulk RNA-seq data. NES: normalized enrichment score. (**I**) Gene-set enrichment analysis profiles depicting the top „Reactome" gene signatures enriched upon *Miz-1* POZ domain deletion in CD34^{-} (left) and CD34^{+} (middle and right) LSKs, generated with bulk RNA-seq data. NES: normalized enrichment score. (**J**) Bar graph depicting biological function annotation by the application DAVID of genes upregulated by *Miz-1^{ΔPOZ}* mutation in CD34^{-} LSKs. X-axis shows the negative log of the Benjamini p-value of the gene ontology term. Gene ontology terms with the lowest Benjamini p-value are ranked at the top of the graph. Color of the bar graph represents the percentage of genes of that gene ontology term that were upregulated DEGs in knockout. (**K**) As in (**J**) but for CD34^{+} LSKs.

Furthermore, gene ontology (GO) analysis using the Database for Annotation, Visualization, and Integrated Discovery (Huang et al., 2009) online resource showed that, among DEGs overexpressed in either CD34⁻ or CD34⁺ LSKs lacking Miz-1 activity, there was a substantial enrichment in biological processes for genes associated with host response to viral infection and the cellular response to interferon (Figures 3.6J, 3.6K). Gene ontology analysis was unable to find enrichment of processes among downregulated genes for either cell type in *Miz-1^{ΔPOZ}* mice. This was confirmed by gene ontology analysis by the PANTHER classification system, which further identified GTPase activity among molecular functions to be upregulated in both cell types and the ISG15 antiviral pathway to be activated in *Miz-1^{ΔPOZ}* CD34⁺ LSKs (data not shown).

Proteins expressed from the mRNA of DEGs shape the biochemical activities of the cell through protein-protein interaction (PPI) networks and these networks can be represented in the program Cytoscape using information from the STRING database searching program. Differentially expressed mRNAs have been visualised in the form of PPI networks by others to understand RNA sequencing data (Fan et al., 2018), (B. Wu et al., 2014). The 119 DEGs from CD34⁻ LSKs and 90 DEGs from CD34⁺ LSK were each analysed in Cytoscape to generate respective PPI networks. For each network generated, not all DEGs formed a part of the network, but all DEGs placed into a network by Cytoscape encode cytoplasmic-residing protein products. STRING identified 1 subnetwork, or cluster, from the RNA-seq dataset of each cell type, with each cluster consisting of mostly upregulated DEGs. In *Miz-1^{ΔPOZ}* CD34⁻ LSKs, this cluster was associated by the functional gene ontology function in Cytoscape most strongly with the response to virus term (Figure 3.6L), whereas the cluster in *Miz-1^{ΔPOZ}* CD34⁺ LSKs was most associated the interferon signaling term. As no other cluster was identified in the PPI networks generated by our RNA-seq data from LSKs upon *Miz-1* POZ domain knockout, this result suggests that Miz-1 knockout exerts its effect on the antiviral response and interferon signaling primarily through an integrated network of mRNAs that share a transcriptional regulation mechanism. Analysis of a PPI network can provide a hint as to which molecules form the core of that network through assessing the node degree, or number of bridges, that each gene has to other genes. As such, *IRF7* was a highly interconnected node in the PPI networks generated from both LSK subtypes (Figures 3.6M, 3.6N), indicating that the effect of Miz-1 on the type I interferon response is potentially taking place primarily through IRF7.

To gain further insight into which molecules may be governing the *Miz-1^{ΔPOZ}* phenotype, we looked to upstream regulator analysis with Ingenuity Pathway Analysis software to find predicted regulators that are known to activate or inhibit the expression of genes affected by *Miz-1* POZ domain deletion. Regulators predicted to be influencing the *Miz-1^{ΔPOZ}* phenotype in both CD34⁻ and CD34⁺ LSKs included STAT1, components of the cytosolic DNA- and viral RNA-sensing pathways such as cGAS, IRF3, IRF7, interferons and their receptors, as well as the bacterial outer membrane component, lipopolysaccharide (Figure 3.6O).

These data show that *Miz-1ΔPOZ* LSK exhibit heightened activity of the type I interferon response, particularly the anti-viral response mechanism and suggest that this may be due to Miz-1 suppression of a network of co-expressed mRNAs through its interaction with a core regulator of the immune response. Furthermore, these results suggest that Miz-1 transcription factor activity directly or indirectly suppresses these processes, resulting in a limitation of the expansion of HSCs and MPPs, while preserving their quiescent and less-differentiated, stem cell-like state.
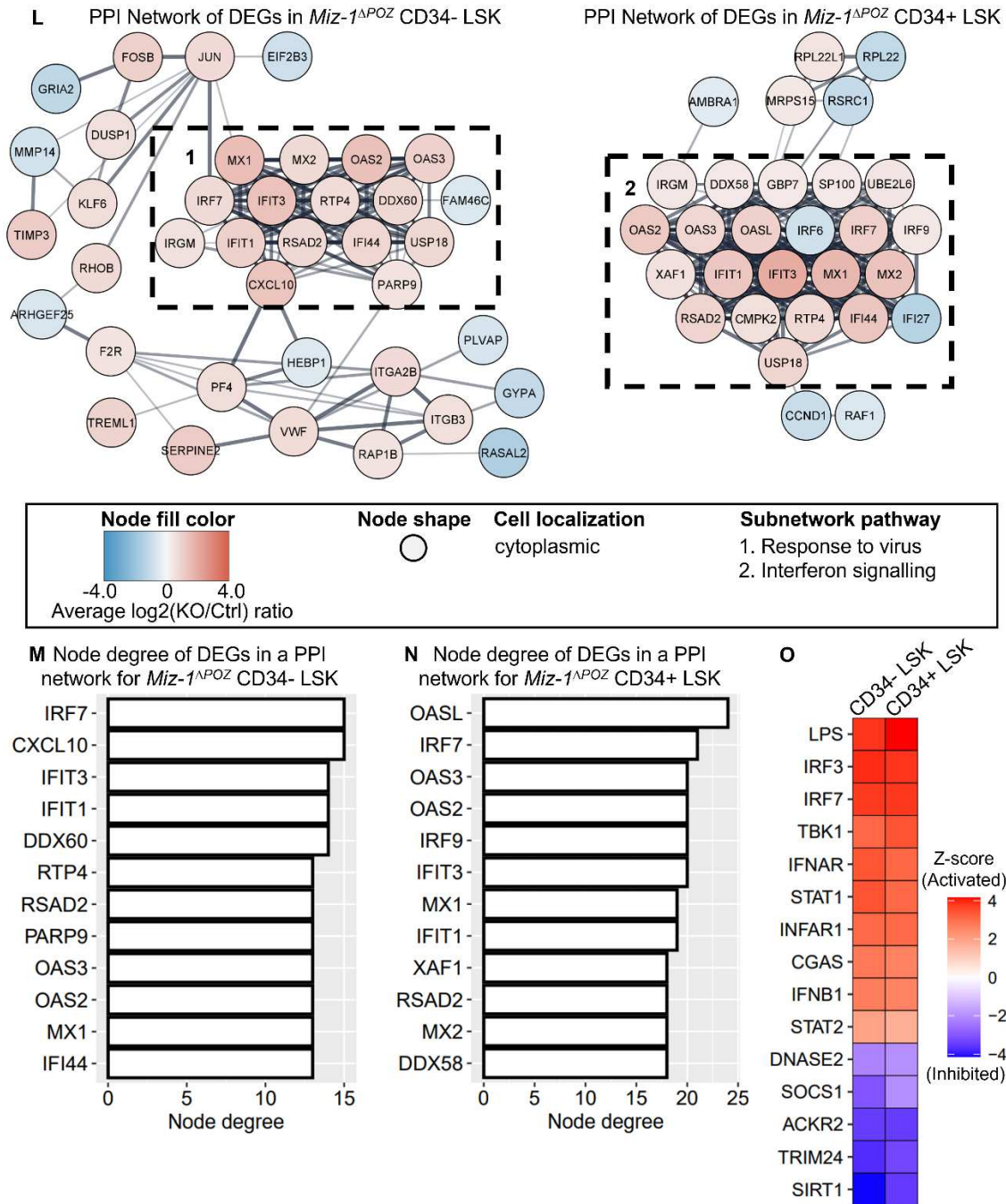

Figure 3.6.: Inactivation of Miz-1 transcriptional activity leads to the transcriptional activation of the type I interferon response pathway (**L**) PPI network of DEGs in *Miz-1ΔPOZ* CD34⁻ (left) and CD34⁺

(right) LSKs. The network pathway term of the highlighted cluster is the gene ontology term with the lowest FDR value for that cluster. Bridge thickness represents the confidence score of the interaction (not shown). Not all DEGs submitted to Cytoscape are shown in this network, as some DEGs do not form bridges to other nodes. In generating the network, default confidence score cutoff was set to 0.6 and maximum additional interactors set to 0. (**M**) Bar graph of node degree (number of bridges) for each gene (node) in the PPI network of DEGs in *Miz-1$^{\Delta POZ}$* CD34$^-$ LSKs. (**N**) as in (**M**) but for CD34$^+$ LSKs. (**O**) A heat map representing Ingenuity upstream regulator analysis. Shown are the 15 regulators with the lowest *p*-value for both cell types. Red are regulators predicted to be activated and those blue are predicted to be inhibited. *P*-values for all regulators shown were between 2 x 10^{-8} and 3 x 10^{-22}.

3.7 *Miz-1$^{\Delta POZ}$* LSKs have disrupted protein networks involved in rRNA processing and mRNA splicing impacting the anti-viral response

To verify that a type I interferon response is activated at the proteomic level and to observe the changes that occur in the proteome of *Miz-1$^{\Delta POZ}$* LSKs, global proteome analysis was performed on freshly isolated LSKs from young (16-18 weeks old) mice (Figure 3.7A). 6 biological repeats were produced for this experiment, from which the best 3 correlated repeats were chosen for further analysis. control and *Miz-1$^{\Delta POZ}$* samples were clearly separated in a principle component analysis (PCA, Figure 3.7B). 2,566 peptide groups (hereafter referred to as proteins) were differentially regulated, defined as having a Q-value (false discovery rate) below 0.05 were revealed. Among these, 1,422 were increased in abundance in *Miz-1$^{\Delta POZ}$* LSKs and 1,144 proteins were decreased in abundance. To refine this large selection of proteins further, a protein was considered to be a differentially abundant protein (DAP) if there was a 2-fold or greater difference in their abundance, measured by their absolute average logarithmic *Miz-1$^{\Delta POZ}$*-over-control expression ratio. This resulted in a shorter list of 170 upregulated and 150 downregulated proteins. These DAPs included VAMP4 protein, the gene of which is bound directly by Miz-1, incurring a 3.3-fold decrease in expression level in *Miz-1$^{\Delta POZ}$* LSKs (Figure 3.7C). Also included among the DAPs of *Miz-1$^{\Delta POZ}$* LSKs were many large (RPL) and small (RPS) ribosomal proteins, six NADH dehydrogenase family proteins and several myosin light and heavy chain isoforms (Figure 3.7J).
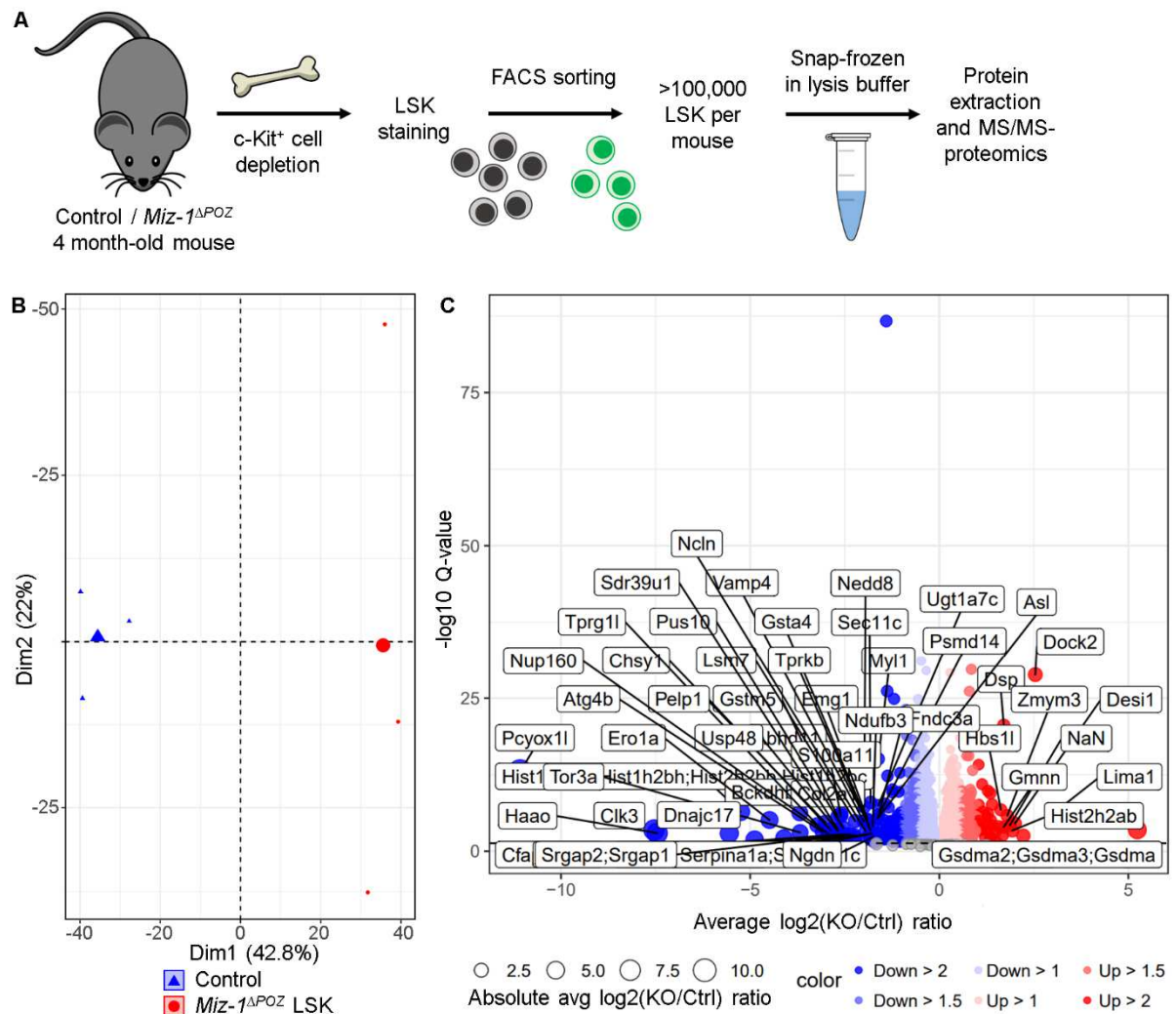
Figure 3.7.: *Miz-1ᐤᴾᴼᶻ* LSKs have disrupted protein networks involved in rRNA processing and mRNA splicing impacting the anti-viral response (**A**) Schematic depicting the set-up of proteomics experiment. Bone marrow cells were taken from young mice and fractionated for c-Kit expressing cells, from which a pure LSK population were sorted and immediately snap-frozen in lysis buffer for protein extraction and mass-spectometry (MS) proteomics. (**B**) Principle component analysis (PCA) of 3 biological replicates of 110,000 or more LSK cells subjected to MS-based proteomics. Large points represent the average position of smaller points. The data of differentially expressed proteins separate the samples into two dimensions: Dim1 separates control from *Miz-1ᐤᴾᴼᶻ* LSKs, Dim2 reveals greater variation in *Miz-1ᐤᴾᴼᶻ* samples, *n* = 3. (**C**) Volcano plot visualising differentially expressed proteins resulting from *Miz-1ᐤᴾᴼᶻ* mutation in LSKs. Larger points had a higher fold expression change, red points were overexpressed in *Miz-1ᐤᴾᴼᶻ* LSKs, while blue points represent underexpressed DAPs.

To gain insight into which cellular compartments are affected by *Miz-1ᐤᴾᴼᶻ* knockout in LSKs, we submitted our list of 320 DAPs to the DAVID bioinformatics tool for functional annotation. Among DAPs overexpressed upon *Miz-1ᐤᴾᴼᶻ* knockout, the most enriched cellular component was cytoplasm, with 57% of DAPs in this category (Figure 3.7D). The terms of intracellular ribosomal complex and ribosome were also highly enriched, as was nucleus, with 50% of DAPs also in this term (genes can be assigned to more than one term). Underexpressed

DAPs were highly enriched in the extracellular exosome term, with this term applying to 46% of the 150 underexpressed DAPs, as was the term mitochondrion with 33% (Figure 3.7E). In addition, the terms of myofibril, myosin complex and myosin filament were also highly enriched with around 6% of underexpressed DAPs represented. These results indicate a reorganisation of the cellular proteome in *Miz-1$^{\Delta POZ}$* LSKs.

To understand the molecular functions affected in *Miz-1$^{\Delta POZ}$* LSKs, DAP lists were also submitted to DAVID Keywords functional annotation for analysis, showing that the terms of acetylation and phosphoprotein were highly enriched in both overexpressed and underexpressed DAP lists (Figure 3.7F, 3.7G). Furthermore, around 10% of overexpressed DAPs were in the terms of ribonucleoprotein and ribosomal protein, while 14% of underexpressed DAPs had the keyword term of muscle protein. This suggests that levels of acetylation and the phosphorylation states of proteins may be altered, while ribosomal activity may be increased, and microtubule function may be reduced in *Miz-1$^{\Delta POZ}$* LSKs.

To obtain an overview of the biological processes and pathways affected by loss of the *Miz-1* POZ domain, we also investigated which biological processes and pathways are associated with the DAPs in *Miz-1$^{\Delta POZ}$* LSKs. Only one term was retrieved by DAVID in the Biological Process category for either the overexpressed or underexpressed DAP lists: for overexpressed DAPs, only translation was a highly enriched term, while among those that were downregulated, muscle contraction was enriched (data not shown). The gene list analysis tool PANTHER accepted 159 DAPs among upregulated proteins and 144 among those downregulated, and provided concurring but more extensive results from our DAP lists: highly enriched PANTHER Reactome pathways associated with overexpressed DAPs were those involved in translation, such as eukaryotic translation initiation, the formation of 40S and 60S ribosomal subunits as well as the processing of rRNAs in particular (Figure 3.7H). Those DAPs that were underexpressed in *Miz-1$^{\Delta POZ}$* LSKs were associated with the Reactome pathways of striated muscle contraction, arginine methyltransferase (RMT) activity, metalloproteinase deubiquitinating enzymes (DUBs) and the nucleolar remodeling complex (NoRC) negatively regulates rRNA expression (Figure 3.7I). Furthermore, when the list of 2,566 proteins not filtered by expression ratio was submitted to PANTHER, the antiviral pathway stimulated by interferon genes Reactome pathway term was included among the results (data not shown), a pathway that was also enriched in the GSEA analysis on RNA-sequencing data (Figure 3.6I). These results suggest that the expression of ribosomal RNAs is influenced by Miz-1 transcription factor activity both through proteins that Miz-1 stimulates the expression of and those it represses.

We wished to visually represent the proteomic consequences of *Miz-1* POZ domain loss in LSKs to observe if its effects are concentrated in particular networks of proteins. A PPI network was generated with the complete list of 320 DAPs in *Miz-1$^{\Delta POZ}$* LSKs using the STRING database and visualized using the Cytoscape program. PPI network analysis revealed 5 identifiable clusters composed of DAPs (Figure 3.7J). The en-suite functional enrichment function in

Cytoscape revealed that the largest cluster of 28 DAPs was associated with the enrichment term major pathway of rRNA processing in the nucleolus and cytosol, while the next largest cluster of 22 DAPs was associated with mRNA splicing, spliceosome and processing of pre-mRNA. Joint-third in size were two clusters, both composed of 19, almost all downregulated DAPs, and was associated with the terms contractile fiber and muscle protein, while the other was associated with the terms membrane trafficking and vesicle-mediated transport.
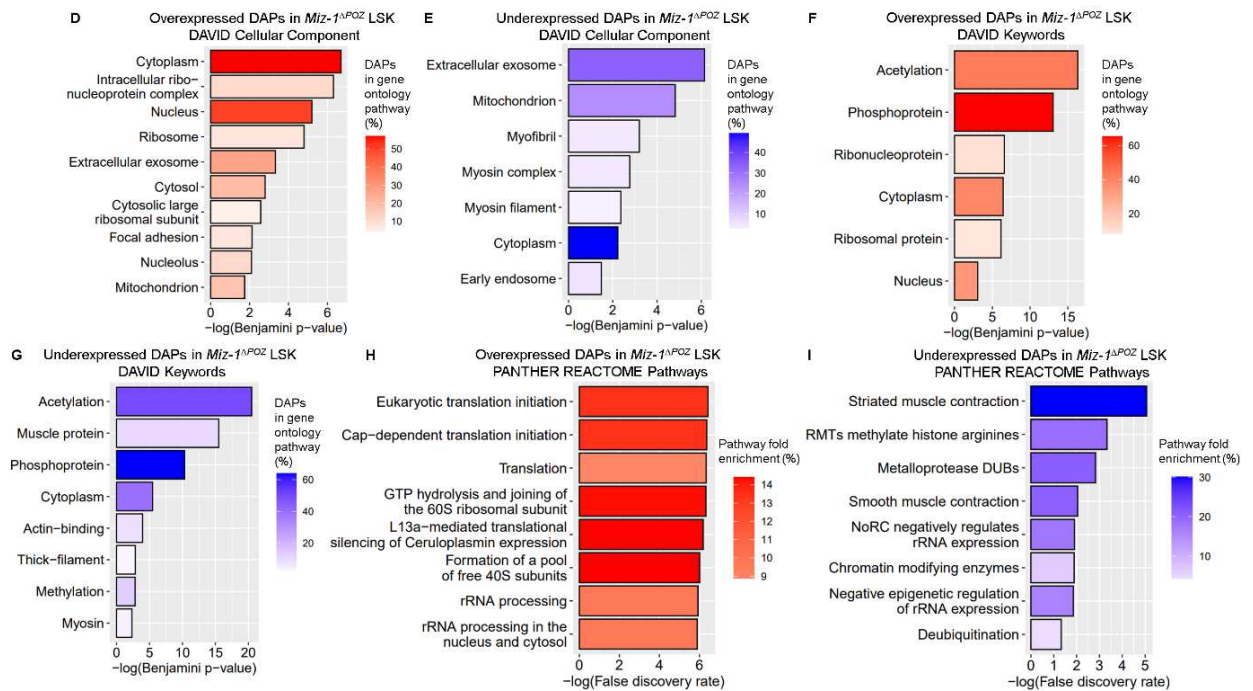
Figure 3.7.: *Miz-1^{ΔPOZ}* LSKs have disrupted protein networks involved in rRNA processing and mRNA splicing impacting the anti-viral response (**D**) Bar graph showing overrepresented gene ontology terms of differentially expressed proteins in *Miz-1^{ΔPOZ}* LSKs revealed by DAVID Cellular Component annotation. The x-axis shows the negative log of the Benjamini p-value of the gene ontology term. Gene ontology terms with the lowest Benjamini p-value are ranked at the top of the graph. The bar graph color represents the percentage of genes of that gene ontology term that were upregulated DAPs in knockout. (**E**) as in (**D**) but for DAPs that were underexpressed. (**F**) as in (**D**) but for DAVID Keyword terms. (**G**) as in (**E**) but for DAVID Keyword terms. (**H**) Bar graph showing overrepresented gene ontology terms of differentially expressed proteins in *Miz-1^{ΔPOZ}* LSKs revealed by PANTHER REACTOME annotation. The x-axis shows the negative log of the false discovery rate (FDR or Q-value) of the gene ontology term. Gene ontology terms with the lowest FDR are ranked at the top of the graph. The bar graph color represents the percentage of genes of that gene ontology term that were upregulated DAPs in knockout. (**I**) as in (**H**) but for DAPs that were underexpressed.

The smallest cluster consisted of 16 mostly mitochondria-localized DAPs and was associated with the respiratory electron transport and oxidative phosphorylation terms. This analysis reiterates the gene ontology analysis given above. Node degree distribution analysis revealed that the most integrated node of this PPI network was NHP2L1 (SNU13), a ribonucleoprotein, followed by large and small ribosomal subunits (Figure S7E), indicating that

changes in expression levels of these proteins may be organising the network across subnetworks as a whole.
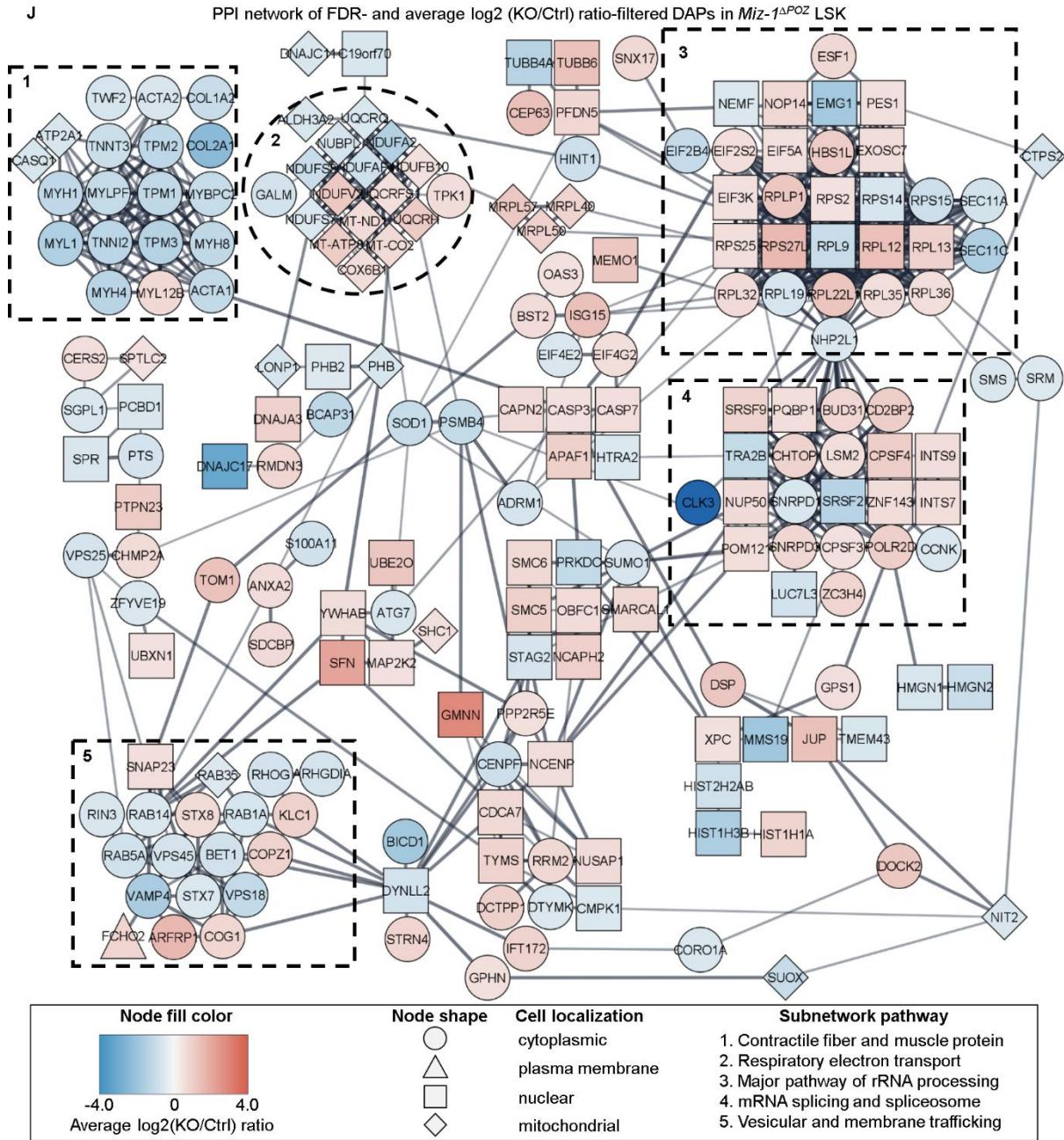
Figure 3.7.: *Miz-1^ΔPOZ* LSKs have disrupted protein networks involved in rRNA processing and mRNA splicing impacting the anti-viral response (**J**) PPI network of DAPs in *Miz-1^ΔPOZ* LSKs. The network pathway term of the highlighted cluster is the gene ontology term with the lowest FDR value for that cluster. Bridge thickness represents the confidence score of the interaction (not shown). Only DAPs included in the network are shown.

To find the common pathways in which both the proteome and transcriptome change upon *Miz-1* POZ domain knockout in LSKs, we combined the DAP list from our proteomic experiment with the DEG lists from our RNA-sequencing experiment. The 320 DAPs that were

filtered for both a logarithmic fold expression change of 2 or greater and a Q-value of <0.05 were combined with DEGs from CD34$^-$ and CD34$^+$ *Miz-1$^{\Delta POZ}$* LSKs as well a DEG list produced from comparing the two LSK subsets of CD34 pooled together. This showed that VAMP4 and OAS3 expression level changes were concordant in both mRNA and protein (Figure 3.7K). Interferon induced GTPase 1 (IIGP1) also showed significant alteration in both protein expression level and transcript expression level in CD34$^-$ and CD34$^+$ LSKs, while CD34$^-$ LSKs alone shared *HEBP1* with DAPs in *Miz-1$^{\Delta POZ}$* LSKs and in CD34$^+$ LSKs the DEG *RPL22L1* was also increased in protein expression level. Furthermore, in the pooled CD34$^-$ and CD34$^+$ LSK dataset, interferon-stimulated gene 15 (*ISG15*) and bone marrow stromal cell antigen 2 (*BST2*) were among the DEGs which also showed expression level changes in protein. When these 7 DAP/DEGs were submitted to PANTHER gene ontology functional analysis, gene ontology terms found to be enriched were those involved in response to viral infection (Figure 3.7L), illustrating that *Miz-1$^{\Delta POZ}$* LSKs do have an antiviral response phenotype at the proteomic level. Among differentially abundant proteins in LSKs, there were 3 genes altered in mRNA expression level in both LSK cell types, as well as 1 in CD34$^-$ LSKs only and 1 in CD34$^+$ LSKs only (Figure 3.7M). In addition to this, there were 315 DAPs not found to have been altered by *Miz-1* POZ domain deletion at their corresponding mRNA level in LSKs, and conversely, 84 RNAs in CD34$^-$ and 55 RNAs in CD34$^+$ LSKs that did not show protein expression level changes. There were also 31 DEGs common to both LSK cell types, 28 of which showed no change in expression in their corresponding protein products. When the full list of 2,566 proteins that were not excluded for having a log expression fold change ratio of less than 2 was combined with our RNA-seq data and subject to the same gene ontology analysis as done here, the results were highly similar, with immune and antiviral response terms being the associated pathways (Figure S7A, S7B). However, the list of DAPs that were also DEGs was twice as large, including *IFIT1* and *RPL22* (Figure S7C).

When the list of 320 DAPs was submitted to Ingenuity softare for upstream regulator analysis, this shed light on the phenotype observed in the proteome of *Miz-1$^{\Delta POZ}$* LSKs by way of predicted upstream regulators. Smoothelin-like protein 1 (SMTNL1), a regulator of smooth muscle contraction, was predicted to be strongly activated, as were the Miz-1 binding partner Myc and the lysine demethylase KDM5A (Figure 3.7N).

Taken together, these results illustrate that Miz-1 transcription factor activity in LSKs serves to suppress translation, ribosome assembly and rRNA processing while maintaining the capacity for microtubule activity and membrane trafficking. This effect may originate in the modulation of acetylation and phosphoprotein activity by Miz-1 through its complexes with Myc and epigenetic regulators and results in reorganisation of the proteome through distinct protein networks, with a subset of these effects being the transcriptional suppression of the interferon signaling and the antiviral response.
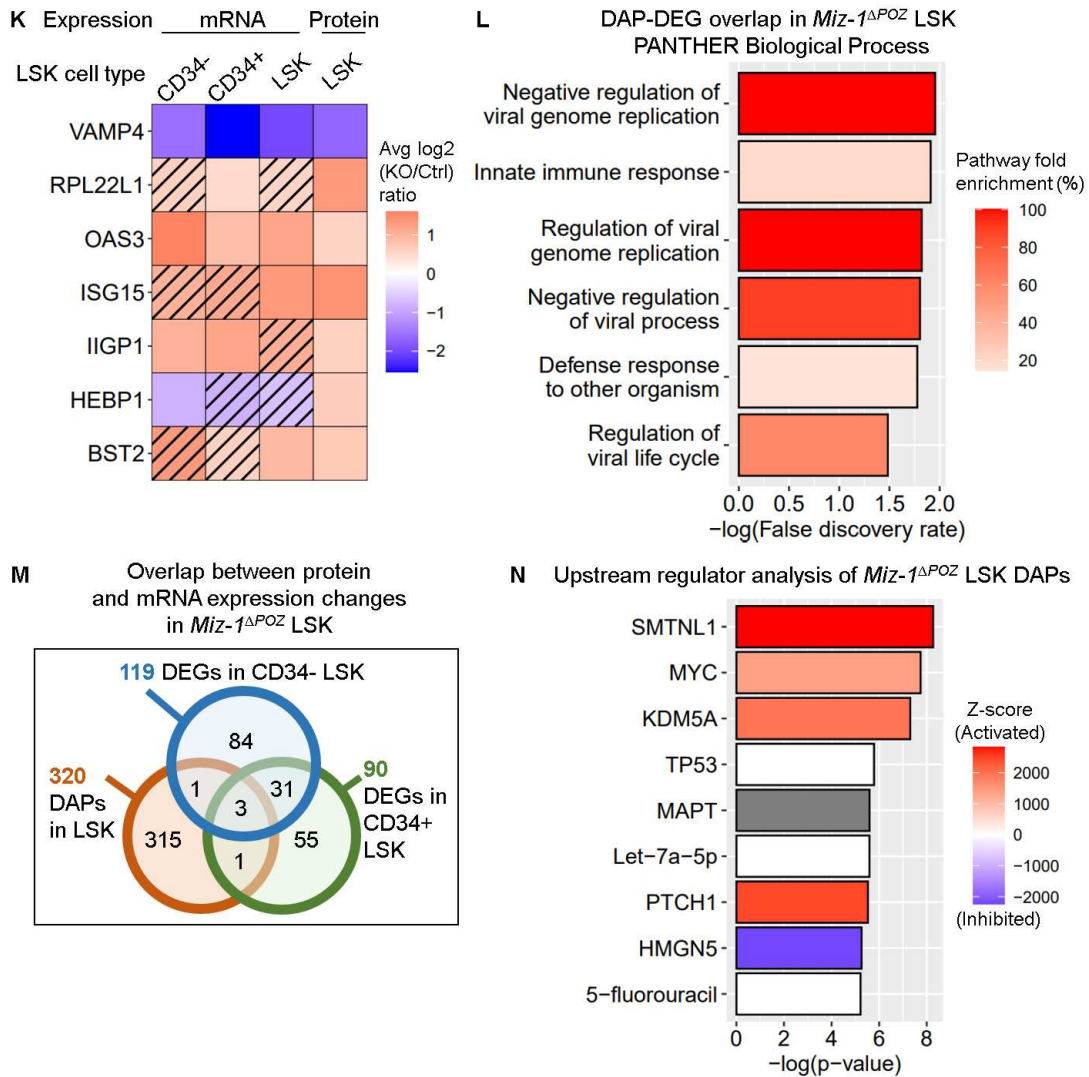
Figure 3.7.: *Miz-1^ΔPOZ* LSKs have disrupted protein networks involved in rRNA processing and mRNA splicing impacting the anti-viral response (**K**) Heat map of DAPs in *Miz-1^ΔPOZ* LSKs the transcripts of which were also DEGs, demonstrating fold expression changes. The color represents the logarithmic knockout over control ratio for each DAP, shaded-out cells have a statistically insignificant fold expression change for the indicated cell type. The first three columns represent the expression fold change of the DEG of the gene while the right-most column represents the expression fold change of the protein of the gene. (**L**) Bar graph showing overrepresented gene ontology terms of DEGs that were also differentially expressed proteins in *Miz-1^ΔPOZ* LSKs revealed by PANTHER Biological Process annotation. The x-axis shows the negative logarithm of the false discovery rate (FDR or Q-value) of the gene ontology term. Gene ontology terms with the lowest FDR are ranked at the top of the graph. The bar graph color represents the percentage of genes of that gene ontology term that were upregulated DAPs in knockout. (**M**) Venn diagram representing the overlap between protein and RNA expression changes in *Miz-1^ΔPOZ* LSK. (**N**) Bar graph representing Ingenuity upstream regulator analysis of 320 DAPs in in *Miz-1^ΔPOZ* LSKs. Shown are the 9 regulators with the lowest p-value for both cell types. Red are regulators predicted to be activated, those blue are predicted to be inhibited and grey represents no prediction. The p-value range was 6 x 10^{-6} to 6 x 10^{-9}.

3.8 Miz-1 does not directly bind to IRF7 or IFIT3 transcriptional start sites in HSPCs

Miz-1 is a transcription factor known to directly stimulate the transcription of mRNA and therefore this may be the primary mechanism of the observed phenotype when the POZ domain is deleted. To further explore the mechanism of Miz-1-orchestrated gene regulation of the type I interferon response pathway in hematopoietic stem cells, we measured Miz-1 transcription factor binding of its potential target loci in the HPC-5 hematopoietic stem cell line. This was performed using chromatin immunoprecipitation followed by qPCR (ChIP-qPCR), employing anti-Miz-1 (Pineda) and anti-IgG (immunoglobulin G) antibodies and primers targeting the promoter transcription start site (TSS) and downstream regions of *KDM8*, *IFIT3* (Interferon-induced protein with tetratricopeptide repeats 3) and *IRF7* (interferon regulatory factor 7) genes. These loci were chosen because *IFIT3* mRNA had a low p-value among the upregulated immune response transcripts in the RNA-sequncing data in *Miz-1^{ΔPOZ}* LSKs, while *IRF7* was also upregulated, is a transcription factor which coordinates the cellular response to interferons and has appeared in the results of several of our analyses.

We found that Miz-1 strongly binds the TSS of the *KDM8* gene, but not to a region 1000 bp downstream of it or any other gene region we immunoprecipitated (Figure 3.8A). Enrichment of Miz-1 binding at the TSS of the *KDM8* gene is consistent with our expression data and studies in other cell lines (Fuhrmann et al., 2018). These ChIP assays show that Miz-1 directly binds the *KDM8* promoter, but not those of *IFIT3* or *IRF7* in HPC-5 cells and suggest that the immune response phenotype observed upon *Miz-1* POZ domain deletion is at least partially independent of the transcription factor function of Miz-1.
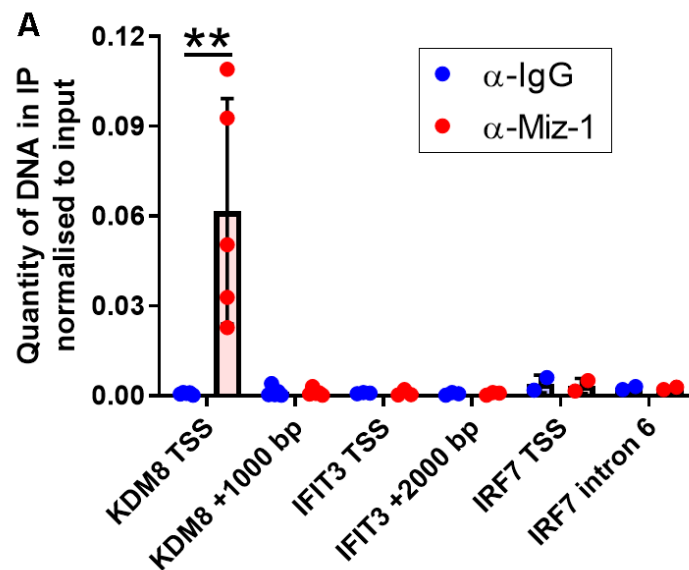
Figure 3.8.: Miz-1 does not directly bind to IRF7 or IFIT3 transcriptional start sites in HSPCs (**A**) Bar graph with dot plot overlay showing analysis of Miz-1 enrichment on *IFIT3* and *IRF7* promoters in

HPC-5 cells via ChIP assay followed by qPCR analysis. ChIP assays were performed with indicated antibodies against Miz-1 and IgG. Data are expressed as the quantity of immunoprecipitated DNA normalised to a standard curve produced from known amounts of HPC-5 DNA. Sample numbers of independent IPs: n = 5 (*KDM8*), n = 3 (*IFIT3*), n = 2 (*IRF7*), mean ± SD; *: p < 0.05; *t* test.

3.9 The transcriptional changes induced by *Miz-1* POZ domain knockout in LSK cells are no longer significant in old-aged mice

Intrigued by the similarity between the *Miz-1ΔPOZ* phenotype in young HSCs and that of aged control HSCs, we decided to repeat our earlier RNA sequencing experiment with 24 month-old control and *Miz-1ΔPOZ* mice to observe whether *Miz-1ΔPOZ* RNA expression signatures are enriched during aging in LSKs. Cells were prepared and RNA was extracted and then sequenced following ribosomal RNA depletion in the same manner as in young mice (Figure S7A). The sequencing depth was again satisfactory with an average number of reads per sample of $4.1 ± 1.2 \times 10^7$, which mapped onto and identified 53,802 unique transcripts. The quality of data was high, with an average of 95% of base calls ranked with a Phred quality score between Q30 and Q40. MDS on the correlation between gene counts for each gene between genotypes revealed that control CD34⁻ LSKs did not separate clearly from *Miz-1ΔPOZ* CD34⁻ LSKs in aged mice, while CD34⁺ LSKs showed slight separation between genotypes (Figure 3.9A). In contrast to this, CD34⁻ LSK samples were separated distinctly from CD34⁺ samples in either genotype of aged mice, showing that CD34⁻ and CD34⁺ LSKs in aged mice remain distinct populations at the transcriptomic level. This is further represented in a heat map (Figure 3.9B) of correlations between control, *Miz-1ΔPOZ*, CD34⁻ and CD34⁺ cell types, which reveals that our samples separate by gene expression in CD34 expression, but not, in contrast in young mice (Figure 3.6E), in control and *Miz-1ΔPOZ* genotype. A heat map representing all samples from both RNA-sequencing experiments further reflects this, showing that control and *Miz-1ΔPOZ* conditions is most distinguishable in CD34⁻ samples from young mice (Figure S8B). CD34⁺ samples from young mice were quite transcriptionally similar to CD34⁺ samples taken from aged mice. Interestingly, *Miz-1ΔPOZ* samples bear greater resemblance to samples from aged mice than their control counterparts, as do CD34⁺ samples compared to CD34⁻ samples. These results indicate that in old age, the statistical differences between control and *Miz-1ΔPOZ* LSK transcriptomes cease to exist. Sample #3 from the *Miz-1ΔPOZ* CD34⁻ LSK group was removed from all other analyses due to it being a statistical outlier.

Comparing RNA-sequencing results between control and *Miz-1ΔPOZ* in CD34⁻ LSK cells from 2 year-old mice revealed 207 DEGs (defined as having an adjusted *p*-value of below 0.05), 37 of which were overexpressed in *Miz-1ΔPOZ* CD34⁻ LSKs and 170 of which were underexpressed. Furthermore, the vast majority of these DEGs (95%) were not expressed in one genotype compared to the other, meaning that these DEGs had "infinite"-fold expression changes. Of further interest, a substantial proportion of these DEGs included uncharacterised predicted genes named with Gm-suffices (35%) or were RIKEN cDNAs (11%). Similarly in CD34⁺ LSKs, 433 genes were differentially expressed between control and *Miz-1ΔPOZ* cells: 125 upregulated

and 308 downregulated in *Miz-1* POZ domain knockout. In total, 31% of these DEGs were uncharacterised predicted genes and 2.3% were RIKEN cDNAs. There were 55 genes that were commonly differentially expressed in both subsets of *Miz-1*^{ΔPOZ} LSKs (Figure 3.9E).
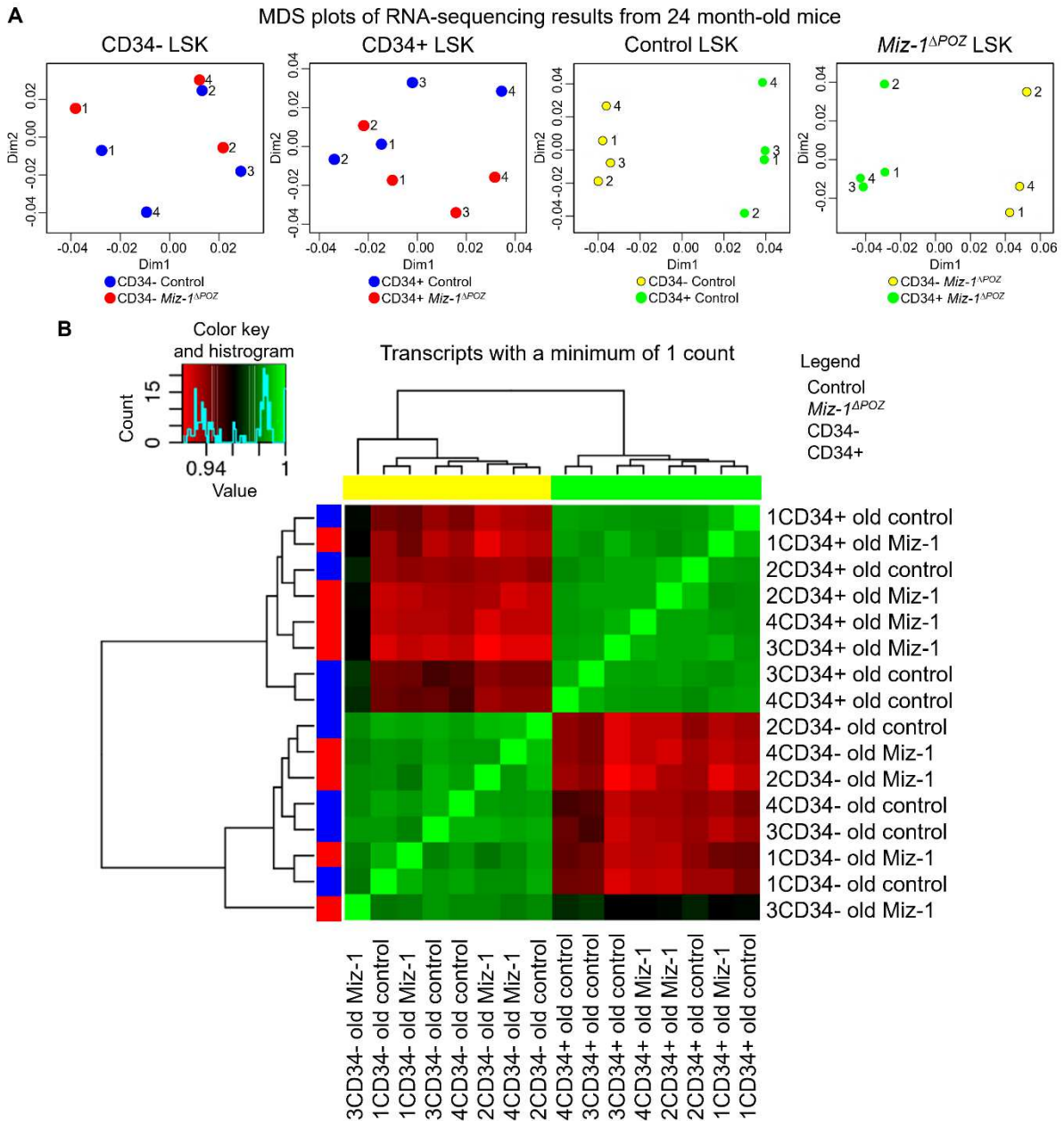
Figure 3.9.: The transcriptional changes induced by *Miz-1* POZ domain knockout in LSK cells are no longer significant in old-aged mice (**A**) MDS plot revealing the characteristics in 2-dimensions of RNA-sequenced samples according to gene expression, measured in read counts. Samples are arranged according to CD34 expression and *Miz-1*^{ΔPOZ} genotype. CD34$^-$ *Miz-1*^{ΔPOZ} samples, *n* = 3; all others, *n* = 4. (**B**) Heat map of sample similarity in terms of gene counts. A heat map displaying comparisons of the spearman correlation of gene counts (for genes with more than one count) per gene for each sample.

Gene ontology analysis using the DAVID online resource did not reveal any terms to be significantly enriched in *Miz-1^{ΔPOZ}* LSKs compared to control in either CD34⁻ or CD34⁺ subsets. When upregulated and downregulated gene lists were submitted to PANTHER for GO analysis, approximately half of the genes submitted were unmapped by PANTHER for each analysis. The only category in which enrichment among upregulated DEGs was observed was in the protein class term immunoglobulin, which was enriched in both CD34⁻ and CD34⁺ LSKs. The only enrichment found among downregulated DEGs was in the biological processes of immune response and phagocytosis, which were enriched in *Miz-1^{ΔPOZ}* CD34⁻ LSKs and in generic differentiation terms, which were enriched in *Miz-1^{ΔPOZ}* CD34⁺ LSKs (Figure 3.9C).

However, when GSEA was performed using the full readout of RNA-sequencing experiments from aged mouse LSKs, we found that in *Miz-1^{ΔPOZ}* CD34⁻ and CD34⁺ LSKs, the Hallmark gene set of interferon alpha response was significantly enriched compared to control (Figure 3.9D). In addition, the gene sets of Myc target genes, E2F targets and interferon gamma response were also enriched in *Miz-1^{ΔPOZ}* CD34⁺ LSKs. Furthermore, Reactome gene sets were also enriched in *Miz-1^{ΔPOZ}* CD34⁺ LSKs: those involved FGFR4 signaling. Notably, the gene sets for interferon alpha and gamma responses that were enriched in aged *Miz-1^{ΔPOZ}* LSKs compared to control had lower enrichment scores than the same comparison in young mice as well as higher p- and q-values. In combination with the fact that analyses on DEGs revealed no clear phenotype in *Miz-1^{ΔPOZ}* LSKs, this indicates that the difference in type I interferon response activity in HSPC between control and *Miz-1^{ΔPOZ}* mice is greatly diminished by 2 years of age.

When DEGs from *Miz-1^{ΔPOZ}* LSKs compared to control were submitted to Ingenuity pathway analysis, details about upstream regulators could not be predicted for either cell type; when they were submitted to STRING, no PPI networks could be created. Furthermore, there were no individual transcripts that were differentially expressed in *Miz-1^{ΔPOZ}* LSKs of both CD34 subsets in young mice that remained so in both subsets of LSKs in aged *Miz-1^{ΔPOZ}* mice (Figure 3.9E). The *Miz-1^{ΔPOZ}* CD34⁻ LSKs of young and aged mice had only 2 DEGs in common: the immunoglobulin light chain mRNA, *IGLC1* and that of *SLCO2A1*. Similarly in CD34⁺ LSKs, the mRNA of *Necdin* and *IRF6* were differentially regulated in both young and aged mice. Only 1 mRNA, that of interferon gamma-induced GTPase (*IGTP*), was differentially expressed in both young *Miz-1^{ΔPOZ}* LSK subsets and *Miz-1^{ΔPOZ}* CD34⁺ LSKs from aged mice (Figure 3.9F). We can therefore conclude that the differences between control and *Miz-1^{ΔPOZ}* LSKs in type I interferon and anti-viral activity have become insignificant in old-aged mice.
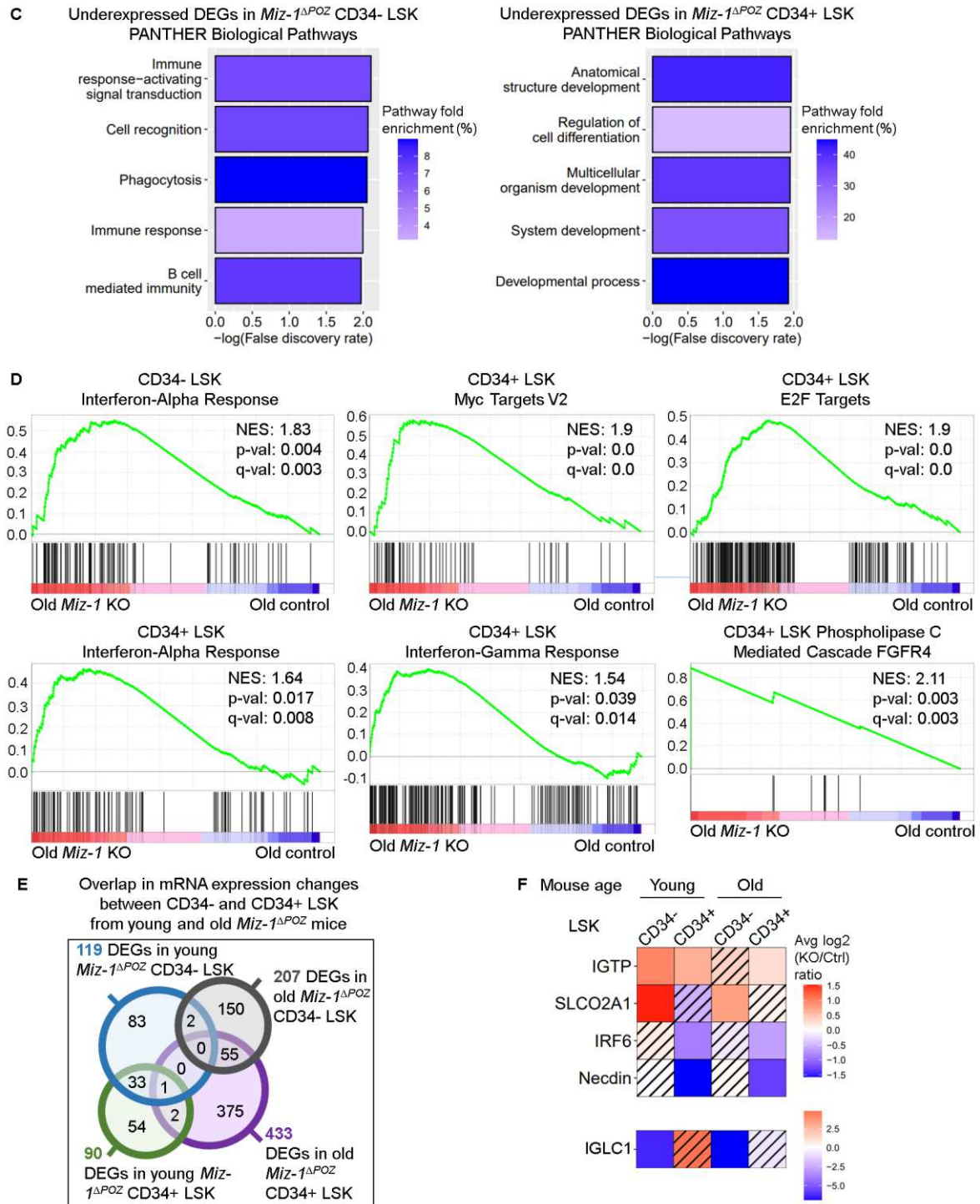
Figure 3.9.: The transcriptional changes induced by *Miz-1* POZ domain knockout in LSK cells are no longer significant in old-aged mice (**C**) Bar graph depicting biological function annotation of genes downregulated by *Miz-1ΔPOZ* mutation using the GO program PANTHER in CD34⁻ LSKs (left) and CD34⁺ LSKs (right) from 2 year-old mice. X-axis shows the negative log of the false discovery rate of the gene ontology term. Gene ontology terms with the lowest FDR are ranked at the top of the graph. The bar graph color represents the percentage of genes of that gene ontology term that were downregulated DEGs in knockout. (**D**) Gene-set enrichment analysis profiles depicting the top „Hallmark" gene signatures enriched upon *Miz-1* POZ domain deletion in CD34⁻ (top left) and CD34⁺ (all others) LSKs in 2 year-old mice, generated with bulk RNA-seq data. NES: normalized enrichment

score. (**E**) Venn diagram representing the overlap in RNA expression changes between LSK subsets of young and aged *Miz-1$^{\Delta POZ}$* mice. (**F**) Heat map of transcripts of *Miz-1$^{\Delta POZ}$*-associated DEGs common to at least one LSK subset in young mice and one LSK subset in aged mice. Color represents the log knockout over control ratio for each transcript RPKM, shaded-out cells have a statistically insignificant fold expression change for the indicated cell type.

We also examined the transcriptional differences in LSKs of both CD34 expression subtypes from young control mice compared to those from their 2 year-old counterparts, to verify that our results are consistent with those of previous studies. As already mentioned, studies have documented that quiescent LSK populations undergo, as mice progress from young to old age, transcriptional changes including an enhancement in biological processes such as the inflammatory response, NF-κB cascade (Chambers et al., 2007) and cell adhesion (Sun et al., 2014), as well as marked decline in gene expression of genes involved in chromatin silencing, cell cycle and DNA repair. Our analysis on CD34$^-$ LSKs from aged control mice robustly affirmed these findings. In control CD34$^-$ LSKs, 9748 genes became differentially expressed in 2 year-old mice compared to 4 month-old mice, while the amount for the same comparison was 662 in CD34$^+$ LSKs. Furthermore, in CD34$^-$ LSK taken from 2 year-old *Miz-1$^{\Delta POZ}$* mice, there were 6337 DEGs in comparison to their young counterparts, and 569 DEGs in *Miz-1$^{\Delta POZ}$* CD34$^+$ LSKs. In CD34$^-$ and CD34$^+$ LSKs, aging induced an expression change in those mRNA transcripts proven to be markers for old HSC in previous studies, such as: *CAVIN2*/*SDPR* (Taiwo et al., 2013), *CLU*, *SELP*, and *APP* (Chambers et al., 2007). In CD34$^-$ LSKs, this included eight different *MCM* transcripts along with *CDKN1A*, *CDKN2C* and *CCNE2* (Noda et al., 2009). Gene ontology analysis using the application DAVID on age-induced genes in control CD34$^-$ LSKs revealed many enriched biological processes, chief among which were protein phosphorylation, DNA transcription, small GTPase and Rho signal transduction, endocytosis, angiogenesis, immunity and NF-κB signaling (Figure 3.9G). Meanwhile, age-repressed genes from control CD34$^-$ LSKs were associated with biological processes including the cell cycle, mRNA and rRNA processing, mitotic cell division, DNA repair and chromatin silencing in rDNA (Figure 3.9H). Furthermore, in control CD34$^+$ LSKs, RNAs which increased in expression from young to old age were associated with immune, anti-viral and inflammatory responses, such as the cellular response to IFN-β; but also, with cell adhesion and cell migration in agreement with previous studies (Figure 3.9I). Only one biological process was associated with age-repressed RNAs in control CD34$^+$ LSKs: that of the cell cycle (data not shown). Aging affected the RNA expression of *Miz-1$^{\Delta POZ}$* CD34$^-$ LSK of mice in a similar fashion (Figure S8C), however immune system processes and NF-κB signaling were much less enriched than in control. Emphasizing these findings were the results of GSEA analysis: in CD34$^-$ LSKs, aging produced an enrichment in the TNF-α via NF-κB and angiogenesis Hallmark gene sets, while in CD34$^+$ LSK, the most enriched gene set was that of interferon alpha response (Figure 3.9J). When gene counts from *Miz-1$^{\Delta POZ}$* CD34$^-$ LSKs were subject to GSEA however, results differed, showing that hypoxia and myogenesis processes were the most enriched among Hallmark gene sets (Figure S8D).

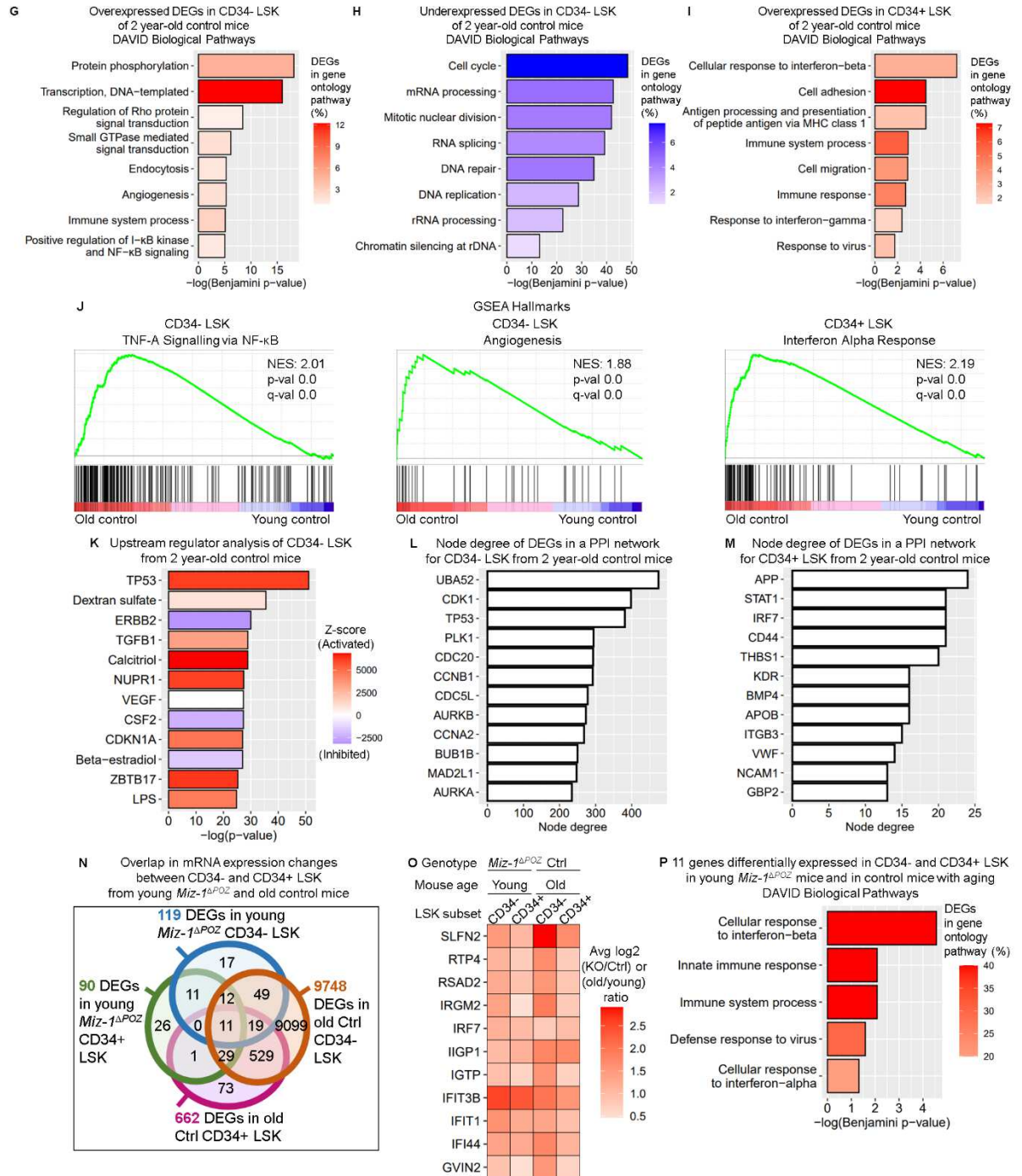**Figure 3.9.: The transcriptional changes induced by *Miz-1* POZ domain knockout in LSK cells are no longer significant in old-aged mice** (**G**) Bar graph presenting the biological function annotation of genes upregulated in 2 year-old control mice compared to young control mice in CD34⁻ LSKs, using the DAVID gene ontology application. X-axis shows the negative log of the Benjamini p-value of the gene ontology term. Gene ontology terms with the lowest Benjamini p-value are ranked at the top of the graph. Color of the bar graph represents the percentage of genes of that gene ontology term that were upregulated DEGs in aged mice. (**H**) as in (**G**) but for downregulated genes. (**I**) as in (**G**) but for CD34⁺ LSKs. (**J**) Gene-set enrichment analysis profiles depicting the top „Hallmark" gene signatures enriched in 2 year-old control mice compared to young control mice in CD34⁻ (left and middle) and CD34⁺ (right) LSKs, generated with bulk RNA-seq data. NES: normalized enrichment score. (**K**) Bar graph

representing Ingenuity upstream regulator analysis of DEGs in CD34⁻ LSKs from 2 year-old control mice compared to young control mice. Shown are the 12 regulators with the lowest p-value for both cell types. Red are regulators predicted to be activated and blue represents predicted inhibition. (**L**) Bar graph of node degree (number of bridges) for each gene (node) in the PPI network of DEGs in CD34⁻ LSKs from 2 year-old control mice. (**M**) as in (**L**) but for CD34⁺ LSKs. (**N**) Venn diagram representing the overlap in RNA expression changes between LSK subsets of young *Miz-1^ΔPOZ* and aged control mice, compared to young control mice. (**O**) Heat map of genes that are differentially expressed in common from young control mice to aged control and young *Miz-1^ΔPOZ* in both CD34⁻ and CD34⁺ LSKs. Color represents the log knockout over control ratio or old control over young control ratio for each transcript RPKM, shaded-out cells have a statistically insignificant fold expression change for the indicated cell type. (**P**) as in (**G**) but for the 11 common genes differentially expressed in both LSK subsets of young *Miz-1^ΔPOZ* and aged control mice, compared to young control mice.

To infer the key regulators responsible for these transcriptional changes over the course of aging in control LSKs, we subjected our DEG lists to upstream regulator analysis with Ingenuity software; only data from CD34⁻ LSKs produced reliable results. We found that the most highly represented key regulator was p53 (Figure 3.9K), predicted to be activated, as was the second most represented regulator, the polysaccharide dextran sulfate, while predicted to be inactivated was Erbb2 (Her2). Of further interest, other upstream regulators found to be enriched were TGF-β, which was found to be an upstream regulator of HSC aging in another study (Sun et al., 2014), NUPR1 and even ZBTB17 (Miz-1). Similar results were found in *Miz-1^ΔPOZ* CD34⁻ LSKs from aged mice (Figure S8E).

To extract information on which protein products of these RNAs may be driving the age-associated phenotype of HSPCs, a PPI network was generated in Cytoscape using DEG lists for the young-to-old comparison of each LSK subset and mouse genotype (data not shown). For control CD34⁻ LSKs, the largest subnetworks formed from age-associated gene expression changes were: mitotic cell cycle, ubiquitination and proteasome, mRNA splicing, ribosome biogenesis and rRNA processing and oxidative phosphorylation. Whereas, for control CD34⁺ LSKs, the major two subnetworks were those associated with interferon signaling and Rho GTPase signaling. Networks generated from the same comparisons in *Miz-1^ΔPOZ* mice were similar, but with alterations in the ranking of subnetworks by size (data not shown). The PPI networks for these comparisons were then subject to degree distribution analysis to infer the relative importance of each DEG in the network from their respective number of predicted interactions with other DEGs. In the PPI network generated from CD34⁻ LSKs from aged mice compared to young mice, the node with the highest degree was *UBA52*, a gene with little known connection to aging, followed by *CDK1* (Figure 3.9L). This gene was included among many cell cycle and mitotic division regulators, which is highly reassuring as cell cycle gene expression has been shown by a single-cell RNA-seq approach to be the main source of variation between young and old HSCs (Kowalczyk et al., 2015), including those with established roles in HSC aging, such as *TP53* (Chambers et al., 2007), *BUB1B* (Beerman et al., 2014) and the epigenetic modifiers *AURKA* and *AURKB* (Sun et al., 2014). Meanwhile, a node degree analysis likewise generated for age-dependent gene expression change in control

CD34$^+$ LSKs found that the most interconnected DEG was the marker for senescent HSCs, the gene *APP*, followed by inflammatory regulators *STAT1* and *IRF7* (Figure 3.9M). When this analysis was applied to *Miz-1$^{\Delta POZ}$* CD34$^-$ LSKs, the topmost nodes were again cell cycle genes (Figure S8F), while in *Miz-1$^{\Delta POZ}$* CD34$^+$ LSKs the node with highest degree was the HSPC differentiation-associated gene *RPS27A*, which has been associated with aging in other models (Figure S8G).

We wanted to assess whether the transcriptional changes associated with type I interferon and anti-viral response pathways resulting from *Miz-1* POZ domain deficiency in the LSKs of young mice constitute an age-related phenotype. Therefore, we looked for overlap in genes that were altered in expression both in LSKs from aged control mice and in *Miz-1$^{\Delta POZ}$* LSKs from young mice, relative to the LSKs of their respective young mice controls. In young mice, there were 119 genes that were differentially expressed in *Miz-1$^{\Delta POZ}$* CD34$^-$ LSKs compared to controls, but 91 (76%) of these genes are also differentially expressed in the CD34$^-$ LSKs of aged control mice (Figure 3.9N). *Miz-1$^{\Delta POZ}$* CD34$^-$ LSKs also shared 40 (34%) DEGs with CD34$^+$ LSKs of aged control mice, while *Miz-1$^{\Delta POZ}$* CD34$^+$ LSKs had 52 (58%) and 41 (46%) DEGs in common with the CD34$^-$ and CD34$^+$ LSKs of aged control mice, respectively. Therefore, a subset of age-related gene expression changes are strongly overrepresented in *Miz-1$^{\Delta POZ}$* LSKs. Of these genes, there were 11 that were differentially expressed in all four of these comparisons with LSKs from young control mice, all of which were overexpressed (Figure 3.9O). When these 11 genes were submitted to gene ontology analysis using the application DAVID, the biological processes they were associated with were the cellular response to interferons, innate immunity and the response to viruses (Figure 3.9P). These data indicate that an activated immune and anti-viral response mediated by interferon pathways is an age-related phenotype of HSPCs which is present in *Miz-1$^{\Delta POZ}$* LSKs.

In an attempt to confirm this by qPCR, we isolated RNA from the LSKs of young and aged mice of both genotypes and measured the fold expression changes in the mRNAs *OAS3*, *IRF7* and *MX1*, which are involved in the interferon and anti-viral responses. The data shown here for *IRF7* and *OAS3* expression changes in young mice have already been shown in Figures 3.6F and 3.6G. We confirmed our earlier RNA-sequencing results indicating that *MX1* mRNA is induced by *Miz-1* POZ domain loss, but interestingly found that *MX1* expression falls in *Miz-1$^{\Delta POZ}$* CD34$^-$ LSK with age (Figure 3.9Q). While *IRF7* appeared to rise in expression level in control LSKs with age, as well as *OAS3* in CD34$^-$ control LSKs, these changes did not reach statistical significance.

We were intrigued by the association between Miz-1 and age-related changes; in particular, the induction of an accumulation of HSCs, MPP1 and myeloid progenitor cells when *Miz-1* function is deficient, the identification of Miz-1 as a potential regulator of young-to-old mRNA expression changes in our Ingenuity upstream regulator analysis and the, albeit statistically insignificant, decrease in expression of *Miz-1* mRNA in quiescent LSK of aged mice shown in a study by Chambers et al. (Chambers et al., 2007). Furthermore, a trend of reduced *Miz-1*

mRNA expression in aged mice was observed in our own RNA-sequencing data (Figure S8H). To investigate a putative change in Miz-1 activity over the course of HSC aging, we attempted to verify the potential differential expression of *Miz-1* mRNA in young versus old HSCs by isolating HSCs (CD34⁻ CD48⁻ CD150⁺ LSKs) from 4 month-old and 24 month-old mice for qPCR using primers targeting the exon 6- and exon 7-spanning region of the *Miz-1/ZBTB17* gene. The result of this experiment suggested a trend of decreased expression of *Miz-1* in HSCs in aged mice compared to young mice, however this was not statistically significant. Furthermore, we also verified the successful knockout of the POZ domain in our *Miz-1^{ΔPOZ}* mice of both young and old ages, by isolating RNA from CD34⁻ and CD34⁺ LSKs from young and aged mice and performing qPCR using primers targeting the POZ domain region of the *Miz-1/ZBTB17* gene, showing that *Miz-1^{ΔPOZ}* mice of either age group do not express *Miz-1* mRNA containing the POZ domain in either LSK cell type (Figure 3.9R), but also showing no age-related change in expression in control mice.

These results show that the phenotype of activated type I interferon response and anti-viral response pathway observed in the LSKs of young *Miz-1^{ΔPOZ}* mice disappears with aging. Our analysis of transcriptional changes in the HSPCs of aged mice is supported by its verification of previous studies. We've found that Miz-1 represses the expression of interferon pathways that are overexpressed in the CD34⁻ and CD34⁺ LSKs of aged mice, and may therefore be a regulator of aging, as our upstream analysis suggests, despite the lack of a confirmed drop in expression levels of *Miz-1* mRNA in HSCs. The hypothesis that Miz-1 regulates HSC aging by restraining the interferon-mediated and anti-viral responses must be tested further.
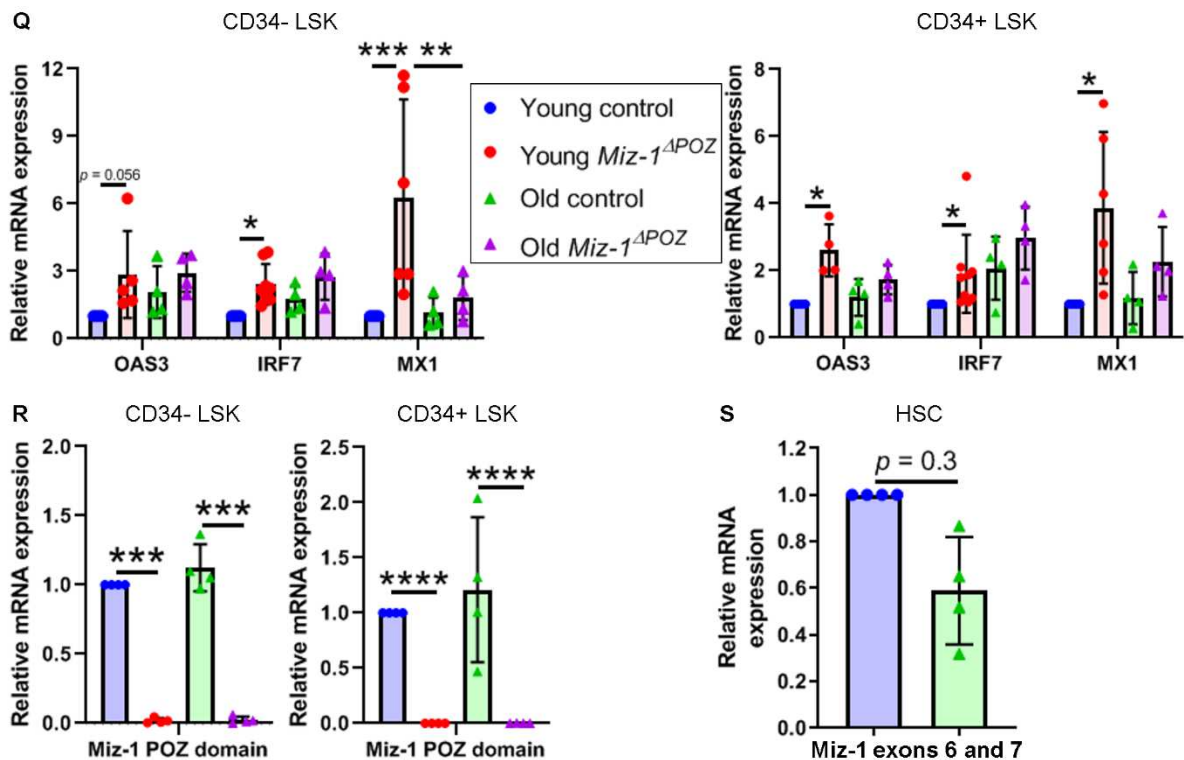
Figure 3.9.: The transcriptional changes induced by *Miz-1* POZ domain knockout in LSK cells are no longer significant in old-aged mice (**Q**) Bar graph overlaid with dot-plot of qPCR results documenting the expression of selected mRNAs altered in expression level by *Miz-1$^{\Delta POZ}$* mutation in CD34$^-$ (left) and CD34$^+$ (right) LSKs from young and old mice. Graphs of *IRF7* and *OAS3* expression show data pooled from two different experiments. $n = 8$ (*IRF7*, young samples), $n = 5$ (*OAS3*, young CD34$^-$ LSK), $n = 4$ (all others); error bars represent mean ± SD; *: $p < 0.05$, **: $p < 0.005$, ***: $p < 0.001$; *t* test. (**R**) Bar graph overlaid with dot-plot of qPCR results of the expression of *Miz-1* POZ domain in CD34$^-$ (left) and CD34$^+$ (right) LSKs from young and aged mice of both genotypes. $n = 4$; error bars represent mean ± SD; ***: $p < 0.001$, ****: $p < 0.0001$; *t* test. (**S**) Bar graph overlaid with dot-plot of qPCR results representing the expression of *Miz-1* mRNA across exons 6 and 7 in HSCs from young and aged control mice. $n = 4$; error bars represent mean ± SD.

3.10 Miz-1 does not modulate the phosphorylation of STAT1 in response to interferon in LSKs

We wished to find a molecular mechanism for our findings and therefore looked to the upstream regulator and canonical pathway predictions in Ingenuity software for suggestions as to which molecular signaling pathways may be altered in *Miz-1$^{\Delta POZ}$* LSKs. In both CD34$^-$ and CD34$^+$ LSKs, STAT1 activity and interferon signaling were suggested to be altered in *Miz-1$^{\Delta POZ}$* mice. Gene ontology analysis also showed that response to interferon pathways were highly enriched. To corroborate the involvement of STAT1 in producing the phenotype seen in *Miz-1$^{\Delta POZ}$* LSKs, we measured the intracellular phosphorylation state of STAT1 in response to stimulation by interferons alpha and gamma in LSKs by flow cytometry. The stimulation of either IFN-α or IFN-γ caused efficient phosphorylation of STAT1 in LSKs, whether isolated from control or *Miz-1$^{\Delta POZ}$* mice (Figures 3.10A, 3.10C). We observed no difference in phosphorylation of STAT1 in *Miz-1$^{\Delta POZ}$* LSKs compared to controls in response to either IFN-α or IFN-γ (Figure 3.10B, 3.10D). Of further note, in our RNA-sequencing results from young mice, *STAT1* mRNA was increased in expression level, albeit with a DESeq p-value that narrowly missed our significance threshold in both *Miz-1$^{\Delta POZ}$* LSK cell types: 0.058 in CD34$^-$ LSKs, 0.055 in CD34$^+$ LSKs.

These results demonstrate that, while both control and *Miz-1$^{\Delta POZ}$* LSKs are able to phosphorylate STAT1 in response to IFNs, *Miz-1$^{\Delta POZ}$* LSKs show no different a level of phosphorylation of STAT1 in response to either IFN, eliminating altered STAT1 sensitivity as an explanation for the phenotype of *Miz-1$^{\Delta POZ}$* LSKs.
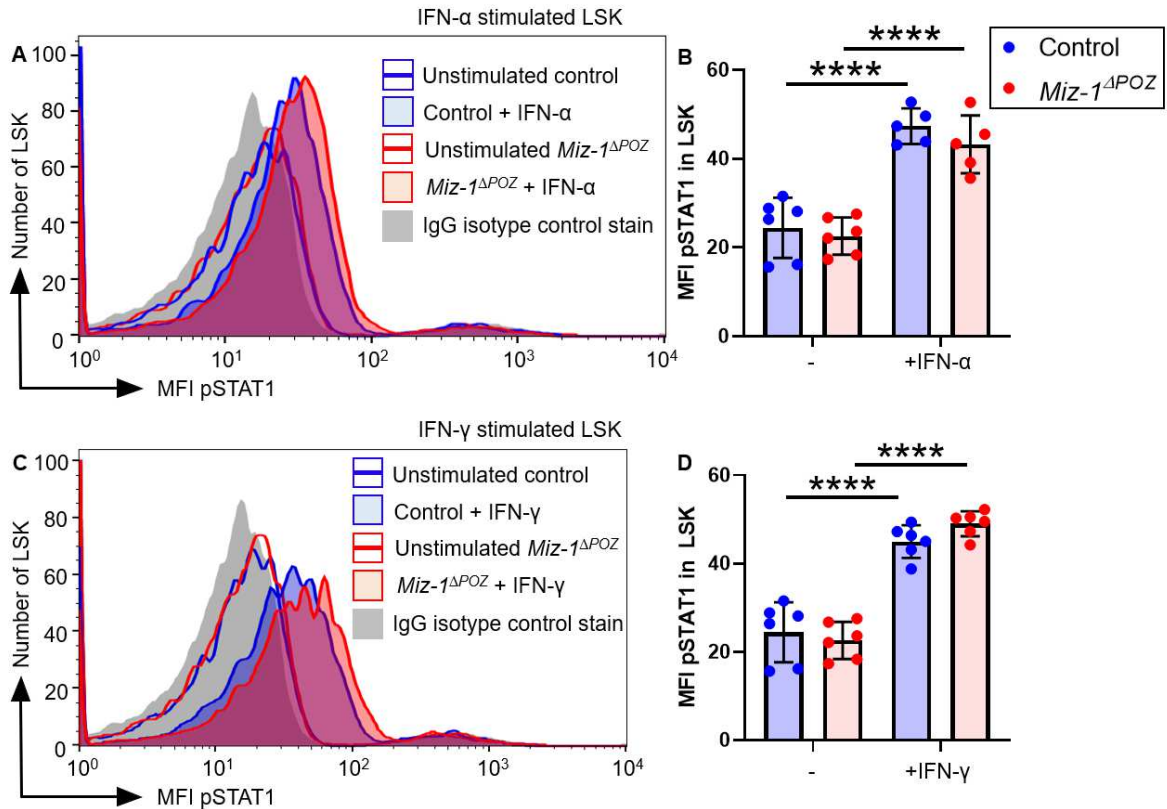
Figure 3.10.: Miz-1 does not modulate the phosphorylation of STAT1 in response to interferon in LSKs (**A**) Representative FACS histograms of the mean fluorescence intensity (MFI) of phosphorylated STAT1-specific fluorescence after IFN-α stimulation versus number of LSKs. Empty colored line graphs represent unstimulated LSKs, filled colored line graphs represent LSKs stimulated with IFN-α and the grey histogram represents LSKs stained with IgG isotype control antibody. (**B**). Bar graphs overlaid with dot plot of the MFI of phosphorylated STAT1 in IFN-α-stimulated control and *Miz-1^{ΔPOZ}* LSKs. $n = 6$ (unstimulated), $n = 5$ (stimulated), mean ± SD; **: $p < 0.01$; 2-way ANOVA test. (**C**). As in (**A**), but for IFN-γ stimulated samples. (**D**) Bar graphs overlaid with dot plot of the MFI of phosphorylated STAT1 in IFN-γ-stimulated control and *Miz-1^{ΔPOZ}* LSKs. $n = 6$, mean ± SD; *: $p < 0.05$; ***: $p < 0.001$; ****; $p < 0.0001$, 2-way ANOVA test.

3.11 *Miz-1* POZ domain deficiency results in diminished thrombopoietin-mediated STAT5 phosphorylation in LSKs

Previous studies have shown that a POZ domain knockout of *Miz-1* results in a phenotype mediated by altered STAT5 phosphorylation in various cell types (Kosan et al., 2010), (Saba et al., 2011), (Sanz-Moreno et al., 2014). Our results also suggest that Miz-1 influences phosphoprotein activity in LSKs. To find out if defective STAT5 phosphorylation is associated with *Miz-1* POZ domain deletion in LSKs, we assessed the efficacy of thrombopoietin-mediated intracellular STAT5 phosphorylation by flow cytometry (Figure 3.11A). This was done in sorted control LSKs, in which thrombopoietin stimulation efficiently resulted in an increase in the MFI of phosphorylated STAT5, whereas in *Miz-1^{ΔPOZ}* LSKs, STAT5 did not show statistically significant phosphorylation by thrombopoietin (Figure 3.11B).

These data suggest that lack of Miz-1 transcription factor function results in a disruption in post-thrombopoietin signaling prior to phosphorylation of STAT5 in HSPCs.
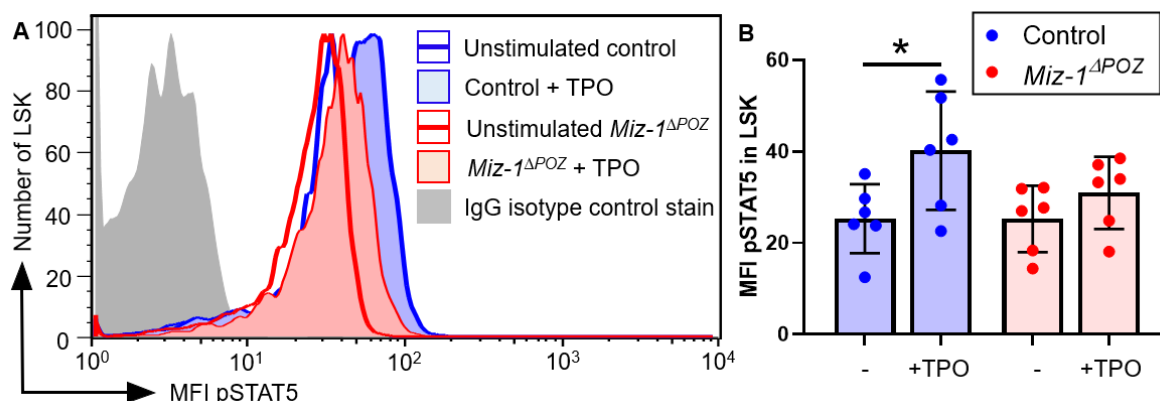
Figure 3.11.: *Miz-1* POZ domain deficiency results in diminished thrombopoietin-mediated STAT5 phosphorylation in LSKs (**A**) Representative FACS histograms of the mean fluorescence intensity (MFI) of phosphorylated STAT5-specific fluorescence versus number of LSKs. Colored line graphs represent unstimulated LSKs, filled line graphs with color represent LSKs stimulated with TPO and the grey histogram represents LSKs stained with IgG isotype control antibody. (**B**). Bar graphs overlaid with dot plot of the MFI of phosphorylated STAT5 in TPO-stimulated control and *Miz-1^{ΔPOZ}* LSKs. n = 6, mean ± SD; *: $p < 0.05$; 2-way ANOVA test.

3.12 The relative expansion of *Miz-1^{ΔPOZ}* LSKs disappears on *in vitro* LPS stimulation

Our gene ontology analysis using DAVID on RNA-sequenced LSKs revealed that the lipopolysaccharide response gene signature is upregulated. Likewise, LPS was predicted to be an upstream regulator of the knockout phenotype from RNA-sequencing data by Ingenuity pathway analysis. In an effort to provide a molecular basis for explaining the relative expansion of HSPCs in *Miz-1^{ΔPOZ}* mice seen in our flow cytometry experiments, we sought to find out if stimulating the anti-bacterial response pathway, stimulated by LPS in lineage marker-depleted cells, results in altered expansion of *Miz-1^{ΔPOZ}* LSKs compared to control. Hence, we depleted bone marrow cells of lineage marker-positive cells and placed them for 18 hours in DMEM media, followed by incubation with LPS at a concentration gradient and measured the percentage of LSKs among lineage-negative cells by FACS analysis (Figure 3.12A).

LSKs from control mice showed a statistically significant expansion as a percentage of lineage-negative cells when cultured in a concentration of 50 ng/mL LPS or greater, from 1.9% without LPS to 10.7% at 200 ng/mL LPS (Figures 3.12B, 3.12C). Similarly, *Miz-1^{ΔPOZ}* LSKs expanded from 4.4% of lineage-negative cells without LPS stimulation to 13.2% with 200 ng/mL LPS. This expansion was statistically significant only at concentrations above 10 ng/mL for control LSKs and at 50 ng/mL or above for *Miz-1^{ΔPOZ}* LSKs. Under unstimulated conditions, the percentage of LSKs among lineage-negative cells from *Miz-1^{ΔPOZ}* mice was significantly

higher compared to control (Figure 3.12C). However, the statistical significance of this difference was no longer present when lineage-negative cells were stimulated with 10 ng/mL or higher concentrations of LPS for 18 hours in DMEM. Therefore, *Miz-1^{ΔPOZ}* lineage-negative bone marrow cells having a greater proportion of LSKs than control was dependent on LPS stimulation *in vitro*.

These results suggest that the lipopolysaccharide-response signaling pathway, which triggers LSKs and HSPCs to proliferate, may be partially responsible for the greater number of LSKs, MPPs and HSCs seen in *Miz-1^{ΔPOZ}* mouse bone marrow. However, these results may be misleading due to the large amount of variation in these data. This experiment requires improvement and would need to be combined with further experiments to draw a clear conclusion.
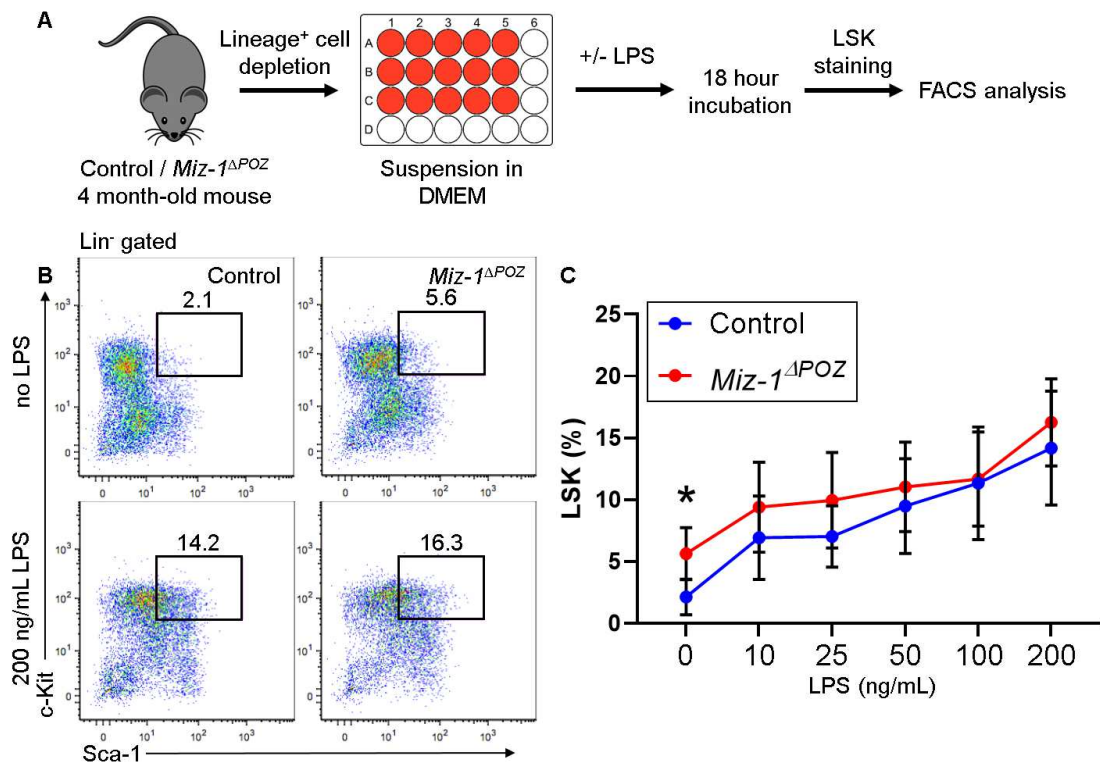
Figure 3.12.: The relative expansion of *Miz-1^{ΔPOZ}* LSKs disappears on *in vitro* LPS stimulation (**A**) Schematic of the experimental set-up of the *in vitro* LPS stimulation of LSKs. Between 1.5×10^5 to 2.5×10^5 lineage⁻ (Lin⁻) BM cells were deposited in a plate before incubation for 18 hours with the amount of LPS indicated in the below figures. Cells were then harvested and stained for LSK markers and acquired by flow cytometry. (**B**) Representative FACS plots of control (top) and 200 ng/mL LPS-stimulated (bottom) control and *Miz-1* KO bone marrow with LSK cells resolved. The proportion of gated cells as a percentage of living lineage-negative cells are shown beside gates. (**C**) Line graph of control and *Miz-1^{ΔPOZ}* LSKs as a percentage of living Lin⁻ cells at rising concentrations of LPS. $n = 5$, mean ± SD; *: $p < 0.05$, *t* test.

3.13 *Miz-1* POZ domain deficient LSKs do not have heightened DNA damage or cytosolic single-stranded DNA

The type I interferon signaling pathway is known to be induced by the appearance of cytosolic DNA due to DNA damage in hematopoietic cells (Härtlova et al., 2015). In an effort to explain the upregulated type I interferon signaling response seen in *Miz-1$^{\Delta POZ}$* LSKs, we decided to assay phospho-γH2A.X as a measure of the extent of DNA damage in sorted LSKs by immunofluorescence and flow cytometry. We began by sorting and dividing LSKs into un-irradiated and irradiated groups for flow cytometry. The irradiated groups were divided further into those left to rest after irradiation for 1 hour and 6 hours in SFEM media at 37°C before staining, in order to find if the *Miz-1$^{\Delta POZ}$* affects the amount of DNA damage repaired post-irradiation. In both control and *Miz-1$^{\Delta POZ}$* LSKs, 2 Gray of irradiation efficiently induced the phosphorylation of γH2A.X (Figures 3.13A, 3.13B). However, we did not find any differences between control and *Miz-1$^{\Delta POZ}$* LSKs in the level of γH2A.X phosphorylation under any conditions: those un-irradiated, those stained 1 hour post-irradiation or those stained 6 hours post-irradiation. Of further note, the level of γH2A.X phosphorylation in LSKs 6 hours post-irradiation was lower than those acquired after only 1 hour post-irradiation in both genotypes, indicating that γH2A.X was appropriately stained.

We wished to verify these findings by directly counting immunofluorescently stained γH2A.X foci. As before, sorted LSKs were left un-irradiated before staining, or irradiated and stained 1 or 6 hours post-irradiation with γH2A.X antibody or IgG control. Irradiation strongly induced the appearance of γH2A.X foci in both control and *Miz-1$^{\Delta POZ}$* LSKs however, no differences between control and *Miz-1$^{\Delta POZ}$* LSKs were found under any condition (Figure 3.13C). While *Miz-1$^{\Delta POZ}$* LSKs showed a tendency to have fewer foci 1 hour or 6 hours after irradiation relative to control, these differences were not statistically significant (Figure 3.13D). As before, 2 Gray irradiation induced a statistically significant increase in the number of γH2A.X foci, which then showed significant decline 5 hours afterwards in both genotypes.

Furthermore, we investigated the potential presence of single-stranded DNA (ssDNA) in the cytosol *Miz-1$^{\Delta POZ}$* LSKs, due to Ingenuity software analyses of our RNA-sequencing data indicating that molecules responding to ssDNA may be altered in their activation (Figure 3.6O). The presence of cytosolic ssDNA in hematopoietic cells is known to trigger activation of the type I interferon response (Härtlova et al., 2015). Therefore, we stained LSKs with the F7-26 anti-ssDNA antibody or no primary antibody control to determine the presence of ssDNA in the cytosol of LSKs by immunofluorescence. In either control or *Miz-1$^{\Delta POZ}$* LSKs, we did not detect any ssDNA signal above that of no-primary antibody controls (Figure 3.13E). Hence, we were unable demonstrate the presence of ssDNA in the cytosol of LSKs.

These results show that the phenotype of activated interferon signaling in *Miz-1^{ΔPOZ}* LSKs cannot be attributed to the presence of cytosolic DNA, of DNA damage or the delayed repair of such damage.
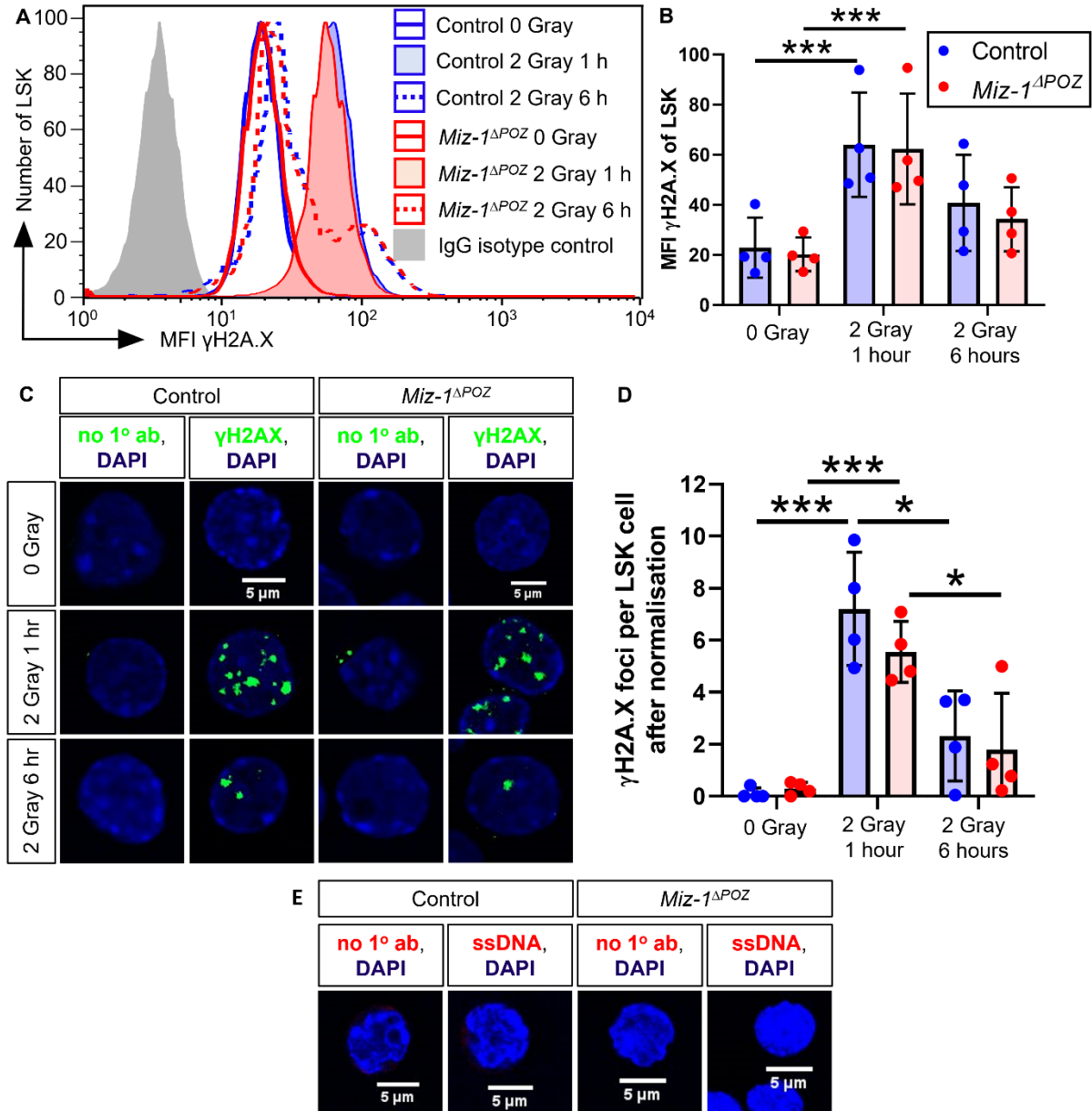
Figure 3.13.: ***Miz-1* POZ domain deficient LSKs do not have heightened DNA damage or cytosolic single-stranded DNA** (**A**) Representative FACS histogram of the MFI of phosphorylated γH2A.X-specific fluorescence versus number of LSKs. Colored line graphs with no fill represent un-irradiated LSKs, colored line graphs filled with color represent 2 Gray irradiated LSKs after 1 hour, colored dotted line graphs represent LSKs 6 hours after 2 Gray of irradiation and the grey histogram represents LSKs from each condition stained with IgG isotype control antibody. (**B**) Bar graphs overlaid with dot plot of the MFI of phosphorylated γH2A.X in control and *Miz-1^{ΔPOZ}* LSKs that are un-irradiated, 1 hour after irradiation or 6 hours after irradiation, $n = 4$, mean ± SD; ***: $p < 0.001$; 2-way ANOVA test. (**C**) Immunofluorescent staining of γH2A.X foci in sorted LSKs attached to polylysine-coated glass slides. Scale bars represent 5 μm. No 1° ab stains refer to those that were stained with only the Alexa Fluor-

488 secondary antibody and no anti-γH2A.X antibody. Middle row shows cells stained 1 hour after irradiation; bottom row 6 hours after. (**D**) Bar graphs overlaid with dot plot of the mean number of γH2A.X foci in control and *Miz-1^{ΔPOZ}* LSKs that are un-irradiated, 1 hour after irradiation or 6 hours after irradiation. $n = 4$, mean ± SD; *: $p < 0.05$; t test. (**E**) Immunofluorescent staining of ssDNA in sorted LSKs attached to polylysine-coated glass slides. Scale bars represent 5 μm. No 1° ab stains refer to those that were stained with only the Alexa Fluor-488 secondary antibody and no anti-γH2A.X antibody.

4. Discussion

We have demonstrated that loss of Miz-1 transcriptional activity in HSCs results in an expansion of Sca-1 high-expressing subsets of lineage-negative cells (Figure 3.1A): among LSKs, HSCs and MPP subtypes all expand at least 2-fold (Figure 3.1D) despite a 28% loss of bone marrow cellularity (Figure 3.1J). While CD41 is overexpressed on the surface of *Miz-1$^{\Delta POZ}$* pHSCs and MPPs (Figure 3.1I), CD41-negative populations did also expand, illustrating that CD41 expression was not a prerequisite for *Miz-1$^{\Delta POZ}$*-dependent expansion (Figure 3.1F, 3.1G, 3.1H). A differential rate of apoptosis is not believed to play a role in the relative expansion of *Miz-1$^{\Delta POZ}$* HSPCs as no difference was detected at the LSK level (Figure 3.1L). Myeloid and lymphoid progenitors CMPs, GMPs, MEPs, LMPPs and CLPs were between 2- and 3-fold enriched in number in *Miz-1$^{\Delta POZ}$* mice compared to controls (Figures 3.1H, 3.3B, 3.3E), while neutrophils were 1.4-fold depleted (Figure 3.4A). We also recapitulated the huge loss of lymphocytes in *Miz-1$^{\Delta POZ}$* mice, which has been accounted for by a previous study. We found that *Miz-1$^{\Delta POZ}$* mice had 20% fewer quiescent cells in the G0 phase of the cell cycle as a percentage of HSCs, while having 18% more HSCs in the G1 phase and 2% more synthesizing DNA, than control mice (Figure 3.2B). As a percentage of MPP3 cells, *Miz-1$^{\Delta POZ}$* mice had 4% more in the S phase than controls (Figure 3.2C). No statistical differences in cell cycle phase between control and *Miz-1$^{\Delta POZ}$* mice were found in any other cell type. BM cells from *Miz-1$^{\Delta POZ}$* mice were found to be hugely deficient in their ability to form myeloid and erythroid colony types (Figures 3.5A, 3,5B, 3.5C). To summarise our RNA-sequencing results, they demonstrated that *Miz-1$^{\Delta POZ}$* LSKs bore more transcriptomic similarity to control CD34$^+$ LSKs than CD34$^-$ LSKs from control mice did (Figure 3.6C), while also showing that the expression of Miz-1 target genes are disrupted in *Miz-1$^{\Delta POZ}$* LSKs (Figure 3.6D) and that IFN and antiviral response genes are overexpressed (Figures 3.6E, 3.6H, 3.6J, 3.6K). Our proteomics experiment found that loss of the Miz-1 POZ domain in LSKs results in a derepression in translation machinery and rRNA processing as well as disruption to subnetworks of proteins involved in vesicular trafficking, respiratory electron transport, muscle contraction and RNA processing (Figure 3.7J), while bioinformatics analysis indicated involvement of Myc (Figure 3.7N) and the antiviral response (Figure 3.7L). In the HPC-5 cell line, we demonstrated that Miz-1 binds the transcriptional start site of *KDM8*, but did not find binding at the transcription start sites of either *IRF7* or *IFIT3* (Figure 3.8A). Our findings discounted double-stranded DNA damage playing a role in the *Miz-1$^{\Delta POZ}$* phenotype of LSK cells, as neither flow cytometric nor immunofluorescent means of measurement showed any difference between control and *Miz-1$^{\Delta POZ}$* cells, even though we used antibodies recognising different antigens (Figures 3.13B, 3.13D). Of interest, we showed that STAT5 in control LSKs is phosphorylated by TPO stimulation, but not *Miz-1$^{\Delta POZ}$* LSKs (Figure 3.11B). While demonstrating that both IFN-α and IFN-γ efficiently phosphorylate STAT1 in both control and *Miz-1$^{\Delta POZ}$* LSKs, we found no difference in phosphorylation of STAT1 by IFNs in *Miz-1$^{\Delta POZ}$* LSKs compared to controls (Figure 3.10D). We also performed an *in vitro* experiment whose results should be treated as preliminary, appearing to show that the greater

proportion of LSKs relative to Lin⁻ cells in *Miz-1^{ΔPOZ}* mice compared to control mice disappears when Lin⁻ cells are cultured with LPS (Figure 3.12C), leaving open the possibility that the relative expansion of *Miz-1^{ΔPOZ}* LSKs *in vivo* is due to TLR signaling.

4.1 Miz-1 represses the expression of interferon response genes in LSK cells

Our RNA-sequencing results and their overlap with the results of our proteomics analysis demonstrated that interferon-mediated inflammatory responses are activated at both the mRNA and protein levels in *Miz-1^{ΔPOZ}* LSKs (Figures 3.6I, 3.6J, 3.6K, 3.7L, S7A, S7B). Miz-1 POZ domain ablation is known to induce the expression of "a group of genes, usually expressed during an immune response" in mammary epithelial cells (Sanz-Moreno et al., 2014), as well as IFN response genes in pancreatic adenocarcinoma cells (Muthalagu et al., 2020), showing that the suppression of the immune response by Miz-1 we've demonstrated agrees with established results in other cell types. When existing studies are looked at comprehensively, this transcriptional response can be interpreted to account for the phenotypes we see in *Miz-1^{ΔPOZ}* HSPCs.

In vivo direct administration of IFN-γ has not only been shown to expand the LSK compartment when administered to mice (Zhao et al., 2010), (Schürch et al., 2014), but deficiency in the function of its receptor results in a drop in HSC and MPP cell numbers at homeostasis compared to controls (MacNamara, Jones, et al., 2011). Furthermore, bacterial infection results in expansion of HSC and MPP cell populations dependently on the IFN-γ receptor (Baldridge et al., 2010). While IFN-α administration has not to date been shown to result in an expansion in absolute numbers of HSCs, it is shown in MPPs (Pietras et al., 2014), (Essers et al., 2009). The expansion of HSCs, MPP1, MPP2 and MPP3 cells seen in *Miz-1^{ΔPOZ}* mice (Figures 3.1B, 3.1D) being the result of a transcriptional type I IFN response is therefore consistent with these studies.

HSCs are also known to leave quiescence in response to IFN-α exposure (Pietras et al., 2014), (Essers et al., 2009) and LSKs become more represented in the S phase of the cell cycle after IFN-γ administration to mice (Zhao et al., 2010). Furthermore, IFN-γ receptor function is necessary for HSC entry into the cell cycle in response to viral infection (Matatall et al., 2014) as well as the increase in CD150⁺ LSK proliferation (as well as LSK cells as a whole) that follows bacterial infection (Baldridge et al., 2010), (Zhang et al., 2013). Our observation that Miz-1 deficiency results in fewer quiescent and more DNA synthesizing HSCs (Figure 3.2B) is therefore a phenocopy of the cellular response to IFN.

Direct treatment of BM cells with IFN-γ or IFN-α is well documented to result in a substantial reduction in CFU plating capacity (Zhao et al., 2010), (Snoeck et al., 1994), (Broxmeyer et al., 1983), (Snoeck et al., 1993), (Zeng et al., 2021) and colony size (Pietras et al., 2014), allowing us to conclude that the hugely deleterious effect of Miz-1 POZ domain loss on the colony forming efficiency of BM cells (Figures 3.5A, 3.5B, 3.5C) owes to the transcriptional interferon response

phenotype that *Miz-1^ΔPOZ* HSPCs show. The depletion of BM cells of *Miz-1^ΔPOZ* mice (Figure 3.1J) also phenocopies IFN-α exposure. For example supplementing mice with IFN-α results in BM hypoplasia (Pietras et al., 2014) of a very similar degree to that observed in *Miz-1^ΔPOZ* mice.

The expansion of CMP and GMP cells in *Miz-1^ΔPOZ* mice (Figure 3.3B) could be explained by the interferon response of *Miz-1^ΔPOZ* LSKs due to the fact that both expand in response to IFN-γ treatment (Zhao et al., 2010), (Mucci et al., 2021), (Schürch et al., 2014). While dsRNA-induced IFN-α signaling has been shown to also have the same effect on GMP cell numbers, in contrast it results in a reduction of in CMPs (Buechler et al., 2013) and CMPs also fall in relative frequency in response to IFN-α administration (Pietras et al., 2014). Evidence of the effects of interferon signaling or models of infection on MEP and LMPP cellularity is somewhat lacking. Whereas, the existing evidence regarding the effect of interferon exposure on CLP cell count in mice contradicts an IFN-based hypothesis of how Miz-1 deficiency exerts its effects, since CLP absolute number was shown to be unaffected by the IFN-γ-dependent effects of bacterial infection (MacNamara, Oduro, et al., 2011) and reduced by IFN-α upregulation (Di Scala et al., 2015). The effects on neutrophil count of IFN exposure differs by IFN type: IFN-α stimulation induces an IFNAR-dependent decrease in Gr-1^+ Mac-1^+ cells (Pietras et al., 2014) and IFNAR-deficient mice exhibit an accumulation of neutrophils (Seo et al., 2011), whereas IFN-γ administration achieves the opposite effect (Zhao et al., 2010), so whether the reduction in BM neutrophils observed in *Miz-1^ΔPOZ* mice (Figure 3.4A) can also be explained by the interferon response is speculative. In light of the evidence, it is uncertain whether *Miz-1^ΔPOZ* mutation in HSCs is associated with an increase in myeloid and lymphoid progenitors and a decrease in neutrophils due to the over-active IFN response in HSPCs. Owing to our observations that myeloid progenitors are not more actively cycling in *Miz-1^ΔPOZ* mice (Figure 3.3C), we can discount the notion that their accumulation is due to IFN (or other factors) directly stimulating them to proliferate. Furthermore, we do not know that IFN levels are altered in the blood or BM of *Miz-1^ΔPOZ* mice, or even whether myeloid progenitor cells exhibit the same IFN response phenotype that *Miz-1^ΔPOZ* LSKs do, so we only have the upstream accumulation of HSPCs and the higher proportion of cycling HSCs from which to speculate why progenitors and neutrophils are altered in number.

The entry of HSCs into the cell cycle in response to dsRNA or IFN-γ stimulation depends on functional STAT1 (Essers et al., 2009), and the expansion of LSK cell count due to IFN-γ exposure partially depends on STAT1 activity (Baldridge et al., 2010). However, our data suggest that STAT1 activity is no different in *Miz-1^ΔPOZ* LSKs compared to controls (Figures 3.10C, 3.10D). This rules out the notion that altered STAT1 phosphorylation in response to IFN activity in *Miz-1^ΔPOZ* LSKs is a part of the mechanism by which HSPC accumulation comes about.

CD41 has been demonstrated to be highly expressed on the surface of HSCs in response to IFN-α signaling via dsRNA stimulation (Haas et al., 2015), which fits the hypothesis that Miz-1 POZ domain loss induces higher CD41 MFI in *Miz-1^ΔPOZ* HSCs (Figure 3.1I) and higher CD41

mRNA expression in *Miz-1^{ΔPOZ}* CD34^- LSKs (data not shown) via a de-repressed interferon response. Two groups of DAPs that are overexpressed in HSCs in response to dsRNA stimulation include many of the RNAs that were overexpressed in *Miz-1^{ΔPOZ}* CD34^- LSKs. They are the "interferon response genes": *BST2*, *ISG15*, *IFIT1*, *IFIT3*, *RSAD2*, *IFI44*, *CXCL10*, *OAS2*, *OAS3* and *DDX60* and the "megakaryocyte and platelet genes": *TIMP3*, *PF4*, *ITGB3* (*CD61*), *VWF*, *SERPINE2*, *SDPR* and *ITGA2B* (*CD41*). Some of these genes, with a few additional different genes, but fewer overall, were also overexpressed in common with the overexpressed proteins from the study in *Miz-1^{ΔPOZ}* CD34^+ LSKs. Such precise and widespread overlap between the phenotypes of the emergency megakaryopoiesis response of HSCs to IFN-α signaling and Miz-1 deficiency in LSKs indicates a common underlying mechanism. This is further supported by the overexpression of the platelet activation biological pathway among *Miz-1^{ΔPOZ}* CD34^- LSK DEGs (Figure 3.6J).

We found that *Miz-1^{ΔPOZ}* LSKs have a deficiency in TPO-mediated STAT5 phosphorylation (Figures 3.11A, 3.11B), which can also be explained by an IFN response mechanism, since when HSCs are exposed to IFN-γ and TPO simultaneously, the STAT5-phosphorylating effect of TPO stimulation is lost (de Bruin et al., 2013). The study showing this found the effect to be due to the ability of IFN-γ to induce *SOCS1* expression, which inhibits STAT5 signaling, however *SOCS1* was not a DEG in our RNA-sequencing or proteomic data, despite it being indicated as an upstream regulator of the *Miz-1^{ΔPOZ}* LSKs transcriptomic phenotype (Figure 3.6O). Just as in Miz-1 deficient CD34^+ LSKs (Figure 3.6G), IFN-γ treated HSCs had lower mRNA levels of *cyclin D1* (de Bruin et al., 2013), the expression of which is associated with TPO signaling through STAT5 (Matsumura et al., 1999). Evidence therefore supports the STAT5 phosphorylation deficiency seen in *Miz-1^{ΔPOZ}* LSKs being a result of their de-repressed IFN response phenotype.

We observed that lineage marker-depleted cells from *Miz-1^{ΔPOZ}* mice cultured for 18 hours showed enrichment of LSK cells compared to controls and that culturing with LPS removes this difference in LSKs as a proportion of Lin^- cells (Figures 3.12B, 3.12C). We also have unpresented preliminary data of the same experiment using IFN-γ indicating the same trend. Our experiment indicates that TLR signaling expands LSKs as a fraction of Lin^- cells *in vitro*, and that the relative expansion of *Miz-1^{ΔPOZ}* LSKs is dependent on whatever mechanisms induced by TLR signaling result in LSK expansion. In support of this, the Miz-1 POZ domain is known to be essential for suppression of LPS-mediated inflammation by Miz-1 in lung cells (Do-Umehara et al., 2013). However the data in this experiment contained a lot of variation in LSK gate percentages, owing to suboptimal culturing conditions, so for the results of this experiment to be reliable enough for a clear conclusion, the culturing conditions should be optimised and the experiment replicated. This experiment indicates that an immune-response mechanism for the expansion of *Miz-1^{ΔPOZ}* HSPCs is worth investigating.

Our ChIP-qPCR experiment would discount a direct transcriptional role of Miz-1 in repressing the expression of *IRF7* and *IFIT3* (Figure 3.8A). In a recent study, Muthalagu et al.

demonstrated that the repression of *IRF7* by the Myc/Miz-1 complex is directly regulated in adenocarcinoma cells from the *IRF7* gene locus, which would appear to contradict the lack of binding we observed at this locus in the HPC-5 cell line (Muthalagu et al., 2020). However, in their ChIP experiment, it was Myc that was immunoprecipitated, not Miz-1 as in ours; furthermore their initial ChIP using an anti-Miz-1 antibody did not enrich *IRF7* gene fragments. But they then verified that *IRF7* is bound by Miz-1 dependently on Myc by performing a re-ChIP on anti-Myc-precipitated fragments with an anti-Miz-1 antibody, revealing that these fragments were highly enriched for Miz-1 binding. Of interest, the authors showed that the *STAT1* promoter is bound by Myc/Miz-1 in the same way and that deletion of either *Miz-1* POZ domain or *c-Myc* resulted in an immunogenic phenotype in a manner dependent on IFNAR function. We can therefore hypothesize that Miz-1 binds the start sequences of *IRF7*, *STAT1* and possibly other ISGs to directly repress them dependently on Myc and that this is no longer possible when Miz-1 DNA binding ability is lost, resulting in the de-repression of IFN response genes. We would also hypothesize that this function of Miz-1 is co-dependent upon c-Myc function in HSPCs.

Taken together, our analysis concludes that the critical role of Miz-1 in suppressing the interferon-response pathway in HSPCs is a fitting explanatory model for the loss of quiescence and gain of cell cycle entry of HSCs, the compartmental expansion of HSC, MPP and GMP cell types, the overexpression of CD41, loss of efficient STAT5 signaling in response to thrombopoietin in HSPCs and the severe colony forming deficits and hypocellularity of bone marrow cells that occur when the Miz-1 POZ domain is ablated. It is unclear whether the increase in LS$^+$K$^-$ cells, CMPs, MEPs, CLPs, LMPPs and decrease in neutrophil absolute numbers is due to interferon response gene upregulation, thanks to either lack of studies or known conflicting roles that IFN-α and IFN-γ play in influencing their cell numbers. The retinue of ISGs that is de-repressed by Miz-1 loss of function does not fall exclusively into either IFN-α or IFN-γ regulated signatures however, and this fact may account for any deviation we see in our phenotypes from the known effects of stimulation by either cytokine. Our results support a model in which Miz-1 is responsible for repressing the expression of IFN response genes; a role critical to maintaining the quiescence of HSCs, preventing the expansion of hematopoietic stem and progenitor cells.
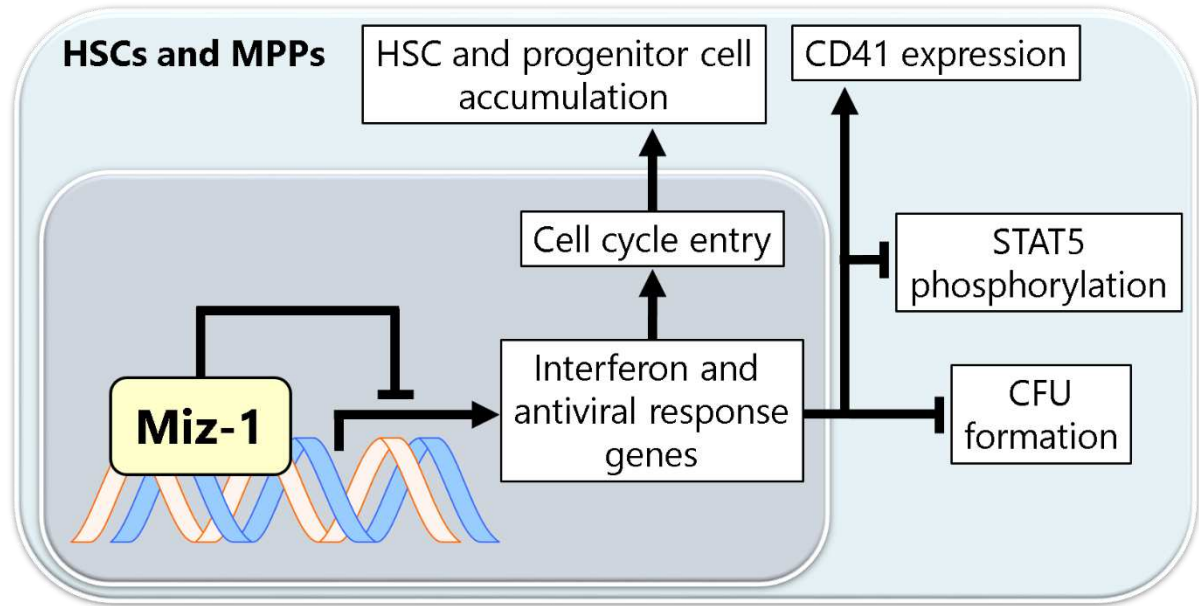
Figure 4.: Miz-1 represses the expression of interferon response genes in LSK cells The expression of interferon and antiviral response genes is repressed by Miz-1 in LSK subsets, maintaining their quiescence and limiting HSPC expansion. When Miz-1 is functionally deficient, interferon and antiviral response genes become expressed, resulting in cell cycle entry of HSCs, their accumulation in the bone marrow and overexpression of the inflammation response marker CD41, and defects in colony formation and thrombopoietin-mediated STAT5 phosphorylation.

4.2 The role of Miz-1 as a transcription factor in LSK cells overlaps with previously defined roles and mechanisms

Miz-1 primarily functions as a transcription factor, so its effects on the transcriptome and proteome are major indicators of its role in a given cell type. The findings of our analysis of the proteomic changes seen in *Miz-1^{ΔPOZ}* LSK cells is at least partially consistent with processes that are perturbed by *Miz-1^{ΔPOZ}* in other tissues. Miz-1 regulates the expression of large and small ribosomal proteins, vesicular and membrane proteins and contraction fibre and muscle proteins in LSK cells (Figure 3.7J).

Miz-1 has been previously demonstrated to regulate and be regulated by, large and small ribosomal proteins. For example, Miz-1 induces the expression of *RPL22* directly at the promoter (Rashkovan et al., 2014), (Wolf et al., 2013) and Miz-1-mediated activation of gene expression can be inhibited by Myc-induced RPL23 (Wanzel et al., 2008), (Qi et al., 2017). While RPL23 appeared nowhere in our data, our RNA-sequencing data revealed *RPL22* downregulation (Figures 3.6D, S6B) and many RPL and RPS proteins were altered in abundance in *Miz-1^{ΔPOZ}* LSK cells (Figure 3.7J), including RPL9, a known Miz-1 direct target gene (Wolf et al., 2013). Miz-1s regulation of this cluster of proteins may account for the enrichment of ribosomal components (Figure 3.7D), translation initiation and rRNA processing (Figure 3.7H) pathways in *Miz-1^{ΔPOZ}* LSKs. Furthermore, a gene ontology analysis on ChIP results of Miz-1-

bound genes in embryonic stem cells found that ribosomal proteins were disproportionately immunoprecipitated (Varlakhanova et al., 2011). The *Miz-1^{ΔPOZ}* proteomic phenotype in LSK cells may therefore be an example of a general mechanism by which Miz-1 regulates cellular processes via RPL and RPS gene expression.

Of keen interest is the fact that the aforementioned study also identified Myc-bound genes and showed that genes co-bound by Myc and Miz-1 included gene sets for muscle development and chromatin regulation gene ontology terms. Miz-1 overexpression is also known to induce hypertrophy in cardiac muscle cells, while heart failure results from full Miz-1 knock out (Buyandelger et al., 2015). The *Miz-1^{ΔPOZ}* transgene is also associated with nerve cell proliferation and hypomethylation due to *KDM8* overexpression (Fuhrmann et al., 2018). A role for Miz-1 in promoting both muscle function (Figures 3.7E, 3.7G, 3.7I, 3.7J) and histone methylation (Figures 3.7G, 3.7I) at the level of protein expression was also seen in our results. The upstream regulator analysis also predicted the activity of SMTNL1, which regulates muscle contraction and KDM5A (it was likely KDM8 that was detected, as MS detects peptide fragments and assigns them each to a group) as the most prominent causes of the proteomic phenotype (Figure 3.7N). These results support the notion that Miz-1 contributes to cellular function in HSPCs through the regulation of the expression of muscle proteins and histone demethylases, as has been found in other cell types.

In cells of the central nervous system Miz-1 targets genes, such as *AMBRA1* and *VAMP4*, that encode proteins involved in vesicular transport pathways, endocytosis and lysosomal biogenesis to ensure cell survival (Wolf et al., 2013). In the case of epithelial mammary gland cells, Miz-1 maintains the expression levels of *AMBRA1, LRP12 and VAMP4* to safeguard proper vesicular trafficking of membrane receptors, which is important for the STAT5 signaling pathway (Sanz-Moreno et al., 2014). In *Miz-1^{ΔPOZ}* LSKs, we saw that *AMBRA1*, *LRP12* and *VAMP4* were downregulated at the mRNA level (Figure 3.6D) and VAMP4, along with VPS18, VPS25, VPS45 and other proteins in the vesicular and membrane trafficking cluster, were less abundant at the protein level (Figure 3.7J). Therefore it appears that positive regulation of vesicular trafficking is a conserved mechanism through which Miz-1 exerts its effects across cell types.

The phenotypes we see in HSPCs of cells bearing the *Miz-1^{ΔPOZ}* mutation are not very similar to those seen in lymphocytes and erythrocytes, the other hematopoetic cell types in which Miz-1 function has been studied. *Miz-1^{ΔPOZ}* HSCs and MPPs do not have high levels of apoptosis or p53-suppressed genes, as developing B and T lymphocytes do, nor do they have an enhancement in STAT5 phosphorylation in response to ligand stimulation, as TER-119⁺ splenocytes do. Unlike either of these cell types (and mammary epithelial cells), *Miz-1^{ΔPOZ}* HSPCs also do not show perturbed levels of *SOCS* mRNAs, although to truly test this in LSKs we would have to assess *SOCS* levels after stimulation with TPO. *Miz-1^{ΔPOZ}* LSKs were akin to both lymphocytes and mammary epithelial cells in their defective STAT5 phosphorylation in response to a ligand (TPO for LSKs; IL-7 for lymphocytes; prolactin for mammary epithelial

cells). Since *Miz-1^(ΔPOZ)* mammary epithelial cells show defective STAT5 phosphorylation when stimulated due to a mechanism mediated by defective vesicular trafficking, they are most similar to *Miz-1^(ΔPOZ)* LSKs. As a result Miz-1 loss of function may form a mechanism with deficient STAT5 responsivity to TPO through insufficient vesicular trafficking or change in *SOCS* levels in LSKs in a similar fashion. Defective TPO responsivity in *Miz-1^(ΔPOZ)* HSPCs may also explain the highly deleterious effect *Miz-1^(ΔPOZ)* mutation had on the colony-forming capacity of BM cells. Because the CFU assay depends on TPO stimulation for colonies to grow, the lack of STAT5 phosphorylation in response to TPO and lower cyclin D1 expression (expression of which is activated by TPO in HSCs) in *Miz-1^(ΔPOZ)* HSPCs may be responsible for their greatly reduced colony formation capability.

4.3 The potential role of a Myc-dependent mechanism of Miz-1-mediated suppression of interferon signaling

Our upstream regulator analysis on the differentially abundant proteins in *Miz-1^(ΔPOZ)* LSKs indicate that Myc is responsible for the phenotype of these cells (Figure 3.7N). This is likely to be due to the ribosomal subunit and rRNA processing proteins in the dataset. It is unlikely that the phenotypes of *Miz-1^(ΔPOZ)* HSCs and MPPs are driven by aberrant Myc activity resulting from loss of Miz-1 DNA-binding ability. There is no known similarity between higher Myc activity and Miz-1 POZ domain loss in HSPCs. Furthermore, enhanced Myc activity has drastic consequences for the BM and PB due to premature cell differentiation. The *Miz-1^(ΔPOZ)* phenotype in HSPCs rather better correlates with Myc deficiency, in that Myc loss leads to LSK accumulation (Wilson et al., 2004) and impaired CFU-forming ability (Y. Guo et al., 2009), (Baena et al., 2007) as well as a HSC-specific increase in cell cycling (Laurenti et al., 2008). However, Myc loss of function serving as an explanation for the effects of Miz-1 deficiency in HSPCs is also unsatisfactory, since Myc^(-/-) mice, at odds with *Miz-1^(ΔPOZ)* mice, experience anemia and leukopenia as well as almost entirely lacking hematopoietic progenitor cell types.

It is most likely that the role Myc plays in producing *Miz-1^(ΔPOZ)*-induced phenotypes in HSPCs owes to the loss of its ability to suppress IFN response genes, as has been demonstrated to occur in pancreatic cells lacking the Miz-1 POZ domain (Muthalagu et al., 2020). To further support this, *c-Myc* expression levels correlate with the suppression of IFN responsivity in other cell types (Tulley et al., 2004). Myc also plays a role in transcriptionally biasing HSCs towards the CD41^(+) (as opposed to CD41^(-)) subtype, which express megakaryocyte and platelet signature genes such as *PF4* and *VWF* (Rao et al., 2021), therefore the bias of *Miz-1^(ΔPOZ)* HSPCs toward megakaryocyte primed HSCs may be a consequence of Myc-dependent de-repression of IFN response genes which induce this bias. IFN signaling (via dsRNA) also induces the expansion of these CD41^(+) HSCs, as well as an increase in c-Myc protein abundance (Ehninger et al., 2014), which provides a connection between the phenotypes of *Miz-1^(ΔPOZ)* HSCs and our proteomics analysis in LSKs, strengthening the notion that Myc is a part of the mechanism.

This model would fit with what is known in undifferentiated pluripotent stem cells, which suppress the antiviral response in order to differentiate appropriately (Eggenberger et al., 2019). The stimulation of the type I IFN response in pluripotent stem cells impairs their ability to properly undergo differentiation; in comparison in *Miz-1*$^{\Delta POZ}$ HSPCs, we see increased self-renewal of stem and progenitor cell types in coincidence with their IFN response phenotype. As discussed in the introduction, c-Myc plays a key role in regulating the decision between self-renewal and differentiation in HSCs. This suggests that c-Myc forming a suppressive complex with Miz-1 against the expression of IFN response genes in HSCs is important for the prevention of HSC expansion and maintenance of their quiescence, and the mechanism by which Myc participates in the *Miz-1*$^{\Delta POZ}$ phenotype.

4.4 *Miz-1* POZ domain deletion emulates aging by de-repression of interferon-induced transcripts in HSPCs

Our findings in comparing young and old mice of the control genotype affirmed those of previously published studies. We observed a large expansion of HSCs and MPP1 cells with age but no statistically significant expansion of MPP2 or MPP3 cells (Figure S1A, S1B), in accordance with what other investigators have found (Rossi et al., 2005), (Porto et al., 2015). The BM of control mice also lost cellularity with age. A potentially novel finding of ours was that LS$^+$K$^-$ cells are 5-fold expanded in control mice of 18 months of age compared to young mice (Figure S1G). While it is contentious whether or not LSK subsets become more active in the cell cycle with aging, we found that the proportion of MPP3 cells in the S phase consistently rose with age in both genotypes of mice studied (Figures S2D, S2E). MEP and GMP absolute numbers in control mice rose with aging (Figure S3A), while CMP numbers were unaffected by age and again in-line with previously published findings (Rossi et al., 2005), CLPs declined with aging in both control as well as in Miz-1-deficient mice. In accordance with the findings of other groups, we observed no aging-related differences in the absolute numbers of BM-situated mature hematopoietic cells (Figure S4A). In another potentially new finding, we saw that BFU-E colony formation became enhanced with age in control mice (Figure 3.5B), while aging did not statistically affect the formation of other colony types. Our comparison of the RNA-sequencing results performed on CD34$^-$ and CD34$^+$ LSK cells from control mice of 4- and 24-month old ages confirmed the findings other groups made studying aging in HSPCs. In control CD34$^-$ LSKs, DAVID gene ontology analysis on age-induced genes revealed that protein phosphorylation, DNA transcription, small GTPase, endocytosis, angiogenesis, immunity and NF-κB signaling processes were enriched (Figure 3.9G), while among age-repressed genes cell cycle, mRNA and rRNA processing, mitotic cell division, DNA repair and chromatin silencing were enriched (Figure 3.9H). Similarly, we found that the transcriptomes of control CD34$^+$ LSK, overexpress immune, anti-viral and inflammatory response, cell adhesion and cell migration processes with age (Figure 3.9I). Many previously identified aging-regulated transcripts were also included in our results, but we also performed upstream regulator analysis which indicated that *TP53*, and potentially, *ZBTB17*, are causally upstream of age-related transcription changes

in CD34⁻ LSKs (Figure 3.9K). Our PPI network analyses showed that while cell cycle regulators are the most highly integrated nodes that become altered with age in CD34⁻ LSKs (Figure 3.9L), this is true of genes involved in the immune response in CD34⁺ LSKs (Figure 3.9M), indicating the importance of these genes for the aging of HSPCs. Our qPCR results did not support the claim that IFN response genes such as *IRF7*, *MX1* and *OAS3* are altered in expression in CD34⁻ᐟ⁺ LSKs in old age in mice. Although *IRF7* should have been higher in LSKs from old mice compared to young, these negative findings could be due to the stringent test for statistical significance that we applied.

The age-related changes seen in *Miz-1ᐟᴾᴼᶻ* mice in some cases had the same tendency as those seen in control mice. HSCs accumulated in absolute number with aging in *Miz-1ᐟᴾᴼᶻ* mice to a greater extent than in controls, indicating, in this case, a compounding of the effects of aging and *Miz-1* POZ domain loss. As in controls, MPP2 and MPP3 cells in *Miz-1ᐟᴾᴼᶻ* mice did not accumulate with age, while MPP3 cells were more enriched in the S phase of the cell cycle (Figures S2D, S2E), CLPs became less abundant and the absolute number of mature cell types as well as CFU-G/-GEMM forming abilities of BM cells, were unaffected by aging. The most enriched biological pathways according to DAVID gene ontology analysis was also the same as controls in *Miz-1ᐟᴾᴼᶻ* CD34⁻ LSKs, as both their overexpressed and underexpressed gene sets were also largely the same as aged controls, although their overexpressed terms did lack the enrichment in immune system processes that CD34⁻ LSKs in old control mice presented.

However, there were some differences in the way *Miz-1ᐟᴾᴼᶻ* mice aged compared with controls. The accumulation of MPP1, MEP, GMP and LS⁺K⁻ cells seen in control mice was not seen in *Miz-1ᐟᴾᴼᶻ* mice, nor was the age-related decline in bone marrow cellularity. Furthermore, *Miz-1ᐟᴾᴼᶻ* CD34⁻ LSKs from old mice did not experience an enrichment of immune system or positive regulation of NF-κB signaling gene ontology terms with age and CD34⁺ LSKs had no age-related enrichment of any gene ontology terms, which consisted entirely of immune, interferon and antiviral response pathways in control mice (Figure 3.9I).

Mechanistically, it can only be said that the processes inhibited by Miz-1 and those of aging overlap in cases where each individually results in the same phenotypic change and wherein the combination of both results in no further increase in the effect, as in the above cases of MPP1, MEP, GMP and LS⁺K⁻ cells not accumulating further when both *Miz-1ᐟᴾᴼᶻ* genotype and old age are combined as well as the disappearance of age-related immune and interferon response gene signature enrichment. The age-related and *Miz-1ᐟᴾᴼᶻ*-associated BM cellularity loss also did not worsen when both conditions were combined. To reinforce this notion, not only did *Miz-1ᐟᴾᴼᶻ* mice not show statistically significant age-related changes in these variables, but the statistical significance of these differences between control and *Miz-1ᐟᴾᴼᶻ* genotypes that were found in young mice also disappeared. However, when a phenotypic change common to two conditions is amplified further when they are combined, as in the case of greater HSC self-renewal with *Miz-1* POZ domain knockout (3.3-fold greater) and aging (11-

fold greater), as well as in the presence of both conditions (15-fold greater), we can conclude that the mechanisms in each condition are different but contribute to the same phenotype.

In cases where *Miz-1$^{\Delta POZ}$*-induced changes and age-associated changes did not align, there is no shared mechanism of action of the phenotypes. Consequently, we cannot infer anything about the role of Miz-1 in aging from those observations. For example, the presence of both *Miz-1$^{\Delta POZ}$* mutation and old age culminated in a measurable decline of monocytes (Figure 3.4B), but this wasn't true for either of these factors alone and we do not know how these factors interact. In contrast, we observed that despite the decline in CLP number with aging, CLPs are still elevated in number in *Miz-1$^{\Delta POZ}$* mice compared with controls in old mice, as they are in young mice (Figure 3.3E), suggesting that Miz-1 deficiency protects against this age-related decline. Similarly, BFU-E forming ability was enhanced with age in control mice but almost absent in both young and old *Miz-1$^{\Delta POZ}$* mice (Figure 3.5B). In such a case, the effect of Miz-1 functional deficiency on colony forming ability is so devastating that even the BFU-E formation-enhancing effect of aging cannot remedy it. We did not detect age-related changes in either B lymphocytes nor neutrophils; while the huge loss of B lymphocytes suffered by *Miz-1$^{\Delta POZ}$* mice was present in both young and old mice due to a known mechanism unrelated to aging (Kosan et al., 2010), the relatively fewer neutrophils in *Miz-1$^{\Delta POZ}$* BM of young mice (Figure 3.4A) likely disappeared in old age due to the high variation in neutrophil count of old mice. Finally, we did not see any age-related changes in MPP2, MPP3 or CMP cells, but all three were consistently higher in number in *Miz-1$^{\Delta POZ}$* BM compared to controls, so therefore we do not believe this effect to be age-related.

One especially intriguing result of the upstream regulator analysis of aging-regulated DEGs from CD34$^-$ LSK cells is that they (Figures 3.9K, S8E) suggested that the Miz-1-encoding gene *ZBTB17* is in a more active state in old-aged cells and an activating regulator of the aging transcriptome. Furthermore, supplementary results from a study by Sun et al. indicated that *Miz-1* may be expressed at slightly lower levels in LSKs from old mice (Sun et al., 2014). Both our read-based and qPCR-based measurements of *Miz-1* mRNA showed no appreciable difference in the CD34$^-$ and CD34$^+$ LSKs of old mice compared to young mice (Figures S8H, 3.9R). When we measured the levels of *Miz-1* mRNA in HSCs, we saw a clearer tendency of reduction in cells from old mice, however it was still not statistically significant (Figure 3.9S, *p* = 0.3). We would conclude that there is a statistically insignificant decline in *Miz-1* mRNA levels in aging and this may be influencing the transcriptome of HSCs as they age.

In conclusion, the mechanism by which Miz-1 transcriptional loss of function contributes to age-related changes, likely takes place via the overexpression of antiviral and IFN-induced transcripts as these genes are overexpressed in LSK subsets from both young *Miz-1$^{\Delta POZ}$* and old control mice compared to their respective controls (Figures 3.9O, 3.9P). Via this mechanism, a small decline in *Miz-1* mRNA levels in HSCs may contribute toward the age-related phenotype of HSPCs as mice age.

4.5 Further experiments and conclusion

In light of these findings, we propose that Myc binds Miz-1 in HSCs to suppress the expression of antiviral and interferon-inducible response genes that are directly bound by Miz-1 dependently on c-Myc as part of their homeostatic role in HSCs. This suppression maintains the quiescence of HSCs and consequently limits the pool sizes of HSPCs, as well as protecting the ability of HSPCs to form colonies.

To test these claims, further experiments should be undertaken. To test the proposal that fully functional Miz-1 is bound by c-Myc and recruited to the loci of IFN-stimulated genes for their repression, the HSPCs of mice bearing the *c-Myc*^{V394D} (in which c-Myc is unable to bind Miz-1) mutation should be transcriptionally profiled by RNA-sequencing and compared with each other and control and *Miz-1*$^{\Delta POZ}$ HSPCs. If c-Myc suppresses IFN-inducible genes dependently on Miz-1, then *c-Myc*^{V394D} HSPCs should show an overexpression of the same genes overexpressed in *Miz-1*$^{\Delta POZ}$ mice. Our claim that the constitutive antiviral response in *Miz-1*$^{\Delta POZ}$ HSPCs is responsible for the loss of quiescence of HSCs and the expansion of HSCs, MPPs and committed progenitors can be tested by analysing the composition of these cells in *Miz-1*$^{\Delta POZ}$ mice bearing a *STAT1*$^{-/-}$ or *IRF7*$^{-/-}$ mutation, or that have been treated with a STAT1/IFN inhibitor, by FACS analysis. Finally, we recommend that the claim that Miz-1 directly binds the genomic loci of IFN-response genes in HSPCs should be tested by full ChIP-sequencing in either HPC-5 cells or primary LSKs, using an anti-Miz-1 antibody, or optionally as a re-ChIP after IP with a c-Myc antibody if this is more practical and to test if Miz-1 binding of these genes is c-Myc-dependent.

Our findings present the possibility that c-Myc maintains the capacity of HSCs to proceed with differentiation instead of self-renewing by suppressing the antiviral interferon response through binding Miz-1.

5. Materials and methods

5.1 Mouse strains

All mice were housed at the BioInstrumenteZentrum (BIZ) Jena animal facility in single ventilated cages under pathogen free conditions. All experiments involving animal procedures were performed according to protocols approved by the Thüringer Landesamt für Verbraucherschutz. All mice were of the C57BL/6 background. Constructs used were *Vav-Cre* (de Boer et al., 2003), bearing a functional Cre-recombinase downstream of the *Vav* gene promoter which is exclusively expressed in all hematopoietic-lineage cells, and *Miz-1$^{flox/flox}$* (*Zbtb17$^{fl/fl}$*) bearing LoxP sites flanking the POZ domain (floxed) of the *Miz-1* gene (Kosan et al., 2010) in all cells.

Miz-1$^{\Delta POZ}$ mice: these mice were bred by crossing a *Vav-Cre^{+}* (transgene); *Miz-1$^{flox/flox}$* mouse, male or female, with a *Vav-Cre^{-}* (control); *Miz-1$^{flox/flox}$* mouse of the opposite sex.

Control mice: these mice were bred by crossing a *Vav-Cre^{-}* (control); *Miz-1$^{flox/flox}$* mouse, male or female, with a *Vav-Cre^{-}* (control); *Miz-1$^{flox/flox}$* mouse of the opposite sex.

5.2 Isolation of bone marrow

5.2.1 Isolation of bone marrow from 2 femurs

Bone marrow cells were flushed with PBS/3% fetal calf serum (FCS, wash buffer) from two femurs and passed into a Falcon tube through a 70 μm filter and placed on ice. Samples were then centrifuged at 300 x g for 4 minutes and after aspiration of the supernatant, 1 mL sterile red cell lysis buffer (150 mM NH4Cl, 0.01 M Tris-HCl, pH 7.1–7.4) was added and samples were placed on ice for 5 minutes. Samples were then centrifuged again and resuspended in 5 mL wash buffer for counting. Cells were counted using a light microscope and a Neubauer chamber.

5.2.2 Isolation of bone marrow from the whole skeleton

All bones except the arms, tail, feet and skull were crushed with a mortar and pestle in 5 mL of PBS/10% FCS. Muscle was carefully removed from the bones using a scalpel and tissue paper. The bone marrow was gently suspended with a pipette and washed into a Falcon through a 70 μm filter, placed on ice and centrifuged at 300 x g for 4 minutes. The pellet was then resuspended in 1 mL PBS/10% FCS. Cells intended for lineage marker-depletion were subject to red cell lysis by a 5 minute incubation on ice in 1 mL sterile red cell lysis buffer (150 mM NH4Cl, 0.01 M Tris-HCl, pH 7.1–7.4) and then counted in a Neubauer chamber. However, if cells were intended for c-Kit^{+} cell enrichment, they were not counted and 2 μL of c-Kit APC antibody (eBioscience™) was added and left for 30 minutes on ice. 5 mL PBS/10% FCS was

then added, the sample was centrifuged at 300 x g for 4 minutes and the supernatant removed and resuspended in 500 μL PBS/10% FCS. 1.5 μL of anti-APC beads (Miltenyi Biotec™) per μL of c-Kit APC antibody were then added and the sample was incubated on ice for 30 minutes. The sample was again washed in 5 mL PBS/10% FCS and centrifuged at 300 x g for 4 minutes, before loading onto LS columns for c-Kit⁺ cell enrichment.

5.3 Lineage positive cell depletion

After counting and red cell lysis, cells were resuspended in wash buffer to a concentration of 1×10^8 / mL in FACS tubes, to which 200 μL of MagniSort™ Enrichment Antibody Cocktail (Thermo Fisher Scientific™) per mL of cell suspension was added and tubes were incubated at room temperature for 10 minutes. Cells were washed in a total of 4 mL wash buffer and centrifuged at 300 x g for 4 minutes, the supernatant was discarded and resuspended in the original volume of wash buffer. MagniSort™ Negative Selection Beads (Thermo Fisher Scientific™) were vortexed and 200 μL of beads per mL of volume was then added to cells, followed by pulse-vortexing and a 5 minute incubation at room temperature. The volume was then filled to 2.5 mL with wash buffer and the FACS tube added to a magnet, after which the contents of the FACS tube were gently poured into a 5 mL tube. FACS tubes containing beads were then taken out of the magnet, resuspended in 2.5 mL wash buffer, left for 5 minutes to incubate at room temperature, and again inserted into a magnet and poured into the 5 mL FACS tube. These lineage marker-depleted cells were then centrifuged and stained for FACS analysis.

5.4 C-Kit positive cell enrichment

Cells isolated from the whole skeleton and stained with c-Kit APC antibody and incubated with anti-APC beads (Miltenyi Biotec™, 130-090-855) were resuspended in 1 mL wash buffer, while an LS column (Miltenyi Biotec™) mounted on a magnet stand was equilibrated with 2 mL PBS with a tray underneath. Filter mesh was then placed over the top of the column, and 1 mL bone marrow suspension pipetted gently through the filter mesh. The filter mesh was then washed with another 1 mL wash buffer, followed by 3 mL PBS which was allowed to run through, and again with 3 mL PBS. The column was then removed from the magnet, placed onto a 5 mL Falcon tube and flushed with 5 mL wash buffer, yielding c-Kit⁺ cells.

5.5 Flow cytometry antibodies

Incubations of cells with flow cytometry antibodies were performed in FACS buffer (0.1 mM EDTA, 0.1% sodium azide, PBS/3% FCS) or wash buffer (PBS/3% FCS) on ice.

5.5.1 Lineage panel antibody cocktail

All antibodies listed in this table are biotin-conjugated.

Antigen	Volume (µL)	Clone	Supplier
B220	100	RA3-6B2	Invitrogen
Gr-1 (Ly-6G/Ly-6C)	100	RB6-8C5	eBioscience
TER-119	100	TER-119	eBioscience
CD11b	50	M1/70	eBioscience
CD3e	25	145-2C11	eBioscience
CD4	25	RM4-5	eBioscience
CD8	25	53-6.7	eBioscience

5.5.2 All other FACS antibodies

Antigen	Fluorophore	Clone	Supplier
c-Kit	APC	2B8	eBioscience
Sca-1	PE-Cy7	D7	BD
CD34	FITC	RAM34	eBioscience
CD48	PerCP-Cy5.5	HM48-1	eBioscience
CD135	PE-Cy5	A2F10	eBioscience
CD150	PE	Q38-480	BD
γH2A.X	FITC	JBW301	Millipore
IgG1	FITC	IS5-21F5	Miltenyi Biotec
CD16/32	PE	93	eBioscience
IL-7Rα (CD127)	Pacific Blue	A7R34	eBioscience
Ki-67	Alexa Fluor 700	B56	BD
ITGA2B (CD41)	BV421	MWReg30	BioLegend
p-STAT1	BV421	4a	BD
p-STAT5	BV421	47/STAT5	BD
IgG1 K isotype	BV421	X40	BD
B220	FITC	RA3-6B2	eBioscience
Gr-1 (Ly-6G/Ly-6C)	APC	RB6-8C5	eBioscience
CD11b	PE-Cy7	M1/70	BioLegend
CD115	PerCP-Cy5.5	AFS98	BioLegend
TER-119	(Biotin-conjugate)	TER-119	eBioscience
Streptavidin	APC-Cy7	Not applicable	BD
Annexin V	FITC	VAA-33	eBioscience

5.6 FACS analysis

FACS antibodies were purchase from several suppliers (see tables 5.51 and 5.5.2). For flow cytometric measurements on cells that were not subjected to lineage-marker depletion or c-

Kit$^+$ cell enrichment, 1 x 15 million (red cell-lysed) cells from each mouse were taken for staining and all such stains were performed in wash buffer (PBS/3% FCS) and incubated on ice.

5.6.1 Staining of hematopoietic stem cells and multipotent progenitors

To stain HSC and MPP, 1.5 x 10^7 bone marrow cells were stained with 15 µL of biotin-conjugated lineage marker panel antibody cocktail shown in table 5.51 in 200 µL wash buffer on ice for 30 minutes. 1 mL of wash buffer was then added and cells were centrifuged at 300 x g for 4 minutes. Supernatant was then discarded and cells were resuspended in 200 µL FACS buffer stained with 1 µL each of antibodies against c-Kit, Sca-1, streptavidin, CD48 and CD150, as well as 3.5 µL of anti-CD34 antibody for 60 to 90 minutes on ice. In experiments assessing CD41 expressing-compartments, 1 µL of CD41 was used to stain HSC and MPP instead of CD48. If LSK cells alone were to be analysed, this stain was performed without CD34, CD48, CD150 and CD41 for 30 to 45 minutes on ice. If CD34$^+$ and CD34$^-$ LSK were to be analysed, this stain was performed without CD48, CD150 and CD41 for 60 to 90 minutes on ice. Cells were then washed in 1 mL of wash buffer, centrifuged at 300 x g for 4 minutes, resuspended in 2 mL wash buffer and passed through 70 µm nylon mesh into new FACS tubes for flow cytometry acquisition.

5.6.2 Staining of GMP, MEP, CMP and CLP cells

For the staining of GMP, MEP, CMP and CLP cells types, 1.5 x 10^7 bone marrow cells were stained with 15 µL of biotin-conjugated lineage marker panel antibody cocktail shown in table 5.51 for 30 minutes in 200 µL FACS buffer on ice before addition of 1 mL wash buffer and centrifugation at 300 x g for 4 minutes. Supernatant was then discarded and cells were resuspended in 200 µL FACS buffer stained with 1 µL each of antibodies against c-Kit, Sca-1, streptavidin, IL-7Ra and CD16/32, as well as 3.5 µL of anti-CD34 antibody for 60 to 90 minutes on ice. Cells were then washed in 2 mL of wash buffer, centrifuged at 300 x g for 4 minutes, resuspended in 1 mL wash buffer and passed through 70 µm nylon mesh into new FACS tubes for flow cytometry acquisition.

5.6.3 Staining of B lymphocytes, erythrocytes, monocytes and neutrophils

For the staining of committed cells types, 1.5 x 10^7 bone marrow cells were stained with 2.5 µL anti-B220 antibody and 1.5 µL each of antibody against Gr-1, CD11b, TER-119 (biotin-conjugated) and CD115 in 200 µL wash buffer and left on ice for 30 minutes before centrifugation at 300 x g for 4 minutes. Supernatant was then discarded and cells were resuspended in 200 µL wash buffer, 1.5 µL streptavidin antibody was then added and incubated on ice for 30 minutes. Cells were then washed in 1 mL of wash buffer, centrifuged at 300 x g for 4 minutes, resuspended in 2 mL wash buffer and passed through 70 µm nylon mesh into new FACS tubes for flow cytometry acquisition.

5.6.4 Acquisition and analysis of flow cytometry data

Prior to analysis of multicolour samples, Anti-Mouse Ig, κ/Negative Control Compensation beads (BD, 552843) were prepared as compensation controls for each antibody in the experiment using either the same antibody or one with the same fluorophore. For flow cytometric acquisition of fluorescently-labelled cells the BD LSR Fortessa™ or BD FACSCanto™ II were used and data recorded with the BD FACSDiva™ 8.0.1 software. Samples were compensated during data analysis post-acquisition using FlowJo or FlowLogic Software.

5.6.5 Fluorescence-assisted cell sorting for pure cell populations

During sorting of pure cell populations cells were recorded using the BD LSR Fortessa™ and sorted using the BD FACSAria™ Fusion. Cells were labelled with Incucyte® CytoTox green dye to exclude dead cells. Singlets were excluded by gating on SSC-A^{low}, FSC-A^{medium}, followed by FSC-W^{low}, FSC-H^{low}, then SSC-W^{low}, SSC-H^{low} cells, before gating out CytoTox^{high} cells, yielding viable non-doublet cells for further gating.

5.7 Apoptosis assay

After bone marrow cell samples were stained for lineage, Sca-1 and c-Kit cell surface markers, cells were washed in 500 µL PBS and centrifuged at 500 x g for 5 minutes and the supernatant was poured off. Cells were then resuspended in 500 µL 1X Annexin Binding Buffer (eBioscience™, BMS500BB) and washed again by centrifuging at 500 x g for 5 minutes. The supernatant was discarded and cells were then resuspended in 100 µL 1X Annexin Binding Buffer and 2 µL of Annexin V antibody was added and samples were incubated for 15 minutes in the dark on ice. Samples were then washed in 500 µL 1X Annexin Binding Buffer and centrifuged at 500 x g for 5 minutes, the supernatant was then poured off and cells were resuspended in 200 µL 1X Annexin Binding Buffer. 3 µL of propidium iodide (PI) was then added and samples were taken for flow cytometry acquisition.

5.8 LPS *in vitro* stimulation of LSK

BM cells were isolated as in section 5.2.1 and lineage marker depleted as in section 5.3. Cells were then counted in a Neubauer chamber and resuspended in Dulbecco's Modified Eagle's Medium (DMEM)/15% FCS/1% penicillin-strepticillin at a final cell concentration between 1.5 x 10^5 – 2.5 x10^5 cells per mL. 1 mL of medium was then added to each well per condition in a 24-well plate. Sterile LPS was then added to wells to the desired concentration and the plate was placed in an incubator to incubate in 5% CO$_2$ at 37°C for 18 hours. Cells were then transferred to FACS tubes and centrifuged at 300 x g for 4 minutes and supernatant was removed. Cells were then resuspended in 25 µL FACS buffer and 15 µL lineage panel antibody cocktail (section 5.5.1) that was 2-fold diluted in FACS buffer was added to cells and left on ice for 30 minutes. Cells were then washed in 250 µL FACS buffer, centrifuged at 300 x

g for 4 minutes and the supernatant was aspirated, then cells were resuspended in 30 µL FACS buffer and 4 µL of LSK-antibody staining solution was added as in section 5.6.1 and incubated on ice in the dark for 35 minutes. Cells were washed in 250 µL FACS buffer, centrifuged and the supernatant removed. Cells were then resuspended in 250 µL of a solution of 0.75 µg/mL DAPI prepared in FACS buffer and samples were taken for flow cytometry acquisition.

5.9 Cell cycle analysis

Lineage marker-depleted cells were stained for HSC and MPP as per section 5.6.1, however after antibody incubation, cells were washed in 1 mL wash buffer and centrifuged at 300 x g for 4 minutes. Supernatant was discarded and cells were resuspended in 50 µL PBS/10% DMSO/0.4% Triton X-100 and incubated for 1-minute at room temperature (RTP). Samples were then washed in 950 µL 1X BD Perm/Wash™ Buffer (BD, 554714) and centrifuged at 300 x g for 4 minutes. The supernatant of samples was discarded from their FACS tubes and the cell pellet was resuspended in 250 µL BD Cytofix/Cytoperm™ Fixation/Permeabilization solution (BD, 554714), vortexed and incubated at 4°C for 20 minutes. Cells were then washed twice in 1 mL 1X BD Perm/Wash™ Buffer by centrifugation at 300 x g for 4 minutes. Supernatant was aspirated and samples were resuspended in 50 µL Ki-67 antibody staining solution (2 µL antibody per million cells) and incubated on ice in the dark for 45 minutes. 1 mL 1X BD Perm/Wash™ Buffer was then added to samples which were then centrifuged at 300 x g for 4 minutes. The supernatant was then aspirated and cells were resuspended in 1 mL PBS/1% Triton-X100 containing 10 µg/mL RNAse A incubated with 5 µg/mL 4′,6-diamidino-2-phenylindole (DAPI) for 10 minutes in the dark followed immediately by flow cytometry acquisition.

5.10 Intracellular phospho-STAT staining

Following isolation of the whole bone marrow and c-Kit⁺ cell enrichment, cells were centrifuged at 300 g for 10 minutes and then resuspended in 100 µL FACS buffer in a FACS tube and incubated with 3 µL of lineage panel antibody cocktail per sample for 30 minutes on ice. A master mix of 2 µL streptavidin APC-Cy7 + 1.5 µL c-Kit APC + 1.5 µL Sca-1 PE-Cy7 for 2 samples was made, and after centrifugation at 300 x g for 4 minutes, the cells were resuspended in 50 µL FACS buffer and incubated with 2.5 µL LSK staining mix for a further 45 minutes on ice. A pure LSK population was then sorted into DMEM/15% FCS via FACS. Samples were made to contain equal numbers of cells to the sample with the least number by discarding volume. Each sample was then centrifuged at 300 g x 4 minutes and resuspended in 820 µL of DMEM/15% FCS, which was then distributed to 4 wells of 200 µL for each sample in a 96-well plate and incubated at 37°C for 30 minutes to equilibrate. For phospho-STAT1 experiments, 2 wells for each sample were then incubated at 37°C with 100 ng/mL IFN-γ or 100 ng/mL IFN-α for 15 minutes, while for phospho-STAT5 experiments, thrombopoietin was added to a concentration of 100 ng/mL and incubated at 37°C for 15 minutes. Cells were then promptly transferred to FACS tubes while adding 500 µL FACS buffer and centrifuged at 300 x

g for 4 minutes, then washed again in 500 µL FACS buffer and centrifuged again at 300 x g for 4 minutes. 250 µL of Fixation Buffer (BD Cytofix™, 554655) was then added to samples and resuspended gently and incubated at 4°C for 15 to 30 minutes. 500 µL FACS buffer was then added and samples centrifuged at 300 x g for 4 minutes and the supernatant was carefully aspirated off. 250 µL of ice cold Perm Buffer III (BD Phosflow™, 558050) was then used to resuspend cells which were then incubated on ice for 30 minutes. Cells were washed in 3 mL of FACS buffer and centrifuged at 300 x g for 4 minutes, resuspended in 3 mL of FACS buffer again, and divided equally into 2 tubes per sample: one designated to be stained with IgG isotype control antibody and the other to be stained with anti-p-STAT1 or anti-p-STAT5 antibody and centrifuged as before. Staining solutions were then prepared in PBS/2% BSA, with p-STAT1 antibody (1 µg per 1 x 10^6 cells) or p-STAT5 antibody (5 µL per 1 x 10^6 cells from a stock concentration of 0.05 mg/mL) and mouse IgG1 K isotype control prepared to the same concentration as the phospho-STAT antibody used. After centrifugation, the supernatant was aspirated and resuspended in 50 µL of respective staining solution and incubated on ice protected from light for 60 minutes. Compensation beads with a BV421 dye were also prepared, samples were washed in 400 µL FACS buffer, centrifuged at 300 x g for 4 minutes, resuspended in 300 µL FACS buffer, filtrated through 70 µm nylon filter mesh and taken for flow cytometry analysis.

5.11 Intracellular γH2A.X staining

Bone marrow cells were isolated from mice as per section 5.2.2, LSK were stained as per section 5.6.1 and sorted as per section 5.6.5. 100,000 LSK were then resuspended in 1 mL Serum-Free Expansion Medium (SFEM, StemSpan™) supplemented with 10% FCS, 100 ng/mL IL-6, 50 ng/mL SCF, 50 ng/mL TPO and divided into two 500 µL volumes, one for irradiation and one for an unirradiated control group with both samples kept on ice. LSK to be treated with irradiation were then irradiated with 2 Gray radiation in a Gammacell® 40 Exactor (Theratonics). All samples were then incubated for 1 hour at 37°C after which 500 µL of both unirradiated samples and 250 µL of both irradiated samples were taken for fixation, leaving 250 µL of irradiated cells for fixation 5 hours later. Cells were fixed by transferring them to FACS tubes and centrifuged at 300 x g for 4 minutes, followed by removal of supernatant and resuspension in 100 µL BD Cytofix/Cytoperm™ Fixation/Permeabilization solution and left to incubate at RTP for 15 minutes. Cells were then washed in 100 µL 1X BD Perm/Wash™ Buffer and kept on ice until the 6 hour post-irradiation cell group were ready for fixing. After all samples were fixed, samples were centrifuged at 300 x g for 4 minutes and the supernatant was aspirated, cells were then resuspended in 50 µL PBS/10% DMSO/0.4% Triton X-100 and incubated for 1-minute at room temperature (RTP). 950 µL 1X BD Perm/Wash™ Buffer was then used to wash cells, samples were transferred to 1.5 mL Eppendorf tubes, then centrifuged in a tabletop centrifuge at 3000 RPM for 3 minutes and the supernatant was aspirated. Unirradiated control cells of both genotypes were divided into two new 500 µL volumes, one tube for an anti-γH2A.X stain and the other for an anti-IgG1 stain. This resulted in 4 tubes each

containing 25,000 LSK per genotype. Fresh BLOCK-9 buffer (1 g/L BSA, 0.03% NaN_3, 0.1% Triton X-100, 5 mM EDTA, 1 mM $NaVO_4$, 1 mM Na_2MoO_4, 10 mM NaF, 0.1 g/L RNase A, H_2O) was prepared the day before, to which Herring Sperm DNA was now added to a concentration of 0.25 g/L. Samples were resuspended in a staining solution of anti-γH2A.X antibody (Millipore) in BLOCK-9 buffer at a concentration of 0.6 µg/mL or a staining solution of anti-IgG1 (Miltenyi Biotec) in BLOCK-9 buffer at a concentration of 0.16 µg/mL and incubated on ice for at least 6 hours. Samples were centrifuges at 3000 RPM for 3 minutes, the supernatant was aspirated and cells were resuspended in 300 µL FACS buffer, transferred to FACS tubes and taken for flow cytometry acquisition.

5.12 mRNA expression analysis

5.12.1 RNA isolation

RNA was isolated from fluorescence-assisted cell sorted HSC for qPCR and $CD34^-$ and $CD34^+$ LSK for RNA-sequencing using the RNeasy® Micro Kit (Qiagen) according to the manufacturer's protocol for purifying total RNA from animal and human cells. RNeasy MinElute® Spin Columns allowed to reach RTP before use and lysis buffer was supplemented with 1% β-mercaptoethanol. 75 µL lysis buffer was used to disrupt cells by gently drawing cells up and down in a 27G needle and syringe. The DNA digestion step of the manufacturer's protocol was included and RNA was eluted in 28 µL RNase-free water for RNA-sequencing and 14 µL for qPCR experiments.

RNA was isolated from fluorescence-assisted cell sorted $CD34^-$ and $CD34^+$ LSK using the Direct-zol™ RNA MiniPrep Kit (Zymo Research) according to the manufacturer's protocol for extracting RNA from ≤ 10^5 animal cells. 100 µL of lysis reagent was used to disrupt cells and the DNase I DNA digestion step was included.

RNA was directly frozen at -80°C and later thawed for cDNA reverse transcription.

5.12.2 Reverse transcription

Reverse transcription of RNA into cDNA was performed using the First Strand cDNA Synthesis Kit (Thermo Fisher Scientific™). Reactions were performed according to the manufacturer's protocol using 10 µL RNA and 10 µL master mix per reaction tube.

5.12.3 Quantitative real-time PCR

For qPCR experiments, a QuantStudio™ 3 Real-Time PCR System machine (Applied Biosystems) was used with MicroAmp™ Optical 96-Well Reaction Plates (Thermo Fisher Scientific™). The reaction mixture of each well consisted of 7.5 µL PowerUp™ SYBR™ Green Master Mix (Thermo Fisher Scientific™) 5.5 µL cDNA, 1 µL forward primer and 1 µL reverse primer. All reactions had 3 technical controls and all target genes had no-template DNA (water)

controls. Primers targeting the β-actin gene were used as a source material control. Primers were kept in stocks of 100 μM and used in a final reaction concentration of 200 nM. Template DNA was amplified through 40 cycles of a 58°C or 60°C annealing-extension step and a 95°C denaturation step.

5.12.4 Primers for qPCR

Gene	Primer	Sequence	Product (nt)
β-actin	fwd	TTGCTGACAGGATGCAGAAG	63
β-actin	rev	TGATCTTGATCTTCATGGTGCT	63
Cyclin D1	fwd	CTGGCTCTGTGCCTTTCTATTA	85
Cyclin D1	rev	CTTCACCTCTTCCCTCACATC	85
IRF7	fwd	CTTCAGCACTTTCTTCCGAGA	68
IRF7	rev	TGTAGTGTGGTGACCCTTGC	68
Kdm8	fwd	GATCAGCCTGCCACCAAG	75
Kdm8	rev	GGGTACCATCCGCTCTAACA	75
Miz-1 exons 6-7	fwd	CCGAAGCCTTATCAGAGAGC	76
Miz-1 exons 6-7	rev	TCCTCTTGTCCGTCTTCTCC	76
Miz-1 POZ domain	fwd	CGTGGTGCACCTAGACATCA	91
Miz-1 POZ domain	rev	GTTCTCAGGGCTAAGGCTCA	91
Mx1	fwd	TGTGGACATTGCTACCACAGA	90
Mx1	rev	AAGGCAGTTTGGACCATCTC	90
Necdin	fwd	CAAGAGATGTGCTGTGCTAAAC	98
Necdin	rev	AGGGCCTTCTTTGTCGATAC	98
OAS3	fwd	AACACTGGTACCGCCAGGT	88
OAS3	rev	AGGAGCTCCAGGGCGTAG	88
RORC	fwd	AGAGACACCACCGGACATCT	78
RORC	rev	TGCAAGGGATCACTTCAATTT	78
RPL22	fwd	TCTTAGCGCCTGCGTAGTG	79
RPL22	rev	TCGCCACAAGCTTTTTCA	79
SVA	fwd	CCTAACACTATCAGCCTCCATTC	89
SVA	rev	ACATTTGGTAAGAGTCGCCATA	89
VAMP4	fwd	TGCAAGAGAATATTACAAAGGTAATTG	95
VAMP4	rev	GAAAGCGGTGGCATTATCC	95
VWF	fwd	GAGGAACAGCGGTGTAAACG	93
VWF	rev	CTGGCATTGCTCCCACAT	93

5.12.5 RNA-Sequencing

Samples for RNA-sequencing were submitted to AG Marco Groth at the CF DNA Sequencing Facility of the Fritz Lipmann Institute and were sequenced by Ivonne Görlich using

the SMARTer® Stranded Total RNA-Seq Kit v2 - Pico Input Mammalian (Takara Bio). Analysis of raw RNA-sequencing data as well as production of multidimensional scaling plots and heat maps of raw gene counts were performed by Dr. Marco Groth.

5.13 Colony-forming unit assay

MethoCult™ GF M3434 media (STEMCELL Technologies) was thawed overnight at $4^{\circ}C$ before use. Bone marrow was isolated under sterile conditions as per section 5.2.1 and 3 x 10^4 BM cells were taken, centrifuged at 300 x g for 4 minutes, the supernatant was discarded and cells were resuspended in 300 µL Opti-MEM™ (Thermo Fisher Scientific™). Cells were then transferred to a round-bottomed 14 mL sterile tube and 3.5 mL MethoCult™ GF M3434 media was added through a syringe and gently drawn up and down. 1.2 mL of cell-media suspension was then transferred to a Petri dish in triplicate under sterile conditions. Cultures were then placed into a 200 mm diameter dish and incubated in 5% CO_2 at $37^{\circ}C$ and imaged 8 days after seeding. Images of colonies were taken using a Nikon light microscope in NIS-Elements Advanced Research version 4.5 imaging software.

5.13.1 Serial colony re-plating assay

MethoCult™ GF M3434 media was thawed overnight at $4^{\circ}C$ before use. After imaging, primary colonies were scraped off the surface of their methylcellulose media using a spatula under sterile conditions, resuspended in PBS and counted in a Neubauer chamber. A volume containing 3 x 10^4 was transferred to a sterile capped FACS tube, centrifuged at 300 x g for 4 minutes, the supernatant was discarded and cells were resuspended suspended in 300 µL Opti-MEM™. Cells were then transferred to a round-bottomed 14 mL sterile tube and 3.5 mL MethoCult™ GF M3434 media was added through a syringe and gently drawn up and down. 1.1 mL of cell-media suspension was then transferred to 3 Petri dishes under sterile conditions in triplicate. Cultures were then placed into a 200 mm diameter dish and incubated in 5% CO_2 at $37^{\circ}C$ and imaged 10 days after seeding. Images of colonies were taken using a Nikon light microscope in NIS-Elements Advanced Research version 4.5 imaging software.

5.14 Proteomics

Bone marrow was isolated from the whole skeleton as described in section 5.2.2, c-Kit$^+$ cells were enriched as per section 5.4 and LSK cells were stained as described in section 5.6.1, but only PBS that does not contain serum was used for all washing and incubation steps. Cells were sorted using a BD FACSAria™ Fusion with the cooler switched off. At least 1.1 x 10^5 LSK were sorted into 1.5 mL Micro tubes (Sarstedt Inc) containing a volume of 10X lysis buffer (10% SDS, 500 mM DTT, 1 M HEPES, pH 8.0) one-tenth of the final sorting volume. Samples were immediately snap frozen in liquid nitrogen upon sorting and stored at $-80^{\circ}C$. All protein extraction and MS was performed by Norman Rahnis of the CF Proteomics Facility of the Fritz Lipmann Institute and raw data was analysed by Dr. Joanna Kirkpatrick.

5.15 Chromatin-Immunoprecipitation (ChIP) followed by qPCR

5.15.1 Culture of the HPC-5 cell line

All ChIP experiments were conducted using cells of the Hematopoetic Progenitor Cell-5 (HPC-5) line, an immortal cell line from C57BL/6-cast mice bearing constitutive retroviral expression of the *Lhx2* gene (Ó et al., 2001). HPC-5 cells were obtained from Prof. Leif Carlsson of the Umeå Center for Molecular Medicine under a Biological Material Transfer Agreement. Thawed HPC-5 were cultured in SFEM (StemSpan™) supplemented with 10% FCS, 50 ng/mL IL-6, 50 ng/mL SCF, 50 ng/mL TPO and 1% penicillin-strepticillin (PENSTREP). When HPC-5 were growing exponentially, IL-6, SCF and TPO cytokines were supplemented to 25 ng/mL each. Media was prepared under sterile conditions by adding PENSTREP and FCS to SFEM upon thawing for use, sterile filtered, with cytokines added last. HPC-5 were passaged before reaching a cell density of 3×10^7 in 5 mL.

5.15.2 Chromatin Immunoprecipitation

2×10^7 HPC-5 cells were transferred from culture to a 5 mL Falcon and centrifuged at 300 x g for 4 minutes, resuspended in 1 mL PBS and transferred to a 1.5 mL Eppendorf tube. 65 µL formaldehyde was added to create a 16% formaldehyde solution and the sample rotated on a wheel for 10 minutes at RTP. Glycine was then added to 125 mM concentration to quench fixation and left for 5 minutes at RTP. Cells were then spun in a tabletop centrifuge at 3,000 RPM for 3 minutes, the supernatant was aspirated and the pellet was resuspended in 1 mL PBS. Cells were then centrifuged again at 3,000 RPM for 3 minutes and resuspended in 1 mL Buffer A and left on ice for 15 minutes, vortexed and then left at 30°C for 15 minutes. Cells were then centrifuged at 5,000 RPM, 4°C for 3 minutes, the supernatant was aspirated and 1 mL Buffer B was added and the sample incubated for 5 minutes on ice. Cells were then centrifuged at 5,000 RPM, 4°C for 3 minutes, the supernatant was aspirated and the pellet was resuspended in 1 mL Buffer C followed by incubation for 5 minutes on ice. Cells were then centrifuged at 5,000 RPM, 4°C for 3 minutes, the supernatant was aspirated and the pellet was resuspended in 50 µL Buffer D, transferred to a Diagenode sonication tube and sonicated in a Bioruptor® Diagenode sonication device for ten 30-second on/off cycles for 10 minutes at 4°C. Samples were then centrifuged at 12,000 RPM at 4°C for 10 minutes and supernatants transferred to new tubes and diluted with 250 µL immunoprecipitation (IP) Buffer. 15 µL of blocked protein A/G Sepharose beads were then added to each sample and spun on a wheel for 1-2 hours at 4°C to pre-clear chromatin. Samples were then spun down and the supernatant transferred to a new tube. 10% of the volume of the supernatant was taken as input to a new tube and NaCl was added to a concentration of 300 mM, input was then heated in a heat block overnight at 65°C. The remaining supernatant was then transferred to new tubes and immunoprecipitated with 0.75 µg anti-Miz-1 antibody (mMiz-1-2a supplied by Pineda) or 0.75 µg normal rabbit IgG control, rotating overnight at 4°C. Samples were then spun down and 20 µL blocked protein A/G Sepharose beads added to tubes and spun at 4°C for 1 hour. Beads

were then washed twice in 1 mL of the following buffers each with a 5 minute incubation period at RTP between washes: low salt washing buffer, high salt washing buffer, LiCl washing buffer and TE buffer. Beads were then spun down and the supernatant aspirated. 60 µL elution buffer was then added to beads and incubated for 20 minutes at RTP, then spun down and the supernatant transferred to a new tube. This was repeated twice, leaving 180 µL of chromatin solution which was decrosslinked in 5M NaCl at 65°C for 5-6 hours. DNA from immunoprecipitates and input was then purified using the ChIP Clean & Concentrator™ Kit (Zymo Research) according to the manufacturer's protocol.

5.15.3 Buffers used in ChIP

All buffer components measured in percentages are weight-over-volume percentages.

Buffer	Composition	pH (reagent)
Buffer A	100 mM Tris-HCl, 10 mM DTT	8.0 (Tris-HCl)
Buffer B	10 mM HEPES, 10 mM EDTA, 0.5 mM EGTA, 0.25% Triton-X100	7.5 (HEPES)
Buffer C	10 mM HEPES, 10 mM EDTA, 0.5 mM EGTA, 200 mM NaCl	7.5 (HEPES)
Buffer D	50 mM Tris-HCl, 10 mM EDTA, 1% SDS, 1 µL protease inhibitor cocktail	8.0 (Tris-HCl)
IP buffer	15 mM Tris-HCl, 1.2 mM EDTA, 180 mM NaCl, 1.2% Triton X-100	8.0 (Tris-HCl)
Low salt washing buffer	20 mM Tris-HCl, 2 mM EDTA, 150 mM NaCl, 0.1% SDS, 1% Triton X-100	8.0 (Tris-HCl)
High salt washing buffer	20 mM Tris-HCl, 2 mM EDTA, 500 mM NaCl, 0.1% SDS, 1% Triton X-100	8.0 (Tris-HCl)
LiCl washing buffer	10 mM Tris-HCl, 1 mM EDTA, 250 mM LiCl, 1% w/v Nonidet P-40, 1% sodium deoxycholate	8.0 (Tris-HCl)
TE buffer	50 mM Tris-HCl, 10 mM EDTA	8.0 (Tris-HCl)
Elution buffer	0.1 M NaHCO$_3$, 1% SDS	-
Protease inhibitor cocktail	2 mg/mL antipain, 1 mg/mL aprotinin, 100 mg/mL benzamidin and 1 mg/mL leupeptin	-

5.15.4 ChIP-qPCR

HPC-5 DNA from 1.3×10^7 cells was isolated using NucleoSpin™ DNA RapidLyse (Macherey-Nagel™) according to the manufacturer's protocol for fresh samples. QPCR was performed as

detailed in section 5.12.3. Target genes for all plates had no-template DNA (water) controls and ten-fold diluted input DNA control reactions. A standard curve composed of technical duplicates of 1:10, 1:100, 1:1000 and 1:10000 dilutions of a known amount of HPC-5 DNA was established using the standard curve function in the QuantStudio™ 3 Real-Time PCR System machine software, from which measurements from IP DNA and ten-fold diluted input DNA was quantified. IP DNA was then expressed as its normalised ratio over ten-fold diluted input DNA. DNA was amplified through 40 cycles of a 60°C annealing-extension step and a 95°C denaturation step.

5.15.5 Primers for ChIP-qPCR

Region	Primer	Sequence	Product (nt)
IFIT3 TSS	fwd	TCTTCCCTTTCACAAACACTGA	86
IFIT3 TSS	rev	GGATTATATAAGGGGGCAGTGG	86
IFIT3 +2000 bp	fwd	AAATATTTATCATGGAAGGATACAAGC	72
IFIT3 +2000 bp	rev	GCTTCCACAGTAGCTAATAACATCAG	72
IRF7 TSS	fwd	CAGGCAGGGTGTGGCTTA	73
IRF7 TSS	rev	GGATTTGCAATTGAGTGCTACA	73
IRF7 intron 6	fwd	GGACCCATTCACCTCCTACTG	91
IRF7 intron 6	rev	AGGCGCTAGCACAGCTTTT	91
KDM8 TSS	fwd	CGATCAGCCGAGTCAGAAGT	62
KDM8 TSS	rev	CTTCGGCTGGCTTTATCACC	62
KDM8 +1000 bp	fwd	AGCCTCTAAATTGGCTTCCC	100
KDM8 +1000 bp	rev	AATTCCACAGTTAGGCCATC	100

5.16 Immunofluorescent staining of γH2A.X foci and cytosolic DNA

5.16.1 LSK isolation, sorting and irradiation

Bone marrow was isolated from the whole skeleton as described in section 5.2.2, c-Kit+ cells were enriched as per section 5.4 and LSK cells were stained as described in section 5.6.1. LSK were sorted as per section 5.6.5 directly into SFEM (StemSpan™) supplemented with 25 ng/mL IL-6, 25 ng/mL SCF, 25 ng/mL TPO. Cells were kept on ice and divided into an irradiation group and a control group. LSKs to be irradiated were then irradiated with 2 Gray radiation in a Gammacell® 40 Exactor (Theratonics). After irradiation, all samples were incubated for 1 hour at 37°C. Unirradiated and irradiated cells were taken for fixation, while some irradiated cells were left to incubate for another 5 hours for later fixation.

5.16.2 LSK slide attachment and fixation

12 mm round coverslips (Carolina Biological) were stored in 100% ethanol and washed in water, placed in the wells of a 12-well plate and air-dried. 20 µL ten-fold water-diluted poly-

L-lysine solution (Sigma-Aldrich) was added to the surface of coverslips and incubated at RTP for 10 minutes, then pipetted off. Required cells were transferred to 1.5 mL Eppendorf tubes and centrifuged at 700 RPM for 4 minutes, supernatant was removed and cells were resuspended in 20 μL PBS, then transferred onto a coverslip and incubated for 30 minutes at 4°C. 400 μL 4% formaldehyde was then added to the well containing the coverslip and the 12-well plate was incubated for 10 minutes at RTP. Coverslips were then washed in 1 mL PBS and solutions were immediately removed by tipping the plate up. Coverslips were then washed twice more in 1 mL PBS, but with 5 minutes incubation at RTP between each wash.

5.16.3 Immunofluorescent staining and mounting of LSK

500 μL PBS/0.3% Triton-X100/2% BSA was added to wells containing coverslips and left for 30 minutes at RTP. This was then discarded by tipping and 0.5 – 1 mL PBS/2% BSA was added and left to incubate for an hour at RTP. Coverslips were then taken out of the 12-well plate using tweezers and placed facing upwards on the frosted side of a microscopic slide and remaining PBS/2% BSA was carefully removed. 15 μL of primary antibody staining solution (PBS/2% BSA/0.1% Triton X-100) containing a 1:200 dilution of anti-γH2A.X antibody (Biolegend), 1:200 dilution of anti-IgG (Invitrogen), or a 1:20 dilution F7-26 anti-ssDNA (Enzo Life Sciences) was then added to coverslips. Coverslips were then left in a humid chamber for 1 – 2 hours at 4°C in the dark. Coverslips were transferred back into the 12-well plate for washing and washed 3 times in 1 mL PBS with 5 minute incubation intervals. Coverslips were transferred again to a humid chamber, excess PBS was removed and 20 μL secondary antibody solution (PBS/2% BSA/0.1% Triton X-100) containing a 1:500 dilution of AF488 secondary antibody (Invitrogen) and were incubated for an hour at 4°C in the dark. Coverslips were then washed in a 12-well plate twice in PBS and twice in water. Microscopic slides were made clean with alcohol and water and mounting medium was prepared. DAPI was added to VECTASHIELD® HardSet™ Antifade Mounting Medium (Vector) to a final concentration of 170 ng/mL, 16 μL of which was added to microscopic slides. Coverslips were lowered onto using tweezers and left in the dark to set.

5.16.4 Imaging, signal normalisation and analysis of immunofluorescent samples

Slides were visualised with a DMi8 SP8 laser scanning confocal microscope (Leica) and images were saved in the LAS X Life Science Microscope Software Platform (Leica). For image analysis and signal quantification, Fiji ImageJ version 1.52p was used. Images were opened as .lif files and concatenated to a stack. A threshold of a required size was then applied such that signal in IgG control samples was insufficient for a count and the number of foci in γH2A.X samples were counted using the analyse particles function. The threshold was adjusted for each biological repeat. The same procedure was used for counting cells in the DAPI channel. The number of foci and the number of cells in the stack were then used to calculate the average number of foci per cell. No such analysis was performed on samples stained for ssDNA as they produced no signal.

5.17 Kits

Name	Company	Order number
ChIP Clean & Concentrator™ Kit	Zymo Research	D5201
Direct-zol™ RNA MiniPrep Kit	Zymo Research	R2051
RNeasy® Micro Kit	Qiagen	74004
First Strand cDNA Synthesis Kit	Thermo Fisher Scientific™	K1622
NucleoSpin™ DNA RapidLyse	Macherey-Nagel™	REF 740100.50

5.18 Data analysis

Data from all flow cytometry, colony assay, qPCR, immunofluorescent microscopy experiments were directly entered into GraphPad Prism®, version 8.4.1 for the creation of bar graphs with dot plot overlays. FACS plots and histograms of MFI for figures are images taken directly from FlowJo or FlowLogic Software. Data from RNA-sequencing experiments was submitted to GSEA 4.0.3 (Broad Institute) for the production of GSEA profiles using the Ensemble_mouse_gene chip file as a chip platform, the h.all.v7.1.symbols.gmt and c2.cp.reactome.v71 databases and with the permutation type set to gene set. Gene lists from RNA-sequencing and proteomics data were submitted to the DAVID Bioinformatics Resources 6.8 (National Institutes of Health) and PANTHER version 16.0 functional annotation tools for gene signature enrichment analysis. RNA-sequencing and proteomics data were also submitted to Ingenuity Pathway Analysis (Qiagen, spring release 2019 version) software for upstream regulator analyses. Bar graphs and heat maps (of specific genes) for RNA-sequencing and proteomics data analyses, were prepared using the programming language R x64 version 4.0.2 in RStudio version 1.1.383, while MDS plots and heat maps of all genes with more than 1 read count were prepared by Dr. Marco Groth also in R. Differentially regulated gene and protein lists were submitted to Cytoscape version 3.8.2, using StringApp version 1.6.0 to construct and design PPI networks. In generating the PPI network, default confidence score cutoff was set to 0.6 and maximum additional interactors set to 0.

5.19 Statistics

All statistical analyses, except those on the results from intracellular pSTAT1, pSTAT5 and γH2A.X FACS experiments, were calculated using the t-test function in GraphPad Prism® version 8.4.1. Results from intracellular pSTAT1, pSTAT5 and γH2A.X FACS experiments were calculated using a 2-way ANOVA function in GraphPad Prism® version 8.4.1 Statistical analysis was performed using paired (for *in vitro* LPS stimulation experiments) or unpaired (all others) t-test. Graphical figures show the mean and the error bars indicate the standard deviation. Statistical significance is indicated by * $p < 0.05$, ** $p < 0.01$, *** $p < 0.001$ and **** $p < 0.0001$.

6. Bibliography

Abramson, S., Miller, R. G., & Phillips, R. A. (1977). The identification in adult bone marrow of pluripotent and restricted stem cells of the myeloid and lymphoid systems. *The Journal of Experimental Medicine*, *145*(6), 1567–1579. https://doi.org/10.1084/jem.145.6.1567

Adhikary, S., Peukert, K., Karsunky, H., Beuger, V., Lutz, W., Elsässer, H.-P., Möröy, T., & Eilers, M. (2003). Miz1 is required for early embryonic development during gastrulation. *Molecular and Cellular Biology*, *23*(21), 7648–7657. https://doi.org/10.1128/MCB.23.21.7648-7657.2003

Adolfsson, J., Borge, O. J., Bryder, D., Theilgaard-Mönch, K., Astrand-Grundström, I., Sitnicka, E., Sasaki, Y., & Jacobsen, S. E. (2001). Upregulation of Flt3 expression within the bone marrow Lin(-)Sca1(+)c-kit(+) stem cell compartment is accompanied by loss of self-renewal capacity. *Immunity*, *15*(4), 659–669. https://doi.org/10.1016/s1074-7613(01)00220-5

Adolfsson, J., Månsson, R., Buza-Vidas, N., Hultquist, A., Liuba, K., Jensen, C. T., Bryder, D., Yang, L., Borge, O.-J., Thoren, L. A. M., Anderson, K., Sitnicka, E., Sasaki, Y., Sigvardsson, M., & Jacobsen, S. E. W. (2005). Identification of Flt3+ lympho-myeloid stem cells lacking erythro-megakaryocytic potential a revised road map for adult blood lineage commitment. *Cell*, *121*(2), 295–306. https://doi.org/10.1016/j.cell.2005.02.013

Akashi, K., Traver, D., Miyamoto, T., & Weissman, I. L. (2000). A clonogenic common myeloid progenitor that gives rise to all myeloid lineages. *Nature*, *404*(6774), 193–197. https://doi.org/10.1038/35004599

Alexopoulou, L., Holt, A. C., Medzhitov, R., & Flavell, R. A. (2001). Recognition of double-stranded RNA and activation of NF-kappaB by Toll-like receptor 3. *Nature*, *413*(6857), 732–738. https://doi.org/10.1038/35099560

Au-Yeung, N., Mandhana, R., & Horvath, C. M. (2013). Transcriptional regulation by STAT1 and STAT2 in the interferon JAK-STAT pathway. *JAK-STAT*, *2*(3), e23931. https://doi.org/10.4161/jkst.23931

Baena, E., Ortiz, M., Martínez-A, C., & de Alborán, I. M. (2007). C-Myc is essential for hematopoietic stem cell differentiation and regulates Lin(-)Sca-1(+)c-Kit(-) cell generation through p21. *Experimental Hematology*, *35*(9), 1333–1343. https://doi.org/10.1016/j.exphem.2007.05.015

Bahr, C., von Paleske, L., Uslu, V. V., Remeseiro, S., Takayama, N., Ng, S. W., Murison, A., Langenfeld, K., Petretich, M., Scognamiglio, R., Zeisberger, P., Benk, A. S., Amit, I., Zandstra, P. W., Lupien, M., Dick, J. E., Trumpp, A., & Spitz, F. (2018). A Myc enhancer cluster regulates normal and leukaemic haematopoietic stem cell hierarchies. *Nature*, *553*(7689), 515–520. https://doi.org/10.1038/nature25193

Baldridge, M. T., King, K. Y., Boles, N. C., Weksberg, D. C., & Goodell, M. A. (2010). Quiescent haematopoietic stem cells are activated by IFN-gamma in response to chronic infection. *Nature*, *465*(7299), 793–797. https://doi.org/10.1038/nature09135

Banerjee, S., Gusho, E., Gaughan, C., Dong, B., Gu, X., Holvey-Bates, E., Talukdar, M., Li, Y., Weiss, S. R., Sicheri, F., Saunthararajah, Y., Stark, G. R., & Silverman, R. H. (2019). OAS-RNase L innate immune pathway mediates the cytotoxicity of a DNA-demethylating drug. *Proceedings of the National Academy of Sciences of the United States of America*, *116*(11), 5071–5076. https://doi.org/10.1073/pnas.1815071116

Basu, S., Liu, Q., Qiu, Y., & Dong, F. (2009). Gfi-1 represses CDKN2B encoding p15INK4B through interaction with Miz-1. *Proceedings of the National Academy of Sciences of the United States of America*, *106*(5), 1433–1438. https://doi.org/10.1073/pnas.0804863106

Beerman, I., Bhattacharya, D., Zandi, S., Sigvardsson, M., Weissman, I. L., Bryder, D., & Rossi, D. J. (2010). Functionally distinct hematopoietic stem cells modulate hematopoietic lineage potential during aging by a mechanism of clonal expansion. *Proceedings of the National Academy of Sciences of the United States of America*, *107*(12), 5465–5470. https://doi.org/10.1073/pnas.1000834107

Beerman, I., Seita, J., Inlay, M. A., Weissman, I. L., & Rossi, D. J. (2014). Quiescent hematopoietic stem cells accumulate DNA damage during aging that is repaired upon entry into cell cycle. *Cell Stem Cell*, *15*(1), 37–50. https://doi.org/10.1016/j.stem.2014.04.016

Bradley, T. R., & Metcalf, D. (1966). The growth of mouse bone marrow cells in vitro. *The Australian Journal of Experimental Biology and Medical Science*, *44*(3), 287–299. https://doi.org/10.1038/icb.1966.28

Broxmeyer, H. E., Lu, L., Platzer, E., Feit, C., Juliano, L., & Rubin, B. Y. (1983). Comparative analysis of the influences of human gamma, alpha and beta interferons on human multipotential (CFU-GEMM), erythroid (BFU-E) and granulocyte-macrophage (CFU-GM) progenitor cells. *Journal of Immunology (Baltimore, Md.: 1950)*, *131*(3), 1300–1305.

Buechler, M. B., Teal, T. H., Elkon, K. B., & Hamerman, J. A. (2013). Cutting edge: Type I IFN drives emergency myelopoiesis and peripheral myeloid expansion during chronic TLR7 signaling. *Journal of Immunology (Baltimore, Md.: 1950)*, *190*(3), 886–891. https://doi.org/10.4049/jimmunol.1202739

Buyandelger, B., Mansfield, C., Kostin, S., Choi, O., Roberts, A. M., Ware, J. S., Mazzarotto, F., Pesce, F., Buchan, R., Isaacson, R. L., Vouffo, J., Gunkel, S., Knöll, G., McSweeney, S. J., Wei, H., Perrot, A., Pfeiffer, C., Toliat, M. R., Ilieva, K., ... Knöll, R. (2015). ZBTB17 (MIZ1) Is Important for the Cardiac Stress Response and a Novel Candidate Gene for Cardiomyopathy and Heart Failure. *Circulation. Cardiovascular Genetics*, *8*(5), 643–652. https://doi.org/10.1161/CIRCGENETICS.113.000690

Buza-Vidas, N., Antonchuk, J., Qian, H., Månsson, R., Luc, S., Zandi, S., Anderson, K., Takaki, S., Nygren, J. M., Jensen, C. T., & Jacobsen, S. E. W. (2006). Cytokines regulate postnatal hematopoietic stem cell expansion: Opposing roles of thrombopoietin and LNK. *Genes & Development*, *20*(15), 2018–2023. https://doi.org/10.1101/gad.385606

Cabezas-Wallscheid, N., Klimmeck, D., Hansson, J., Lipka, D. B., Reyes, A., Wang, Q., Weichenhan, D., Lier, A., von Paleske, L., Renders, S., Wünsche, P., Zeisberger, P., Brocks, D., Gu, L., Herrmann, C., Haas, S., Essers, M. A. G., Brors, B., Eils, R., … Trumpp, A. (2014). Identification of regulatory networks in HSCs and their immediate progeny via integrated proteome, transcriptome, and DNA methylome analysis. *Cell Stem Cell*, *15*(4), 507–522. https://doi.org/10.1016/j.stem.2014.07.005

Carlin, A. F., Plummer, E. M., Vizcarra, E. A., Sheets, N., Joo, Y., Tang, W., Day, J., Greenbaum, J., Glass, C. K., Diamond, M. S., & Shresta, S. (2017). An IRF-3-, IRF-5-, and IRF-7-Independent Pathway of Dengue Viral Resistance Utilizes IRF-1 to Stimulate Type I and II Interferon Responses. *Cell Reports*, *21*(6), 1600–1612. https://doi.org/10.1016/j.celrep.2017.10.054

Carrelha, J., Meng, Y., Kettyle, L. M., Luis, T. C., Norfo, R., Alcolea, V., Boukarabila, H., Grasso, F., Gambardella, A., Grover, A., Högstrand, K., Lord, A. M., Sanjuan-Pla, A., Woll, P. S., Nerlov, C., & Jacobsen, S. E. W. (2018). Hierarchically related lineage-restricted fates of multipotent haematopoietic stem cells. *Nature*, *554*(7690), 106–111. https://doi.org/10.1038/nature25455

Chambers, S. M., Shaw, C. A., Gatza, C., Fisk, C. J., Donehower, L. A., & Goodell, M. A. (2007). Aging hematopoietic stem cells decline in function and exhibit epigenetic dysregulation. *PLoS Biology*, *5*(8), e201. https://doi.org/10.1371/journal.pbio.0050201

Chanprasert, S., Geddis, A. E., Barroga, C., Fox, N. E., & Kaushansky, K. (2006). Thrombopoietin (TPO) induces c-myc expression through a PI3K- and MAPK-dependent pathway that is not mediated by Akt, PKCzeta or mTOR in TPO-dependent cell lines and primary megakaryocytes. *Cellular Signalling*, *18*(8), 1212–1218. https://doi.org/10.1016/j.cellsig.2005.09.010

Choi, U. Y., Kang, J.-S., Hwang, Y. S., & Kim, Y.-J. (2015). Oligoadenylate synthase-like (OASL) proteins: Dual functions and associations with diseases. *Experimental & Molecular Medicine*, *47*, e144. https://doi.org/10.1038/emm.2014.110

Civin, C. I., Strauss, L. C., Brovall, C., Fackler, M. J., Schwartz, J. F., & Shaper, J. H. (1984). Antigenic analysis of hematopoiesis. III. A hematopoietic progenitor cell surface antigen defined by a monoclonal antibody raised against KG-1a cells. *Journal of Immunology (Baltimore, Md.: 1950)*, *133*(1), 157–165.

Coffman, R. L., & Weissman, I. L. (1981). B220: A B cell-specific member of th T200 glycoprotein family. *Nature*, *289*(5799), 681–683. https://doi.org/10.1038/289681a0

Comoglio, F., Park, H. J., Schoenfelder, S., Barozzi, I., Bode, D., Fraser, P., & Green, A. R. (2018). Thrombopoietin signaling to chromatin elicits rapid and pervasive epigenome remodeling within poised chromatin architectures. *Genome Research*, gr.227272.117. https://doi.org/10.1101/gr.227272.117

Coppola, J. A., & Cole, M. D. (1986). Constitutive c-myc oncogene expression blocks mouse erythroleukaemia cell differentiation but not commitment. *Nature*, *320*(6064), 760–763. https://doi.org/10.1038/320760a0

Dahlin, J. S., Hamey, F. K., Pijuan-Sala, B., Shepherd, M., Lau, W. W. Y., Nestorowa, S., Weinreb, C., Wolock, S., Hannah, R., Diamanti, E., Kent, D. G., Göttgens, B., & Wilson, N. K. (2018). A single-cell hematopoietic landscape resolves 8 lineage trajectories and defects in Kit mutant mice. *Blood*, *131*(21), e1–e11. https://doi.org/10.1182/blood-2017-12-821413

de Boer, J., Williams, A., Skavdis, G., Harker, N., Coles, M., Tolaini, M., Norton, T., Williams, K., Roderick, K., Potocnik, A. J., & Kioussis, D. (2003). Transgenic mice with hematopoietic and lymphoid specific expression of Cre. *European Journal of Immunology*, *33*(2), 314–325. https://doi.org/10.1002/immu.200310005

de Bruin, A. M., Demirel, Ö., Hooibrink, B., Brandts, C. H., & Nolte, M. A. (2013). Interferon-γ impairs proliferation of hematopoietic stem cells in mice. *Blood*, *121*(18), 3578–3585. https://doi.org/10.1182/blood-2012-05-432906

Dexter, T. M., Allen, T. D., & Lajtha, L. G. (1977). Conditions controlling the proliferation of haemopoietic stem cells in vitro. *Journal of Cellular Physiology*, *91*(3), 335–344. https://doi.org/10.1002/jcp.1040910303

Di Scala, M., Gil-Fariña, I., Vanrell, L., Sánchez-Bayona, R., Alignani, D., Olagüe, C., Vales, A., Berraondo, P., Prieto, J., & González-Aseguinolaza, G. (2015). Chronic exposure to IFNα drives medullar lymphopoiesis towards T-cell differentiation in mice. *Haematologica*, *100*(8), 1014–1022. https://doi.org/10.3324/haematol.2014.115410

Diamond, M. S., & Farzan, M. (2013). The broad-spectrum antiviral functions of IFIT and IFITM proteins. *Nature Reviews. Immunology*, *13*(1), 46–57. https://doi.org/10.1038/nri3344

Ding, L., Saunders, T. L., Enikolopov, G., & Morrison, S. J. (2012). Endothelial and perivascular cells maintain haematopoietic stem cells. *Nature*, *481*(7382), 457–462. https://doi.org/10.1038/nature10783

Do-Umehara, H. C., Chen, C., Urich, D., Zhou, L., Qiu, J., Jang, S., Zander, A., Baker, M. A., Eilers, M., Sporn, P. H. S., Ridge, K. M., Sznajder, J. I., Budinger, G. R. S., Mutlu, G. M., Lin, A., & Liu, J. (2013). Suppression of inflammation and acute lung injury by Miz1 via repression of C/EBP-δ. *Nature Immunology*, *14*(5), 461–469. https://doi.org/10.1038/ni.2566

Du, J., Wang, J., Kong, G., Jiang, J., Zhang, J., Liu, Y., Tong, W., & Zhang, J. (2012). Signaling profiling at the single-cell level identifies a distinct signaling signature in murine hematopoietic stem cells. *Stem Cells (Dayton, Ohio)*, *30*(7), 1447–1454. https://doi.org/10.1002/stem.1127

Duesberg, P. H., & Vogt, P. K. (1979). Avian acute leukemia viruses MC29 and MH2 share specific RNA sequences: Evidence for a second class of transforming genes. *Proceedings of the National Academy of Sciences of the United States of America*, *76*(4), 1633–1637. https://doi.org/10.1073/pnas.76.4.1633

Dykstra, B., Olthof, S., Schreuder, J., Ritsema, M., & de Haan, G. (2011). Clonal analysis reveals multiple functional defects of aged murine hematopoietic stem cells. *The Journal of Experimental Medicine*, *208*(13), 2691–2703. https://doi.org/10.1084/jem.20111490

Eggenberger, J., Blanco-Melo, D., Panis, M., Brennand, K. J., & tenOever, B. R. (2019). Type I interferon response impairs differentiation potential of pluripotent stem cells. *Proceedings of the National Academy of Sciences of the United States of America*, *116*(4), 1384–1393. https://doi.org/10.1073/pnas.1812449116

Ehninger, A., Boch, T., Uckelmann, H., Essers, M. A., Müdder, K., Sleckman, B. P., & Trumpp, A. (2014). Posttranscriptional regulation of c-Myc expression in adult murine HSCs during homeostasis and interferon-α-induced stress response. *Blood*, *123*(25), 3909–3913. https://doi.org/10.1182/blood-2013-10-531038

Ema, H., Takano, H., Sudo, K., & Nakauchi, H. (2000). In vitro self-renewal division of hematopoietic stem cells. *The Journal of Experimental Medicine*, *192*(9), 1281–1288. https://doi.org/10.1084/jem.192.9.1281

Eskildsen, S., Justesen, J., Schierup, M. H., & Hartmann, R. (2003). Characterization of the 2′-5′-oligoadenylate synthetase ubiquitin-like family. *Nucleic Acids Research*, *31*(12), 3166–3173. https://doi.org/10.1093/nar/gkg427

Esplin, B. L., Shimazu, T., Welner, R. S., Garrett, K. P., Nie, L., Zhang, Q., Humphrey, M. B., Yang, Q., Borghesi, L. A., & Kincade, P. W. (2011). Chronic exposure to a TLR ligand injures hematopoietic stem cells. *Journal of Immunology (Baltimore, Md.: 1950)*, *186*(9), 5367–5375. https://doi.org/10.4049/jimmunol.1003438

Essers, M. A. G., Offner, S., Blanco-Bose, W. E., Waibler, Z., Kalinke, U., Duchosal, M. A., & Trumpp, A. (2009). IFNalpha activates dormant haematopoietic stem cells in vivo. *Nature*, *458*(7240), 904–908. https://doi.org/10.1038/nature07815

Fan, P., Lin, Q.-H., Guo, Y., Zhao, L.-L., Ning, H., Liu, M.-Y., & Wei, D.-Q. (2018). The PPI network analysis of mRNA expression profile of uterus from primary dysmenorrheal rats. *Scientific Reports*, *8*(1), 351. https://doi.org/10.1038/s41598-017-18748-2

Fauser, A. A., & Messner, H. A. (1979). Proliferative state of human pluripotent hemopoietic progenitors (CFU-GEMM) in normal individuals and under regenerative conditions after bone marrow transplantation. *Blood*, *54*(5), 1197–1200.

Finver, S. N., Nishikura, K., Finger, L. R., Haluska, F. G., Finan, J., Nowell, P. C., & Croce, C. M. (1988). Sequence analysis of the MYC oncogene involved in the t(8;14)(q24;q11) chromosome translocation in a human leukemia T-cell line indicates that putative regulatory regions are not altered. *Proceedings of the National Academy of Sciences of the United States of America*, *85*(9), 3052–3056. https://doi.org/10.1073/pnas.85.9.3052

Fuhrmann, D., Mernberger, M., Nist, A., Stiewe, T., & Elsässer, H.-P. (2018). Miz1 Controls Schwann Cell Proliferation via H3K36me2 Demethylase Kdm8 to Prevent Peripheral Nerve Demyelination. *Journal of Neuroscience*, *38*(4), 858–877. https://doi.org/10.1523/JNEUROSCI.0843-17.2017

Gebhardt, A., Kosan, C., Herkert, B., Möröy, T., Lutz, W., Eilers, M., & Elsässer, H.-P. (2007). Miz1 is required for hair follicle structure and hair morphogenesis. *Journal of Cell Science*, *120*(Pt 15), 2586–2593. https://doi.org/10.1242/jcs.007104

Gekas, C., & Graf, T. (2013). CD41 expression marks myeloid-biased adult hematopoietic stem cells and increases with age. *Blood*, *121*(22), 4463–4472. https://doi.org/10.1182/blood-2012-09-457929

Golub, E. S. (1972). BRAIN-ASSOCIATED STEM CELL ANTIGEN: AN ANTIGEN SHARED BY BRAIN AND HEMOPOIETIC STEM CELLS. *The Journal of Experimental Medicine*, *136*(2), 369–374.

Gregory, C. J. (1976). Erythropoietin sensitivity as a differentiation marker in the hemopoietic system: Studies of three erythropoietic colony responses in culture. *Journal of Cellular Physiology*, *89*(2), 289–301. https://doi.org/10.1002/jcp.1040890212

Grinenko, T., Eugster, A., Thielecke, L., Ramasz, B., Krüger, A., Dietz, S., Glauche, I., Gerbaulet, A., von Bonin, M., Basak, O., Clevers, H., Chavakis, T., & Wielockx, B. (2018). Hematopoietic stem cells can differentiate into restricted myeloid progenitors before cell division in mice. *Nature Communications*, *9*(1), 1898. https://doi.org/10.1038/s41467-018-04188-7

Grubeck-Loebenstein, B., Della Bella, S., Iorio, A. M., Michel, J.-P., Pawelec, G., & Solana, R. (2009). Immunosenescence and vaccine failure in the elderly. *Aging Clinical and Experimental Research*, *21*(3), 201–209. https://doi.org/10.1007/BF03324904

Guo, G., Luc, S., Marco, E., Lin, T.-W., Peng, C., Kerenyi, M. A., Beyaz, S., Kim, W., Xu, J., Das, P. P., Neff, T., Zou, K., Yuan, G.-C., & Orkin, S. H. (2013). Mapping cellular hierarchy by single-cell analysis of the cell surface repertoire. *Cell Stem Cell*, *13*(4), 492–505. https://doi.org/10.1016/j.stem.2013.07.017

Guo, Y., Niu, C., Breslin, P., Tang, M., Zhang, S., Wei, W., Kini, A. R., Paner, G. P., Alkan, S., Morris, S. W., Diaz, M., Stiff, P. J., & Zhang, J. (2009). C-Myc-mediated control of cell fate in megakaryocyte-erythrocyte progenitors. *Blood*, *114*(10), 2097–2106. https://doi.org/10.1182/blood-2009-01-197947

Gurney, A. L., Carver-Moore, K., de Sauvage, F. J., & Moore, M. W. (1994). Thrombocytopenia in c-mpl-deficient mice. *Science (New York, N.Y.)*, *265*(5177), 1445–1447. https://doi.org/10.1126/science.8073287

Haas, S., Hansson, J., Klimmeck, D., Loeffler, D., Velten, L., Uckelmann, H., Wurzer, S., Prendergast, Á. M., Schnell, A., Hexel, K., Santarella-Mellwig, R., Blaszkiewicz, S., Kuck, A., Geiger, H., Milsom, M. D., Steinmetz, L. M., Schroeder, T., Trumpp, A., Krijgsveld, J., & Essers, M. A. G. (2015). Inflammation-Induced Emergency Megakaryopoiesis Driven by Hematopoietic Stem Cell-like Megakaryocyte Progenitors. *Cell Stem Cell*, *17*(4), 422–434. https://doi.org/10.1016/j.stem.2015.07.007

Hancks, D. C., Hartley, M. K., Hagan, C., Clark, N. L., & Elde, N. C. (2015). Overlapping Patterns of Rapid Evolution in the Nucleic Acid Sensors cGAS and OAS1 Suggest a Common Mechanism of Pathogen Antagonism and Escape. *PLoS Genetics*, *11*(5), e1005203. https://doi.org/10.1371/journal.pgen.1005203

Härtlova, A., Erttmann, S. F., Raffi, F. A., Schmalz, A. M., Resch, U., Anugula, S., Lienenklaus, S., Nilsson, L. M., Kröger, A., Nilsson, J. A., Ek, T., Weiss, S., & Gekara, N. O. (2015). DNA damage primes the type I interferon system via the cytosolic DNA sensor STING to promote anti-microbial innate immunity. *Immunity*, *42*(2), 332–343. https://doi.org/10.1016/j.immuni.2015.01.012

Hérault, L., Poplineau, M., Mazuel, A., Platet, N., Remy, É., & Duprez, E. (2021). Single-cell RNA-seq reveals a concomitant delay in differentiation and cell cycle of aged hematopoietic stem cells. *BMC Biology*, *19*(1), 19. https://doi.org/10.1186/s12915-021-00955-z

Herkert, B., Dwertmann, A., Herold, S., Abed, M., Naud, J.-F., Finkernagel, F., Harms, G. S., Orian, A., Wanzel, M., & Eilers, M. (2010). The Arf tumor suppressor protein inhibits Miz1 to suppress cell adhesion and induce apoptosis. *The Journal of Cell Biology*, *188*(6), 905–918. https://doi.org/10.1083/jcb.200908103

Herold, S., Wanzel, M., Beuger, V., Frohme, C., Beul, D., Hillukkala, T., Syvaoja, J., Saluz, H.-P., Haenel, F., & Eilers, M. (2002). Negative regulation of the mammalian UV response by Myc through association with Miz-1. *Molecular Cell*, *10*(3), 509–521. https://doi.org/10.1016/s1097-2765(02)00633-0

Hodgson, G. S., & Bradley, T. R. (1979). Properties of haematopoietic stem cells surviving 5-fluorouracil treatment: Evidence for a pre-CFU-S cell? *Nature*, *281*(5730), 381–382. https://doi.org/10.1038/281381a0

Hönnemann, J., Sanz-Moreno, A., Wolf, E., Eilers, M., & Elsässer, H.-P. (2012). Miz1 is a critical repressor of cdkn1a during skin tumorigenesis. *PloS One*, *7*(4), e34885. https://doi.org/10.1371/journal.pone.0034885

Huang, D. W., Sherman, B. T., & Lempicki, R. A. (2009). Systematic and integrative analysis of large gene lists using DAVID bioinformatics resources. *Nature Protocols*, *4*(1), 44–57. https://doi.org/10.1038/nprot.2008.211

Ichikawa, Y., Pluznik, D. H., & Sachs, L. (1966). In vitro control of the development of macrophage and granulocyte colonies. *Proceedings of the National Academy of Sciences of the United States of America*, *56*(2), 488–495. https://doi.org/10.1073/pnas.56.2.488

Ikonomi, N., Kühlwein, S. D., Schwab, J. D., & Kestler, H. A. (2020). Awakening the HSC: Dynamic Modeling of HSC Maintenance Unravels Regulation of the TP53 Pathway and Quiescence. *Frontiers in Physiology*, *11*, 848. https://doi.org/10.3389/fphys.2020.00848

Inoue, S., Hao, Z., Elia, A. J., Cescon, D., Zhou, L., Silvester, J., Snow, B., Harris, I. S., Sasaki, M., Li, W. Y., Itsumi, M., Yamamoto, K., Ueda, T., Dominguez-Brauer, C., Gorrini, C., Chio, I. I. C., Haight, J.,

You-Ten, A., McCracken, S., … Mak, T. W. (2013). Mule/Huwe1/Arf-BP1 suppresses Ras-driven tumorigenesis by preventing c-Myc/Miz1-mediated down-regulation of p21 and p15. *Genes & Development*, *27*(10), 1101–1114. https://doi.org/10.1101/gad.214577.113

Iriuchishima, H., Takubo, K., Matsuoka, S., Onoyama, I., Nakayama, K. I., Nojima, Y., & Suda, T. (2011). Ex vivo maintenance of hematopoietic stem cells by quiescence induction through Fbxw7α overexpression. *Blood*, *117*(8), 2373–2377. https://doi.org/10.1182/blood-2010-07-294801

Jacobson, L. O., Simmons, E. L., Marks, E. K., Robson, M. J., Bethard, W. F., & Gaston, E. O. (1950). The role of the spleen in radiation injury and recovery. *The Journal of Laboratory and Clinical Medicine*, *35*(5), 746–770.

Jefferies, C. A. (2019). Regulating IRFs in IFN Driven Disease. *Frontiers in Immunology*, *10*, 325. https://doi.org/10.3389/fimmu.2019.00325

Johnson, G. R., & Metcalf, D. (1977). Pure and mixed erythroid colony formation in vitro stimulated by spleen conditioned medium with no detectable erythropoietin. *Proceedings of the National Academy of Sciences of the United States of America*, *74*(9), 3879–3882. https://doi.org/10.1073/pnas.74.9.3879

Kaushansky, K. (1997). Thrombopoietin: Understanding and manipulating platelet production. *Annual Review of Medicine*, *48*, 1–11. https://doi.org/10.1146/annurev.med.48.1.1

Kerosuo, L., & Bronner, M. E. (2016). CMyc Regulates the Size of the Premigratory Neural Crest Stem Cell Pool. *Cell Reports*, *17*(10), 2648–2659. https://doi.org/10.1016/j.celrep.2016.11.025

Kiel, M. J., Yilmaz, O. H., Iwashita, T., Yilmaz, O. H., Terhorst, C., & Morrison, S. J. (2005). SLAM family receptors distinguish hematopoietic stem and progenitor cells and reveal endothelial niches for stem cells. *Cell*, *121*(7), 1109–1121. https://doi.org/10.1016/j.cell.2005.05.026

Kondo, M., Weissman, I. L., & Akashi, K. (1997). Identification of clonogenic common lymphoid progenitors in mouse bone marrow. *Cell*, *91*(5), 661–672. https://doi.org/10.1016/s0092-8674(00)80453-5

Konstantinov, I. E. (2000). In search of Alexander A. Maximow: The man behind the unitarian theory of hematopoiesis. *Perspectives in Biology and Medicine*, *43*(2), 269–276. https://doi.org/10.1353/pbm.2000.0006

Korać, P., Dotlić, S., Matulić, M., Zajc Petranović, M., & Dominis, M. (2017). Role of MYC in B Cell Lymphomagenesis. *Genes*, *8*(4), E115. https://doi.org/10.3390/genes8040115

Kosan, C., Rashkovan, M., Ross, J., Schaffer, A.-M., Saba, I., Lemsaddek, W., Trudel, M., & Möröy, T. (2014). The transcription factor Miz-1 is required for embryonic and stress-induced erythropoiesis but dispensable for adult erythropoiesis. *American Journal of Blood Research*, *4*(1), 7–19.

Kosan, C., Saba, I., Godmann, M., Herold, S., Herkert, B., Eilers, M., & Möröy, T. (2010). Transcription factor miz-1 is required to regulate interleukin-7 receptor signaling at early commitment stages of B cell differentiation. *Immunity*, *33*(6), 917–928. https://doi.org/10.1016/j.immuni.2010.11.028

Kowalczyk, M. S., Tirosh, I., Heckl, D., Rao, T. N., Dixit, A., Haas, B. J., Schneider, R. K., Wagers, A. J., Ebert, B. L., & Regev, A. (2015). Single-cell RNA-seq reveals changes in cell cycle and differentiation programs upon aging of hematopoietic stem cells. *Genome Research*, *25*(12), 1860–1872. https://doi.org/10.1101/gr.192237.115

Ku, H., Yonemura, Y., Kaushansky, K., & Ogawa, M. (1996). Thrombopoietin, the ligand for the Mpl receptor, synergizes with steel factor and other early acting cytokines in supporting proliferation of primitive hematopoietic progenitors of mice. *Blood*, *87*(11), 4544–4551.

Kumar, R., Fossati, V., Israel, M., & Snoeck, H.-W. (2008). Lin-Sca1+kit- bone marrow cells contain early lymphoid-committed precursors that are distinct from common lymphoid progenitors. *Journal of Immunology (Baltimore, Md.: 1950)*, *181*(11), 7507–7513. https://doi.org/10.4049/jimmunol.181.11.7507

Kunisaki, Y., Bruns, I., Scheiermann, C., Ahmed, J., Pinho, S., Zhang, D., Mizoguchi, T., Wei, Q., Lucas, D., Ito, K., Mar, J. C., Bergman, A., & Frenette, P. S. (2013). Arteriolar niches maintain haematopoietic stem cell quiescence. *Nature*, *502*(7473), 637–643. https://doi.org/10.1038/nature12612

Larbi, A., Fülöp, T., & Pawelec, G. (2008). Immune receptor signaling, aging and autoimmunity. *Advances in Experimental Medicine and Biology*, *640*, 312–324. https://doi.org/10.1007/978-0-387-09789-3_21

Laurenti, E., Varnum-Finney, B., Wilson, A., Ferrero, I., Blanco-Bose, W. E., Ehninger, A., Knoepfler, P. S., Cheng, P.-F., MacDonald, H. R., Eisenman, R. N., Bernstein, I. D., & Trumpp, A. (2008). Hematopoietic stem cell function and survival depend on c-Myc and N-Myc activity. *Cell Stem Cell*, *3*(6), 611–624. https://doi.org/10.1016/j.stem.2008.09.005

Lorenz, E., Uphoff, D., Reid, T. R., & Shelton, E. (1951). Modification of irradiation injury in mice and guinea pigs by bone marrow injections. *Journal of the National Cancer Institute*, *12*(1), 197–201.

Lu, J., Chen, M., Ren, X.-R., Wang, J., Lyerly, H. K., Barak, L., & Chen, W. (2013). Regulation of hedgehog signaling by Myc-interacting zinc finger protein 1, Miz1. *PloS One*, *8*(5), e63353. https://doi.org/10.1371/journal.pone.0063353

MacNamara, K. C., Jones, M., Martin, O., & Winslow, G. M. (2011). Transient activation of hematopoietic stem and progenitor cells by IFNγ during acute bacterial infection. *PloS One*, *6*(12), e28669. https://doi.org/10.1371/journal.pone.0028669

MacNamara, K. C., Oduro, K., Martin, O., Jones, D. D., McLaughlin, M., Choi, K., Borjesson, D. L., & Winslow, G. M. (2011). Infection-induced myelopoiesis during intracellular bacterial infection is critically dependent upon IFN-γ signaling. *Journal of Immunology (Baltimore, Md.: 1950)*, *186*(2), 1032–1043. https://doi.org/10.4049/jimmunol.1001893

Malathi, K., Dong, B., Gale, M., & Silverman, R. H. (2007). Small self-RNA generated by RNase L amplifies antiviral innate immunity. *Nature*, *448*(7155), 816–819. https://doi.org/10.1038/nature06042

Mann, M., Mehta, A., de Boer, C. G., Kowalczyk, M. S., Lee, K., Haldeman, P., Rogel, N., Knecht, A. R., Farouq, D., Regev, A., & Baltimore, D. (2018). Heterogeneous Responses of Hematopoietic Stem Cells to Inflammatory Stimuli Are Altered with Age. *Cell Reports*, *25*(11), 2992-3005.e5. https://doi.org/10.1016/j.celrep.2018.11.056

Matatall, K. A., Shen, C.-C., Challen, G. A., & King, K. Y. (2014). Type II interferon promotes differentiation of myeloid-biased hematopoietic stem cells. *Stem Cells (Dayton, Ohio)*, *32*(11), 3023–3030. https://doi.org/10.1002/stem.1799

Matsumura, I., Kitamura, T., Wakao, H., Tanaka, H., Hashimoto, K., Albanese, C., Downward, J., Pestell, R. G., & Kanakura, Y. (1999). Transcriptional regulation of the cyclin D1 promoter by STAT5: Its involvement in cytokine-dependent growth of hematopoietic cells. *The EMBO Journal*, *18*(5), 1367–1377. https://doi.org/10.1093/emboj/18.5.1367

Matsunaga, T., Kato, T., Miyazaki, H., & Ogawa, M. (1998). Thrombopoietin promotes the survival of murine hematopoietic long-term reconstituting cells: Comparison with the effects of FLT3/FLK-2 ligand and interleukin-6. *Blood*, *92*(2), 452–461.

Mellon, P., Pawson, A., Bister, K., Martin, G. S., & Duesberg, P. H. (1978). Specific RNA sequences and gene products of MC29 avian acute leukemia virus. *Proceedings of the National Academy of Sciences of the United States of America*, *75*(12), 5874–5878. https://doi.org/10.1073/pnas.75.12.5874

Miller, J. P., & Allman, D. (2003). The decline in B lymphopoiesis in aged mice reflects loss of very early B-lineage precursors. *Journal of Immunology (Baltimore, Md.: 1950)*, *171*(5), 2326–2330. https://doi.org/10.4049/jimmunol.171.5.2326

Min, H., Montecino-Rodriguez, E., & Dorshkind, K. (2006). Effects of aging on the common lymphoid progenitor to pro-B cell transition. *Journal of Immunology (Baltimore, Md.: 1950)*, *176*(2), 1007–1012. https://doi.org/10.4049/jimmunol.176.2.1007

Morales, A. J., Carrero, J. A., Hung, P. J., Tubbs, A. T., Andrews, J. M., Edelson, B. T., Calderon, B., Innes, C. L., Paules, R. S., Payton, J. E., & Sleckman, B. P. (2017). A type I IFN-dependent DNA damage response regulates the genetic program and inflammasome activation in macrophages. *ELife*, *6*, e24655. https://doi.org/10.7554/eLife.24655

Morita, Y., Ema, H., & Nakauchi, H. (2010). Heterogeneity and hierarchy within the most primitive hematopoietic stem cell compartment. *The Journal of Experimental Medicine*, *207*(6), 1173–1182. https://doi.org/10.1084/jem.20091318

Morrison, S. J., Wandycz, A. M., Akashi, K., Globerson, A., & Weissman, I. L. (1996). The aging of hematopoietic stem cells. *Nature Medicine*, *2*(9), 1011–1016. https://doi.org/10.1038/nm0996-1011

Morrison, S. J., Wandycz, A. M., Hemmati, H. D., Wright, D. E., & Weissman, I. L. (1997). Identification of a lineage of multipotent hematopoietic progenitors. *Development (Cambridge, England)*, *124*(10), 1929–1939. https://doi.org/10.1242/dev.124.10.1929

Morrison, S. J., & Weissman, I. L. (1994). The long-term repopulating subset of hematopoietic stem cells is deterministic and isolatable by phenotype. *Immunity*, *1*(8), 661–673. https://doi.org/10.1016/1074-7613(94)90037-x

Mucci, A., Antonarelli, G., Caserta, C., Vittoria, F. M., Desantis, G., Pagani, R., Greco, B., Casucci, M., Escobar, G., Passerini, L., Lachmann, N., Sanvito, F., Barcella, M., Merelli, I., Naldini, L., & Gentner, B. (2021). Myeloid cell-based delivery of IFN-γ reprograms the leukemia microenvironment and induces anti-tumoral immune responses. *EMBO Molecular Medicine*, *13*(10), e13598. https://doi.org/10.15252/emmm.202013598

Muller-Sieburg, C. E., Whitlock, C. A., & Weissman, I. L. (1986). Isolation of two early B lymphocyte progenitors from mouse marrow: A committed pre-pre-B cell and a clonogenic Thy-1-lo hematopoietic stem cell. *Cell*, *44*(4), 653–662. https://doi.org/10.1016/0092-8674(86)90274-6

Muthalagu, N., Monteverde, T., Raffo-Iraolagoitia, X., Wiesheu, R., Whyte, D., Hedley, A., Laing, S., Kruspig, B., Upstill-Goddard, R., Shaw, R., Neidler, S., Rink, C., Karim, S. A., Gyuraszova, K., Nixon, C., Clark, W., Biankin, A. V., Carlin, L. M., Coffelt, S. B., … Murphy, D. J. (2020). Repression of the Type I Interferon Pathway Underlies MYC- and KRAS-Dependent Evasion of NK and B Cells in Pancreatic Ductal Adenocarcinoma. *Cancer Discovery*, *10*(6), 872–887. https://doi.org/10.1158/2159-8290.CD-19-0620

Nestorowa, S., Hamey, F. K., Pijuan Sala, B., Diamanti, E., Shepherd, M., Laurenti, E., Wilson, N. K., Kent, D. G., & Göttgens, B. (2016). A single-cell resolution map of mouse hematopoietic stem and progenitor cell differentiation. *Blood*, *128*(8), e20-31. https://doi.org/10.1182/blood-2016-05-716480

Nishikawa, S., Arai, S., Masamoto, Y., Kagoya, Y., Toya, T., Watanabe-Okochi, N., & Kurokawa, M. (2014). Thrombopoietin/MPL signaling confers growth and survival capacity to CD41-positive cells in a mouse model of Evi1 leukemia. *Blood*, *124*(24), 3587–3596. https://doi.org/10.1182/blood-2013-12-546275

Nishikii, H., Kanazawa, Y., Umemoto, T., Goltsev, Y., Matsuzaki, Y., Matsushita, K., Yamato, M., Nolan, G. P., Negrin, R., & Chiba, S. (2015). Unipotent Megakaryopoietic Pathway Bridging Hematopoietic Stem Cells and Mature Megakaryocytes. *Stem Cells (Dayton, Ohio)*, *33*(7), 2196–2207. https://doi.org/10.1002/stem.1985

Noda, S., Ichikawa, H., & Miyoshi, H. (2009). Hematopoietic stem cell aging is associated with functional decline and delayed cell cycle progression. *Biochemical and Biophysical Research Communications*, *383*(2), 210–215. https://doi.org/10.1016/j.bbrc.2009.03.153

Notta, F., Zandi, S., Takayama, N., Dobson, S., Gan, O. I., Wilson, G., Kaufmann, K. B., McLeod, J., Laurenti, E., Dunant, C. F., McPherson, J. D., Stein, L. D., Dror, Y., & Dick, J. E. (2016). Distinct routes of

lineage development reshape the human blood hierarchy across ontogeny. *Science (New York, N.Y.)*, *351*(6269), aab2116. https://doi.org/10.1126/science.aab2116

Ó, P. P. do, Wandzioch, E., Kolterud, Å., & Carlsson, L. (2001). Multipotent hematopoietic progenitor cells immortalized by Lhx2 self-renew by a cell nonautonomous mechanism. *Experimental Hematology*, *29*(8), 1019–1028. https://doi.org/10.1016/S0301-472X(01)00666-X

Obinata, M., Ohmori, Y., Takada, S., & Shoji, W. (1994). Function of c-myc on erythroid differentiation and heme synthesis. *Stem Cells*, *12*(S1), 55–63. https://doi.org/10.1002/stem.5530120708

Oedekoven, C. A., Belmonte, M., Bode, D., Hamey, F. K., Shepherd, M. S., Che, J. L. C., Boyd, G., McDonald, C., Belluschi, S., Diamanti, E., Bastos, H. P., Bridge, K. S., Göttgens, B., Laurenti, E., & Kent, D. G. (2021). Hematopoietic stem cells retain functional potential and molecular identity in hibernation cultures. *Stem Cell Reports*, *16*(6), 1614–1628. https://doi.org/10.1016/j.stemcr.2021.04.002

Ogawa, M., Matsuzaki, Y., Nishikawa, S., Hayashi, S., Kunisada, T., Sudo, T., Kina, T., Nakauchi, H., & Nishikawa, S. (1991). Expression and function of c-kit in hemopoietic progenitor cells. *The Journal of Experimental Medicine*, *174*(1), 63–71. https://doi.org/10.1084/jem.174.1.63

Oguro, H., Ding, L., & Morrison, S. J. (2013). SLAM family markers resolve functionally distinct subpopulations of hematopoietic stem cells and multipotent progenitors. *Cell Stem Cell*, *13*(1), 102–116. https://doi.org/10.1016/j.stem.2013.05.014

Okada, S., Nakauchi, H., Nagayoshi, K., Nishikawa, S., Nishikawa, S., Miura, Y., & Suda, T. (1991). Enrichment and characterization of murine hematopoietic stem cells that express c-kit molecule. *Blood*, *78*(7), 1706–1712.

Orford, K. W., & Scadden, D. T. (2008). Deconstructing stem cell self-renewal: Genetic insights into cell-cycle regulation. *Nature Reviews. Genetics*, *9*(2), 115–128. https://doi.org/10.1038/nrg2269

Osawa, M., Hanada, K., Hamada, H., & Nakauchi, H. (1996). Long-term lymphohematopoietic reconstitution by a single CD34-low/negative hematopoietic stem cell. *Science (New York, N.Y.)*, *273*(5272), 242–245. https://doi.org/10.1126/science.273.5272.242

Pang, W. W., Price, E. A., Sahoo, D., Beerman, I., Maloney, W. J., Rossi, D. J., Schrier, S. L., & Weissman, I. L. (2011). Human bone marrow hematopoietic stem cells are increased in frequency and myeloid-biased with age. *Proceedings of the National Academy of Sciences of the United States of America*, *108*(50), 20012–20017. https://doi.org/10.1073/pnas.1116110108

Papathanasiou, P., Attema, J. L., Karsunky, H., Xu, J., Smale, S. T., & Weissman, I. L. (2009). Evaluation of the long-term reconstituting subset of hematopoietic stem cells with CD150. *Stem Cells (Dayton, Ohio)*, *27*(10), 2498–2508. https://doi.org/10.1002/stem.170

Peukert, K., Staller, P., Schneider, A., Carmichael, G., Hänel, F., & Eilers, M. (1997). An alternative pathway for gene regulation by Myc. *The EMBO Journal*, *16*(18), 5672–5686. https://doi.org/10.1093/emboj/16.18.5672

Phan, R. T., Saito, M., Basso, K., Niu, H., & Dalla-Favera, R. (2005). BCL6 interacts with the transcription factor Miz-1 to suppress the cyclin-dependent kinase inhibitor p21 and cell cycle arrest in germinal center B cells. *Nature Immunology*, *6*(10), 1054–1060. https://doi.org/10.1038/ni1245

Pietras, E. M., Lakshminarasimhan, R., Techner, J.-M., Fong, S., Flach, J., Binnewies, M., & Passegué, E. (2014). Re-entry into quiescence protects hematopoietic stem cells from the killing effect of chronic exposure to type I interferons. *The Journal of Experimental Medicine*, *211*(2), 245–262. https://doi.org/10.1084/jem.20131043

Porto, M. L., Rodrigues, B. P., Menezes, T. N., Ceschim, S. L., Casarini, D. E., Gava, A. L., Pereira, T. M. C., Vasquez, E. C., Campagnaro, B. P., & Meyrelles, S. S. (2015). Reactive oxygen species contribute to dysfunction of bone marrow hematopoietic stem cells in aged C57BL/6 J mice. *Journal of Biomedical Science*, *22*(1), 97. https://doi.org/10.1186/s12929-015-0201-8

Pulit-Penaloza, J. A., Scherbik, S. V., & Brinton, M. A. (2012). Activation of Oas1a gene expression by type I IFN requires both STAT1 and STAT2 while only STAT2 is required for Oas1b activation. *Virology*, *425*(2), 71–81. https://doi.org/10.1016/j.virol.2011.11.025

Qi, Y., Li, X., Chang, C., Xu, F., He, Q., Zhao, Y., & Wu, L. (2017). Ribosomal protein L23 negatively regulates cellular apoptosis via the RPL23/Miz-1/c-Myc circuit in higher-risk myelodysplastic syndrome. *Scientific Reports*, *7*(1), 2323. https://doi.org/10.1038/s41598-017-02403-x

Qian, H., Buza-Vidas, N., Hyland, C. D., Jensen, C. T., Antonchuk, J., Månsson, R., Thoren, L. A., Ekblom, M., Alexander, W. S., & Jacobsen, S. E. W. (2007). Critical role of thrombopoietin in maintaining adult quiescent hematopoietic stem cells. *Cell Stem Cell*, *1*(6), 671–684. https://doi.org/10.1016/j.stem.2007.10.008

Rao, T. N., Hansen, N., Stetka, J., Luque Paz, D., Kalmer, M., Hilfiker, J., Endele, M., Ahmed, N., Kubovcakova, L., Rybarikova, M., Hao-Shen, H., Geier, F., Beisel, C., Dirnhofer, S., Schroeder, T., Brümmendorf, T. H., Wolf, D., Koschmieder, S., & Skoda, R. C. (2021). JAK2-V617F and interferon-α induce megakaryocyte-biased stem cells characterized by decreased long-term functionality. *Blood*, *137*(16), 2139–2151. https://doi.org/10.1182/blood.2020005563

Rashkovan, M., Vadnais, C., Ross, J., Gigoux, M., Suh, W.-K., Gu, W., Kosan, C., & Möröy, T. (2014). Miz-1 regulates translation of Trp53 via ribosomal protein L22 in cells undergoing V(D)J recombination. *Proceedings of the National Academy of Sciences of the United States of America*, *111*(50), E5411-5419. https://doi.org/10.1073/pnas.1412107111

Rodriguez-Fraticelli, A. E., Wolock, S. L., Weinreb, C. S., Panero, R., Patel, S. H., Jankovic, M., Sun, J., Calogero, R. A., Klein, A. M., & Camargo, F. D. (2018). Clonal analysis of lineage fate in native haematopoiesis. *Nature*, *553*(7687), 212–216. https://doi.org/10.1038/nature25168

Ross, J., Rashkovan, M., Fraszczak, J., Joly-Beauparlant, C., Vadnais, C., Winkler, R., Droit, A., Kosan, C., & Möröy, T. (2019). Deletion of the Miz-1 POZ Domain Increases Efficacy of Cytarabine Treatment in T- and B-ALL/Lymphoma Mouse Models. *Cancer Research*, *79*(16), 4184–4195. https://doi.org/10.1158/0008-5472.CAN-18-3038

Rossi, D. J., Bryder, D., Seita, J., Nussenzweig, A., Hoeijmakers, J., & Weissman, I. L. (2007). Deficiencies in DNA damage repair limit the function of haematopoietic stem cells with age. *Nature*, *447*(7145), 725–729. https://doi.org/10.1038/nature05862

Rossi, D. J., Bryder, D., Zahn, J. M., Ahlenius, H., Sonu, R., Wagers, A. J., & Weissman, I. L. (2005). Cell intrinsic alterations underlie hematopoietic stem cell aging. *Proceedings of the National Academy of Sciences of the United States of America*, *102*(26), 9194–9199. https://doi.org/10.1073/pnas.0503280102

Saba, I., Kosan, C., Vassen, L., Klein-Hitpass, L., & Möröy, T. (2011). Miz-1 is required to coordinate the expression of TCRbeta and p53 effector genes at the pre-TCR 'beta-selection' checkpoint. *Journal of Immunology (Baltimore, Md.: 1950)*, *187*(6), 2982–2992. https://doi.org/10.4049/jimmunol.1101451

Saba, I., Kosan, C., Vassen, L., & Möröy, T. (2011). IL-7R-dependent survival and differentiation of early T-lineage progenitors is regulated by the BTB/POZ domain transcription factor Miz-1. *Blood*, *117*(12), 3370–3381. https://doi.org/10.1182/blood-2010-09-310680

Sadler, A. J., & Williams, B. R. G. (2008). Interferon-inducible antiviral effectors. *Nature Reviews. Immunology*, *8*(7), 559–568. https://doi.org/10.1038/nri2314

Sanz-Moreno, A., Fuhrmann, D., Wolf, E., von Eyss, B., Eilers, M., & Elsässer, H.-P. (2014). Miz1 deficiency in the mammary gland causes a lactation defect by attenuated Stat5 expression and phosphorylation. *PloS One*, *9*(2), e89187. https://doi.org/10.1371/journal.pone.0089187

Schürch, C. M., Riether, C., & Ochsenbein, A. F. (2014). Cytotoxic CD8+ T cells stimulate hematopoietic progenitors by promoting cytokine release from bone marrow mesenchymal stromal cells. *Cell Stem Cell*, *14*(4), 460–472. https://doi.org/10.1016/j.stem.2014.01.002

Seita, J., Ema, H., Ooehara, J., Yamazaki, S., Tadokoro, Y., Yamasaki, A., Eto, K., Takaki, S., Takatsu, K., & Nakauchi, H. (2007). Lnk negatively regulates self-renewal of hematopoietic stem cells by modifying thrombopoietin-mediated signal transduction. *Proceedings of the National Academy of Sciences of the United States of America*, *104*(7), 2349–2354. https://doi.org/10.1073/pnas.0606238104

Selleri, C., Sato, T., Anderson, S., Young, N. S., & Maciejewski, J. P. (1995). Interferon-gamma and tumor necrosis factor-alpha suppress both early and late stages of hematopoiesis and induce programmed cell death. *Journal of Cellular Physiology*, *165*(3), 538–546. https://doi.org/10.1002/jcp.1041650312

Seo, S.-U., Kwon, H.-J., Ko, H.-J., Byun, Y.-H., Seong, B. L., Uematsu, S., Akira, S., & Kweon, M.-N. (2011). Type I interferon signaling regulates Ly6C(hi) monocytes and neutrophils during acute viral pneumonia in mice. *PLoS Pathogens*, *7*(2), e1001304. https://doi.org/10.1371/journal.ppat.1001304

Seoane, J., Pouponnot, C., Staller, P., Schader, M., Eilers, M., & Massagué, J. (2001). TGFbeta influences Myc, Miz-1 and Smad to control the CDK inhibitor p15INK4b. *Nature Cell Biology*, *3*(4), 400–408. https://doi.org/10.1038/35070086

Shahbazian, L. M., Quinton, L. J., Bagby, G. J., Nelson, S., Wang, G., & Zhang, P. (2004). Escherichia coli pneumonia enhances granulopoiesis and the mobilization of myeloid progenitor cells into the systemic circulation. *Critical Care Medicine*, *32*(8), 1740–1746. https://doi.org/10.1097/01.ccm.0000132900.84627.90

Siminovitch, L., Mcculloch, E. A., & Till, J. E. (1963). THE DISTRIBUTION OF COLONY-FORMING CELLS AMONG SPLEEN COLONIES. *Journal of Cellular and Comparative Physiology*, *62*, 327–336. https://doi.org/10.1002/jcp.1030620313

Singh, P., Yao, Y., Weliver, A., Broxmeyer, H. E., Hong, S.-C., & Chang, C.-H. (2008). Vaccinia virus infection modulates the hematopoietic cell compartments in the bone marrow. *Stem Cells (Dayton, Ohio)*, *26*(4), 1009–1016. https://doi.org/10.1634/stemcells.2007-0461

Smith, J. N. P., Zhang, Y., Li, J. J., McCabe, A., Jo, H. J., Maloney, J., & MacNamara, K. C. (2018). Type I IFNs drive hematopoietic stem and progenitor cell collapse via impaired proliferation and increased RIPK1-dependent cell death during shock-like ehrlichial infection. *PLoS Pathogens*, *14*(8), e1007234. https://doi.org/10.1371/journal.ppat.1007234

Snoeck, H. W., Lardon, F., Lenjou, M., Nys, G., Van Bockstaele, D. R., & Peetermans, M. E. (1993). Interferon-gamma and interleukin-4 reciprocally regulate the production of monocytes/macrophages and neutrophils through a direct effect on committed monopotential bone marrow progenitor cells. *European Journal of Immunology*, *23*(5), 1072–1077. https://doi.org/10.1002/eji.1830230514

Snoeck, H. W., Van Bockstaele, D. R., Nys, G., Lenjou, M., Lardon, F., Haenen, L., Rodrigus, I., Peetermans, M. E., & Berneman, Z. N. (1994). Interferon gamma selectively inhibits very primitive CD342+CD38- and not more mature CD34+CD38+ human hematopoietic progenitor cells. *The Journal of Experimental Medicine*, *180*(3), 1177–1182. https://doi.org/10.1084/jem.180.3.1177

Spangrude, G. J., Heimfeld, S., & Weissman, I. L. (1988). Purification and characterization of mouse hematopoietic stem cells. *Science (New York, N.Y.)*, *241*(4861), 58–62. https://doi.org/10.1126/science.2898810

Staller, P., Peukert, K., Kiermaier, A., Seoane, J., Lukas, J., Karsunky, H., Möröy, T., Bartek, J., Massagué, J., Hänel, F., & Eilers, M. (2001). Repression of p15INK4b expression by Myc through association with Miz-1. *Nature Cell Biology*, *3*(4), 392–399. https://doi.org/10.1038/35070076

Stephenson, J. R., Axelrad, A. A., McLeod, D. L., & Shreeve, M. M. (1971). Induction of colonies of hemoglobin-synthesizing cells by erythropoietin in vitro. *Proceedings of the National Academy of Sciences of the United States of America*, *68*(7), 1542–1546. https://doi.org/10.1073/pnas.68.7.1542

Sudo, K., Ema, H., Morita, Y., & Nakauchi, H. (2000). Age-associated characteristics of murine hematopoietic stem cells. *The Journal of Experimental Medicine*, *192*(9), 1273–1280. https://doi.org/10.1084/jem.192.9.1273

Sun, D., Luo, M., Jeong, M., Rodriguez, B., Xia, Z., Hannah, R., Wang, H., Le, T., Faull, K. F., Chen, R., Gu, H., Bock, C., Meissner, A., Göttgens, B., Darlington, G. J., Li, W., & Goodell, M. A. (2014). Epigenomic profiling of young and aged HSCs reveals concerted changes during aging that reinforce self-renewal. *Cell Stem Cell*, *14*(5), 673–688. https://doi.org/10.1016/j.stem.2014.03.002

Taiwo, O., Wilson, G. A., Emmett, W., Morris, T., Bonnet, D., Schuster, E., Adejumo, T., Beck, S., & Pearce, D. J. (2013). DNA methylation analysis of murine hematopoietic side population cells during aging. *Epigenetics*, *8*(10), 1114–1122. https://doi.org/10.4161/epi.26017

Takizawa, H., Regoes, R. R., Boddupalli, C. S., Bonhoeffer, S., & Manz, M. G. (2011). Dynamic variation in cycling of hematopoietic stem cells in steady state and inflammation. *The Journal of Experimental Medicine*, *208*(2), 273–284. https://doi.org/10.1084/jem.20101643

Till, J. E., & McCulloch, E. A. (1961). A Direct Measurement of the Radiation Sensitivity of Normal Mouse Bone Marrow Cells. *Radiation Research*, *14*(2), 213–222. https://doi.org/10.2307/3570892

Tulley, P. N., Neale, M., Jackson, D., Chana, J. S., Grover, R., Cree, I., Grobbelaar, A. O., & Wilson, G. D. (2004). The relation between c-myc expression and interferon sensitivity in uveal melanoma. *The British Journal of Ophthalmology*, *88*(12), 1563–1567. https://doi.org/10.1136/bjo.2003.033498

van Riggelen, J., Müller, J., Otto, T., Beuger, V., Yetil, A., Choi, P. S., Kosan, C., Möröy, T., Felsher, D. W., & Eilers, M. (2010). The interaction between Myc and Miz1 is required to antagonize TGFbeta-dependent autocrine signaling during lymphoma formation and maintenance. *Genes & Development*, *24*(12), 1281–1294. https://doi.org/10.1101/gad.585710

Varlakhanova, N., Cotterman, R., Bradnam, K., Korf, I., & Knoepfler, P. S. (2011). Myc and Miz-1 have coordinate genomic functions including targeting Hox genes in human embryonic stem cells. *Epigenetics & Chromatin*, *4*, 20. https://doi.org/10.1186/1756-8935-4-20

Vo, B. T., Wolf, E., Kawauchi, D., Gebhardt, A., Rehg, J. E., Finkelstein, D., Walz, S., Murphy, B. L., Youn, Y. H., Han, Y.-G., Eilers, M., & Roussel, M. F. (2016). The Interaction of Myc with Miz1 Defines Medulloblastoma Subgroup Identity. *Cancer Cell*, *29*(1), 5–16. https://doi.org/10.1016/j.ccell.2015.12.003

Wanzel, M., Kleine-Kohlbrecher, D., Herold, S., Hock, A., Berns, K., Park, J., Hemmings, B., & Eilers, M. (2005). Akt and 14-3-3eta regulate Miz1 to control cell-cycle arrest after DNA damage. *Nature Cell Biology*, *7*(1), 30–41. https://doi.org/10.1038/ncb1202

Wanzel, M., Russ, A. C., Kleine-Kohlbrecher, D., Colombo, E., Pelicci, P.-G., & Eilers, M. (2008). A ribosomal protein L23-nucleophosmin circuit coordinates Miz1 function with cell growth. *Nature Cell Biology*, *10*(9), 1051–1061. https://doi.org/10.1038/ncb1764

Whitlock, C. A., & Witte, O. N. (1982). Long-term culture of B lymphocytes and their precursors from murine bone marrow. *Proceedings of the National Academy of Sciences of the United States of America*, *79*(11), 3608–3612. https://doi.org/10.1073/pnas.79.11.3608

Wilden, H., Fournier, P., Zawatzky, R., & Schirrmacher, V. (2009). Expression of RIG-I, IRF3, IFN-beta and IRF7 determines resistance or susceptibility of cells to infection by Newcastle Disease Virus. *International Journal of Oncology*, *34*(4), 971–982. https://doi.org/10.3892/ijo_00000223

Wilson, A., Laurenti, E., Oser, G., van der Wath, R. C., Blanco-Bose, W., Jaworski, M., Offner, S., Dunant, C. F., Eshkind, L., Bockamp, E., Lió, P., Macdonald, H. R., & Trumpp, A. (2008). Hematopoietic stem cells reversibly switch from dormancy to self-renewal during homeostasis and repair. *Cell*, *135*(6), 1118–1129. https://doi.org/10.1016/j.cell.2008.10.048

Wilson, A., Murphy, M. J., Oskarsson, T., Kaloulis, K., Bettess, M. D., Oser, G. M., Pasche, A.-C., Knabenhans, C., Macdonald, H. R., & Trumpp, A. (2004). C-Myc controls the balance between hematopoietic stem cell self-renewal and differentiation. *Genes & Development*, *18*(22), 2747–2763. https://doi.org/10.1101/gad.313104

Wolf, E., Gebhardt, A., Kawauchi, D., Walz, S., von Eyss, B., Wagner, N., Renninger, C., Krohne, G., Asan, E., Roussel, M. F., & Eilers, M. (2013). Miz1 is required to maintain autophagic flux. *Nature Communications*, *4*, 2535. https://doi.org/10.1038/ncomms3535

Wu, B., Xie, J., Du, Z., Wu, J., Zhang, P., Xu, L., & Li, E. (2014). PPI network analysis of mRNA expression profile of ezrin knockdown in esophageal squamous cell carcinoma. *BioMed Research International*, *2014*, 651954. https://doi.org/10.1155/2014/651954

Wu, S., Cetinkaya, C., Munoz-Alonso, M. J., von der Lehr, N., Bahram, F., Beuger, V., Eilers, M., Leon, J., & Larsson, L.-G. (2003). Myc represses differentiation-induced p21CIP1 expression via Miz-1-dependent interaction with the p21 core promoter. *Oncogene*, *22*(3), 351–360. https://doi.org/10.1038/sj.onc.1206145

Yamamoto, R., Morita, Y., Ooehara, J., Hamanaka, S., Onodera, M., Rudolph, K. L., Ema, H., & Nakauchi, H. (2013). Clonal analysis unveils self-renewing lineage-restricted progenitors generated directly from hematopoietic stem cells. *Cell*, *154*(5), 1112–1126. https://doi.org/10.1016/j.cell.2013.08.007

Yamamoto, R., Wilkinson, A. C., Ooehara, J., Lan, X., Lai, C.-Y., Nakauchi, Y., Pritchard, J. K., & Nakauchi, H. (2018). Large-Scale Clonal Analysis Resolves Aging of the Mouse Hematopoietic Stem Cell Compartment. *Cell Stem Cell*, *22*(4), 600-607.e4. https://doi.org/10.1016/j.stem.2018.03.013

Yang, L., Bryder, D., Adolfsson, J., Nygren, J., Månsson, R., Sigvardsson, M., & Jacobsen, S. E. W. (2005). Identification of Lin(-)Sca1(+)kit(+)CD34(+)Flt3- short-term hematopoietic stem cells capable of rapidly reconstituting and rescuing myeloablated transplant recipients. *Blood*, *105*(7), 2717–2723. https://doi.org/10.1182/blood-2004-06-2159

Yoshihara, H., Arai, F., Hosokawa, K., Hagiwara, T., Takubo, K., Nakamura, Y., Gomei, Y., Iwasaki, H., Matsuoka, S., Miyamoto, K., Miyazaki, H., Takahashi, T., & Suda, T. (2007). Thrombopoietin/MPL signaling regulates hematopoietic stem cell quiescence and interaction with the osteoblastic niche. *Cell Stem Cell*, *1*(6), 685–697. https://doi.org/10.1016/j.stem.2007.10.020

Zaro, B. W., Noh, J. J., Mascetti, V. L., Demeter, J., George, B., Zukowska, M., Gulati, G. S., Sinha, R., Flynn, R. A., Banuelos, A., Zhang, A., Wilkinson, A. C., Jackson, P., & Weissman, I. L. (2020). Proteomic analysis of young and old mouse hematopoietic stem cells and their progenitors reveals post-transcriptional regulation in stem cells. *ELife*, *9*, e62210. https://doi.org/10.7554/eLife.62210

Zeng, X., Li, X., Shao, M., Xu, Y., Shan, W., Wei, C., Li, X., Wang, L., Hu, Y., Zhao, Y., Qian, P., & Huang, H. (2021). Integrated Single-Cell Bioinformatics Analysis Reveals Intrinsic and Extrinsic Biological Characteristics of Hematopoietic Stem Cell Aging. *Frontiers in Genetics*, *12*, 745786. https://doi.org/10.3389/fgene.2021.745786

Zhang, Y., Jones, M., McCabe, A., Winslow, G. M., Avram, D., & MacNamara, K. C. (2013). MyD88 signaling in CD4 T cells promotes IFN-γ production and hematopoietic progenitor cell expansion in response to intracellular bacterial infection. *Journal of Immunology (Baltimore, Md.: 1950)*, *190*(9), 4725–4735. https://doi.org/10.4049/jimmunol.1203024

Zhao, X., Ren, G., Liang, L., Ai, P. Z., Zheng, B., Tischfield, J. A., Shi, Y., & Shao, C. (2010). Brief report: Interferon-gamma induces expansion of Lin(-)Sca-1(+)C-Kit(+) Cells. *Stem Cells (Dayton, Ohio)*, *28*(1), 122–126. https://doi.org/10.1002/stem.252

# 7. Appendix

7.1 Supplementary figures
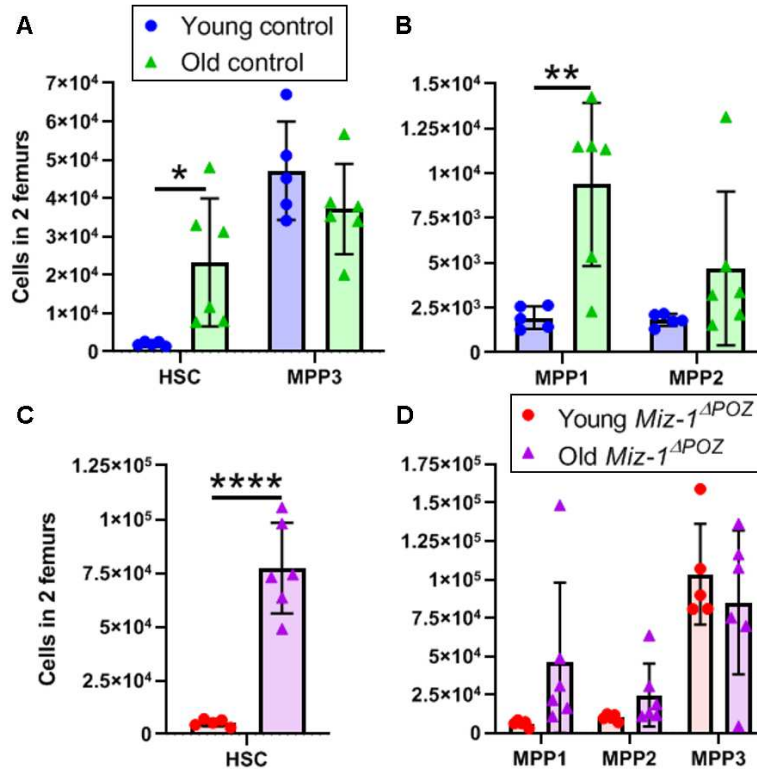
Figure S1.: Supplementary figure for flow cytometry experiments on HSPCs (**A**) Bar graph with overlaid dot plot of the total number of gated HSCs and MPP3 found in 2 femurs of young control and old control mice, $n = 5$ (young), $n = 6$ (old); mean ± SD; *: $p < 0.05$; t test. (**B**) as in (**A**) but for MPP1 and MPP2 cells, mean ± SD; *: $p < 0.05$, **: $p < 0.01$, ****: $p < 0.0001$; t test. (**C**) Bar graph with overlaid dot plot of the total number of gated HSCs found in 2 femurs of young and old $Miz\text{-}1^{\Delta POZ}$ mice, $n = 5$ (young), $n = 6$ (old); mean ± SD; ****: $p < 0.0001$; t test. (**D**) as in (**C**) but for MPP1, MPP2 and MPP3 cells, mean ± SD; t test.
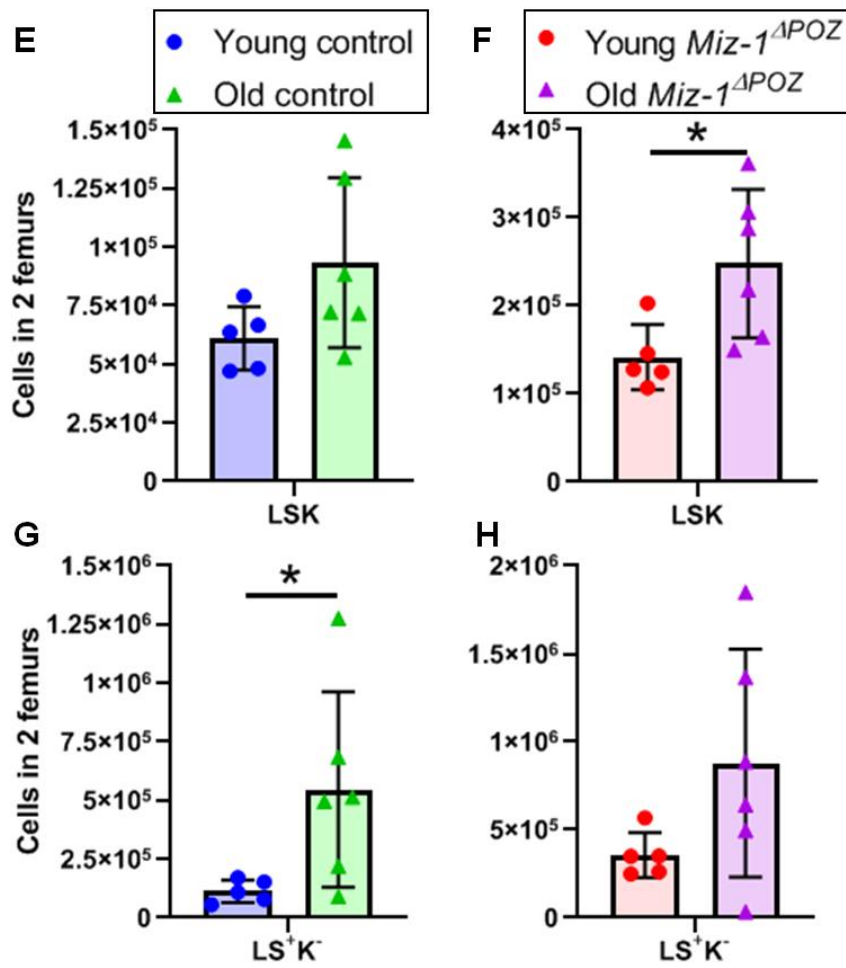
Figure S1.: Supplementary figure for flow cytometry experiments on HSPCs (**E**) Bar graph with overlaid dot plot of the total number of gated LSKs found in 2 femurs of young control and old control mice, n = 5 (young), n = 6 (old); mean ± SD. (**F**) as in (**E**) but young and old $Miz-1^{ΔPOZ}$ mice, n = 5 (young), n = 6 (old); mean ± SD; *: $p < 0.05$; t test. (**G**) Bar graph with overlaid dot plot of the total number of gated LS$^+$K$^-$ cells found in 2 femurs of young control and old control mice, n = 5 (young), n = 6 (old); mean ± SD; *: $p < 0.05$; t test. (**H**) as in (**G**) but young and old $Miz-1^{ΔPOZ}$ mice, n = 5 (young), n = 6 (old); mean ± SD.
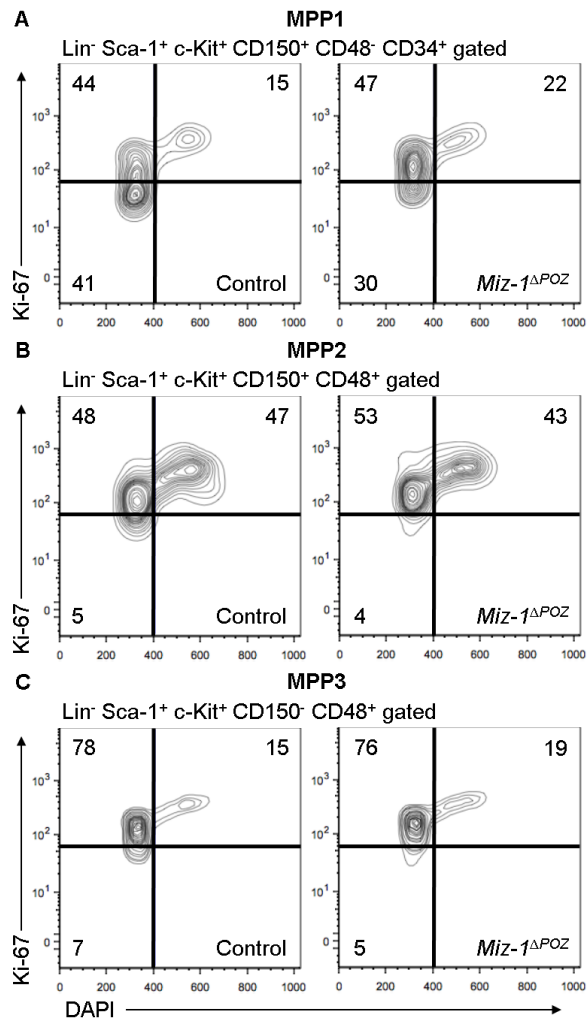
Figure S2.: Supplementary figure for intracellular Ki-67 staining experiments (**A**) Representative FACS plots showing the percentages of MPP1 from young mice in the G0 (Ki-67⁻, DAPI⁻, lower left quadrant), G1 (Ki-67⁺, DAPI⁻, upper left quadrant) and S+G2M (Ki-67⁺, DAPI⁺, upper right quadrant) cell cycle phases. (**B**) as in (**A**), but for MPP2 cells. (**C**) as in (**A**), but for MPP3 cells.
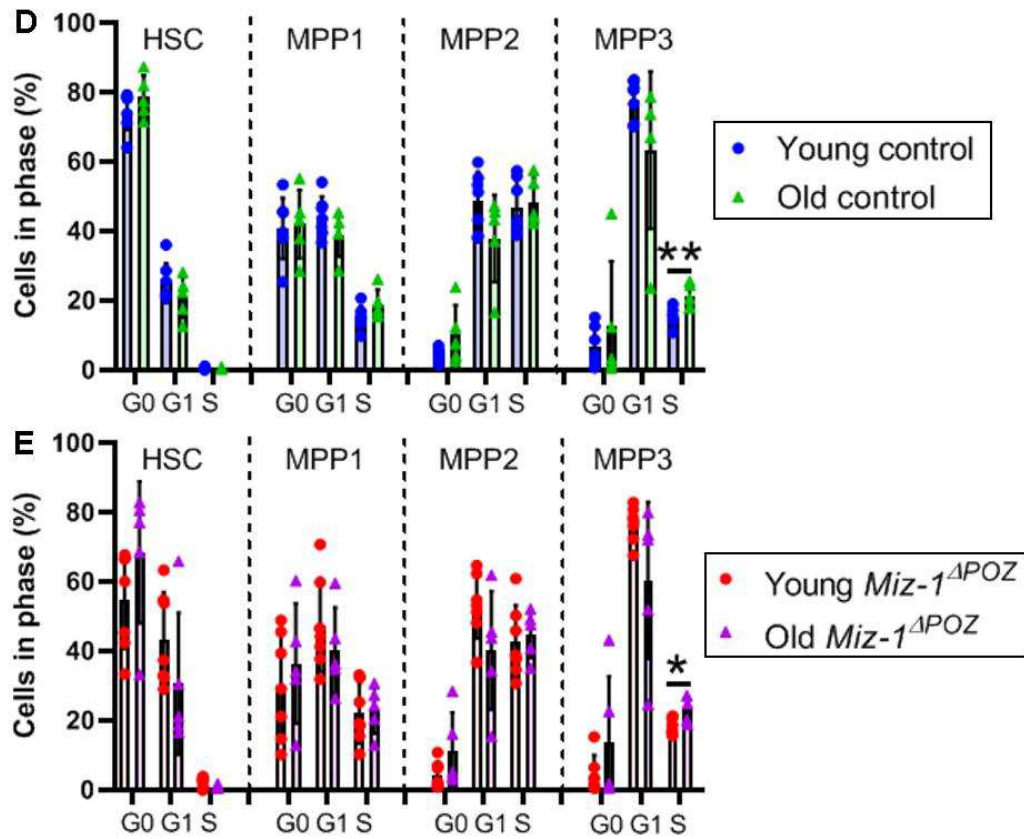
Figure S2.: Supplementary figure for intracellular Ki-67 staining experiments (**D**) Bar graphs with dot plot overlays displaying the mean percentage of HSCs, MPP1, MPP2 and MPP3 cells by cell cycle phase from young and old control mice. n = 7 (young), n = 5 (old); mean ± SD; **: $p < 0.01$; t test. (**E**) as in (**D**) but for *Miz-1^ΔPOZ^* mice. n = 7 (young), n = 5 (old); mean ± SD; *: $p < 0.05$; t test.
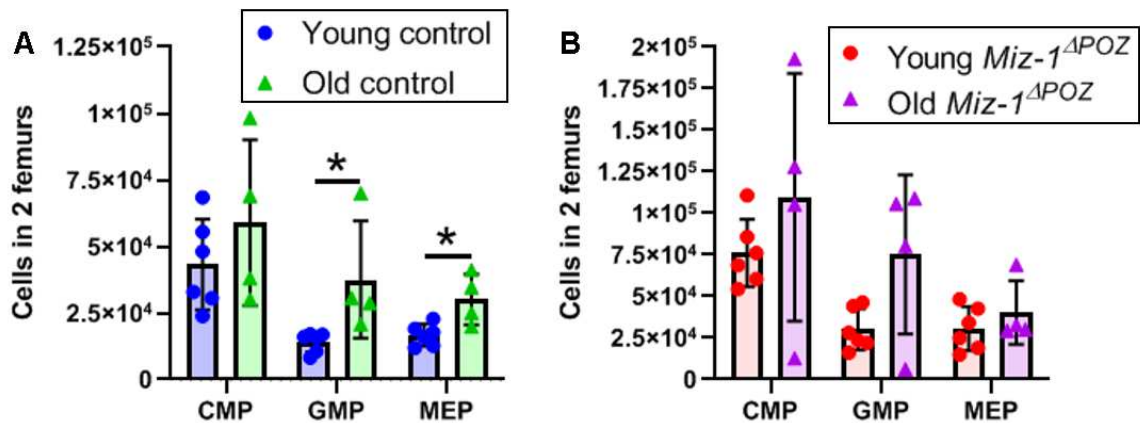
Figure S3.: Supplementary figure for flow cytometry experiments on myeloid and lymphoid cells (**A**) Bar graph with dot plot overlay displaying the mean number of CMP, GMP, MEP cells in 2 femurs from young and old control mice. n = 6 (young), n = 4 (old); mean ± SD; **: $p < 0.01$; t test. (**B**) as in (**A**) but for *Miz-1^ΔPOZ^* mice. n = 6 (young), n = 4 (old); mean ± SD; t test.
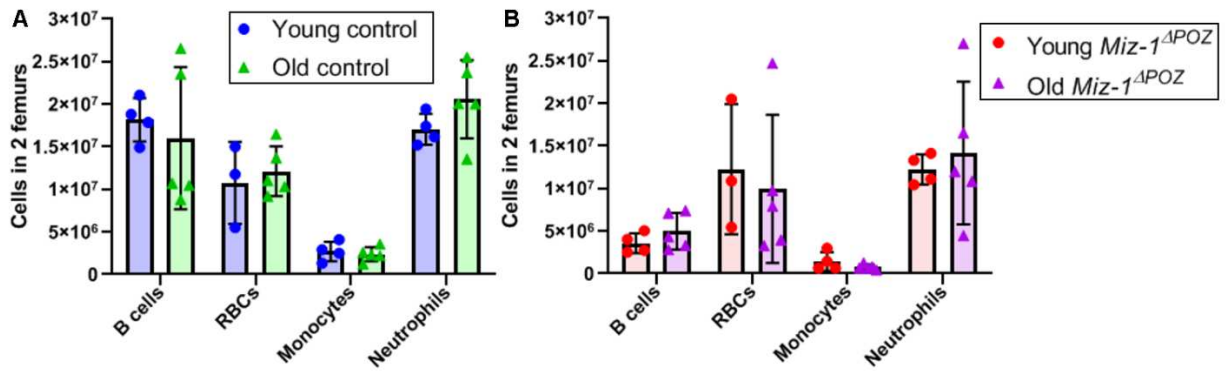
Figure S4.: Supplementary figure for flow cytometry experiments on mature hematopoietic cells (**A**) Bar graph with dot plot overlay displaying the mean number of B lymphocytes, erythrocytes (RBCs), monocytes and neutrophils in 2 femurs from young and old control mice. n = 3-4 (young), n = 5 (old); mean ± SD; t test. (**B**) as in (**A**) but for $Miz-1^{\Delta POZ}$ mice. n = 3-4 (young), n = 5 (old); mean ± SD; t test.
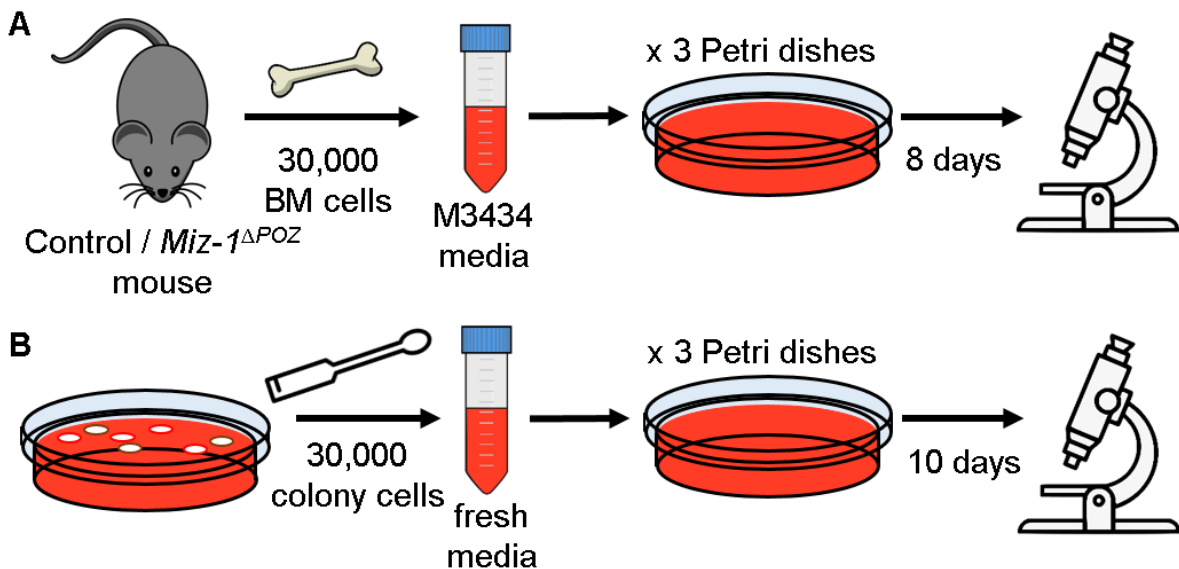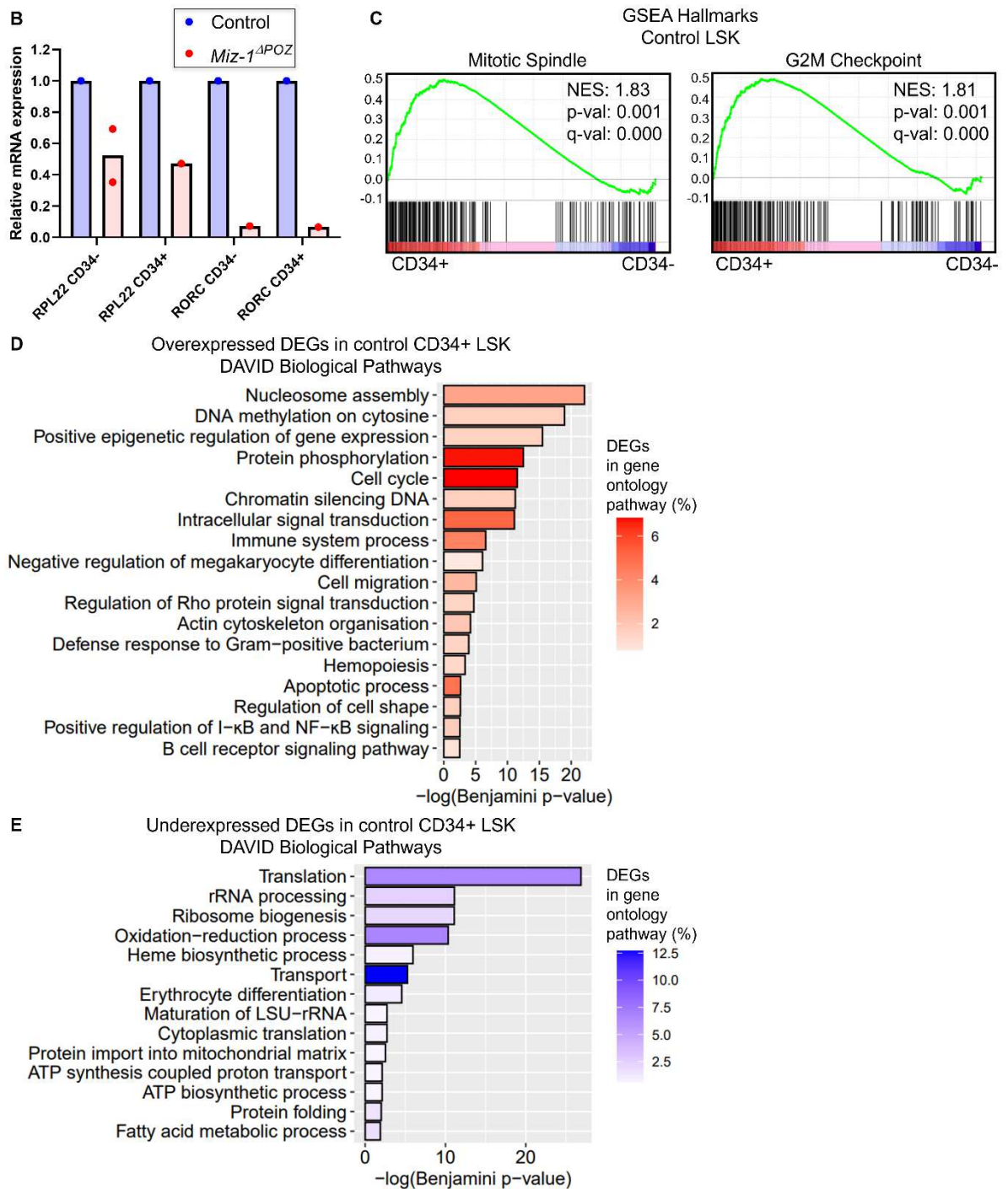

Figure S5.: Supplementary figure showing the experimental plan of colony-forming assays (**A**) Schematic depicting the set-up of colony assays on methylcellulose media. (**B**) Schematic depicting the set-up of serial colony assays on methylcellulose media.
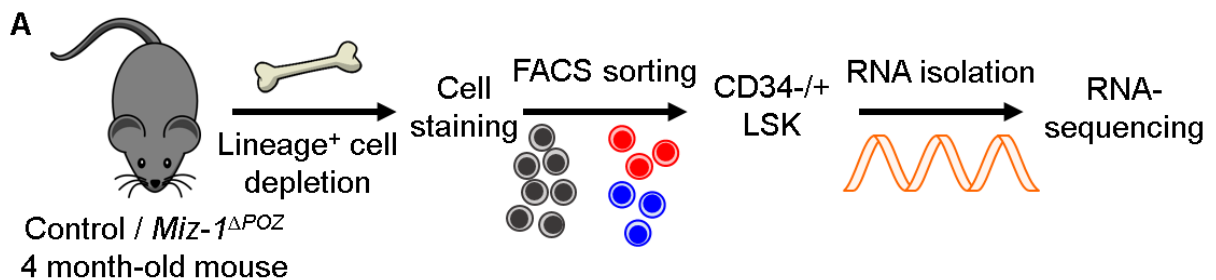
Figure S6.: Inactivation of Miz-1 transcriptional activity leads to the transcriptional activation of the type I interferon response pathway (**A**) Schematic of the RNA-sequencing experimental set-

up. BM cells were depleted of cells expressing lineage markers, fluorescently labelled and sorted by flow cytometry into CD34⁻ and CD34⁺ LSK populations before RNA isolation and freezing prior to RNA-sequencing.
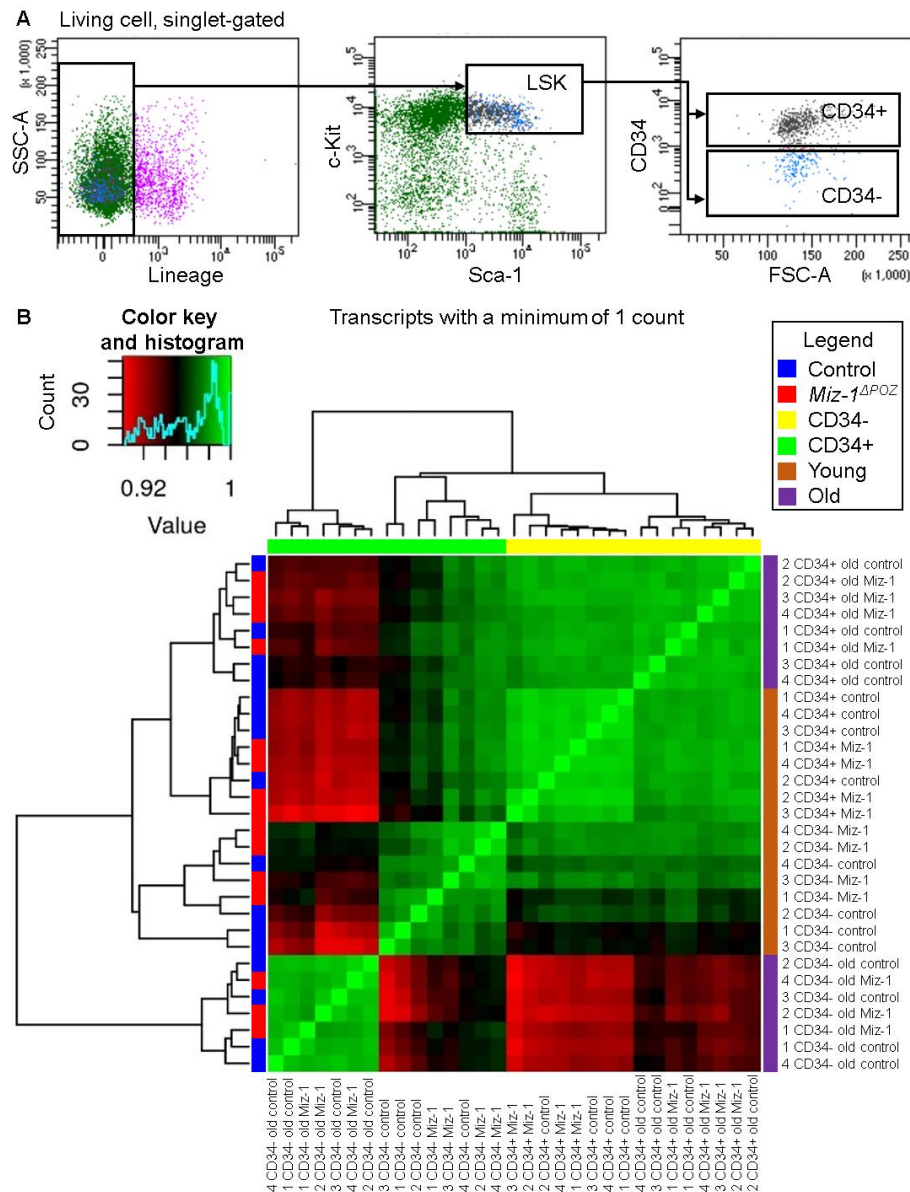

Figure S6.: Supplementary figure for qPCR results and RNA-sequencing in young mice (**B**) Bar graph overlaid with dot-plot of qPCR results documenting the expression of *RPL22* and *RORC* mRNAs altered in expression level by *Miz-1^ΔPOZ* mutation in CD34⁻ and CD34⁺ LSKs. *n* = 2 (*RPL22* CD34⁻ LSKs), *n* = 1 (others). (**C**) Gene-set enrichment analysis profiles depicting the top „Hallmark" gene signatures enriched upon CD34 expression in control LSKs, generated with bulk RNA-seq data. NES: normalized enrichment score. (**D**) Bar graph depicting biological function annotation of genes upregulated in CD34⁺

control LSKs compared to CD34⁻ control LSKs using the functional annotation software DAVID. X-axis shows the negative log of the Benjamini p-value of the gene ontology term. Gene ontology terms with the lowest Benjamini p-value are ranked at the top of the graph. Color of the bar graph represents the percentage of genes of that gene ontology term that were upregulated DEGs in CD34⁺ LSKs. (**E**) as in (**D**) but for downregulated genes.
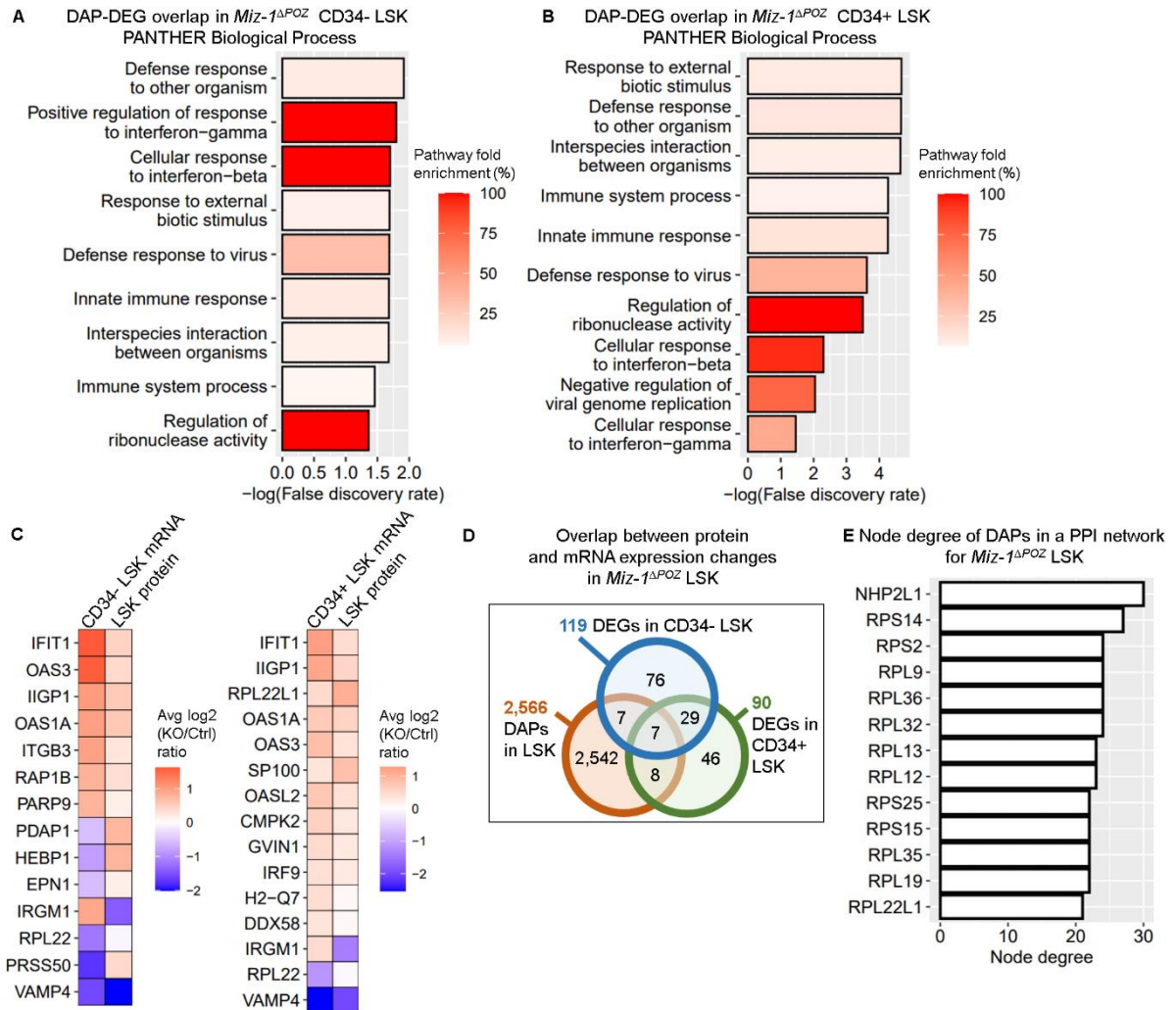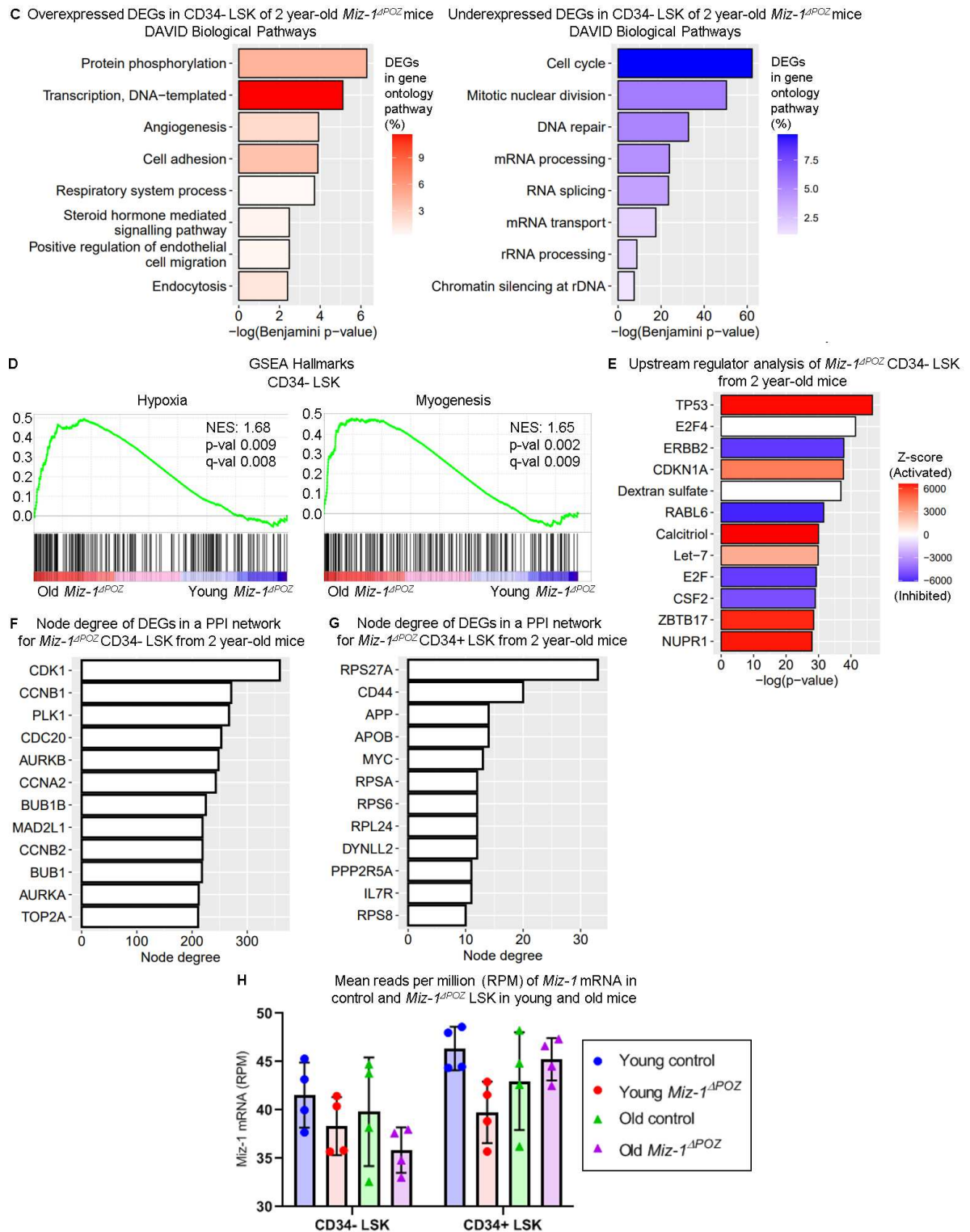

Figure S7.: Supplementary figure for the proteomic analysis (**A**) Bar graph showing overrepresented gene ontology terms of DEGs that were also differentially expressed proteins in CD34⁻ *Miz-1^ΔPOZ* LSKs revealed by PANTHER Biological Process annotation. The DAPs in this figure were not filtered for their logarithmic fold expression change. The x-axis shows the negative logarithm of the false discovery rate (FDR or Q-value) of the gene ontology term. Gene ontology terms with the lowest FDR are ranked at the top of the graph. The bar graph color represents the percentage of genes of that gene ontology term that were upregulated DAPs in knockout. (**B**) As in (**A**) but for CD34⁺ LSKs. (**C**) Heat map of DAPs in CD34⁻ (left) and CD34⁺ (right) *Miz-1^ΔPOZ* LSKs the transcripts of which were also DEGs, demonstrating fold expression changes. The color represents the logarithmic knockout over control ratio for each DAP. (**D**) Venn diagram representing the overlap between protein (Q-value-only filtered DAPs) and RNA expression changes in *Miz-1^ΔPOZ* LSKs. (**E**) Bar graph of node degree (number of bridges) for each gene (node) in the PPI network of 320 Q-value- and fold-change-filtered DAPs in *Miz-1^ΔPOZ* LSKs.

Figure S8.: Supplementary figure for RNA-sequencing of aged mice (**A**) FACS sorting scheme for CD34⁻ and CD34⁺ LSKs from which RNA was isolated for RNA-sequencing. A sample from a 24 month-old control mouse is shown. (**B**) Heat map of sample similarity in terms of gene counts. A heat map displaying comparisons of the spearman correlation of gene counts (for genes with more than one count) per gene for each sample.

Figure S8.: Supplementary figure for RNA-sequencing of aged mice (**C**) Bar graph presenting the biological function annotation by DAVID of genes upregulated (left) and downregulated (right) in 2 year-old *Miz-1^ΔPOZ* mice compared to young *Miz-1^ΔPOZ* mice in CD34^- LSKs. X-axis shows the negative log of the Benjamini p-value of the gene ontology term. Gene ontology terms with the lowest Benjamini p-value are ranked at the top of the graph. Color of the bar graph represents the percentage of genes of that gene ontology term that were up-or-downregulated in aged mice. (**D**) Gene-set enrichment analysis profiles depicting the top „Hallmark" gene signatures enriched in 2 year-old *Miz-1^ΔPOZ* mice

compared to young *Miz-1$^{\Delta POZ}$* mice in CD34$^-$ LSKs, generated with bulk RNA-sequencing data. NES: normalized enrichment score. (**E**) Bar graph representing Ingenuity upstream regulator analysis of DEGs in CD34$^-$ LSKs from 2 year-old *Miz-1$^{\Delta POZ}$* mice compared to young *Miz-1$^{\Delta POZ}$* mice. Shown are the 12 regulators with the lowest p-value for both cell types. Red are regulators predicted to be activated and blue represents predicted inhibition. (**F**) Bar graph of node degree (number of bridges) for each gene (node) in the PPI network (not shown) of DEGs in *Miz-1$^{\Delta POZ}$* CD34$^-$ LSKs from 24 month-old mice. (**G**) as in (**F**) but for CD34$^+$ LSKs. (**H**) Bar graph overlaid with dot plot of the reads per million reads (RPM) of *Miz-1/ZBTB17* RNAs sequenced in CD34$^-$ and CD34$^+$ LSKs from control and *Miz-1$^{\Delta POZ}$* mice of young and old ages.

8. Acknowledgements and contributions

I would firstly like to thank everyone at the Center for Molecular Biomedicine (CMB) who kept the kitchen coffee machine stocked with coffee grounds and milk, thereby making the work presented in this thesis possible.

I am indebted to several colleagues at the Fritz Lipmann Institute on Aging (FLI) who had the patience to lend me their professional assistance in developing the methods used in my doctoral work: Dr. **Yohei Morita**, who helped me design the flow cytometric cell staining scheme I used, Dr. Prof. **Helmut Pospiech** and Dr. **Yulin Chen**, who gave me indispensable guidance in performing the immunofluorescent DNA damage assay, Dr. **Elias Amro**, who shared with me his method of purifying HSCs, and Dr. **Zhiyang Chen** who assisted me in setting up the culturing of HPC-5 cells.

The proteomics data presented in this work was produced from our samples by Dr. **Joanna Kirkpatrick** and **Norman Rahnis** of the Proteomics Facility of the FLI and the RNA-sequencing data by Dr. **Marco Groth**, Dr. **Martin Bens** and **Ivonne Görlich** of the DNA Sequencing Facility of the FLI. I am extremely grateful for their highly important work in providing us with these results, as well as their bioinformatics analysis. I deeply thank Dr. **Amod Godbole** for his guidance and allowance in using the confocal microscope for my immunofluorescent experiments.

I extend thanks to **Katrin Schubert**, **Linda Rothenburger** and **Maria Locke** of the FACS facility of the FLI for enabling me to properly sort cells for my experiments and for their professionalism in their work.

I must thank **Andy Greifenstein**, Dr. **Holger Bierhoff** and Dr. **Maren Godmann** for their advice in setting up the ChIP protocol and analysing the results, as well as immunofluorescent reagents provided to us by **Maren**.

Special thanks go to Dr. **Christian Kosan**, Dr. **Karl Lenhard Rudolph** and Dr. **Helen Morrison** for refining the direction of my research project on my annual project reviews.

I must extend my gratitude to Dr. **Claudia Müller** for her help in guiding me through the administrative aspects of my studentship at the FLI.

I am grateful to **Carmen Martens** for her warmth and technical support throughout the whole of my Ph.D. My thanks also go to the staff of the mouse facility of the BIZ for their professionalism and effort, upon which all of my mouse experiments depended.

My deepest thanks go to my laboratory colleagues and fellow members of the ground floor of the CMB, especially my fellow students in **AG Kosan** and my supervisor **Christian**.

9. Declaration of independent assignment

I hereby certify that I am aware of the applicable doctoral regulations of the Faculty of Biological Sciences of the Friedrich Schiller University of Jena. I have prepared the submitted doctoral thesis myself and have not adopted any text sections from third parties or my own previous theses without citing them. I have indicated all sources and tools used. In addition, all persons who supported me in the production and analysis of the results, and the evaluation and in the writing of this doctoral thesis have been named. I did not receive any services from specialized consultants or third parties who would receive any monetary benefits from me in connection with this thesis. The doctoral thesis has never before been submitted as an examination paper to a governmental or scientific examination. In addition, I have never before submitted the thesis to another university as a doctoral dissertation or anything similar to it as a paper as a publication.

Jena, 08.10.2023

_____

Adam Charles Summerfield